DIGEST OF SELECTED WEATHER PROBLEMS OF THE MEDITERRANEAN

Elmar R. Reiter

Navy Weather Research Facility
Norfolk, Virginia

April 1971

NAVWEARSCHFAC Technical Paper No. 9–71

DIGEST
OF SELECTED WEATHER PROBLEMS
OF THE MEDITERRANEAN

by
DR. ELMAR R. REITER

NAVY WEATHER RESEARCH FACILITY
BLDG. R-48, NAVAL AIR STATION
NORFOLK, VIRGINIA 23511

APRIL 1971

(BASED ON THE PROCEEDINGS OF THE WORKSHOP ON MEDITERRANEAN WEATHER, JUNE 1970)

FOREWORD

As an initial step in the preparation of a forecaster's handbook for the Mediterranean area, an international group of experts was invited to a Working Panel at WEARSCHFAC in June 1970.

The purpose of the Panel was to consolidate and evaluate present knowledge of operational analysis and forecasting techniques in the area and to determine major forecasting problems, thus assisting WEARSCHFAC in formulating a research program.

Although the complete proceedings of the Working Panel are to be published, it was decided that a digest of the significant material presented would be of more immediate value to those interested in forecasting in the Mediterranean area. Dr. E. R. Reiter, the scientific coordinator of the Panel, undertook the task of preparing this digest; in addition to selecting and including pertinent information from contributions made to the Working Panel, he has also included material from other sources. Other valuable information presented to the Panel but not included in Dr. Reiter's digest will greatly assist further studies to be made by WEARSCHFAC personnel. The results of these studies will form the basis of the planned forecaster's handbook, wherein due acknowledgement will be made to all contributors.

G. D. HAMILTON
Commander, U.S. Navy
Commanding Officer
Navy Weather Research Facility

TABLE OF CONTENTS

TABLE OF CONTENTS (CONTINUED)

LIST OF FIGURES AND TABLES

LIST OF FIGURES AND TABLES (CONTINUED)

LIST OF FIGURES AND TABLES (CONTINUED)

1. GENERAL BACKGROUND

1.1 Introduction

At the request of the Commander, SIXTH Fleet, the Navy Weather Research Facility has been tasked with producing a handbook of forecasting techniques for use in the Mediterranean. As a preliminary it was decided to assemble a body of experts for a "Workshop on Mediterranean Weather". This was held between 15 June and 24 June 1970 at the Navy Weather Research Facility in Norfolk, Virginia. Among those participating were:

Maj. Gen. Prof. G. FEA	Supervisor of Italian Meteorological Service, Air Force Staff.
Prof. N.H. FLOHN	Director, Institute of Meteorology, Bonn University.
Dr. Z.O. GÖKART	General Director, Turkish State Meteorological Service.
Dr. E.C. KINDLE	Director of Research, WEARSCHFAC.
Dr. D. METAXAS	Chief, National Analysis Centre, Hellenic National Meteorological Service, Greece.
Lt. Col. A. NANIA	Meteorological Service, Italian Air Force.
Cdr. N. ÖNÜR	Turkish Navy.
Mr. A. ORIEUX	Chief of the Meteorological Center, Marignane, France.
Mr. D.E. PEDGLEY	Anti-Locust Research Centre, London.
Dr. E.R. REITER	Professor and Head, Department of Atmospheric Science, Colorado State University.

Dr. R.J. RENARD	Professor of Meteorology, Naval Postgraduate School, Monterey, California.
Inst. Cdr. D. ROE, R.N.	Chief Meteorological Officer, NAVSOUTH, Malta G.C.
Mr. I.I. SCHELL	Senior Scientist, Ocean-Atmosphere Research Institute, Cambridge, Mass.
CAPT. W.L. SOMERVELL, JR., USN	Commanding Officer, WEARSCHFAC
Mr. H. B. WOBUS	Senior Scientist, WEARSCHFAC.

The results of this Workshop, expressed in formal papers as well as informal discussions, are presented here in a condensed form; the individual papers are to be published shortly.

Wherever possible, the authors who contributed to the various statements contained in this Digest are identified individually in the text. Apologies are extended to those participants who find themselves misquoted or whose names have been omitted from the appropriate places.

In this Digest, emphasis has been placed on field applications. It is hoped, therefore, that forecasters both aboard ship and ashore may find it of value.

1.2 Wind Systems

The Mediterranean is a virtually enclosed inland sea with a complex and mountainous coastline that splits the region into a western and eastern basin and provides several semi-enclosed water bodies. The rugged mountains and wide gaps between them serve as barriers and guides, channeling and controlling the movements of air masses. These features

are shown in the general locator map (fig. 1.1). This map also includes place names which will be referred to throughout this paper. Resulting from this complex orography there are a large number of "local" winds; these are illustrated in figure 1.2. In addition, the desert climate of North Africa, the maritime climate of western Europe, and the continental climate of eastern Europe, give rise to an interesting but complicated variability in weather conditions.

1.3 Pressure Regime

It would exceed the scope of this report to attempt to give the complete climatology of the Mediterranean and its surroundings. Useful background information may be found in the Air Ministry publication [1] and Sailing Directions for the Mediterranean (Port information) [35]. It should suffice therefore, to point out that the regional climatology is strongly shaped by the complex land-sea distribution and by the differential heating resulting therefrom. The global tropospheric flow patterns are strongly modified by these local thermal effects and by the orographic obstacles surrounding the Mediterranean basin. The interplay between the global circulation patterns and these local effects leads to the wind systems given in figure 1.2, to preferred regions of cyclogenesis, such as in the Gulf of Genoa, and to preferred cyclone tracks. The juxtaposition of dry and moist air masses also causes one of the world's problem areas of radio- and radar-wave propagation [2].

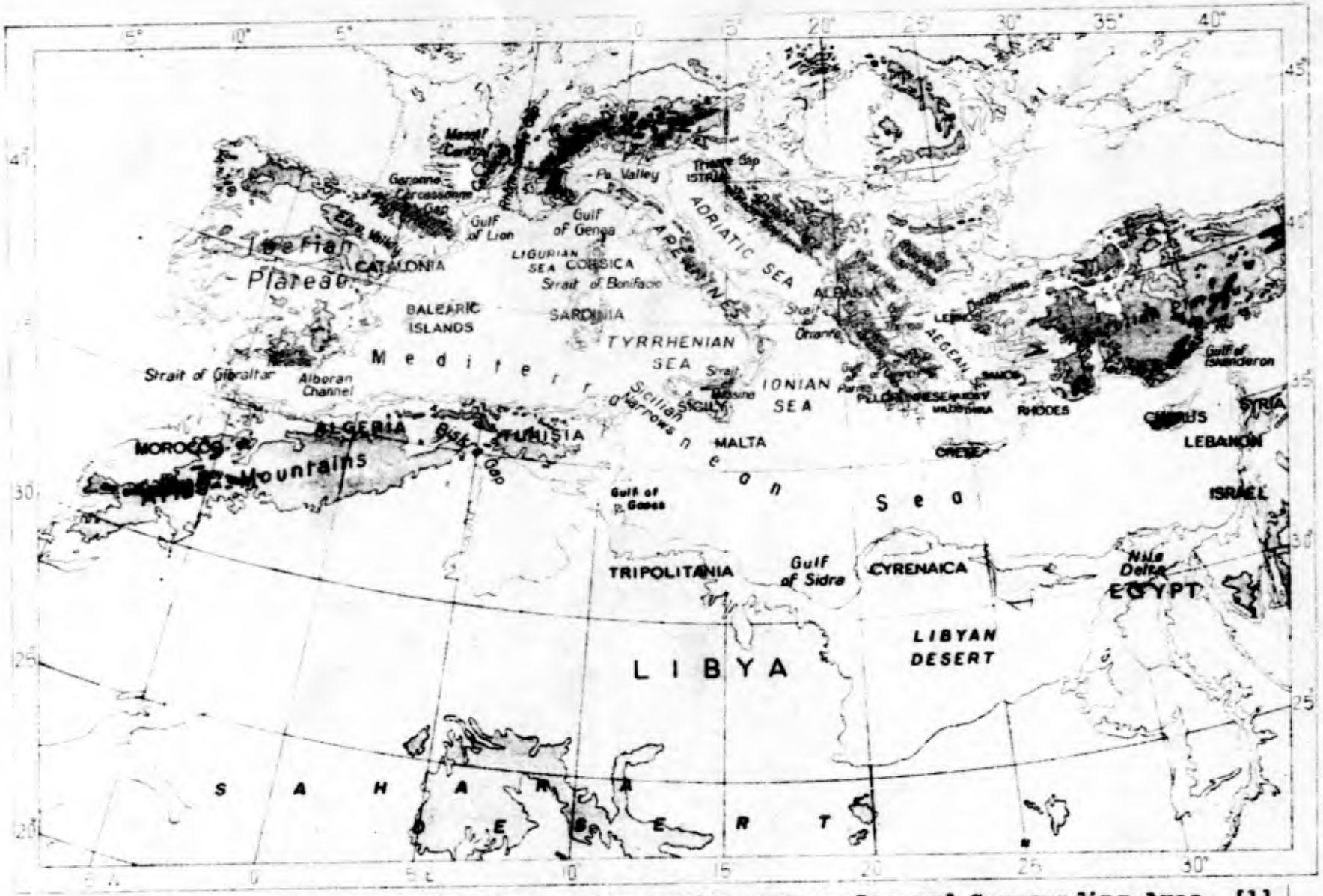

Figure 1.1 General Locator Map of the Mediterranean Sea and Surrounding Area. [1]

Figure 1.2 Regional Wind Systems of the Mediterranean. [1]

The complicated orographic conditions and their thermal effects are reflected in the diurnal pressure variations which by no means conform to a simple tidal wave. Appendix A gives detailed analyses of 3-hourly mean pressure changes for each season. These maps should be consulted by the weather forecaster who is faced with the problem of monitoring the deepening or filling of cyclonic disturbances. As an example, Nania presented the cyclogenetic activity in the lee of the Alps between 16 and 19 February 1958, measured by the mean radial pressure differences in the disturbance (fig. 1.3). The 24-hour periodicity in these pressure differences is in excellent agreement with the pressure tendencies shown in appendix A. Such short-term variations in radial pressure gradients will have an effect on the surface wind regimes.

Even without the presence of a cyclone, the diurnal variations of pressure shown in appendix A, when superimposed on the normal synoptic pressure gradients, should provide valuable clues to the development of local land- and sea-breeze systems, and to the diurnal variations of other wind systems, such as the mistral.

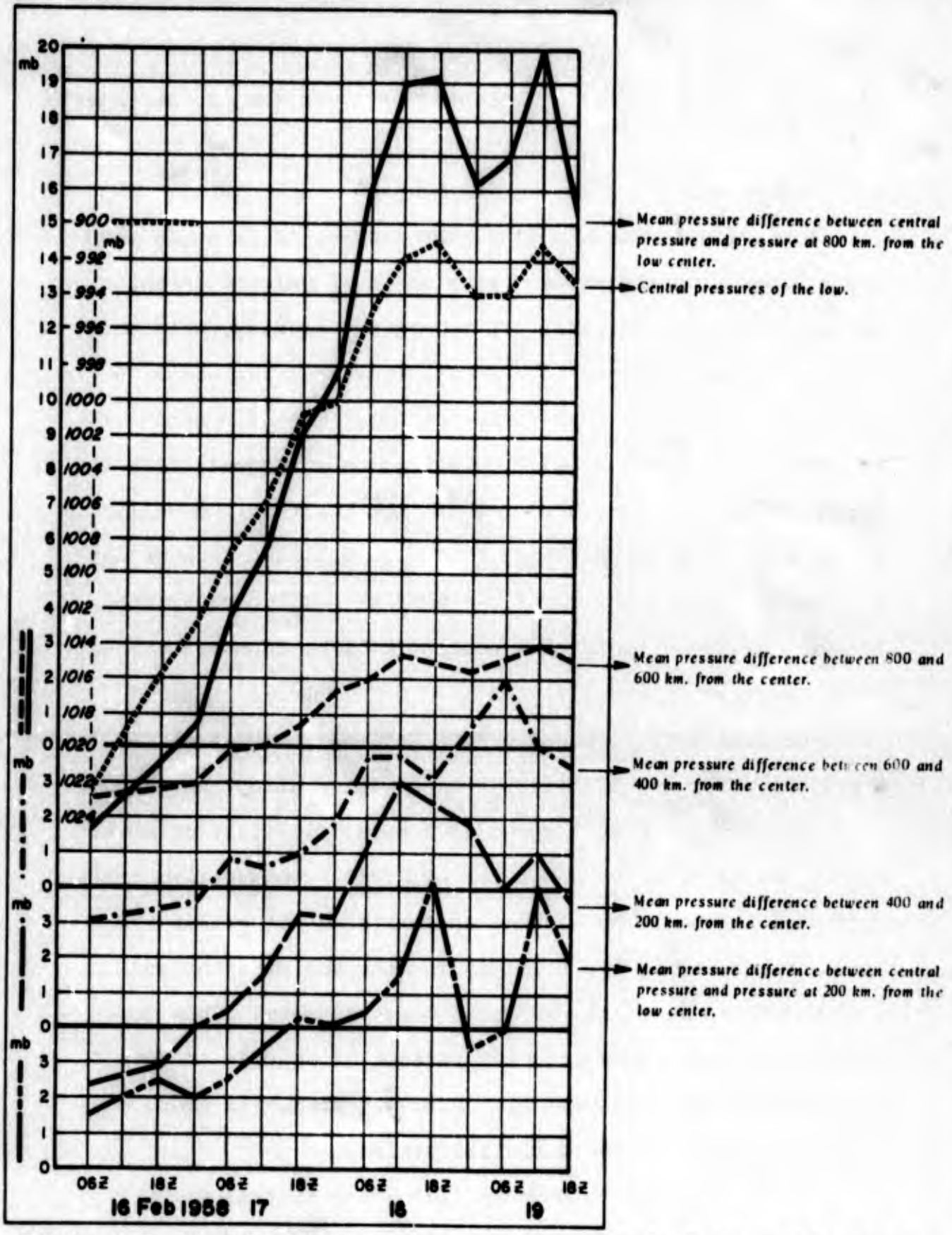

Figure 1.3 Quantitative Estimate of Cyclogenesis Between 16 and 19 February 1958 in the Lee of the Alps. [4]

2. THE MISTRAL

(Based mainly on material presented by A. Orieux, J. Bocchieri, R. Brody and E. R. Reiter.)

2.1 Definition

According to Huschke [13], the mistral is "a north wind which blows down the Rhône valley south of Valence, France and into the Gulf of Lion. It is strong, squally, cold and dry; it is the combined result of the basic circulation, a fall wind, and jet-effect wind. It blows from the north or northwest in the Rhône Delta, where it is strongest; from the northwest in Provence; and from the northeast in the valley of the Durance below Sisteron." Figure 2.1 is a locator map for use in the discussion of the mistral. All geographical features referred to in this section will be found in either this figure or figure 1.1.

For practical purposes Orieux defines the mistral (at Marignane, sta. no. 07650) as a wind with a direction between 280° and 360° and with a speed of 5 m./s. (10 kts.) or more. Both criteria have to be met for at least 6 consecutive hours. A mistral period is considered as terminated if either the speed criterion, or the direction criterion, or both, are violated for a time interval of 6 hours or more. This definition not only eliminates the passage of squalls or fronts from being counted as mistrals, but also prohibits short lulls from interrupting a mistral period.

Again according to Huschke [13], "the mistral has a variety of local names; mangofango in Provence; sécaire,

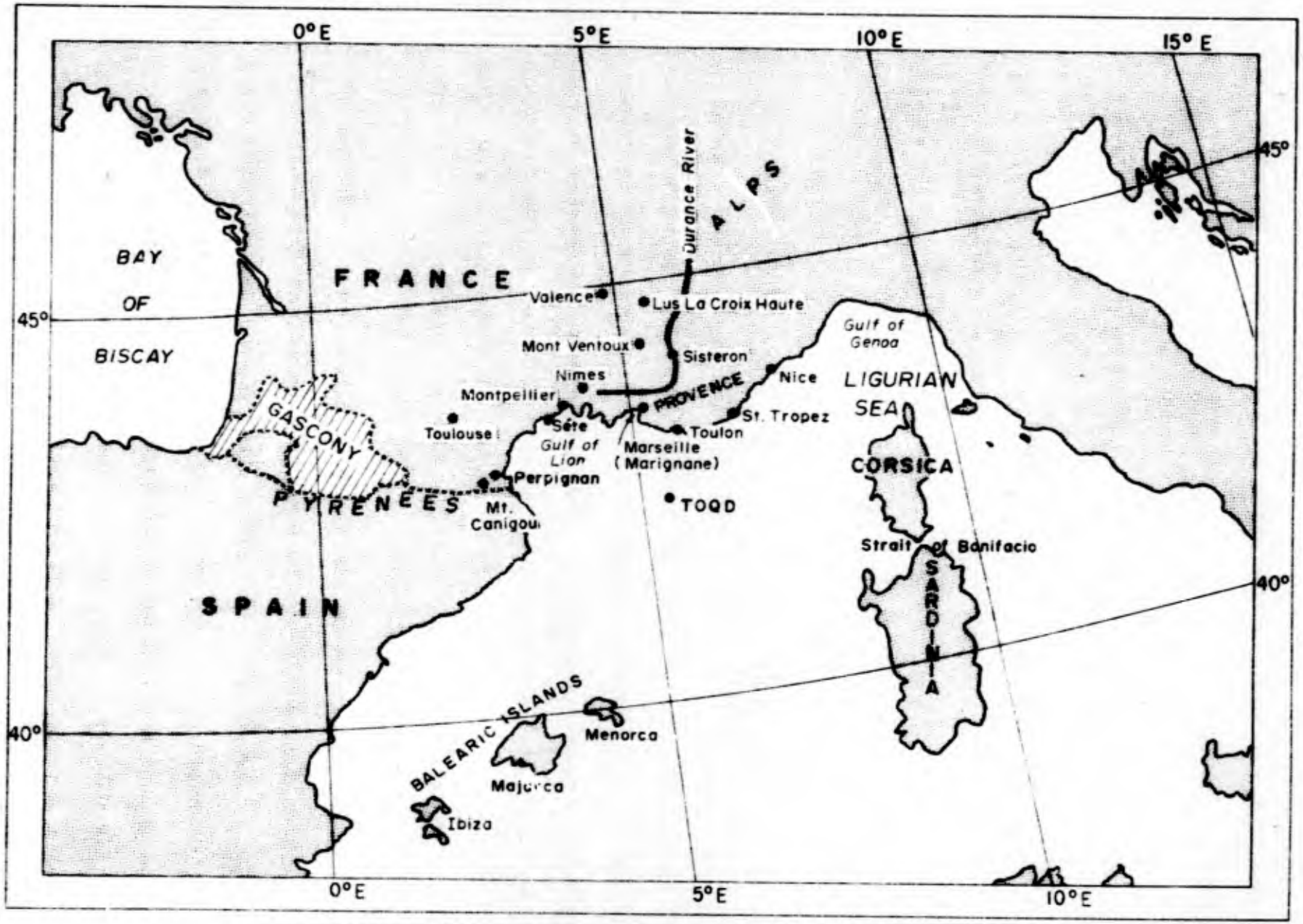

Figure 2.1 Locator Map for the Mistral.

maistrau, maistre or magistral in the Cevennes; dramundan in Perpignan (sta. no. 07747); cierzo in Spain; cers in the Pyrenees, etc. South of Mont Ventoux (sta. no. 07585) a similar wind is named bise. A local west wind of mistral type which descends from Mt. Canigou to the plains of Roussillon is called "canigonenc."

Phenomena often associated with the mistral are:

(1) Cyclogenesis in the Gulf of Genoa.

(2) A strong wind in the Straits of Bonifacio.

(3) A blocking situation.

2.2 General Description

A general mistral is characterized by off-shore winds along part, or all, of the coast of the Gulf of Lion. Wind speeds often exceed 60 knots and reach 85 knots in the lower Rhône valley. Even higher velocities are encountered at sea where the braking effect of surface friction in the planetary boundary layer is greatly reduced. At times gale force winds may extend across the Mediterranean all the way to Malta and the Algerian coast.

Strong off-shore winds, whose direction is modified by surface friction, require a pressure gradient from west to east. Strong winds along the coast of the Gulf of Lion will be enhanced by a component of the pressure gradient directed toward the Mediterranean and parallel to one or all of the major valleys of the Garonne, the Rhône, and the Durance. Maximum winds occur when the surface isobars are at an angle of 30° to these valleys. (Orieux)

Such pressure gradients are due to synoptic disturbances which cause depressions to form over northern Italy, the Ligurian Sea (Gulf of Genoa), or the central Mediterranean in general. Anticyclones over Spain, northern France and/or central Europe may complement the required surface pressure gradient. Changes in the gradient may bring about lulls and surges in the mistral.

The sheltering effects of the Pyrenees and the Alps may lead to the formation of sharp shear lines between high and low wind-speed regimes. These shear lines may extend far out over the sea. On occasion, but by no means always, cloud formations have been observed along these shear lines (USS FORRESTAL). In general, however, the mistral is a katabatic wind, associated with the low-level divergent flow of cold air. Mass continuity requires a sinking motion and hence cloud-free conditions would be expected.

The divergent mistral wind regime is usually a low-level phenomenon reaching to a height of about 2 to 3 km. (Orieux; Huschke [13]) It is, however, intimately associated with the jet-stream regime in the upper troposphere and with the baroclinic waves embedded in the upper flow.

2.3 Occurrence

2.3.1 Types of Mistral

Orieux distinguishes between four different type of mistral.

Type I: (Fig. 2.2(a)) A northwesterly flow in the lower troposphere extends between a surface ridge of high pressure

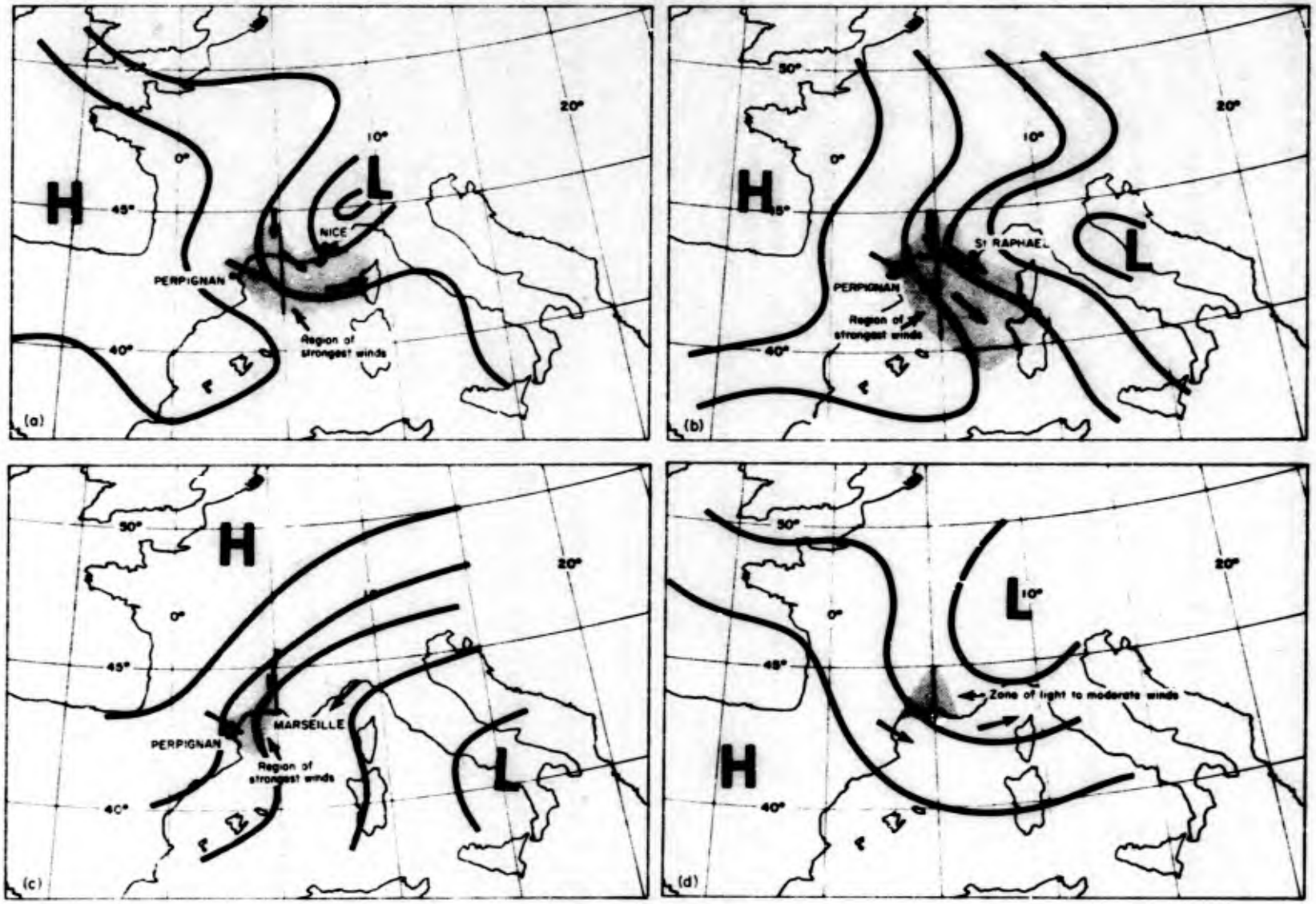

Figure 2.2 Typical Surface Isobar Patterns During 4 Types of Mistrals: (a) Type I, (b) Type II, (c) Type III and (d) Type IV. (Orieux)

covering the Bay of Biscay, the Ebro valley (Spain) and Gascony (France), and a depression located over the Po valley (northern Italy). The latter is typical of summer conditions where a heat low is frequently present to the south of the Alps. According to Orieux, this heat low leads to a preference for the Type I mistral to occur in summer.

Gale force winds of the Type I mistral usually do not persist for longer than 24 hours. (Orieux) This type of mistral is strongly subject to disturbances (short baroclinic waves) traveling in the northwesterly jet stream. Pressure-fall centers moving into the Mediterranean will cause a resurgence of the mistral, whereas the arrival of a pressure-rise region will lead to a temporary or permanent cessation, at least of the gale force off-shore winds.

According to figure 2.2(a), the Type I mistral may affect the whole Riviera coast to Nice (sta. no. 07690) and beyond. Veering of the wind associated with the approach of an anti-cyclone over central France may bring about a westward retreat of the shear line that marks the easternmost extent of the mistral. A Type II mistral situation may ensue with such a veering of the wind. (Orieux)

Type II: (Fig. 2.2(b)) A northerly jet stream flows over the gap between the Pyrenees and the Alps, with a high pressure region extending over the British Isles and a low pressure area covering central and eastern Europe. Strong winds may extend to Corsica and Sardinia, and even to Sicily and North Africa. The surface wind regime is enhanced by

Genoa cyclogenesis. Local channeling may lead to strong westerly winds in the Straits of Bonifacio.

According to Rex [27, 28] blocking anticyclones have a preferred tendency to occur at the longitude of the British Isles and during the early months of the year (figs. 2.3 and 2.4). Since these highs may persist for many days, they may give rise to prolonged mistral episodes, especially if the northerly-to-northwesterly jet stream assumes a favorable position with respect to the orographic gap between the Pyrenees and Alps. Wave disturbances and cold outbreaks imbedded in the northerly flow over France may lead to individual surges within an extended mistral period.

According to Orieux, the Type II mistral accounts for approximately 75% of the observed mistral cases. This type also favors the development of the most severe mistral incidences. In line with the frictional effects mentioned in section 2.2, wind speeds reach a maximum when the surface isobars are oriented at an angle of 30° with respect to the Rhône valley. (Orieux)

The sheltering effect of the Alps usually prevents the Type II mistral from penetrating into the Ligurian Sea (fig. 2.2(b)).

Type III: (Fig. 2.2(c)) A high-pressure ridge extends from the Atlantic into France and central Europe. Low pressure prevails over the central Mediterranean. This situation often develops out of the Type II mistral if the blocking high over northern Europe proceeds eastward. In such a case

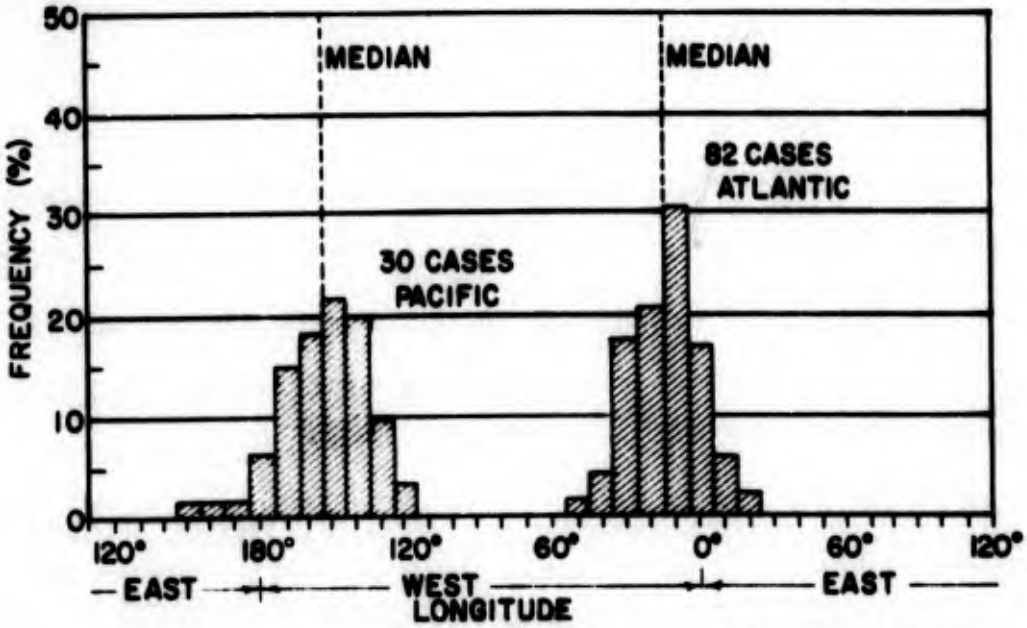

Figure 2.3 Percent Frequency Distribution of the Appearance of Blocking Anticyclones at the 500-Mb. Level Over the Atlantic and Pacific at Various Longitudes (112 cases between 1933 and 1940, 1945 and 1949). [28]

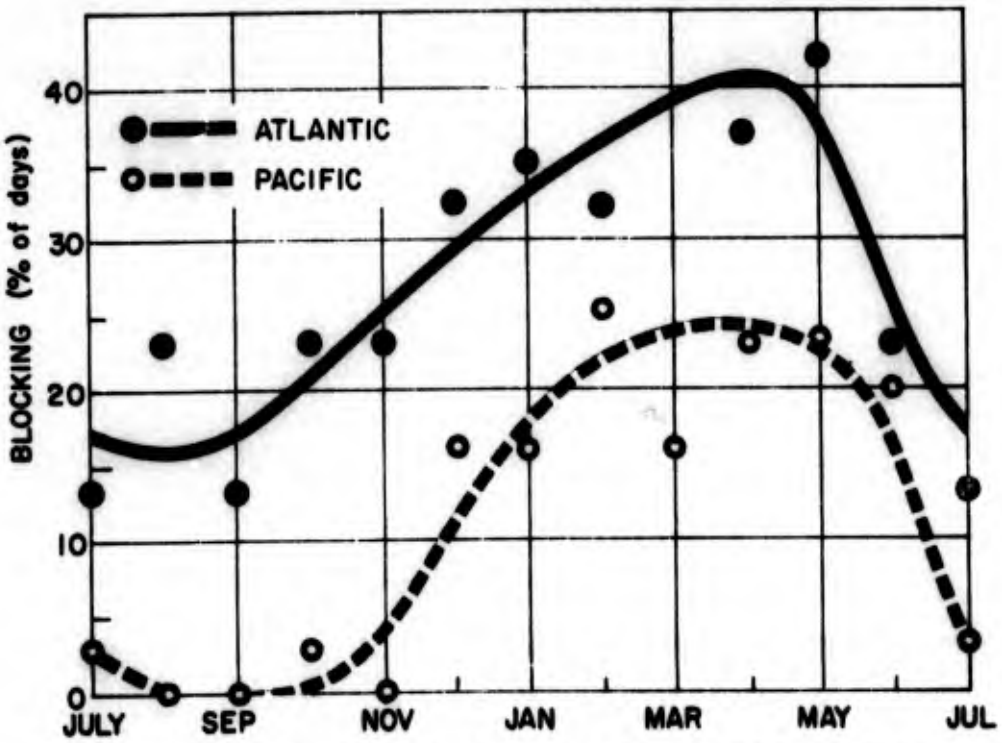

Figure 2.4 Mean Number of Days (Monthly) (%) on Which Blocking Anticyclones Are Observed. [28]

the Type III mistral usually heralds the cessation of the mistral episode within a short time. The Type III mistral is usually short-lived, persisting for one or two days. (Orieux) Strong winds are confined to the region between Marseilles (sta. no. 07650) and Perpignan (sta. no. 07747). Winds at Perpignan are from the west to northwest and almost parallel to the direction of the surface pressure gradient.

Type IV: (Fig. 2.2(d)) As for Type I, high pressure prevails over Spain but the depression to the east is at a higher latitude, being located over the Alps. The orientation of the isobars is not conducive to the development of strong mistral winds, but light to moderate katabatic mistral winds still may occur locally in the Rhône valley. Frontal passages with this type of mistral are always associated with cloud systems and showers. However, if the pressure gradient is sufficiently tight, strong winds may occur in the Perpignan area and along the coast of Provence. (Orieux)

2.3.2 Preferred Wind Direction

The mistral winds were defined in section 2.1 as having a direction between 280° and 360°. Figure 2.5 gives the wind rose for the French buoy TOQD stationed in the Gulf of Lion at 42°13' N. and 05°34' E. from 1 June 1968 to 31 March 1970. According to this diagram, mistral winds are encountered most frequently from the NW (320° to 340°). This direction also has the highest incidence of strong winds >50 knots. (Brody) The wind statistics for TOQD conform rather closely to those computed by Orieux for Marignane (sta. no.

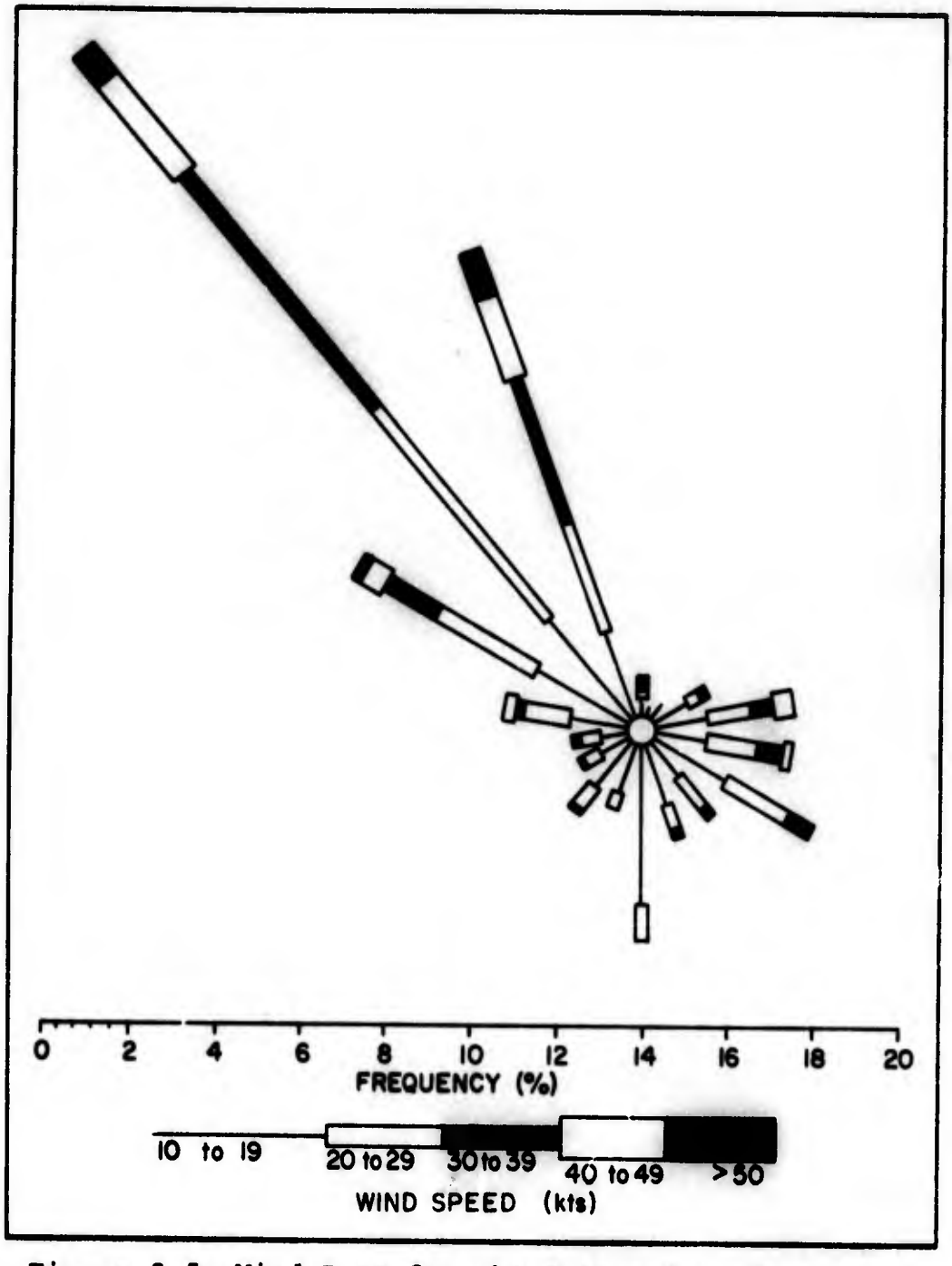

Figure 2.5 Wind Rose for the French Buoy TOQD at 42°13' N. and 05°34' E. From 1 June 1968 to 31 March 1970. (Brody)

07650), with the exception that wind speeds tend to be considerably higher over the open ocean than at coastal stations.

2.3.3 Extent of the Mistral Region

Bocchieri has analysed the wind conditions in the Gulf of Lion for the 1975 occasions during the period 1964-1968 in which at least one of the stations Marseille (sta. no. 7650), Montpellier (sta. no. 07643), Séte (sta. no. 07641) or Perpignan (sta. no. 07747) reported winds of 21 knots or more. Figure 2.6 shows the number of mistrals ascertained from ship reports (available for the analysis) in 1° lat. x 1° long. "squares." It has to be realized that ship traffic tends to avoid the Gulf of Lion during mistral periods. Hence the analysis has a certain "low-wind" bias, favoring conditions during the onset rather than the peak of the mistral.

In spite of these shortcomings, several interesting conclusions may be reached. Figures 2.7 and 2.8, giving the mean wind speeds during mistral conditions (defined by coastal stations) and the frequency of gale force winds (>33 kts.), show that the most severe conditions are encountered off the French coast west of Montpellier. The sheltering effects of the Pyrenees and of the mountains in Provence are clearly evident. Horizontal wind shears produced by this sheltering effect may be very strong indeed.

FORRESTAL reported during her 1965-1966 deployment:

"A definite shear line was found to exist during all mistrals. It was oriented from the northeast tip of Spain, southeast to Menorca. FORRESTAL passed through

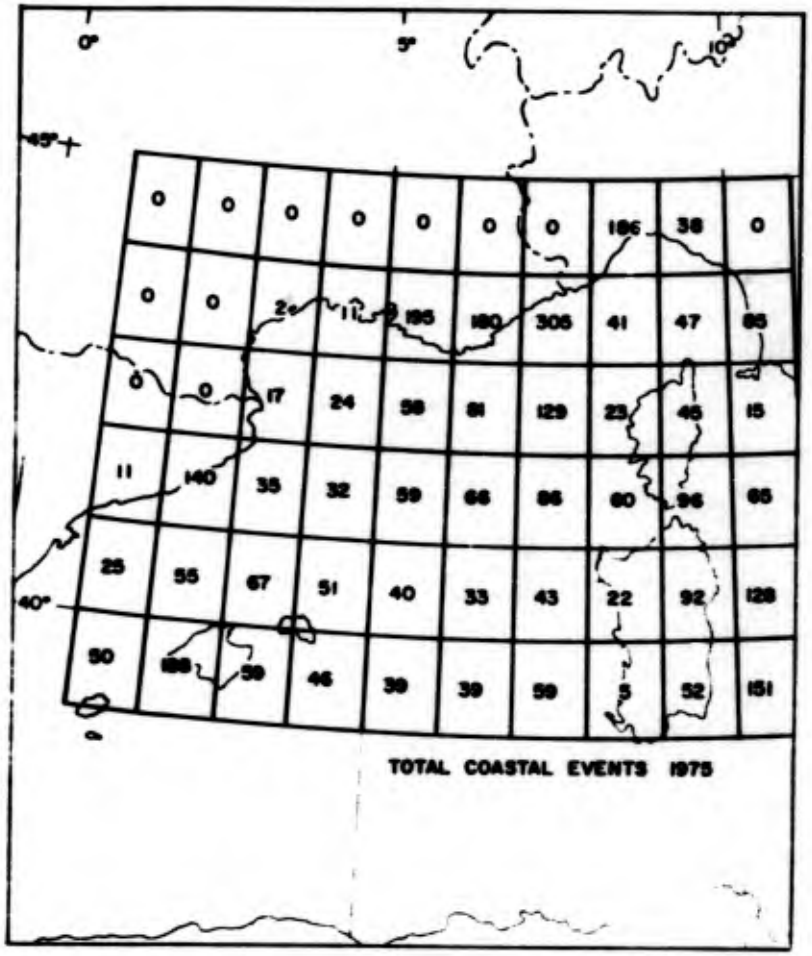

Figure 2.6 Number of Occurrences of Ship Observations in 1° x 1° Squares When Mistral Is Observed at Least on One Coastal Station. (Bocchieri)

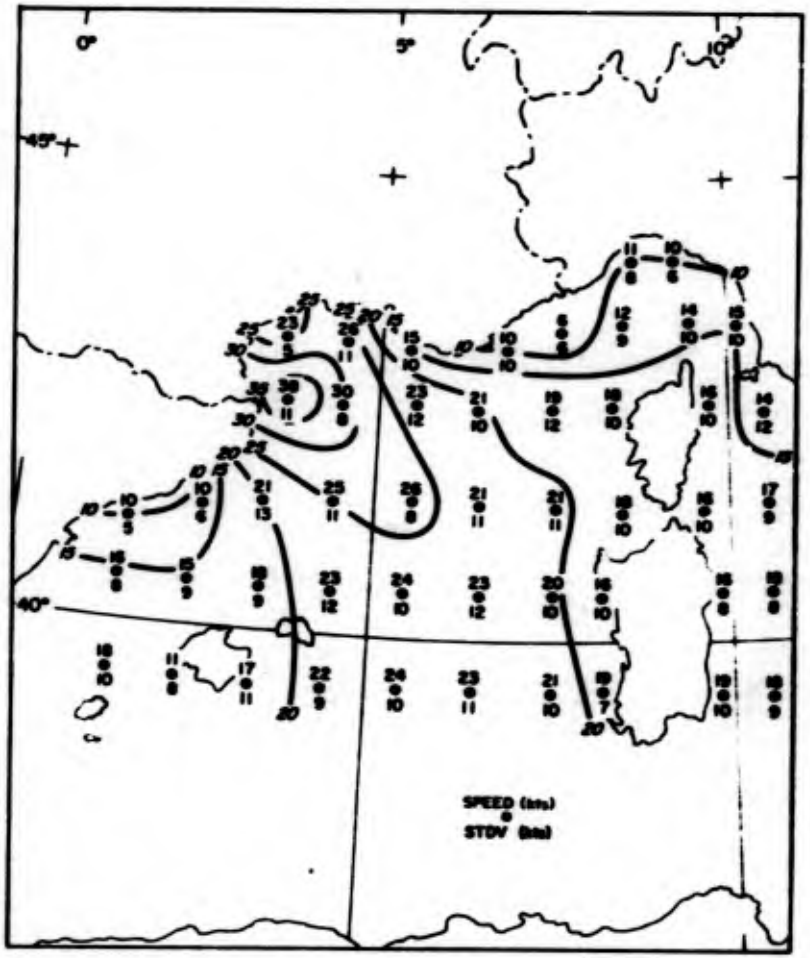

Figure 2.7 Mean Wind During Mistral as Defined in Figure 2.6. (Bocchieri)

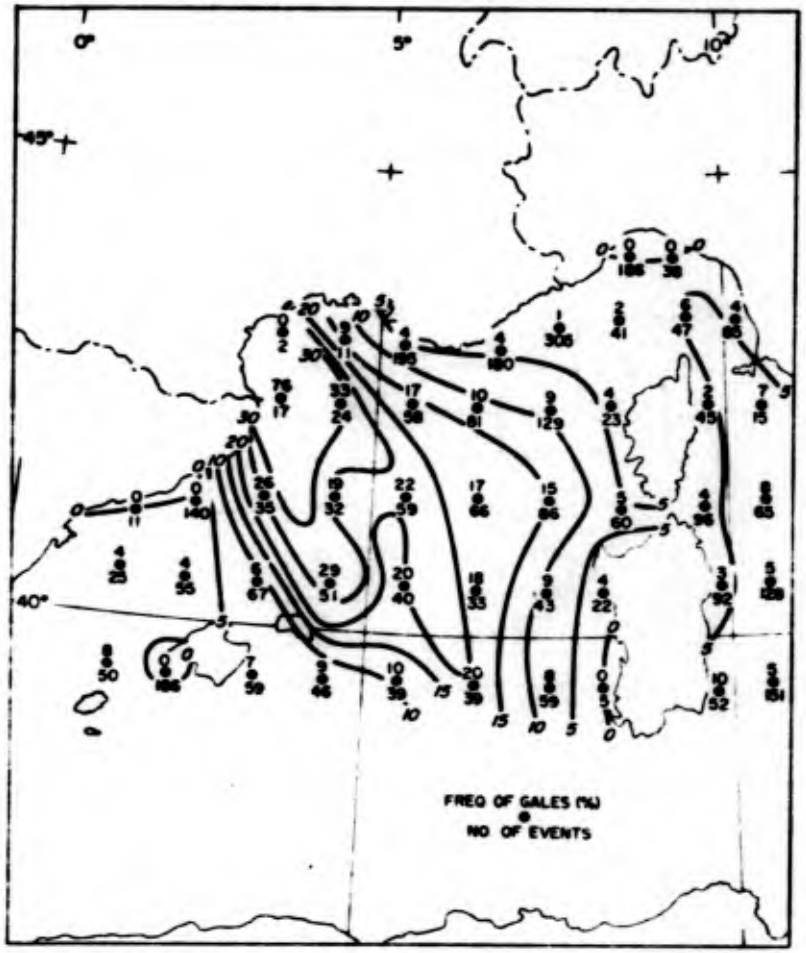

Figure 2.8 Relative Frequency Distribution of Gale Force Winds (>33 kts.) for Mistral Situations as Defined in Figure 2.6. (Bocchieri)

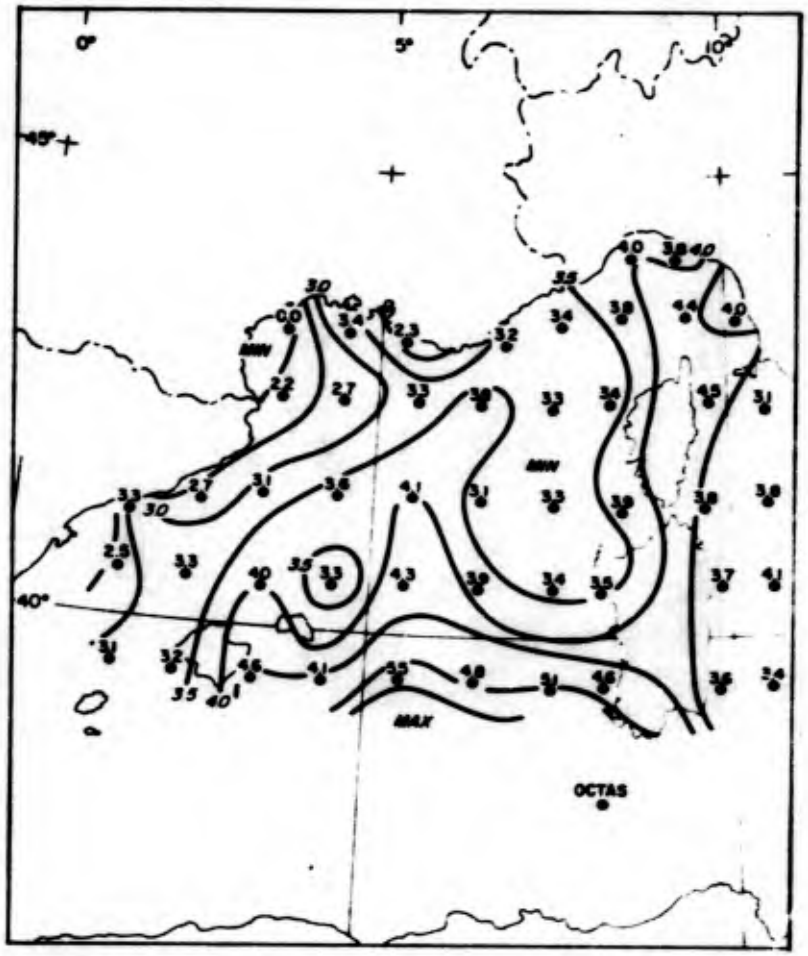

Figure 2.9 Amount of Low Clouds in 1° x 1° Squares When Mistral Is Observed at Least at One Coastal Station. (Bocchieri)

the shear line in the vicinity of 41° N., 03° E. during the first mistral encountered. Winds to the west of the shear line were northerly 8 to 16 knots and the seas were 3 to 5 feet. In the shear line, winds and seas increased markedly; to the east of the shear line winds were 35 to 45 knots and the seas were 14 to 20 feet. The width of the line varied. Based on many aircraft observations taken during the four different mistrals, the shear line at times was as narrow as 2 to 3 miles, or as wide as 20 miles. On some occasions it was marked by clouds; on others it was perfectly clear and could only be observed by the different effects of the wind on the surface of the sea. In several instances the surface effects were markedly distinctive and pilots were able to reports its location with ease, even from high altitudes. When the line was marked by clouds, the shear usually seemed to be very sharp. Carrier flight operations were easily conducted on the west or calm side, although the amount of cloud cover near the line caused some concern. Attempts to find clearer skies by penetration of the line to the east resulted in an immediate clearing, and an extremely rapid increase of winds and seas, often to the extent that flight operations were no longer safely feasible. Under these circumstances, flight operations in pleasant conditions were possible just 20 or 30 miles west of the line. Since the line

was observed by aircraft to move from east to west, especially at the southern end, operations should be conducted at some distance from it. This movement may displace the line from Menorca as far as Majorca and back again several times during a 24-hour period."

Note: The four mistrals encountered by FORRESTAL were probably Type II. It is likely that the shear line would not be so pronounced with the weaker types.

Even though the mistral is a katabatic wind, characterized by the sinking and spreading of cold air (evident from the minima in cloudiness shown in fig. 2.9), FORRESTAL's report quoted above indicates the possibility of low-level convergence and rising motions at the edges of the mistral region.

2.3.4 Seasonal Variation

Figure 2.10 shows the mean monthly frequency distribution of mistral episodes for Marignane (sta. no. 07650), as defined by Orieux (see section 2.1). Two seasonal peaks are evident for the lowest wind-speed threshold (≥5 m./sec. (10 kts.)), one in April and one in July. Orieux ascribes the summer maximum to the relatively frequent occurrence of the Type I mistral (see section 2.3.1). With higher wind speed thresholds, the winter and spring mistral cases become more prominent, with a prevalence of Types II and III.

2.3.5 Diurnal Variation

Based on measurements made at Marignane (Orieux) and at the buoy TOQD (Brody and Reiter), the diurnal variation of

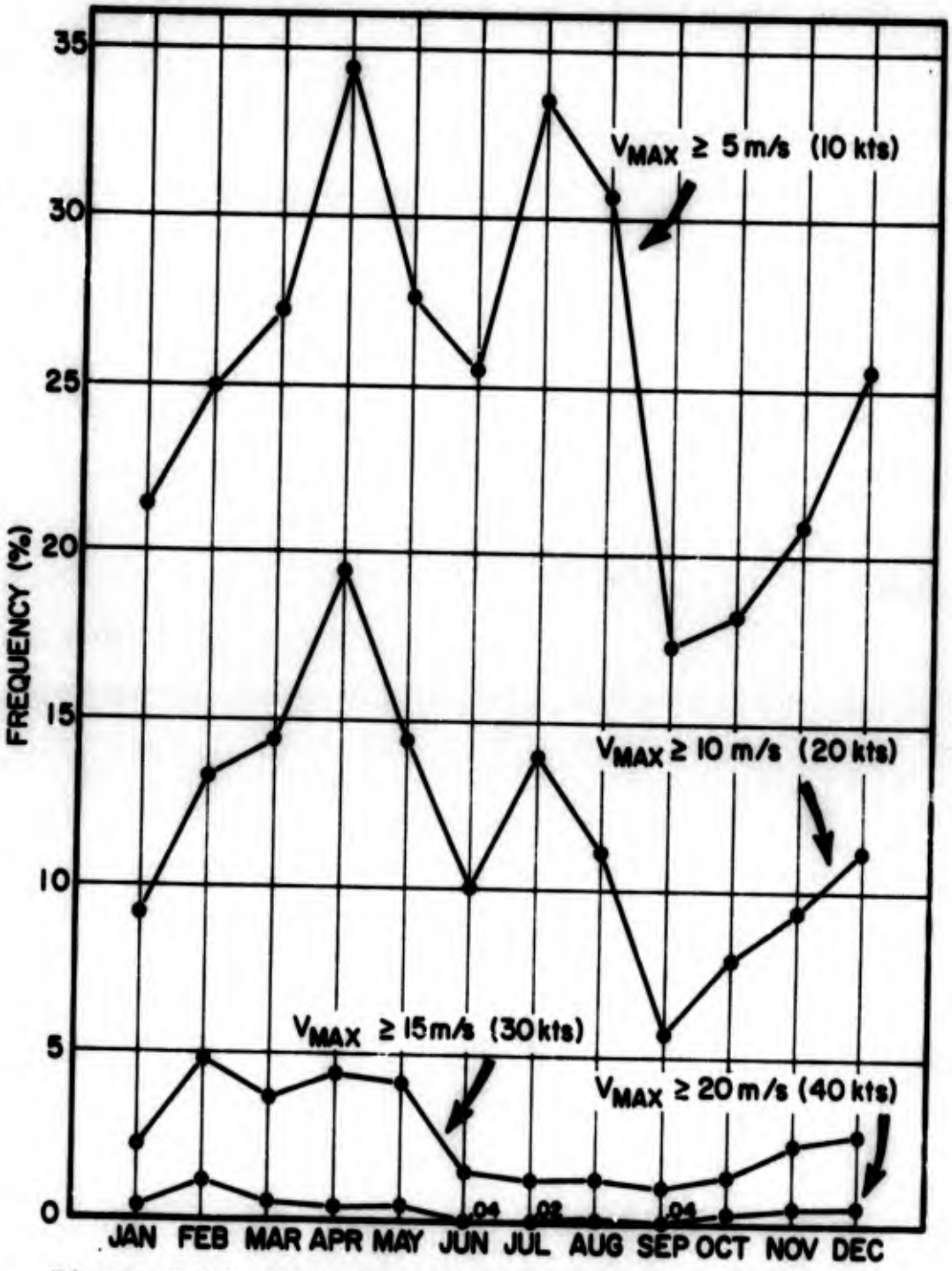

Figure 2.10 Mean Monthly Frequency of Mistrals at Marignane (1957-1966) for Different Threshold Values of Wind Speed. (Orieux)

mistral winds at a coastal station differs from that at a point some 60 miles offshore.

Considering the coastal station, figure 2.11 shows two maxima for the times at which the strongest mistral winds occur. Although a secondary maximum might be expected at midnight ([32], p. 229), it would appear that the method chosen to analyze the data gives an exaggerated maximum. Figure 2.11 was obtained by taking the time at which the maximum mistral wind speed occurred during any given day. If mistral winds increase or decrease from one day to the next, the strongest winds will be recorded at the end or the beginning of the day, that is, at midnight in each case. (Reiter) Discounting this bias in the data, the strongest winds along the coast occur during the afternoon. However, from figure 2.12, it can be seen that at the buoy TOQD the strongest mistral winds occur during the night, a different analysis technique being used to avoid a false midnight maximum. The technique adopted was to consider a particular hour and a selected wind speed (5, 10, 20 or 30 kts.), and then to calculate the mean wind-speed for speeds greater than or equal to the selected value. For example, from figure 2.12, at 1200 GMT the mean wind speed was 32 knots for all mistral wind speeds of 20 knots or more.

The diurnal variation of the boundary layer stability, of course, explains the surface daytime maximum (and gradient-level nighttime maximum) over land. However, the diurnal stability variation over the sea is much smaller; and it is

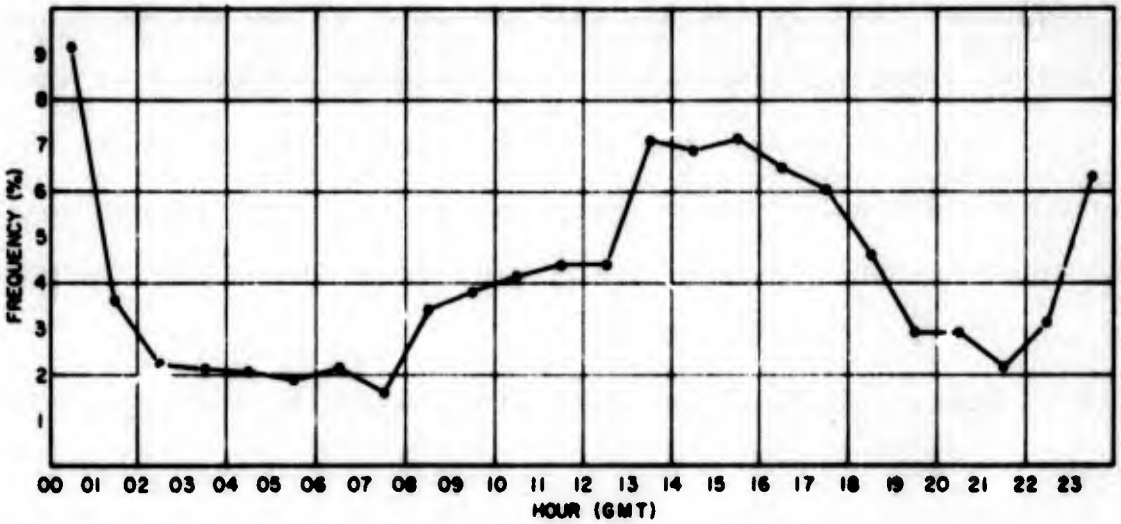

Figure 2.11 Hourly Distribution (%) of the Occurrence of Maximum Wind Speeds in Mistral Situations (>20 kts.) at Marignane (1957-1966). (Orieux)

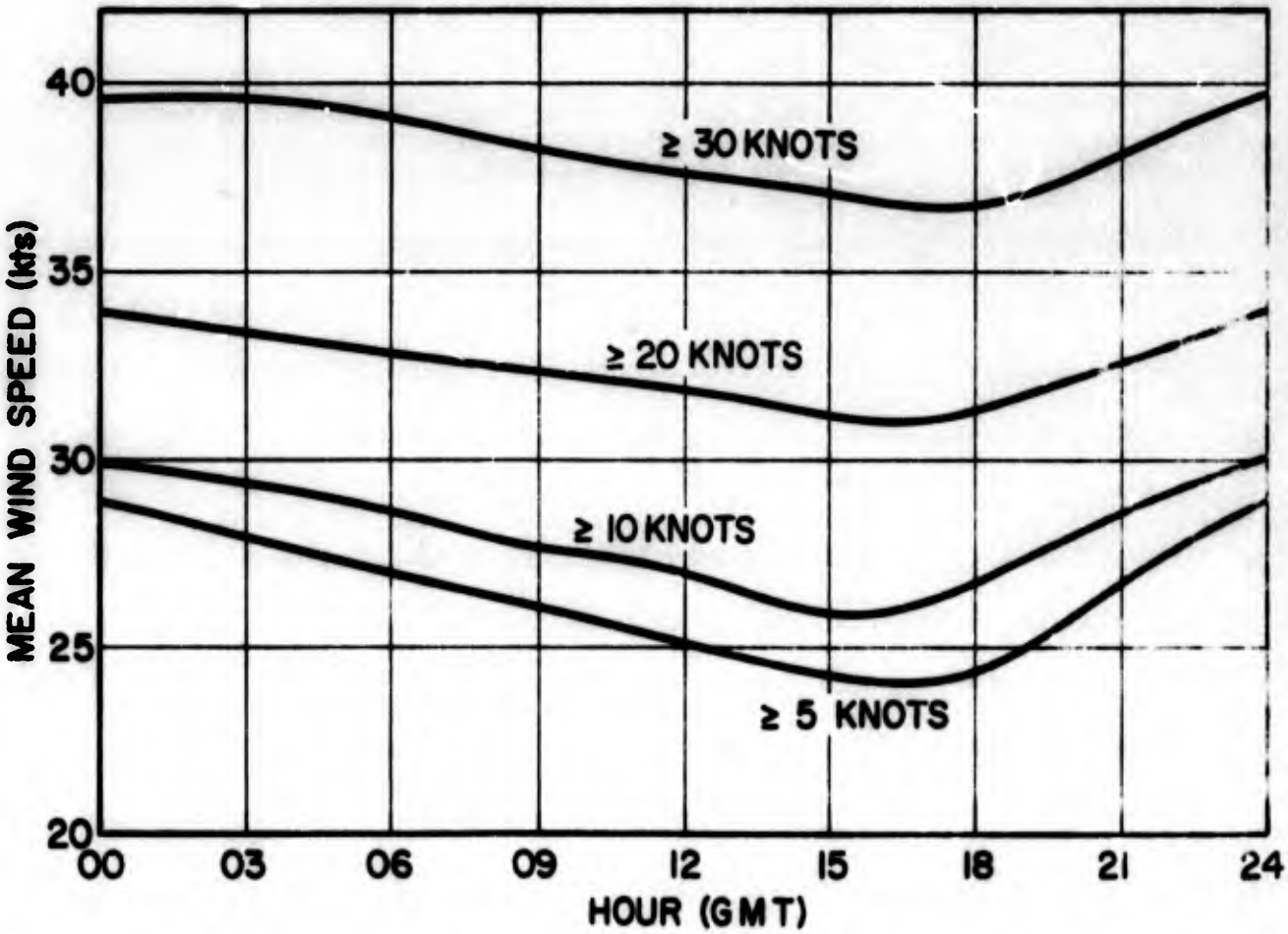

Figure 2.12 Diurnal Variation of Mean Mistral Winds Beyond Indicated Speed Thresholds at TOQD. (Brody)

suggested that by inertia the momentum of the stronger nocturnal gradient-level winds over land is reflected at the gradient levels over the sea. This would result in an increased downward fl. of momentum at night and higher nocturnal surface winds over adjacent ocean areas such as TOQD (see figs. 2.11 and 2.12).

Other effects, e.g. diurnal pressure-variation and land-sea breezes, also may play a minor part in determining the time of maximum wind-speed. It should also be noted that the effect detectable at TOQD may not be detectable farther out to sea.

2.3.6 Onset and Cessation of the Mistral

The mistral at Marignane (sta. no. 07650) has a tendency to start in the morning -- somewhat earlier during the summer months than during the rest of the year (fig. 2.13). It is most likely to cease in the late evening or early morning (fig. 2.14). A secondary frequency maximum of cessation between 1400 and 1500 GMT is especially well-marked during the summer.

The data available from TOQD are not sufficient to allow a reliable statement to be made concerning the preferred time for commencement and cessation of mistral winds. Those data which are available suggest night or early morning as a preferred starting time, and early forenoon or near noon for cessation. (Reiter and Brody)

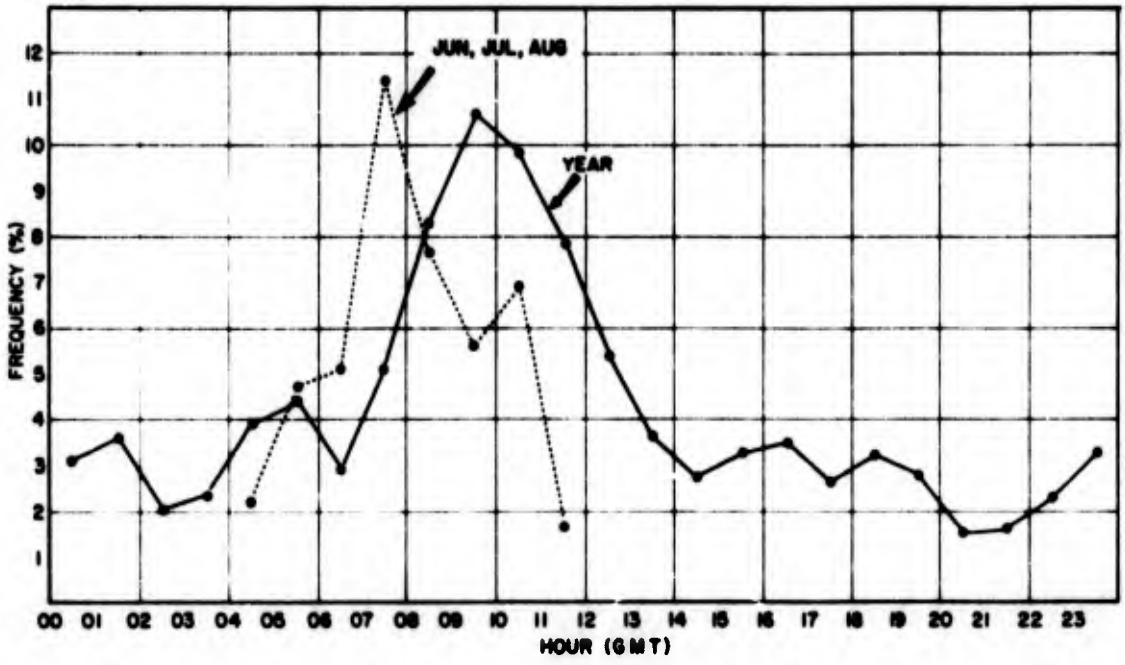

Figure 2.13 Frequency Distribution (%) of the Hours During Which Mistral Starts at Marignane (1957-1966). (Orieux)

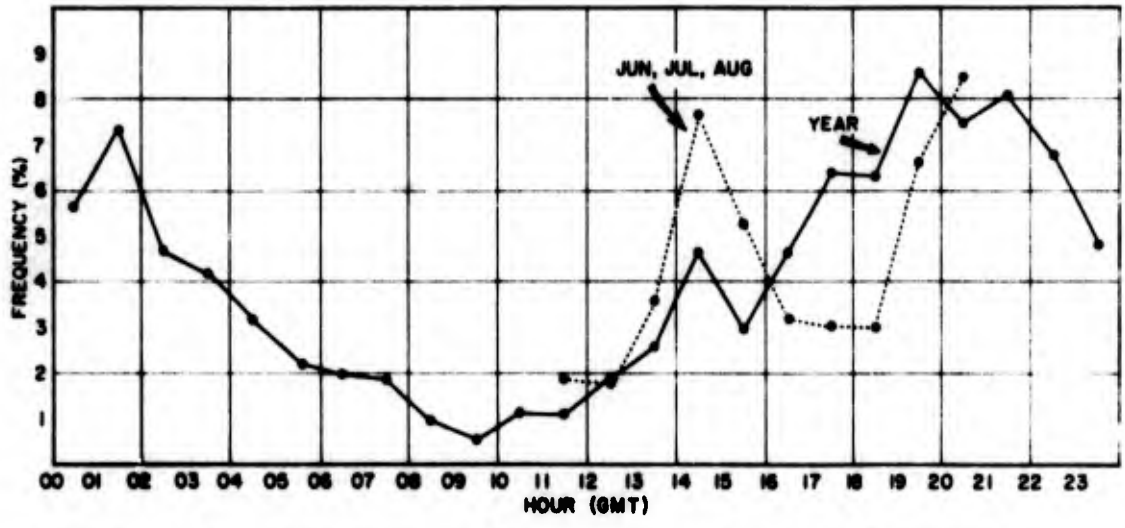

Figure 2.14 Frequency Distribution (%) of the Hours During Which Mistral Ends at Marignane (1957-1966). (Orieux)

2.3.7 Duration of the Mistral

From 10 years of data taken at Marignane (sta. no. 07650), Orieux investigated the persistence of the mistral. From the 172 cases where the mistral lasted two days or more, figure 2.15 shows that for every day increase in the persistence, the percentage of mistral episodes having that duration is approximately halved. The broken line shows an accurate "halving" process.

In the 10 years of observations there were 5 cases in which the mistral lasted between 7 and 8 days. Over a longer period of time one should expect mistral episodes lasting more than 8 days but, as can be seen from figure 2.15, the probability of any particular mistral having a duration in excess of 8 days is very small.

2.3.8 Maximum Velocities of the Mistral

Figures 2.16 and 2.17 show the cumulative number of cases of maximum wind-speed observed during mistral periods at Marignane (sta. no. 07650) and Toulon (sta. no. 07660), respectively. (Orieux) The two stations show good agreement considering that the observational sample from Toulon was obtained over twice the period as that from Marignane. According to these data, winds with 55 m./sec. (107 kts.) may be expected about once every 20 years at these coastal stations. A certain increase of wind speeds over the open water is to be expected, although the "rule-of-thumb", by which one doubles the speed observed at Perpignan or Marignane (Marseille) in order to arrive at speeds offshore near the

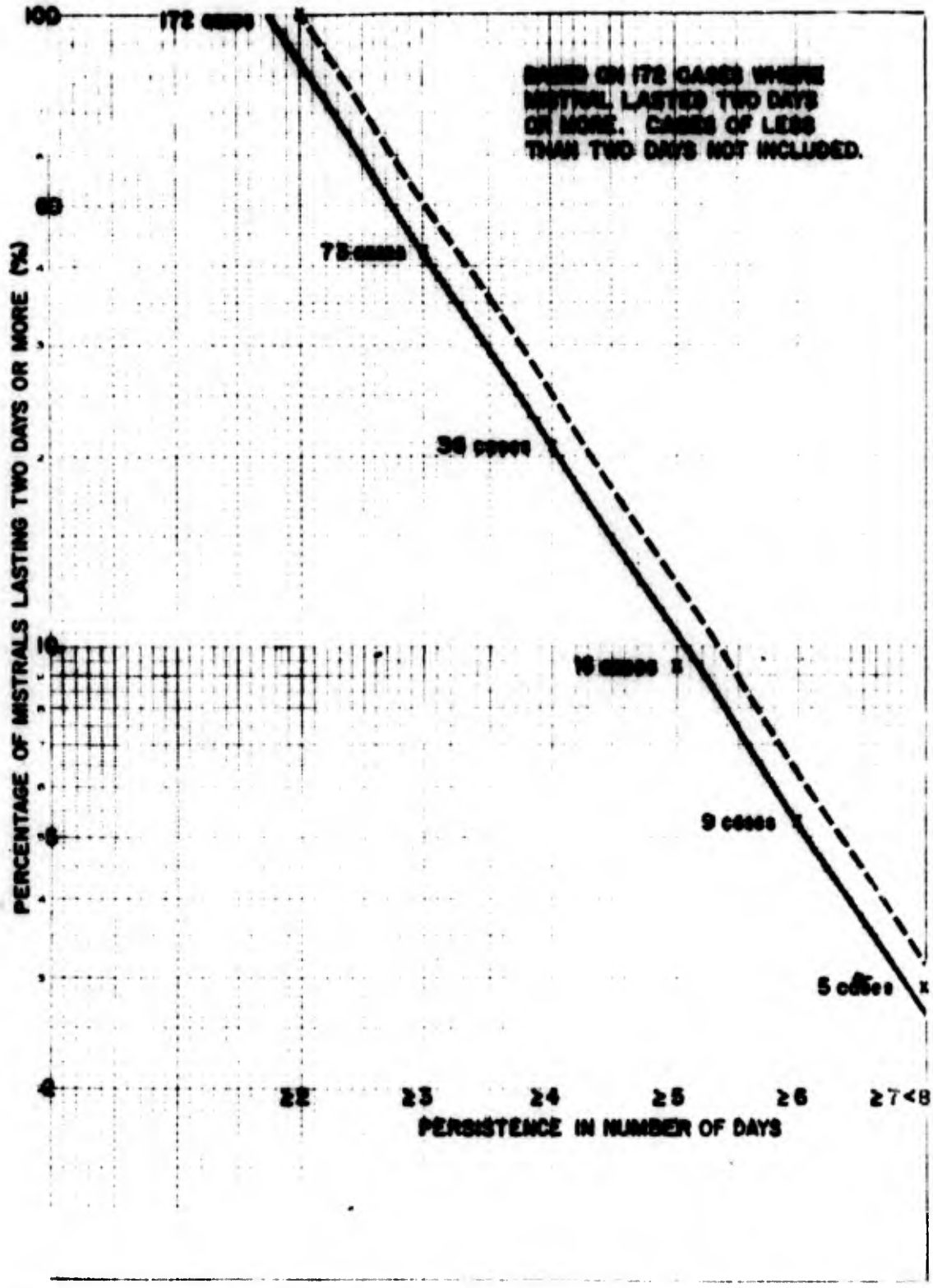

Figure 2.15 Percentage of Mistrals Lasting Two Days or More. (Cuming)

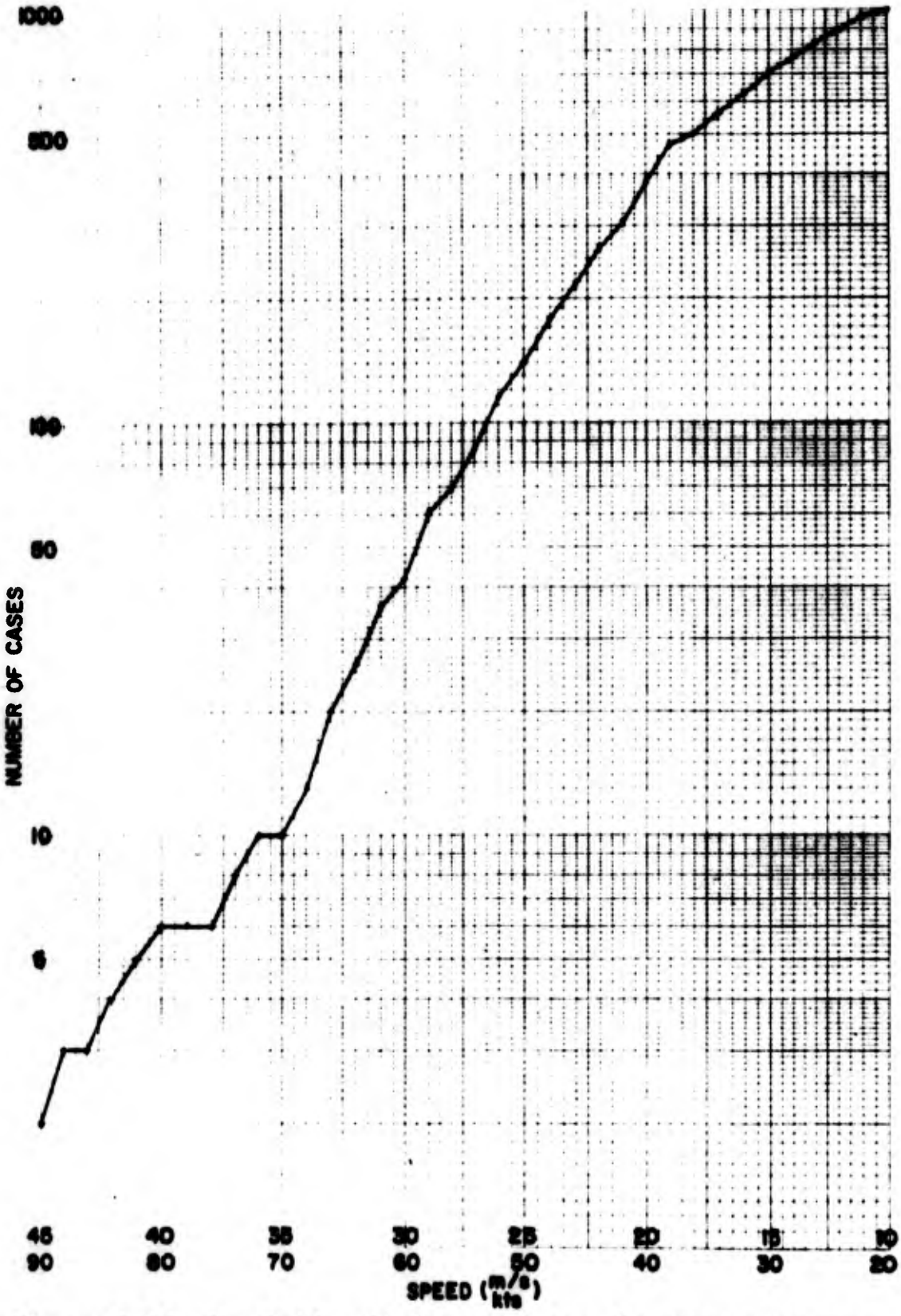

Figure 2.16 Cumulative Number of Cases for Given Maximum Winds During Mistral Periods at Marignane (1957-1966). (Orieux)

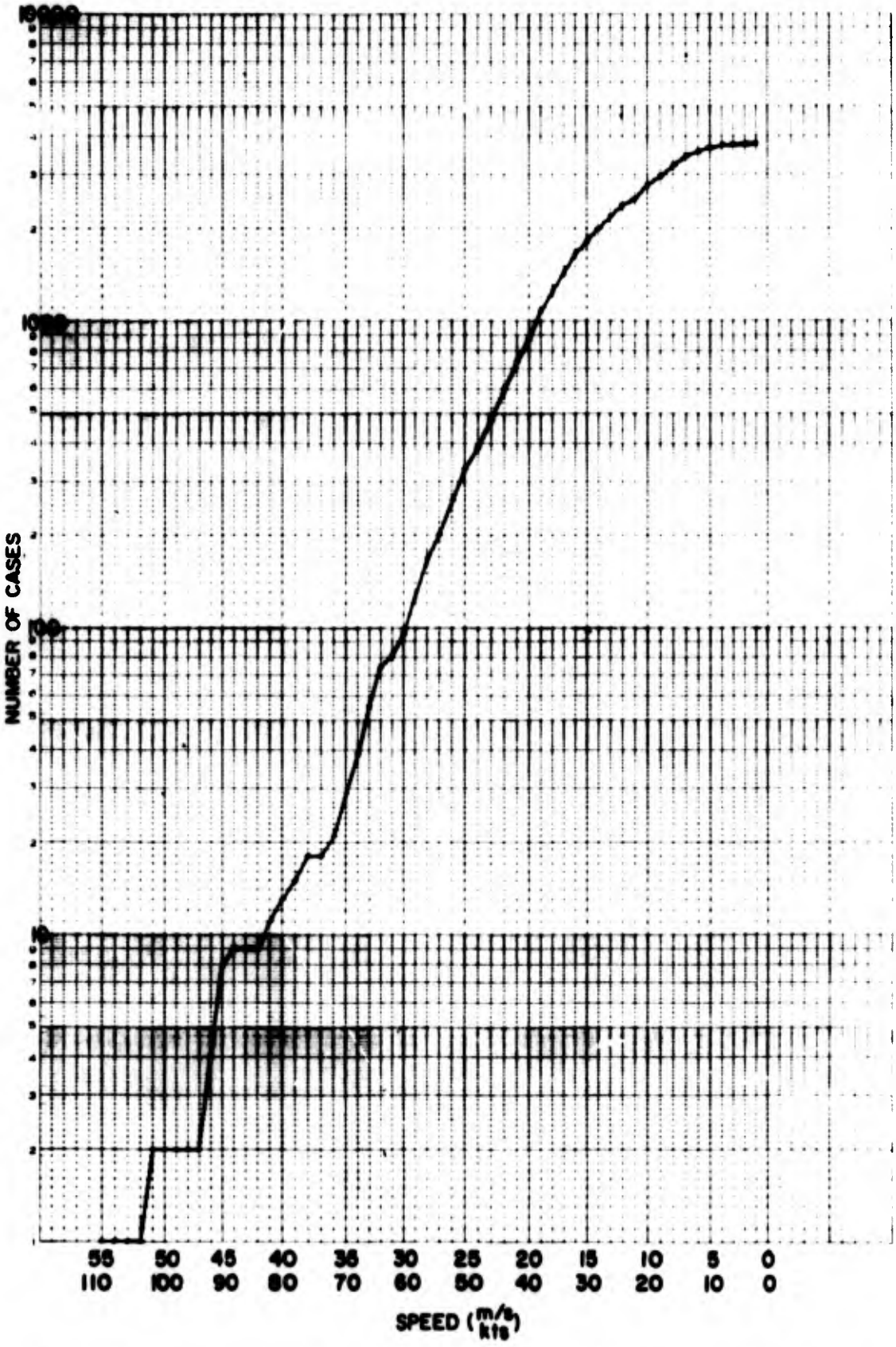

Figure 2.17 Cumulative Number of Cases for Given Maximum Winds During Mistral Periods at Toulon (1947-1966). (Orieux)

TOQD location will certainly yield over-estimates for extreme gale conditions.

Barring these extreme cases, the following rules apply for wind warnings in the Gulf of Lion:

A surface pressure gradient of 6 mb. between Perpignan (sta. no. 07747) and Nice (sta. no. 07690), yields 30-35 knots, 8 mbs. yields 40 knots, and 10 mbs. yields 45-50 knots. A pressure gradient of 3 mbs. between Perpignan and Marignane (sta. no. 07650) or between Marignane and Nice will yield 30-35 knots, 4 mbs. will yield 40 knots, and 5 mbs. will yield 45-50 knots. Forecasters at Perpignan utilize an empirical relationship valid only at Perpignan and then only if the isobars are cyclonically curved in the Gulf of Lion; it is no longer valid at the end of a mistral regime, notably when high pressure over central Europe causes a northeast wind regime. The rule is that the wind gusts (maximum value) measured in knots are 10 times the pressure difference (in millibars) between Toulouse (sta. no. 07630) and Perpignan.

2.4 Case Description

The following sequence is presented as an example of the Type II mistral which occurs most frequently during winter and spring (see fig. 2.2(b)). Figure 2.18 shows TOQD buoy

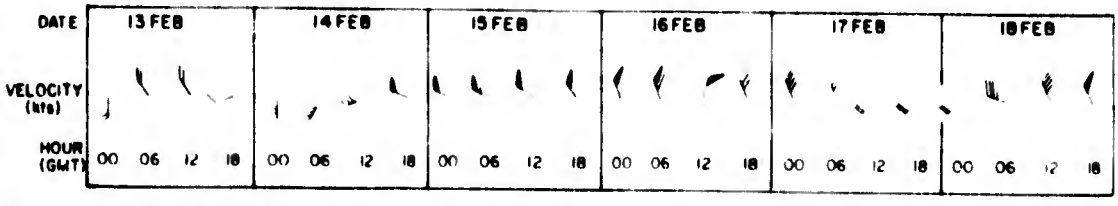

Figure 2.18 Winds at TOQD Between 13 and 18 February 1970. (Orieux)

wind data for the period 13 to 18 February 1970. (Orieux) The mistral regime started on the evening of 14 February and lasted until the morning of 17 February. It was generated by a cold outbreak in the wake of a depression that moved from England into southern France (fig. 2.19). On the 15th, with a low pressure system present in the Gulf of Genoa (fig. 2.20), the mistral regime assumed the typical characteristics of Type II (see fig. 2.2(b)). On the 16th (fig. 2.21), the peak of the mistral development was reached (see also fig. 2.18), with the pressure pattern resembling something in between Type II and III (figs. 2.2(b) and 2.2(c)).

The 500-mb. patterns shown in figures 2.22 and 2.23 are not the best indicators of the jet-stream structure. They reveal, however, the close correlation of the mistral development with the passage of the jet stream aloft. Strongest surface winds are experienced while the jet axis is to the west of, or over, the French Mediterranean coast. The mistral regime is interrupted when a short-wave ridge moves into France on 17 February 1970 (figs. 2.23 and 2.24). Now the northwesterly jet stream has its axis to the east of the French Mediterranean coast.

On 18 February 1970, a new surge of cold air, travelling behind a cold front, arrives at the coast, leading to a renewed outbreak of the mistral (figs. 2.18 and 2.25).

The soundings at Nimes (sta. no. 07645) at 1200 GMT 15 February and 0000 and 1200 GMT 17 February (figs. 2.26(a) and 2.26(b)), show the warming of the troposphere that is

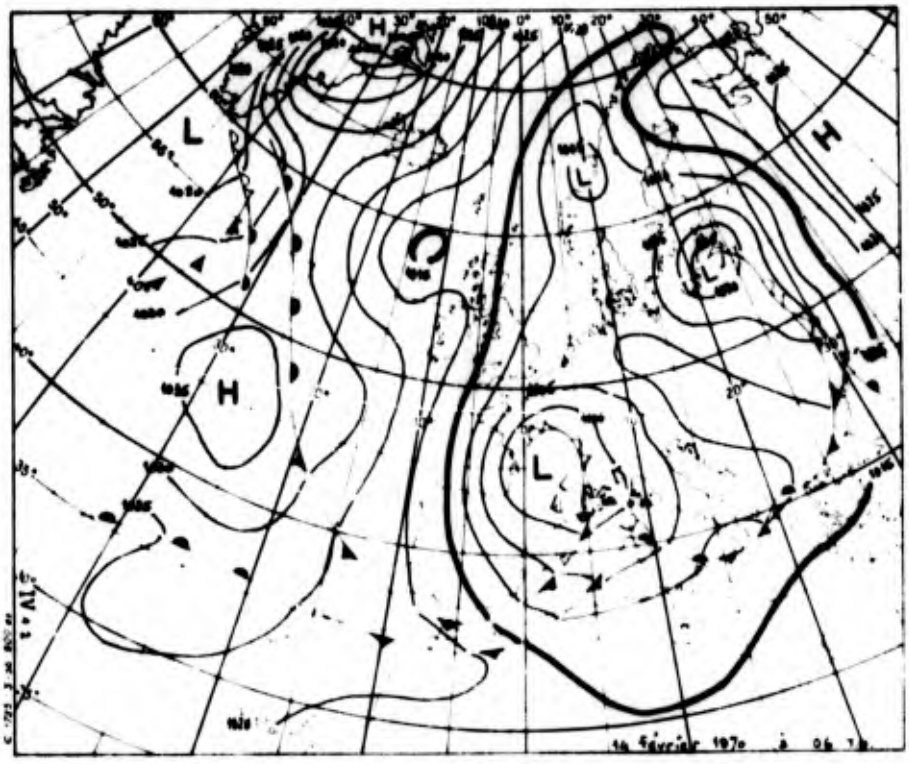

Figure 2.19 Surface Analysis, 0600 GMT 14 February 1970. (Orieux)

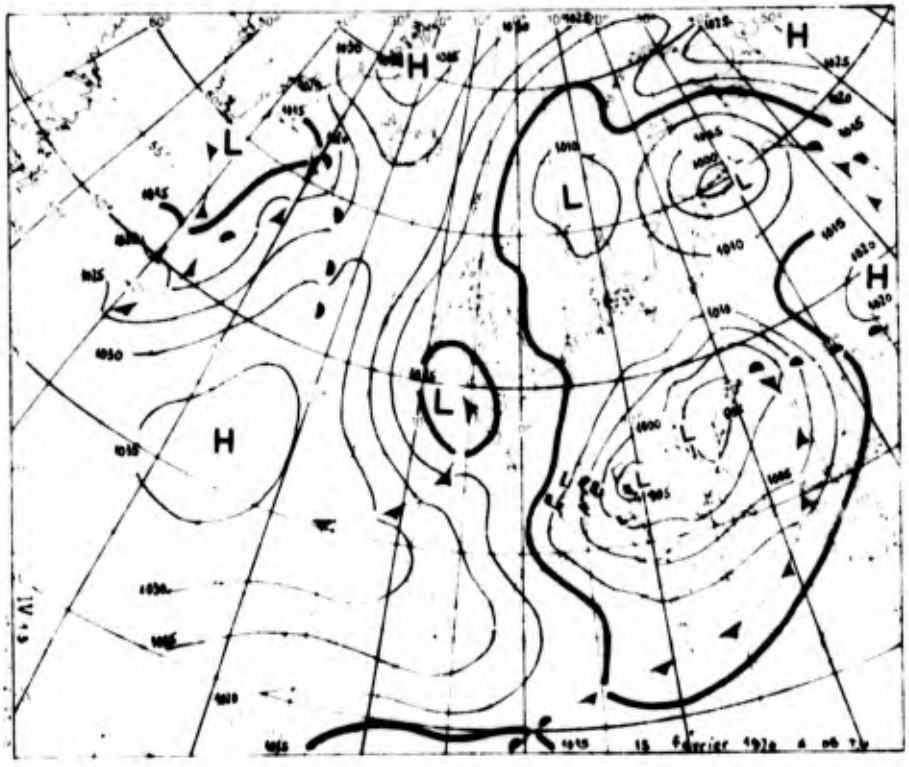

Figure 2.20 Surface Analysis, 0600 GMT 15 February 1970. (Orieux)

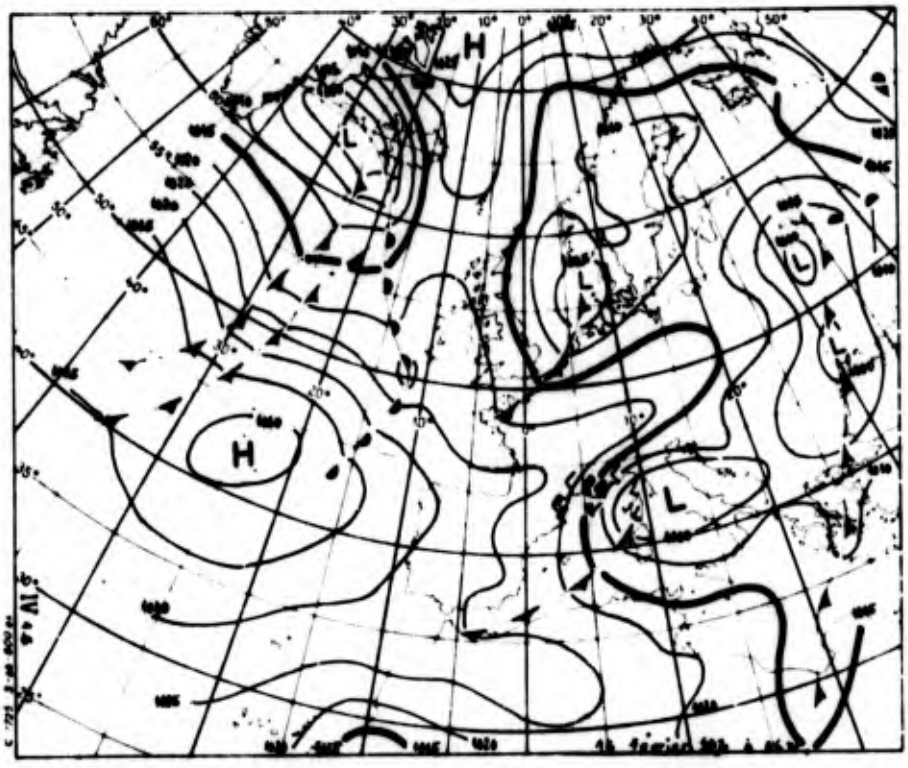

Figure 2.21 Surface Analysis, 0600 GMT 16 February 1970. (Orieux)

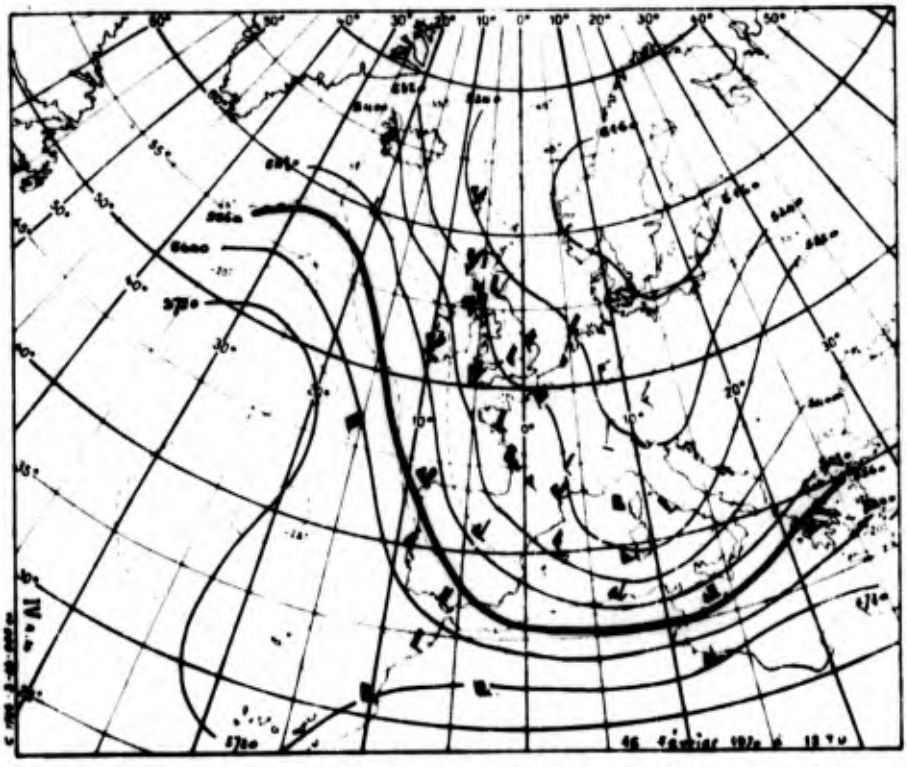

Figure 2.22 500-mb. Analysis, 1200 GMT 15 February 1970 (dashed lines are isotherms). (Orieux)

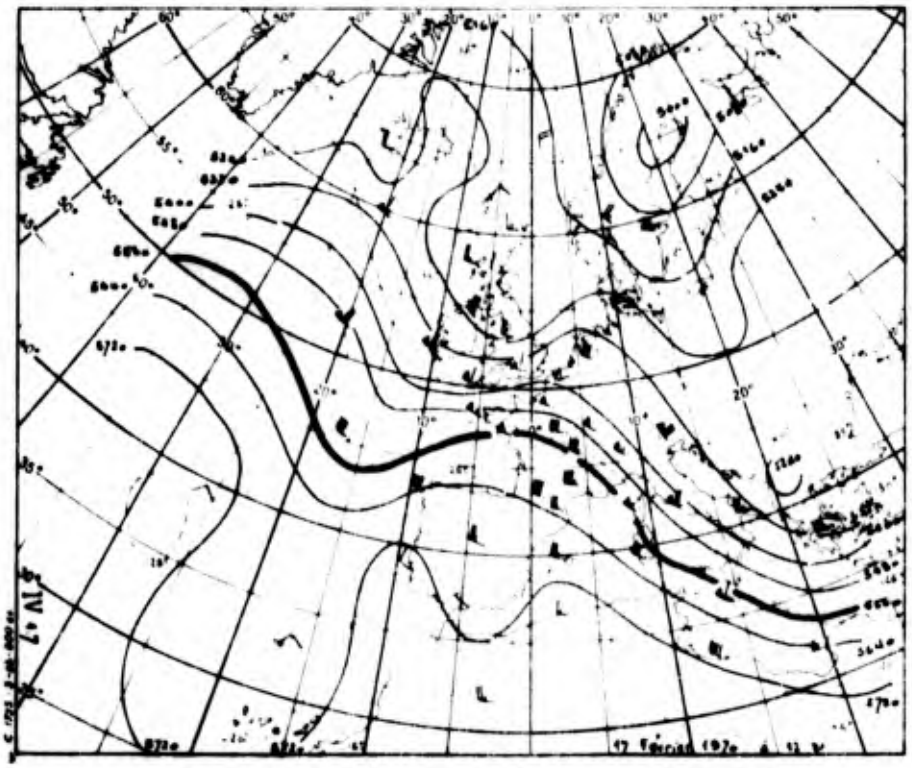

Figure 2.23 500-mb. Analysis, 1200 GMT 17 February 1970 (dashed lines are isotherm). (Orieux)

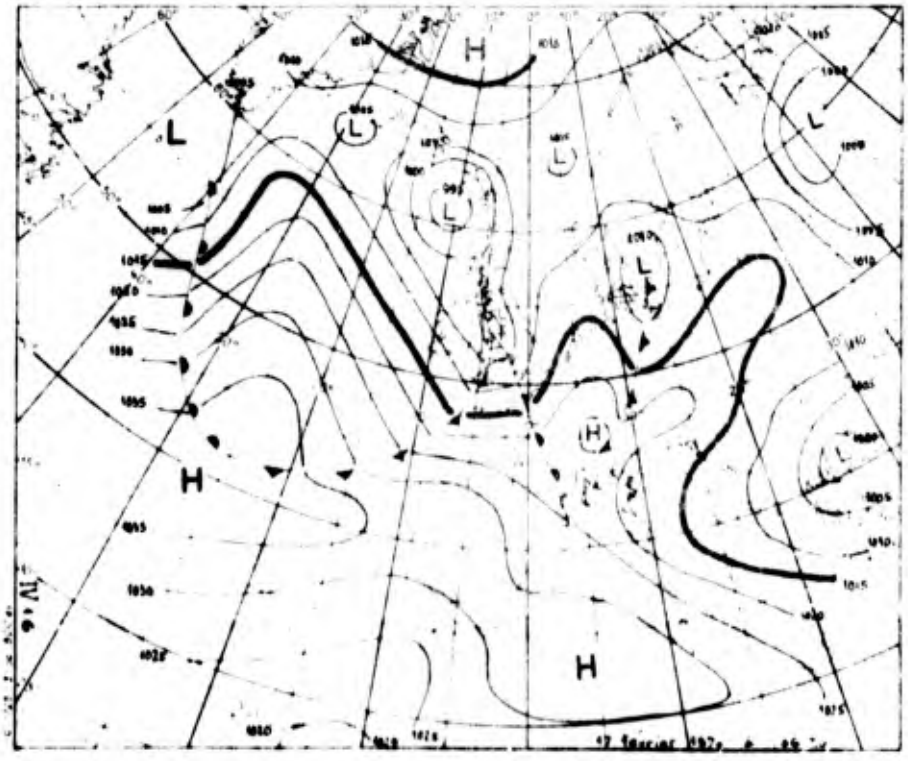

Figure 2.24 Surface Analysis, 0600 GMT 17 February 1970. (Orieux)

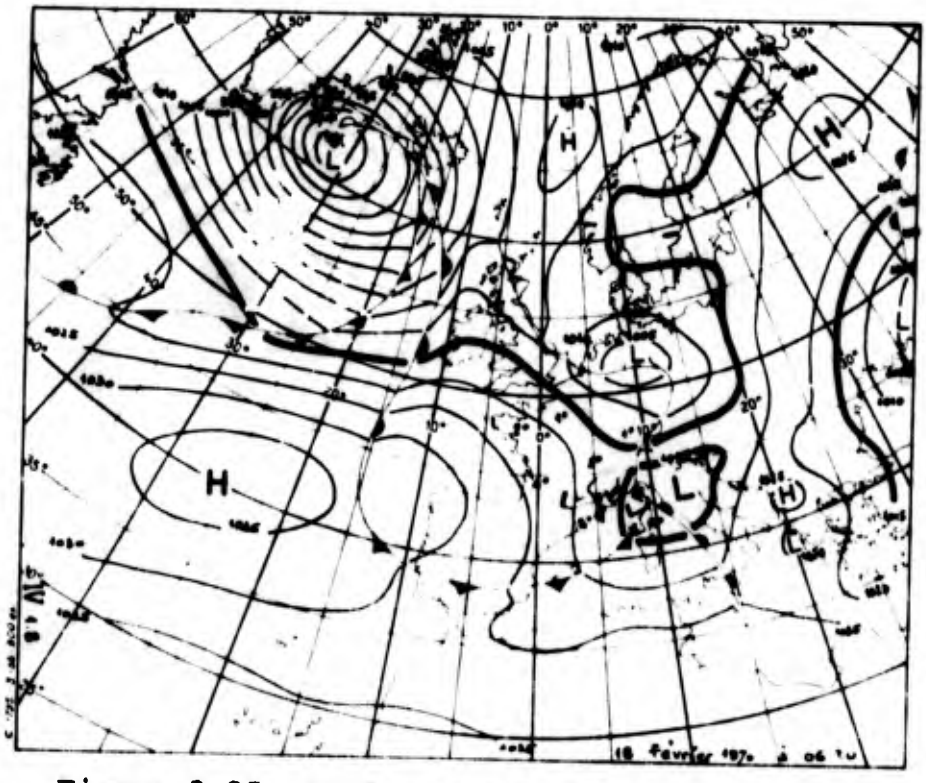

Figure 2.25 Surface Analysis, 0600 GMT 18 February 1970. (Orieux)

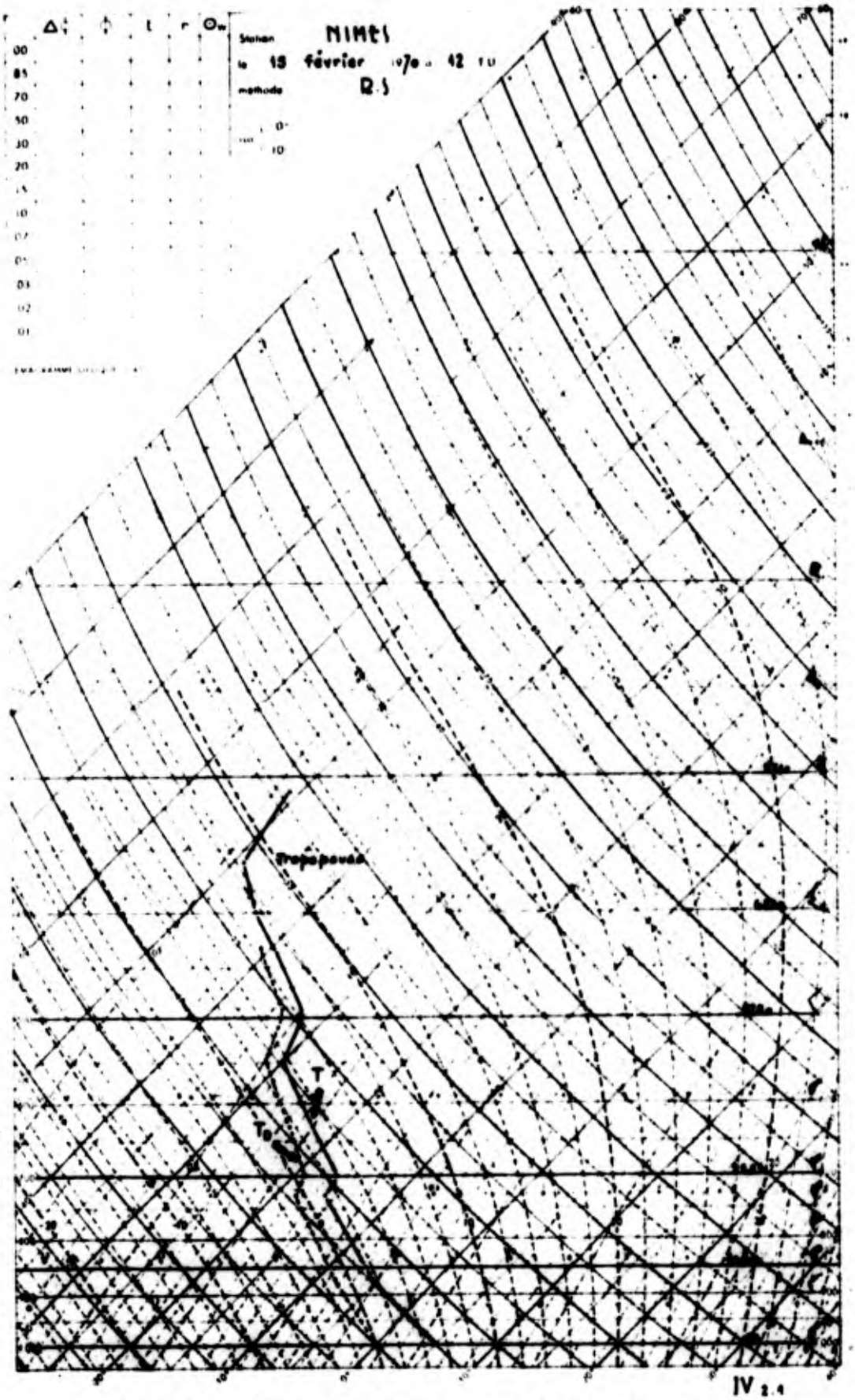

Figure 2.26(a) Sounding at Nimes, (a) 1200 GMT 15 February 1970. (Orieux)

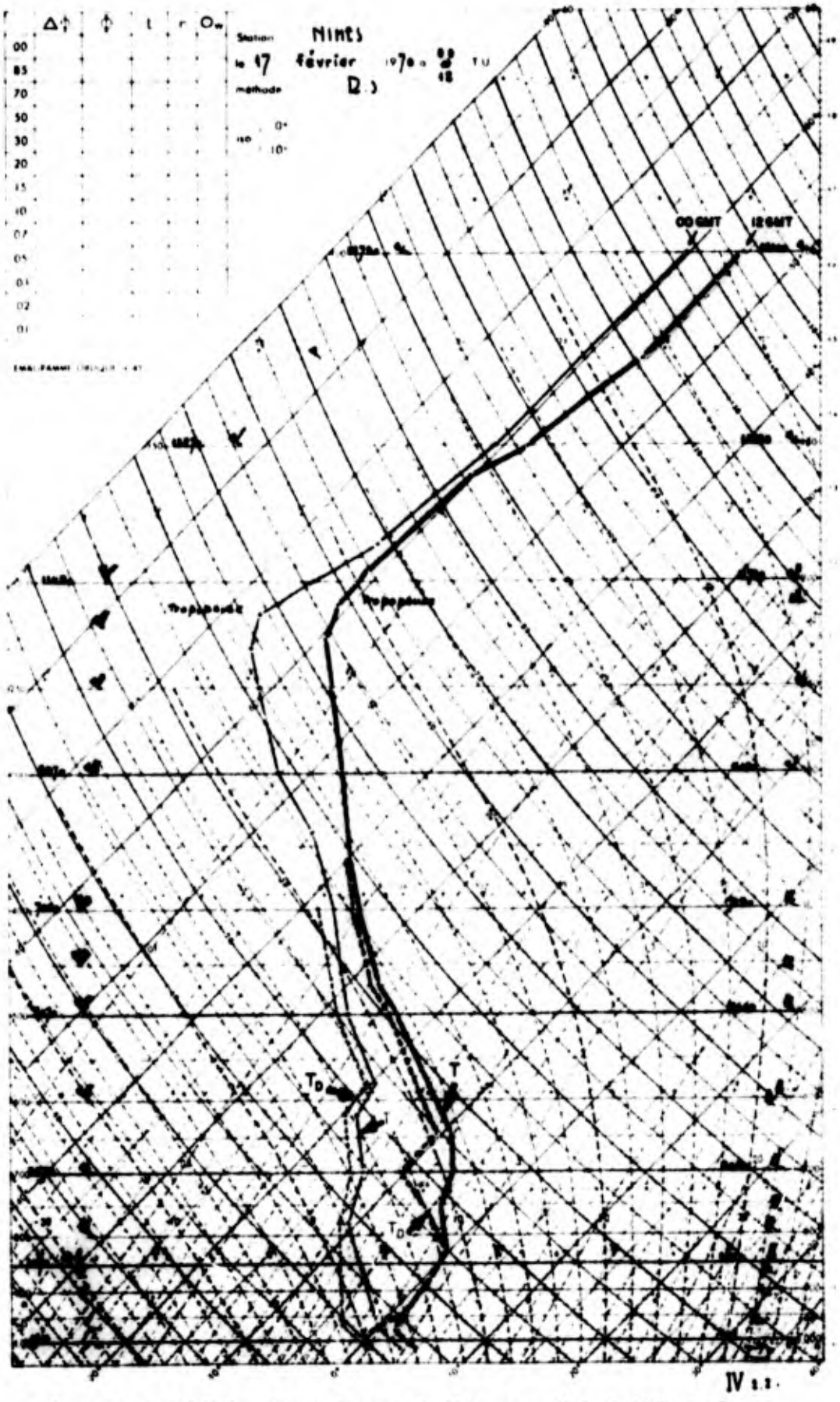

Figure 2.26(b) Sounding at Nimes, (b) 0000 and 1200 GMT 17 February 1970. (Orieux)

associated with the passage of the jet stream aloft and the cessation of the mistral. The adiabatic layer that reaches to almost 850 mb. on 15 February is indicative of the strong turbulent mixing in the lower layers of the atmosphere. The mistral regime of this time and over this station is confined to the region below the near-isothermal layer in the vicinity of 700 mb.

The situation described above is typical of the Air Ministry Type A mistral ([1] Vol. 1, pg. 46). That this is so may be seen by comparison with appendix B, which shows normalized mean and standard deviation charts for incipient Air Ministry Type A mistrals. Appendix B also shows similar charts for incipient Air Ministry Type C mistrals ([1] Vol. 1, pg. 49).

2.5 Forecasting of the Mistral

2.5.1 Short-Range Forecasting

We define this range as extending to approximately 12 hours. Winds at Lus la Croix Haute (sta. no. 07587), located on a tributary of the Durance River, usually give a 2-3 hour advance notice of the onset of a northerly mistral. Wind speeds at this station closely resemble those to be expected later in the Gulf of Lion.

The progress of cold fronts across France in Type I and II situations should be closely studied. In cases where the isobars behind a cold front are closely packed and nearly normal to the frontal line, the post-frontal winds give a good indication of the rate of progress of the front. The

mistral starts, or pre-existing mistral conditions are intensified, with the passage of cold fronts from the north or northwest.

Rules of thumb have been given (section 2.3.8) for maximum wind speeds to be expected in mistral situations. In general, one may state that wind of gale force or more ($\geq$34 kts. according to U.S. definition, $\geq$28 kts. according to Italian definition) may be expected behind cold fronts moving into the Mediterranean in mistral situations.

The areal extent of the mistral must be estimated qualitatively. Shear lines caused by the sheltering effect of the Pyrenees and the Alps may be expected off the coast south of Perpignan and near St. Tropez (sta. no. 07677). As stated in section 2.3.3, the wind speed changes sharply across these shear lines. The orientation of the shear lines is indicated schematically in figures 2.2(a)-(c). Type II is expected to have the sharpest shear lines. The mistral winds associated with this type also extend farthest into the Mediterranean, sometimes as far as Sicily, Malta and the North African coast. The southward extent of the mistral, especially Type II, is forecast empirically by its relation to the jet stream. If a deep trough extends all the way to Sicily, the northwesterly jet stream to the west will cause frontal disturbances to follow its course, and consequently the mistral will extend into the region of Sicily and Malta. As we have seen from the case study, strong mistral winds should be forecast on the cyclonic side of, and

underneath, the jet axis. Surface winds usually decrease as the jet axis moves past the area and an anticyclonic regime is established.

Corner and channel effects may locally increase the wind speed, such as near the southwest tip of Sardinia and in the Straits of Bonifacio.

2.5.2 Synoptic-Range Forecasting

This range comprises the time period 12 to 48 hours. Forecasting in this range has to rely heavily on the quality of upper air and surface prognostic charts. Unfortunately, the present numerical output does not completely meet the required standards. Special consideration of the Mediterranean and its surrounding terrain in a fine-grid analysis and forecasting scheme is advocated. The shortcomings in numerical forecasting techniques which still exist over the Mediterranean place a heavy burden on the local forecaster and his empirical skill. The following rather crude rules should be kept in mind:

(1) The establishment of a mistral situation, as well as a surge in an already existing situation, is tied to the passage of cold fronts across France and into the Mediterranean. This means that the position and movement of short-wave troughs should be charted carefully.

(2) Mistral Types I and II require a long-wave ridge over the eastern Atlantic and a long-wave trough over central Europe. As long as this trough-ridge pattern remains stationary, short-wave passages will cause surges within an extended mistral period. The Type I mistral is typical for a "high-index" flow pattern, whereas Types II and III conform to a "low-index" pattern. Numerical prognoses should be watched for indications of a shift in the long-wave pattern. Climatology provides some help, inasmuch as blocking ridges, responsible for the

> Type II mistral are relatively stable and long lived. Cold advection on the western flanks of such a ridge may herald the breakdown of the long wave pattern. Strong cold advection along the eastern flanks of the ridge and into the long-wave trough may signal a retrogression of the long-wave pattern, or the establishment of an "Ω" pattern which is typical of the Type III mistral.

As stated in section 2.4, Brody, Reiter and Godfrey presented normalized mean and standard deviation charts for incipient mistral situations. These are given in appendix B. At the same time they presented similar charts for periods of 1, 2 and 3 days prior to the mistral development; these are also contained in appendix B. Some of what has been said above concerning synoptic range forecasting is reflected in these charts and may provide useful forecasting hints.

2.5.3 Extended-Range Forecasting

This is intended to cover a period in excess of 48 hours prior to mistral development. Appropriate normalized mean and standard deviation charts are presented and discussed in appendix B.

3. GENOA DEPRESSIONS

(Based upon material supplied mainly by Gen. G. FEA and Lt. Col. A. NANIA.)

3.1 Definition

Genoa depressions are low-pressure systems which form in the Gulf of Genoa and in the Ligurian Sea. Depressions in the upper Po valley are often included in the consideration. In a broader sense one may also include lee cyclogenesis south of the Alps and associated depressions over the northern Adriatic Sea. Associated Weather Phenomena: Mistral, Bora.

3.2 General Description

Outbreaks of cold air over France described in chapter 2 under "mistral" frequently lead to the formation of cyclones over the Ligurian Sea. Several factors listed below, not necessarily in the order of priority, seem to play an important role in the development of these depressions:

(1) The thermal contrast between land and sea has an effect on the surface pressure pattern and its development.

(2) Jet maxima proceeding southeastward over the Alps favor cyclogenesis in their left-front quadrant due to positive vorticity advection [22]. As this quadrant comes to lie over the Ligurian Sea, the Po valley, and even the northern portion of the Adriatic Sea, the divergent flow pattern at jet-stream level induces pressure falls at the earth's surface.

(3) It has been demonstrated in various text books (see e.g. [22]) that a westerly jet stream traversing the Rocky Mountains causes favorable conditions for trough formation and cyclogenesis in the lee of the mountains because of the tendency towards conservation of potential vorticity. This may be expressed by:

$$P = \frac{\zeta + f}{\Delta p} = \text{constant} \qquad (1)$$

where ζ is the relative vorticity, f is the coriolis parameter, and Δp is the thickness (in mb.) of the air layer overflowing the mountain range. As the air descends on the lee side of the mountain range, a vertical air column in the troposphere will stretch, i.e. Δp will increase. In order to balance the equation given above, $(\zeta+f)$ increases proportionately. Since f is constant in a westerly flow, the increase must take place in ζ. Thus the flow pattern will acquire more cyclonic shear and/or curvature, most likely the latter. This sets the stage for divergence and pressure fall patterns to develop.

The situation over northern Italy in the lee of the Alps is different in that the jet streams causing cyclogenesis have a strong northerly wind component, whereas the Alps run nearly in a west-east direction. As Δp increases in an air column descending on the south side of the Alps, $(\zeta+f)$ also must increase. However, f decreases along a northerly air current and thus ζ, the relative vorticity, will have to increase to balance the increase in Δp as well as the loss in f; enhanced cyclogenetic activity will result over northern Italy.

(4) Frequently the cold air mass behind a cold front moving southwards is not deep enough to "spill" over the crest of the Alps. A time-lapse movie shown by General FEA suggests that the cold air may eventually flow around the eastern edge of the Alps and invade northern Italy from the east. Thus the pressure rise at the surface associated with the advancing cold air will be delayed in reaching northern Italy and any conditions favorable to cyclogenesis in that area will persist for a longer period of time than might be expected by timing the southward movement of the high pressure pulse. It should also be mentioned that the advance of cold air around the eastern edge of the Alps may cause strong bora winds along the Adriatic coast of northern Yugoslavia. (The bora is a cold, gusty, katabatic wind that descends the coastal mountain range from the interior to the Adriatic Sea. These katabatic winds can present a considerable hazard to local naval operations.)

3.3 Occurrence

3.3.1 Types of Genoa Depressions

According to CENFAM (1963), surface cyclogenesis in the lee of the Alps may be classified into four general categories each of which may contain several sub-types. In their investigation, examinations of the surface and 500-mb. patterns were carried out independently in arriving at a classification scheme. A "best fit" was then made relating the two independent classifications. For example, the 500-mb. type A_1' has related surface cyclogenesis which was frequently associated with the surface classification type A_1, although not invariably so. This will be discussed later.

Type A(A') -- orographic cyclogenesis in prevailing zonal flow.

Surface sub-type A_1 is characterized by having the strongest 500-mb. geopotential gradient (sub-type A_1') located south of the Alps; A_2 has the strongest 500-mb. gradient roughly at the latitude of the Alps; A_3 shows the strongest 500-mb. gradient north of the Alps. Examples of surface (A) and 500-mb. (A') patterns are given in figures 3.1 to 3.6.

Type B(B') -- cyclogenesis associated with deep troughs of very large, slow moving, upper waves.

Surface sub-type B_1 is characterized by having the 500-mb. trough axis (sub-type B_1') running nearly meridionally from the North Sea through France into the Mediterranean; in B_2 the 500-mb. trough axis lies from northeast to southwest; in B_3 the 500-mb. trough axis is oriented from northwest to

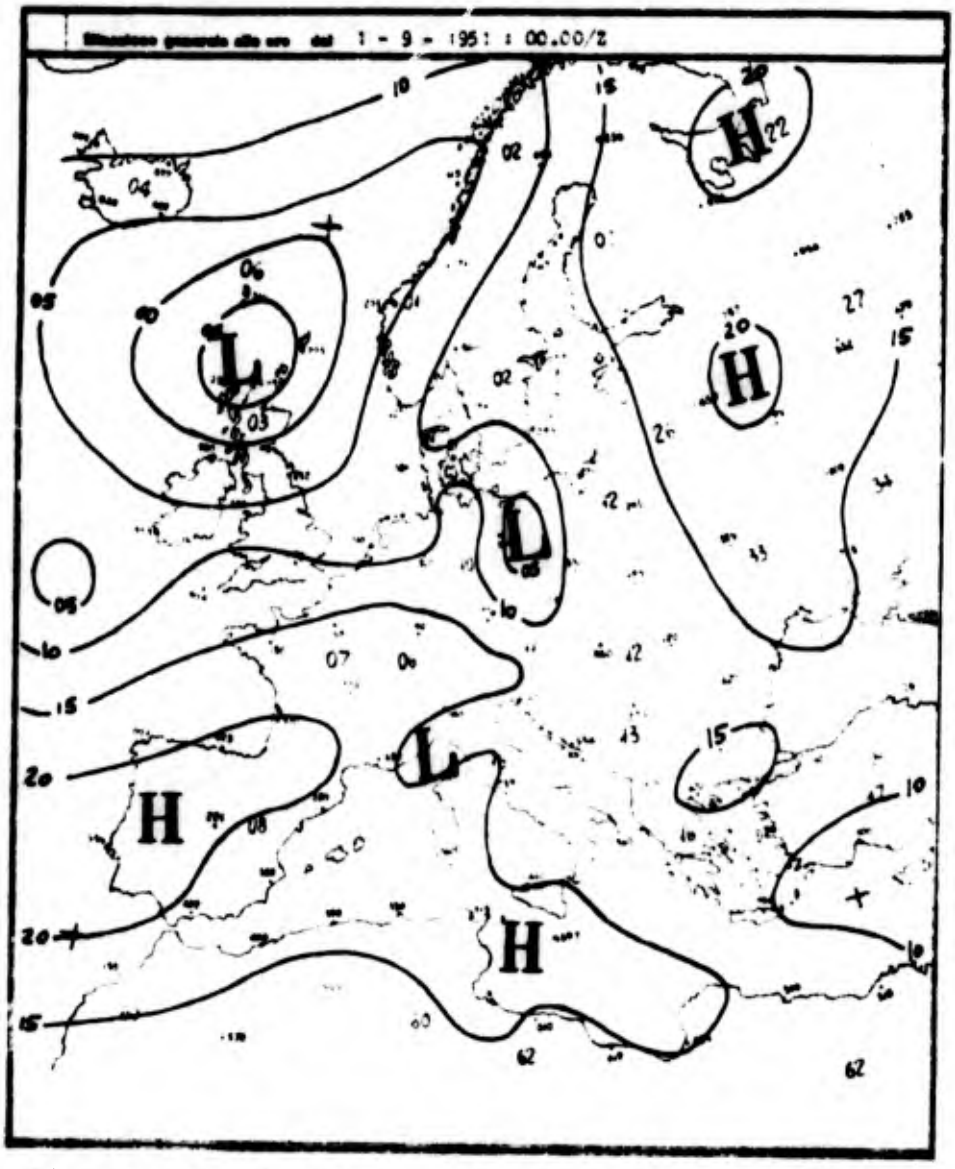

Figure 3.1 Surface Pressure Pattern for Cyclogenesis, Type A_1. [4]

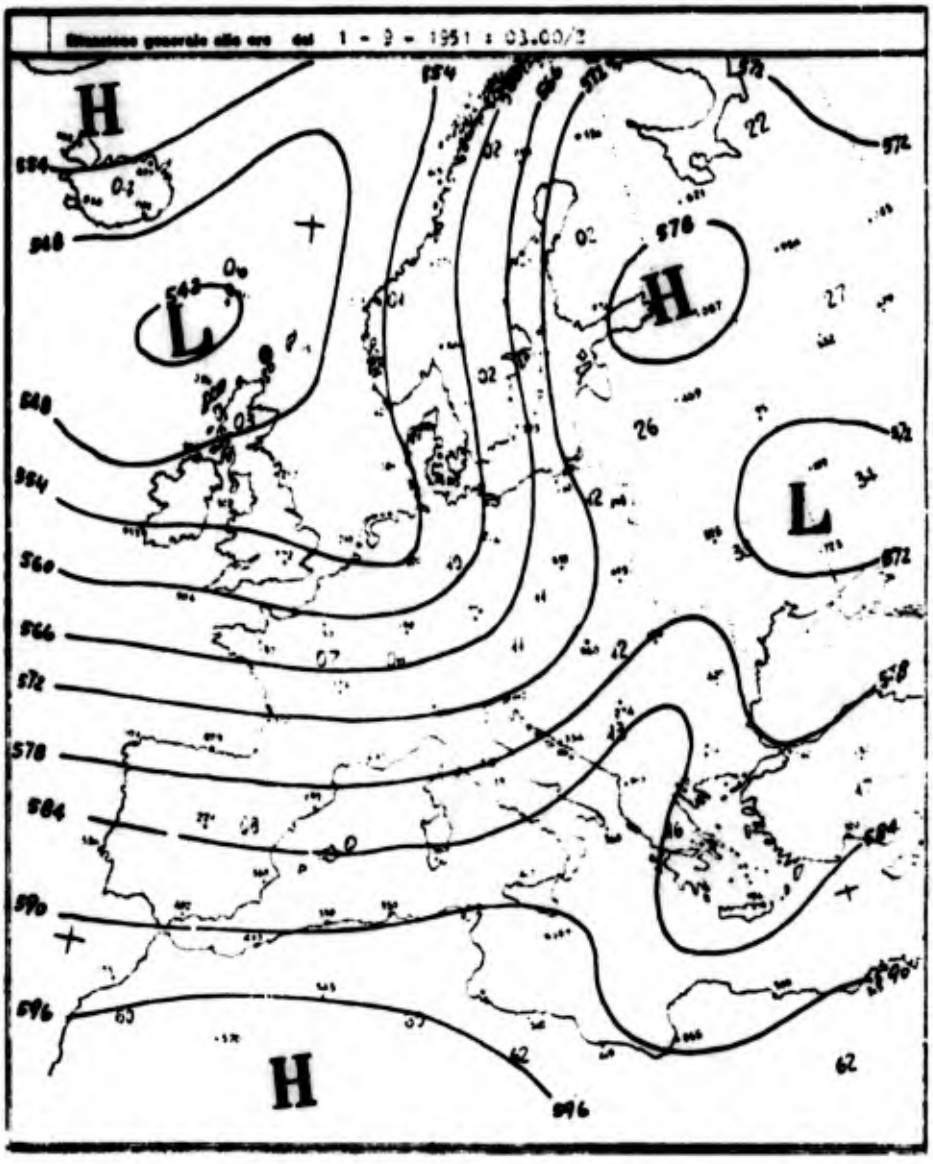

Figure 3.2 500-Mb. Pattern for Cyclogenesis, Type A_1'. [4]

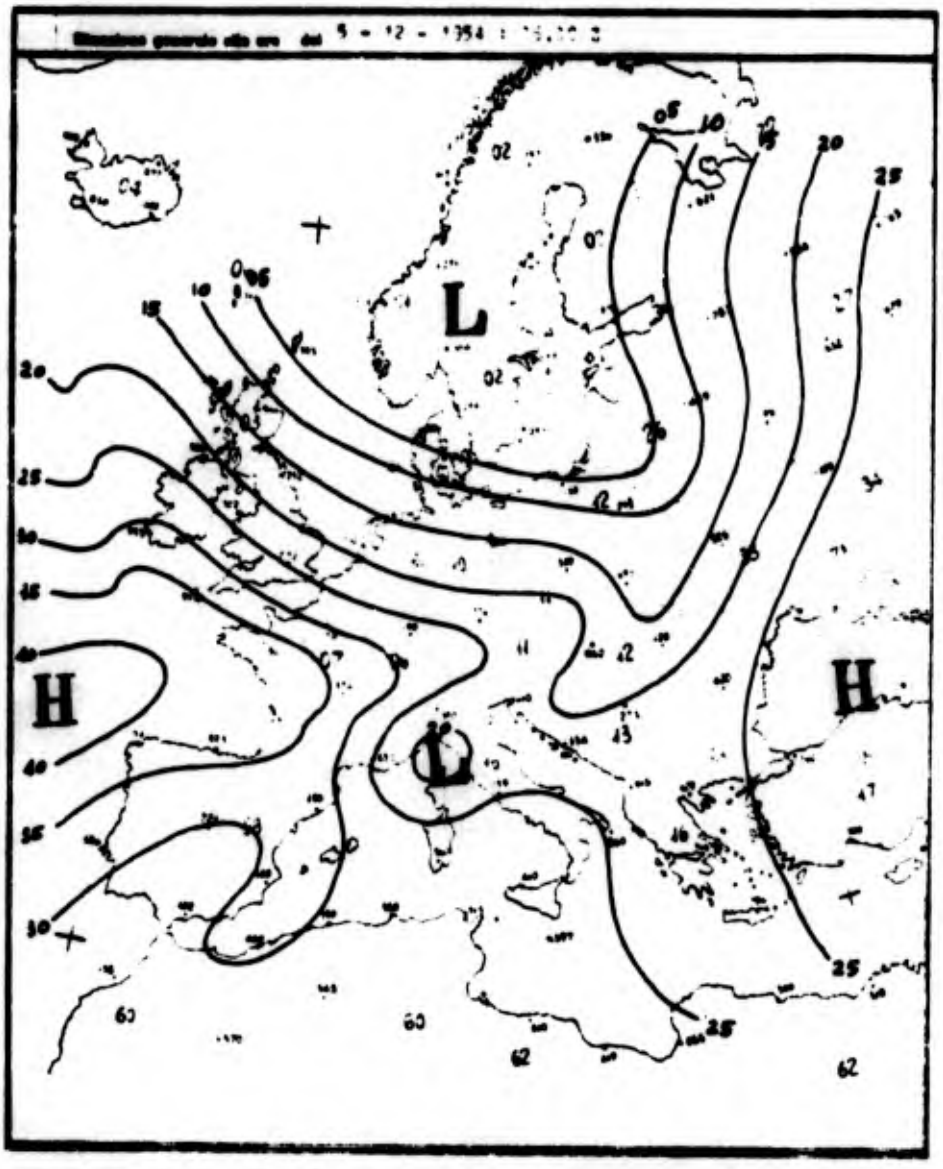

Figure 3.3 Surface Pressure Pattern for Cyclogenesis, Type A_2. [4]

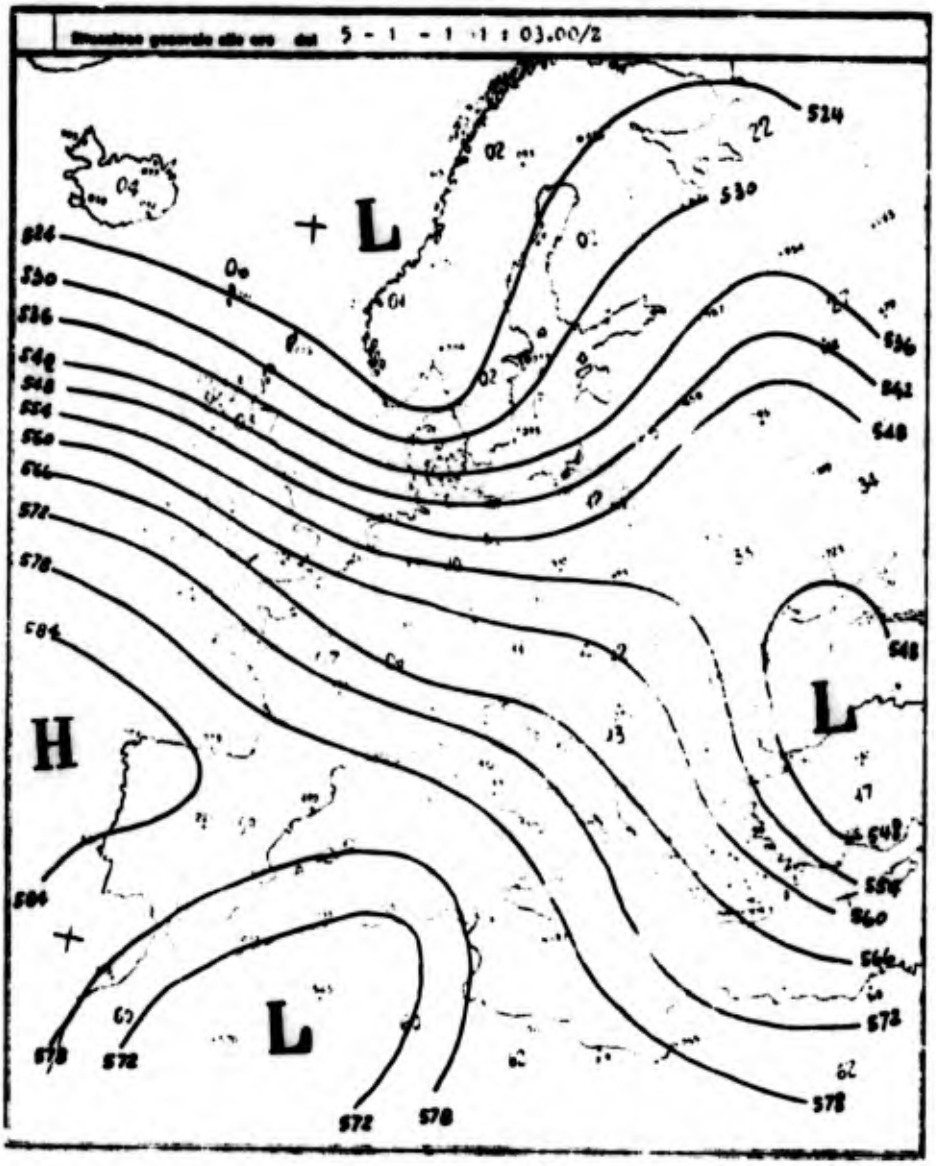

Figure 3.4 500-Mb. Pattern for Cyclogenesis, Type A_2'. [4]

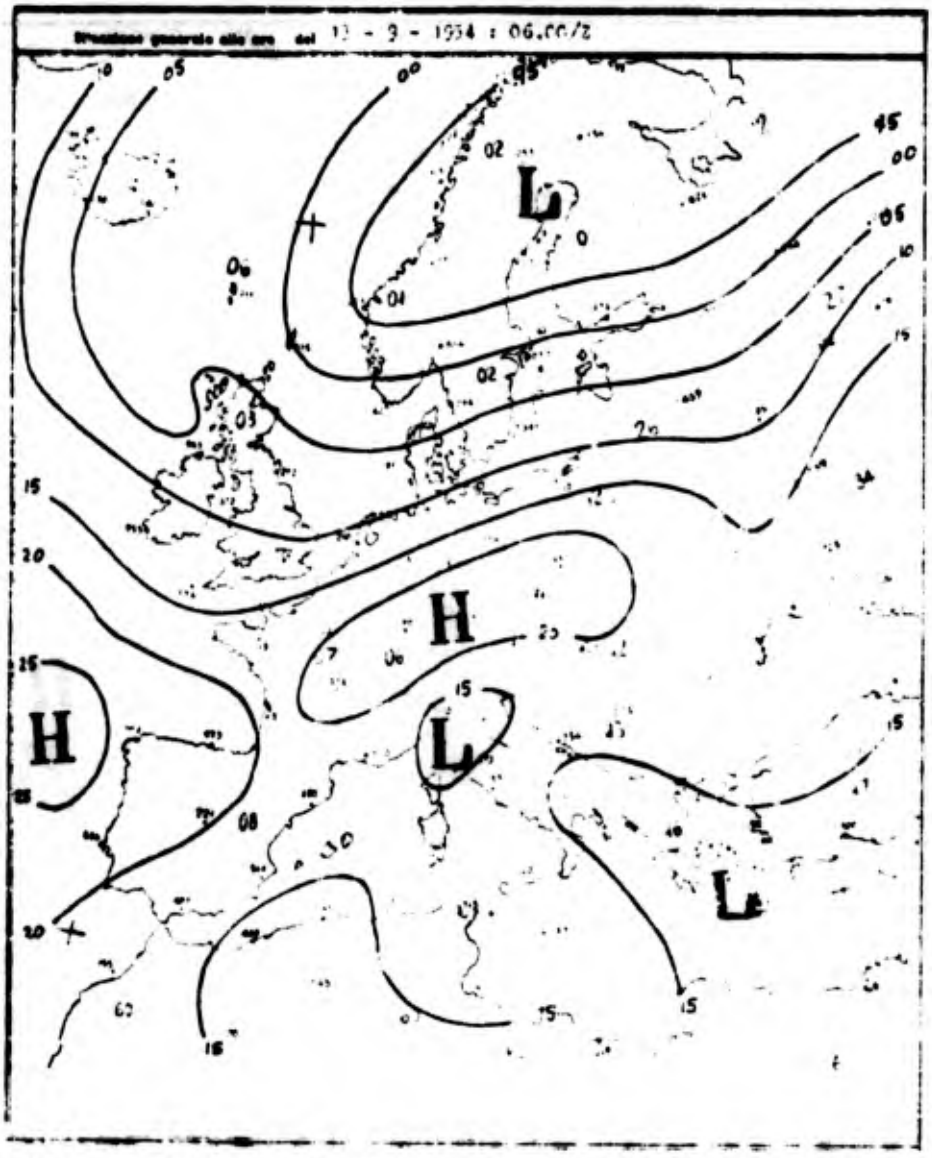

Figure 3.5 Surface Pressure Pattern for Cyclogenesis, Type A_3. [4]

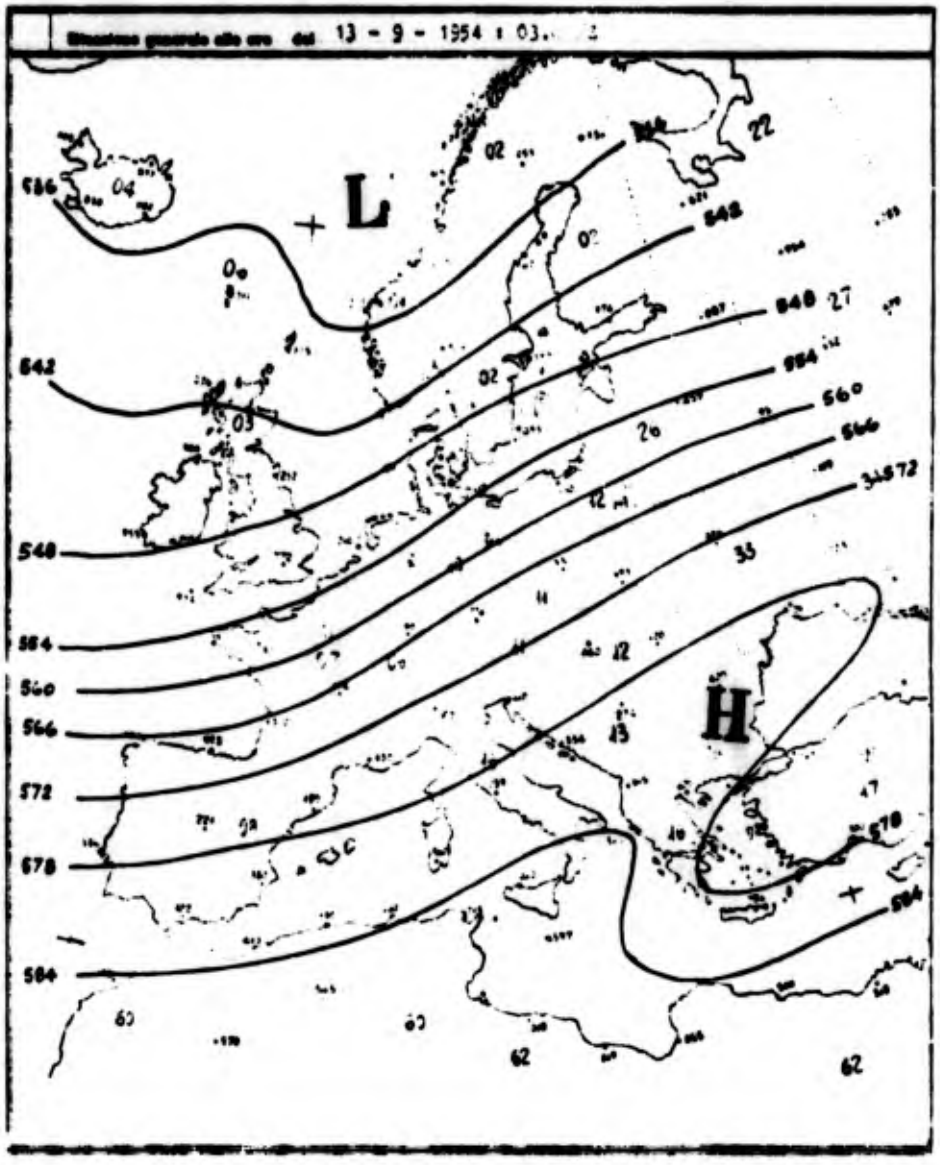

Figure 3.6 500-Mb. Pattern for Cyclogenesis, Type A'_3. [4]

southeast; and in B_4 a cut-off low at 500 mb. dominates central Europe and northern Italy. Examples of both the surface (B) and 500-mb. (B') patterns are given in figures 3.7 to 3.14.

Type C(C') -- cyclogenesis occurring in troughs having more or less zonal axes.

Surface type C is characterized by having a 500-mb. cut-off low (type C') dominating the central Mediterranean and a ridge extending from the Atlantic across northern Europe. Examples of both the surface (C) and the 500-mb. (C') patterns are given in figures 3.15 and 3.16.

Type F(F') -- "föhn" cyclogenesis north of the Alps.

Surface type F is associated with a 500-mb. pattern (F') having an Ω-shaped blocking ridge centered over central and northern Europe and a low located over the British Isles and the Bay of Biscay. Examples of both the surface (F) and the 500-mb. (F') patterns are given in figures 3.17 and 3.18. The surface cyclogenesis in this case is the trough shown to the north of the Alps in figure 3.17.

Basically types A(A') characterize high-index conditions, at least west of the Alps, whereas the other types conform to low-index situations. In particular, types C(C') and F(F') are associated with blocking action over western or central Europe.

3.3.2 Seasonal Variation

The formation of cyclones in the lee (south) of the Alps is a relatively frequent phenomenon. In the 15-year period 1947-1961, the average number of cases was 67 per year.

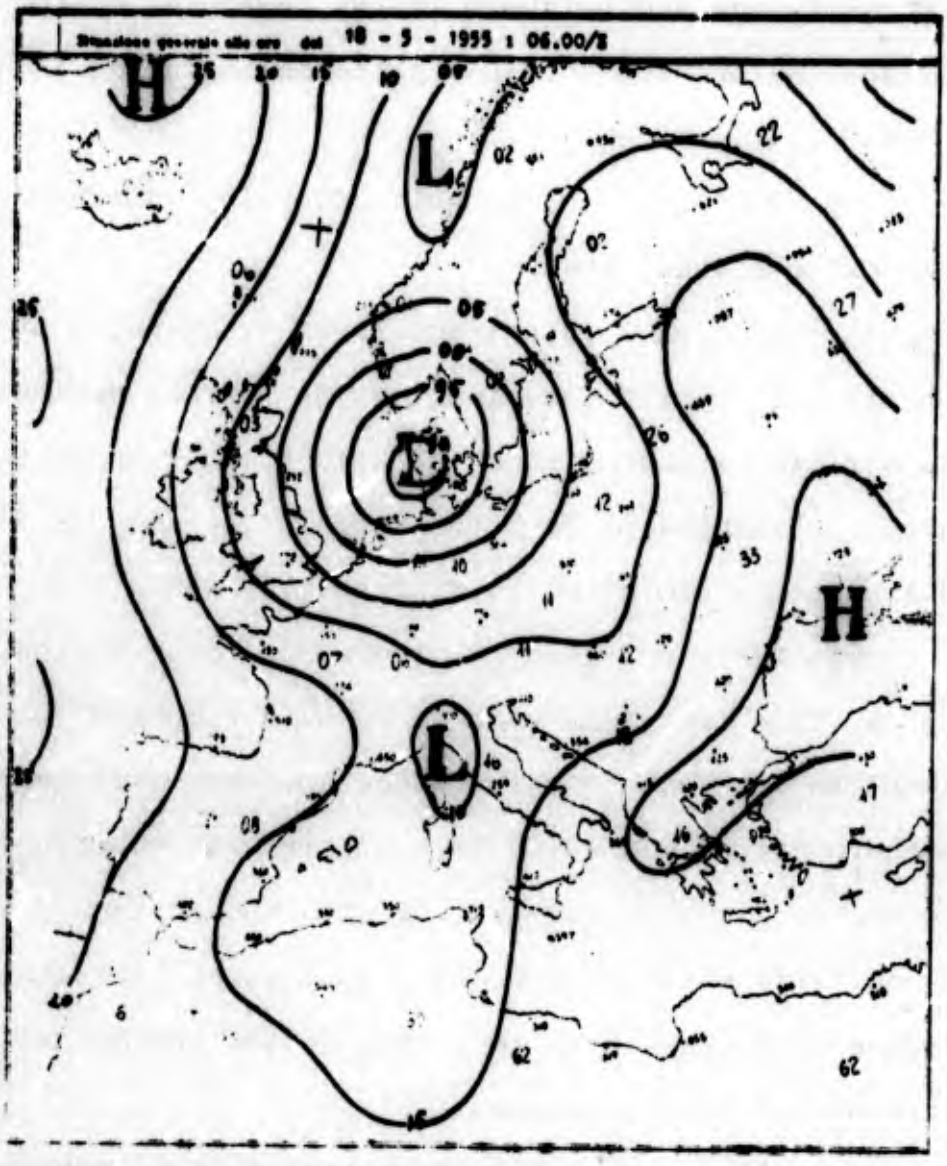

Figure 3.7 Surface Pressure Pattern for Cyclogenesis, Type B_1. [4]

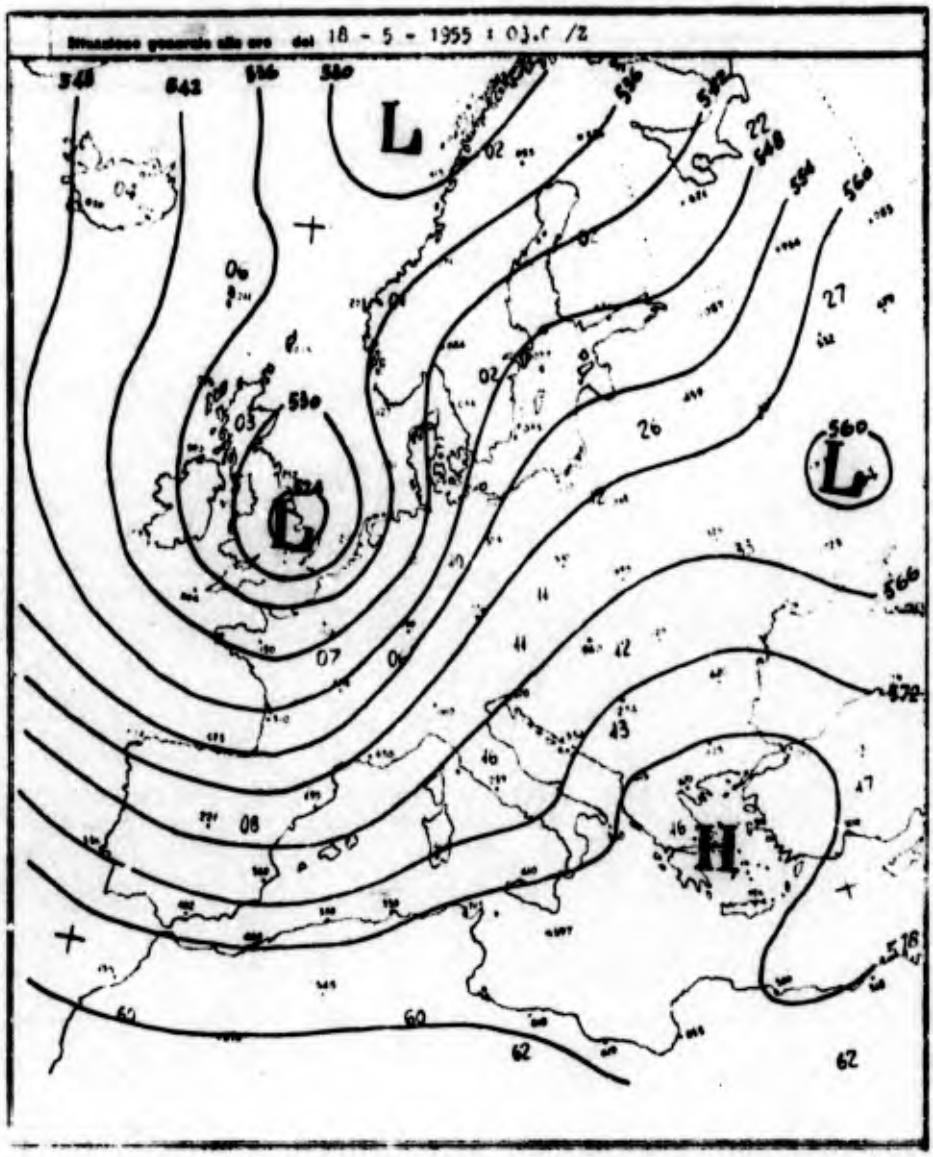

Figure 3.8 500-Mb. Pattern for Cyclogenesis, Type B_1'. [4]

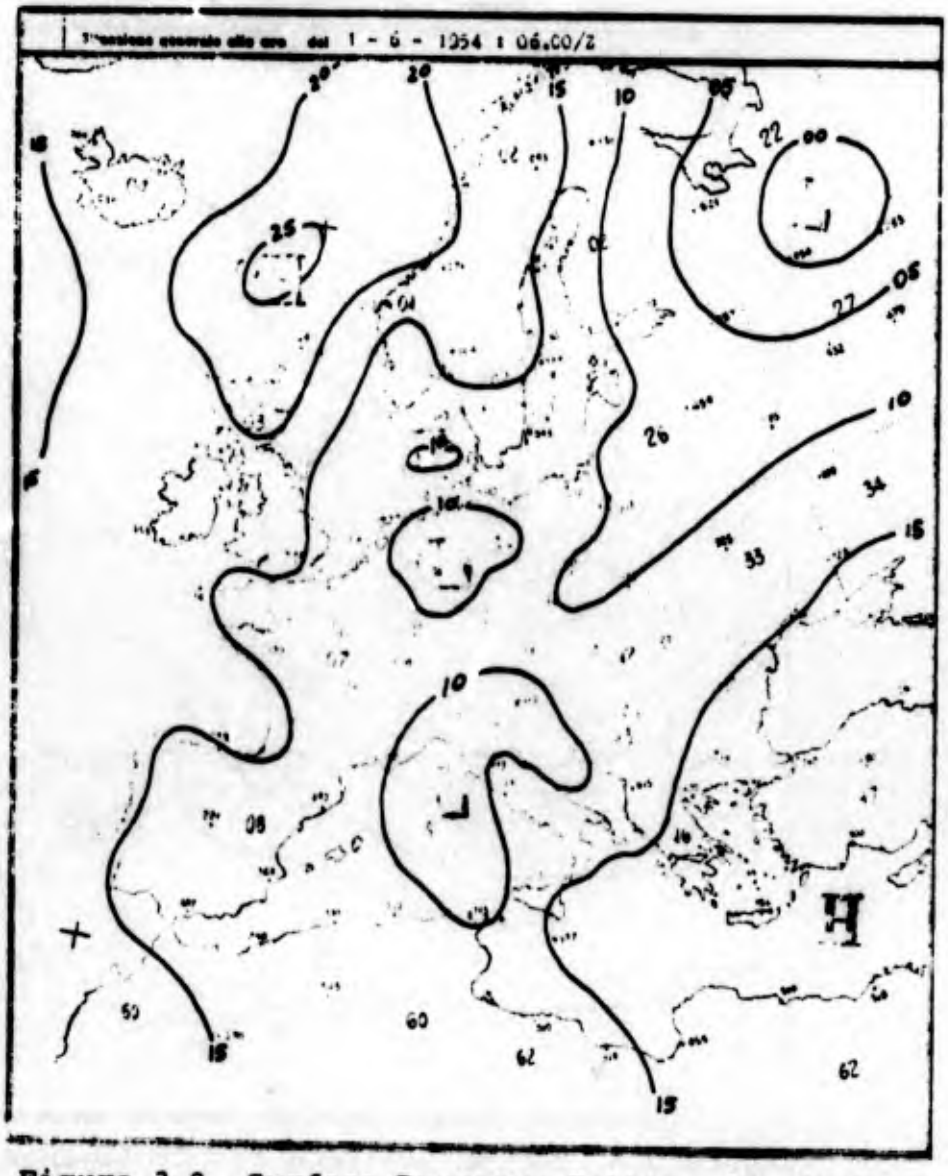

Figure 3.9 Surface Pressure Pattern for Cyclogenesis, Type B_2. [4]

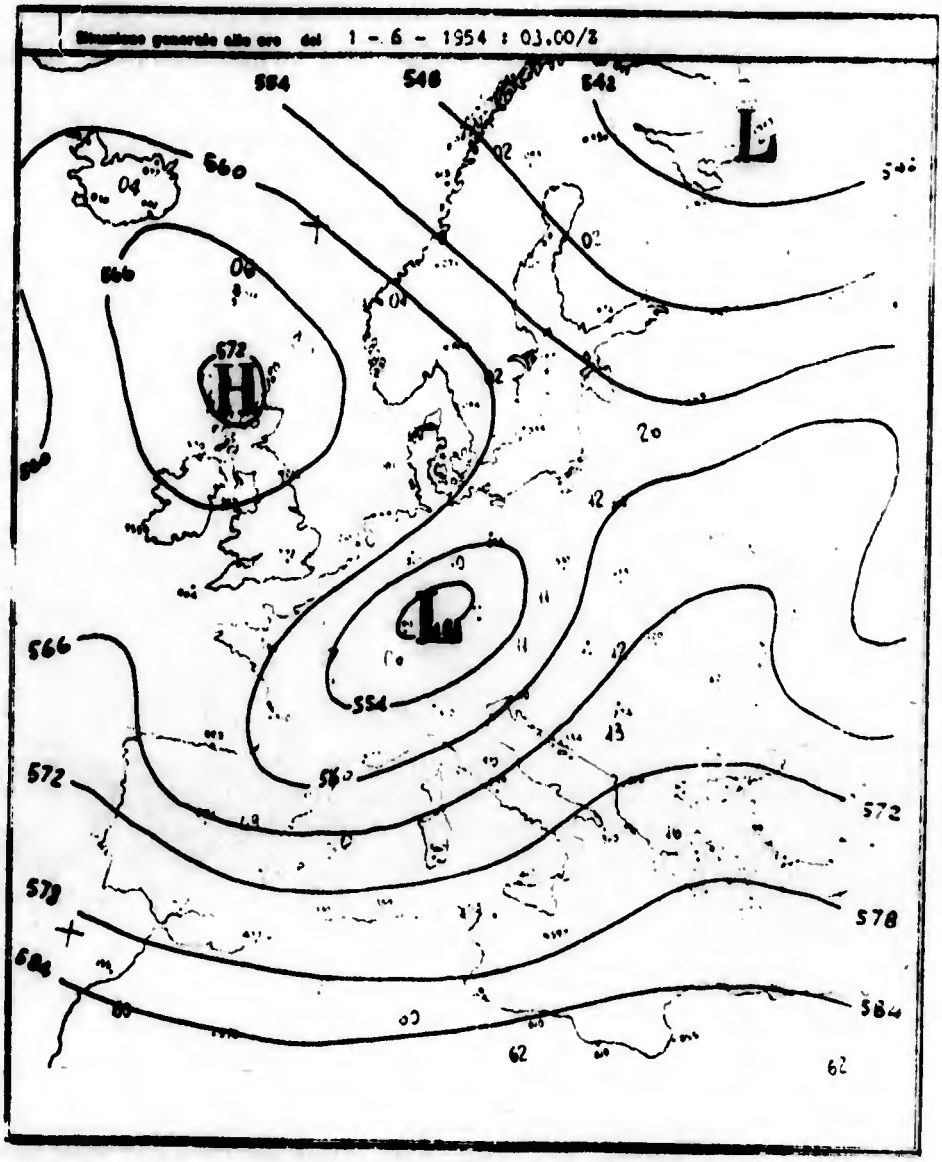

Figure 3.10 500-Mb. Pattern for Cyclogenesis, Type B_2'. [4]

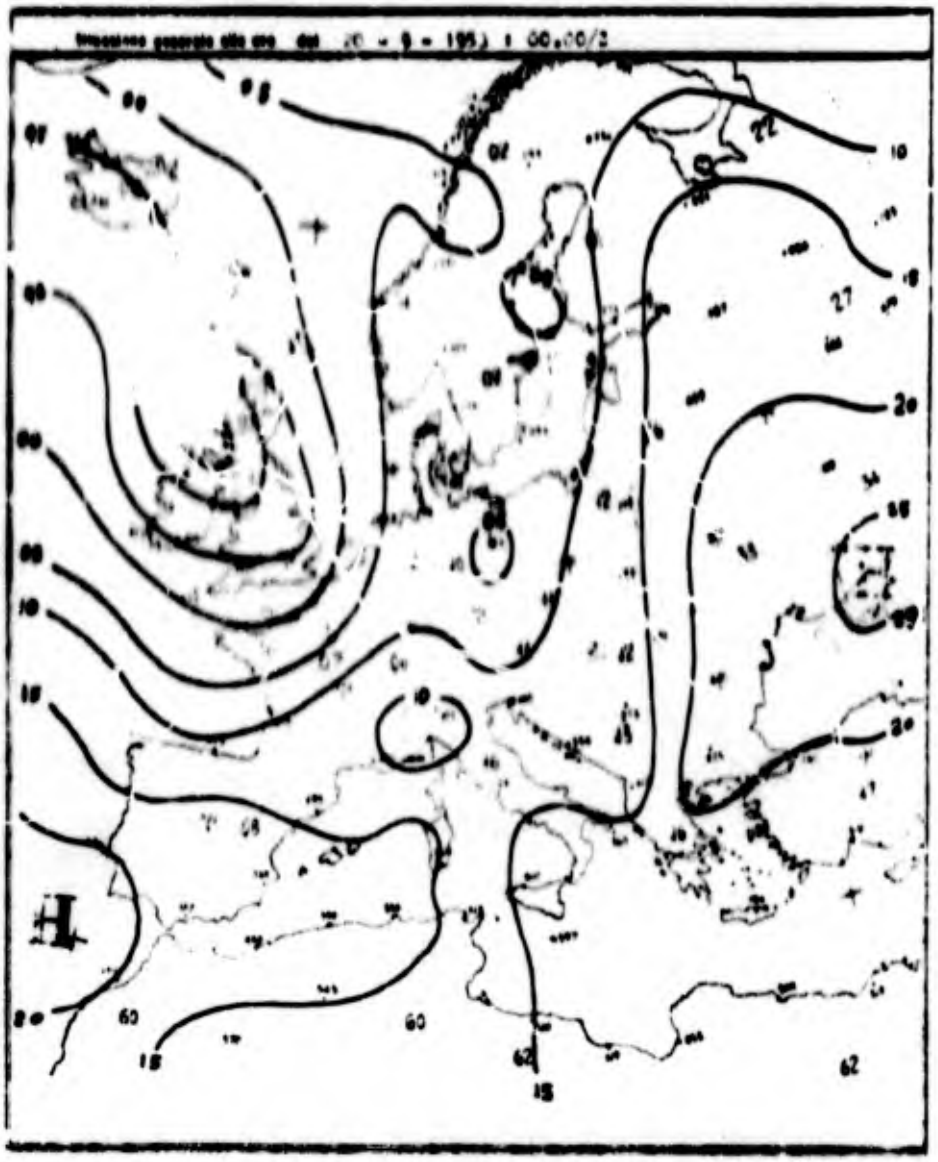

Figure 3.11 Surface Pressure Pattern for Cyclogenesis, Type B_3. [4]

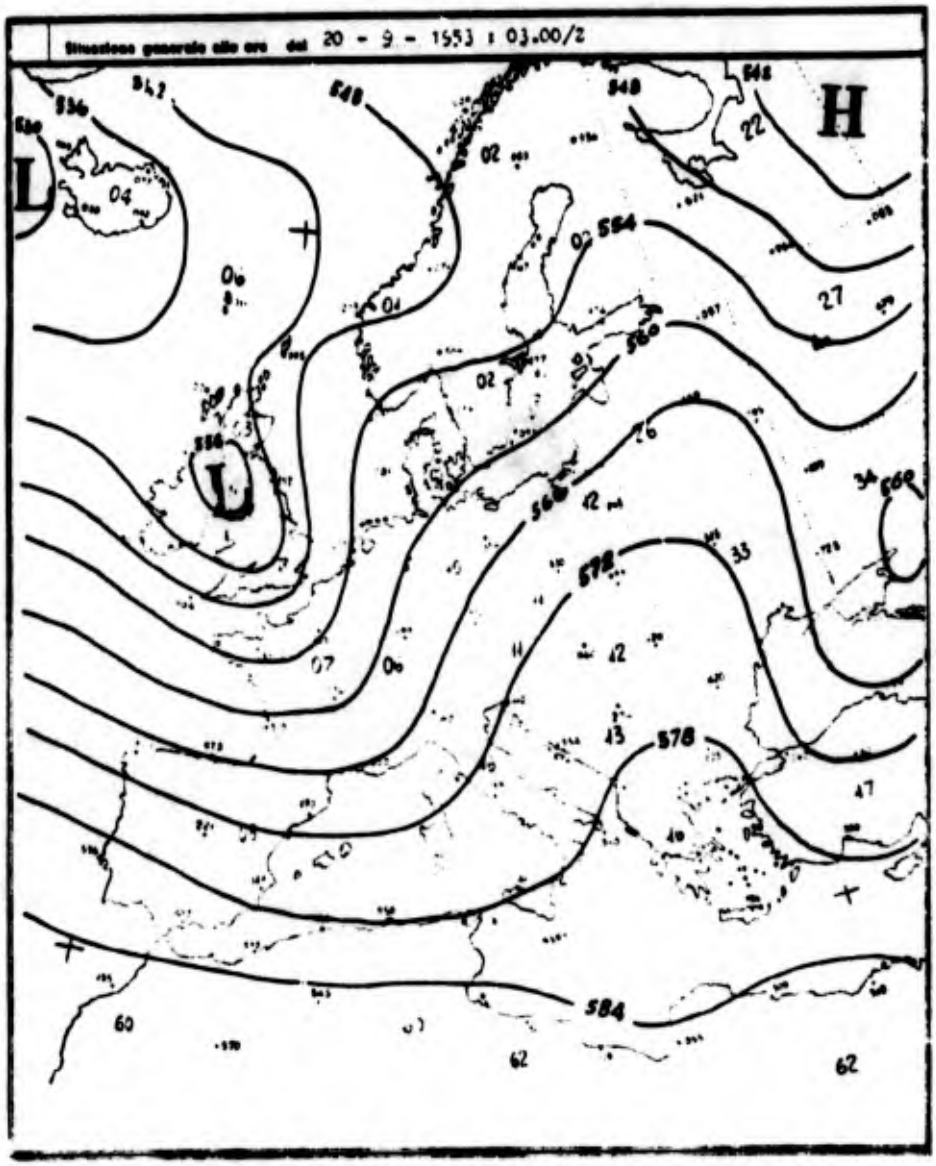

Figure 3.12 500-Mb. Pattern for Cyclogenesis, Type B_3'. [4]

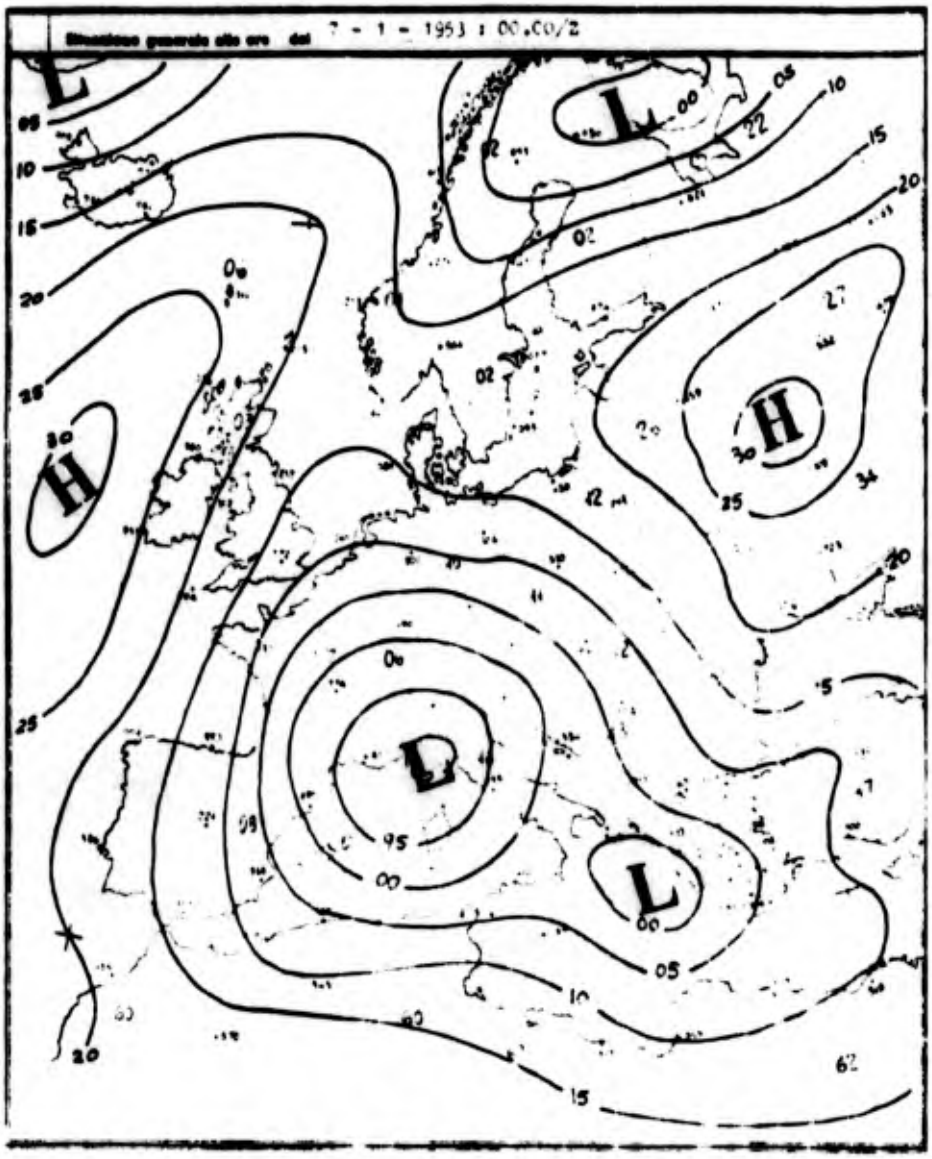

Figure 3.13 Surface Pressure Pattern for Cyclogenesis, Type B_4. [4]

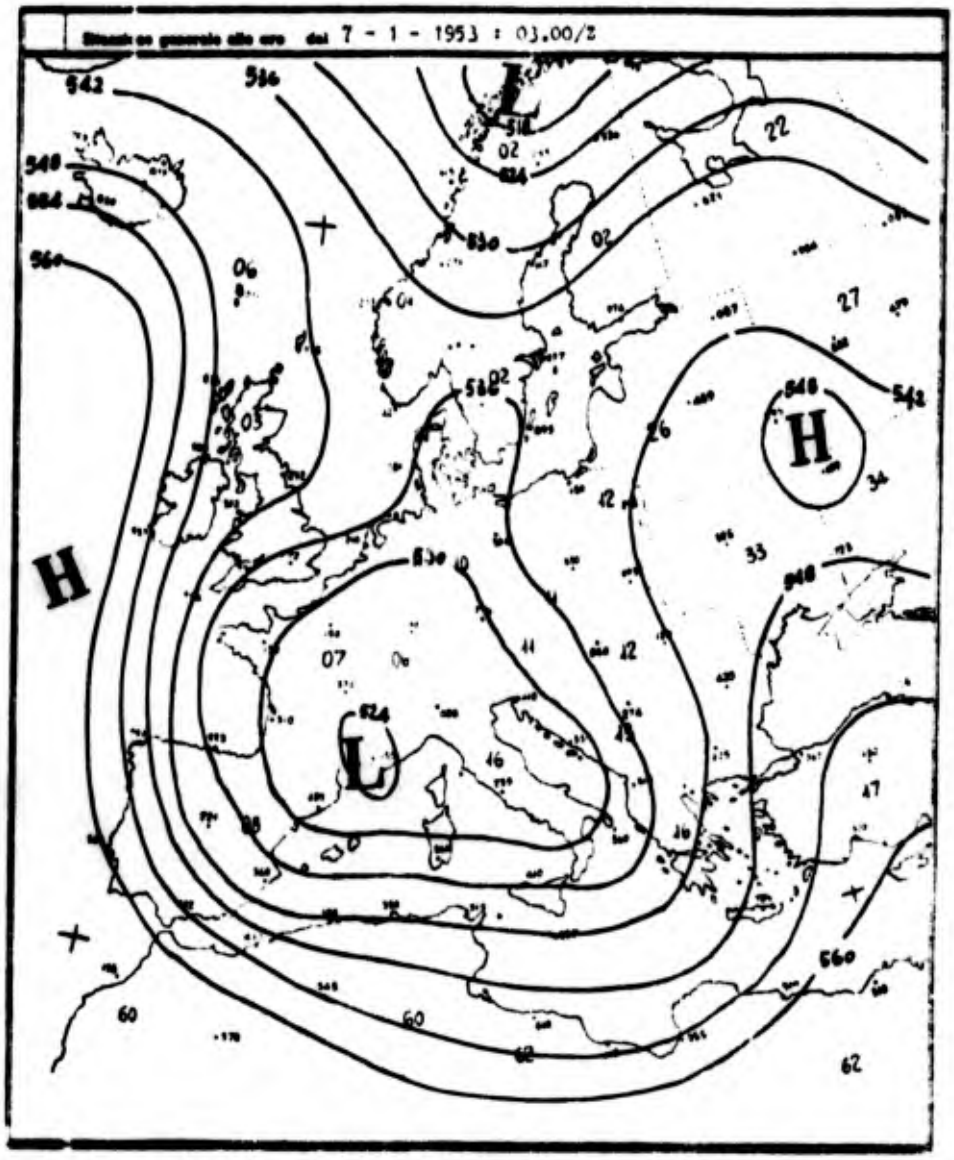

Figure 3.14 500-Mb. Pattern for Cyclogenesis, Type B'_4. [4]

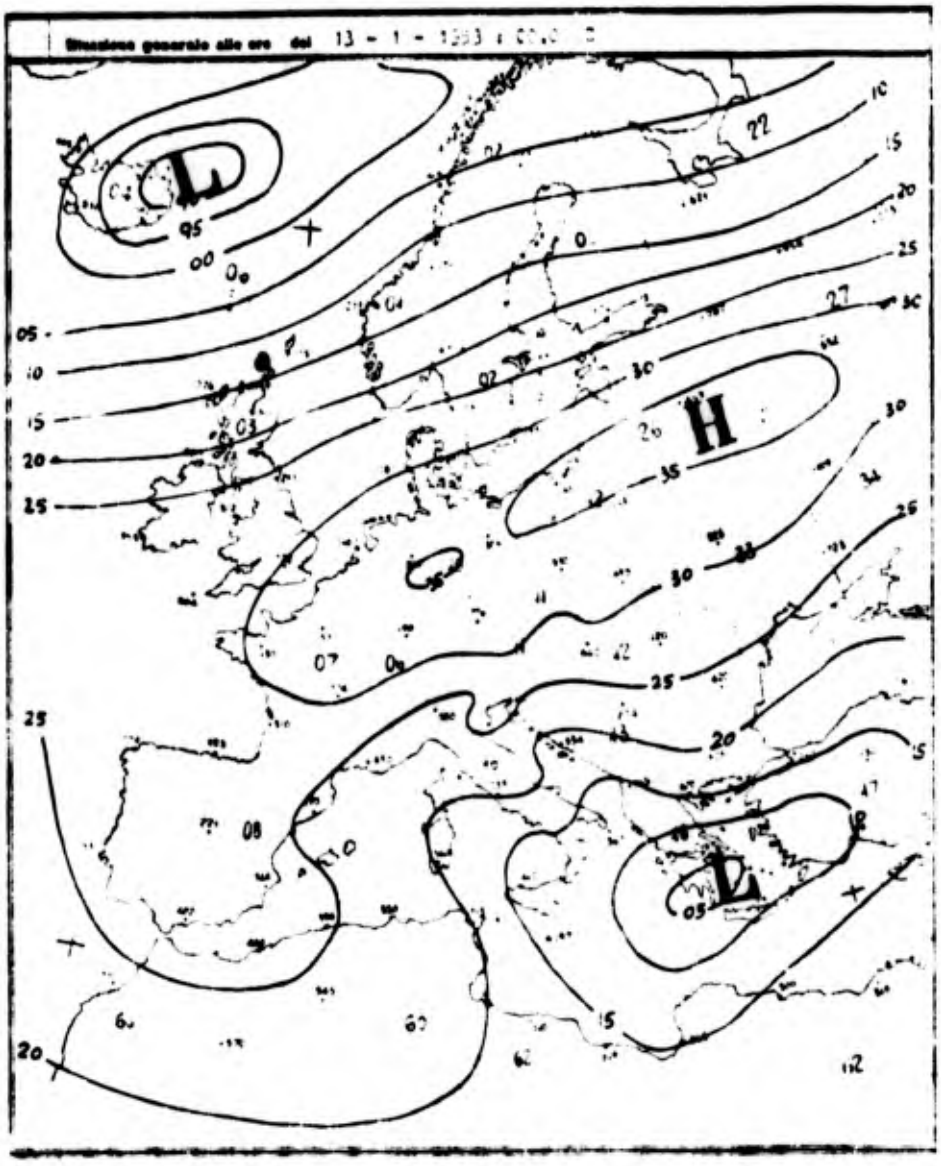

Figure 3.15 Surface Pressure Pattern for Cyclogenesis, Type C. [4]

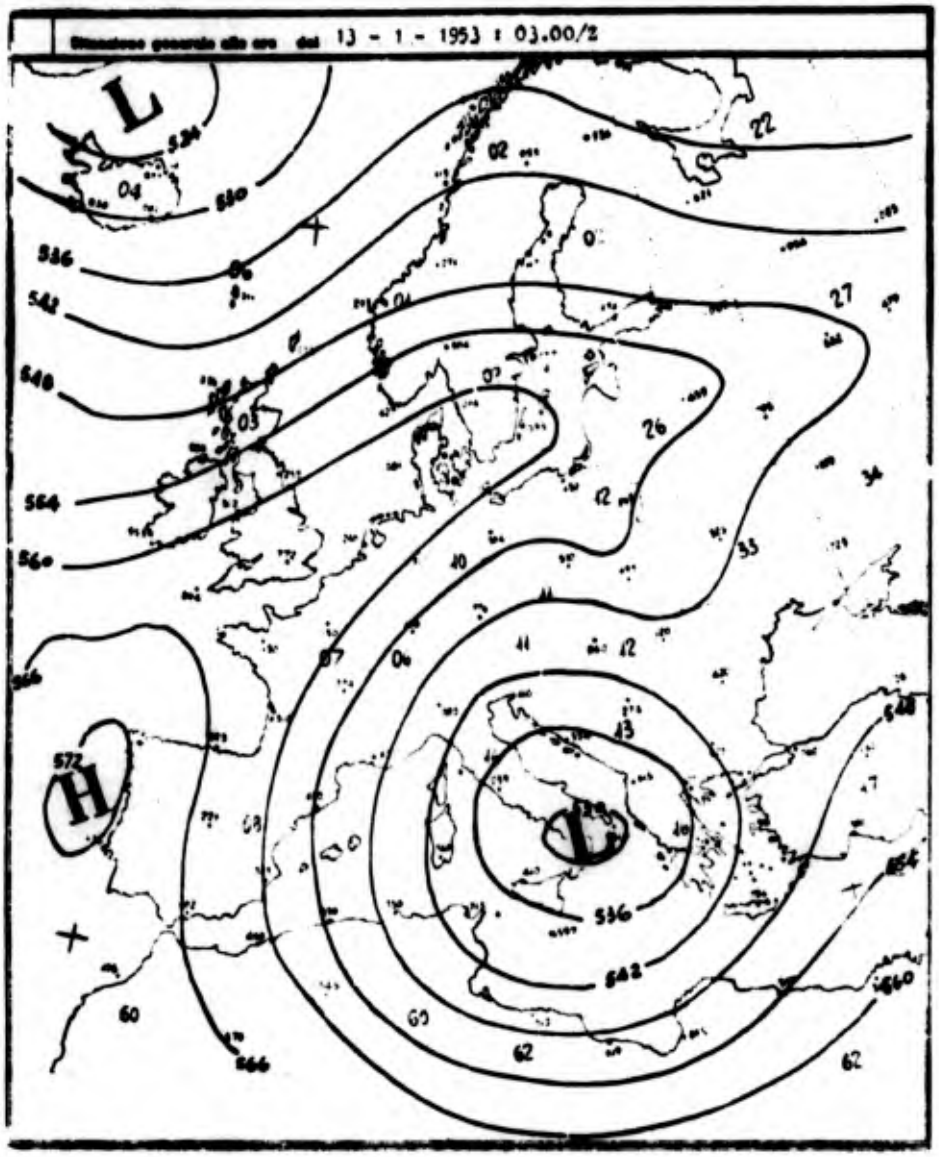

Figure 3.16 500-Mb. Pattern for Cyclogenesis, Type C'. [4]

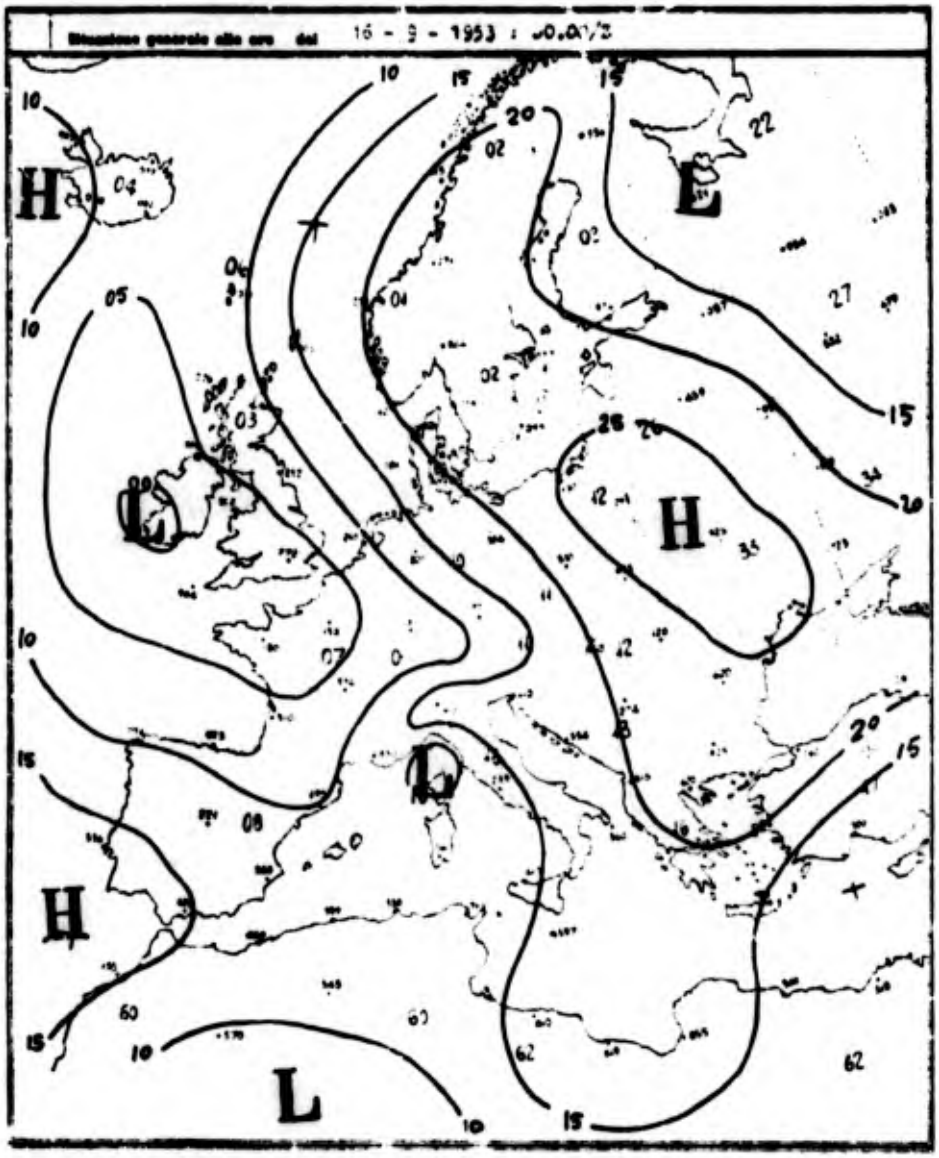

Figure 3.17 Surface Pressure Pattern for Cyclogenesis, Type F. [4]

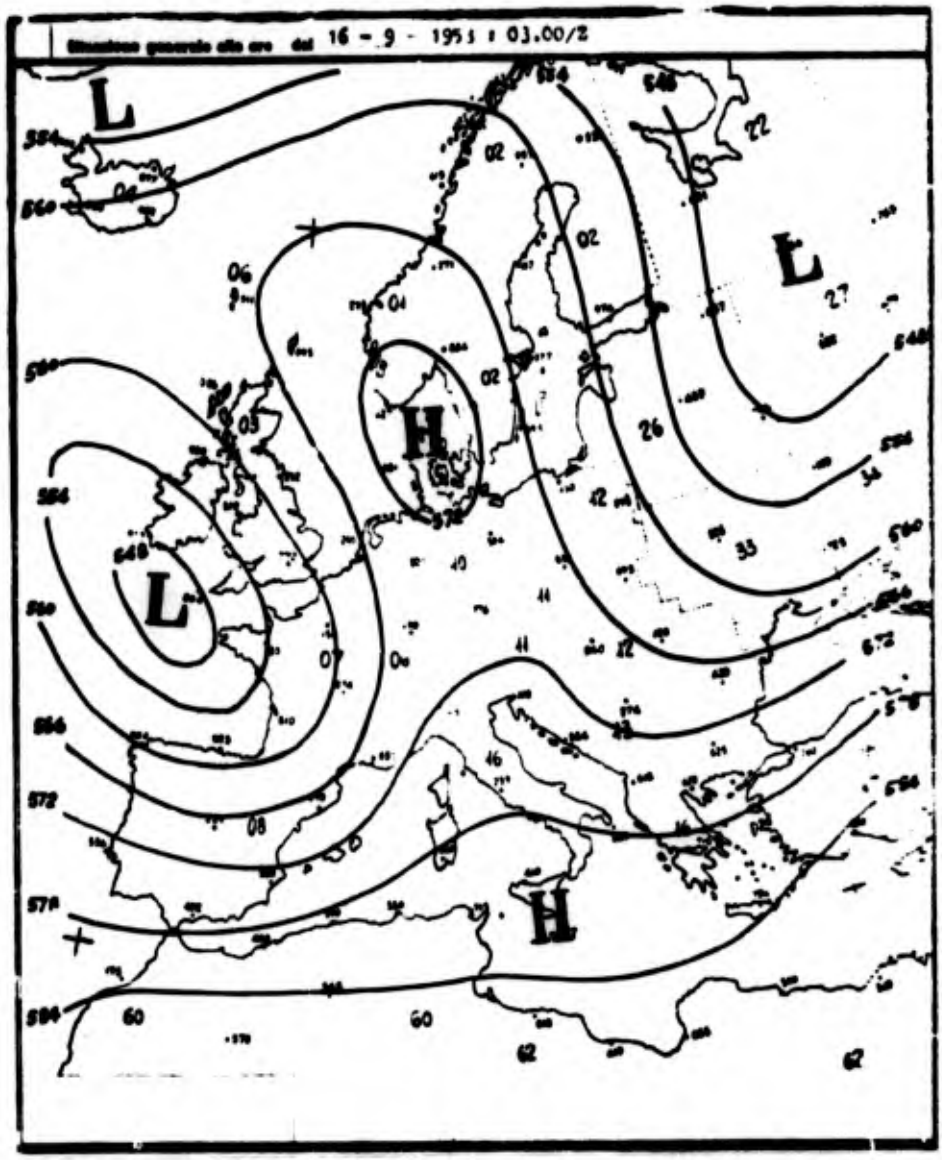

Figure 3.18 500-Mb. Pattern for Cyclogenesis, Type F'. [4]

The maximum number of cases in any one year was 86 (1947) and the minimum 41 (1961) [4].

Types B (B') occur most frequently, with B_3 most common for the surface and B_1' for the upper air (see figs. 3.19(a) and (c)). A comparison with section 2 reveals that types B (B') also favor mistral development, perhaps more so than most of the other types of cyclogenesis. (The surface pressure pattern of type C is suggestive of mistral Type III which is relatively short-lived.)

Surface cyclogenesis in the lee of the Alps -- irrespective of the type -- may occur throughout the year. There is an indication of a weak maximum in the frequency of upper-air patterns associated with surface cyclogenesis during the autumn and winter (fig. 3.19(b)). From the surface patterns two rather weak frequency maxima appear, one in winter and one in summer (fig. 3.19(d)). The latter is probably caused by the thermal effect of warm air over the Po valley. Figure 3.20 suggests that the summer maximum of the surface patterns related to cyclogenesis is mainly of types A_1 and B_1, whereas type B_3 reveals a pronounced summer minimum. In upper-air patterns related to surface cyclogenesis, the frequency distribution among the various types is much more random. Only type B_3' seems to have a pronounced preference for autumn and winter (fig. 3.21).

The actual occurrence of cyclones observed over the Ligurian Sea reveals a maximum in autumn and spring as indicated by table 3.1 [5]:

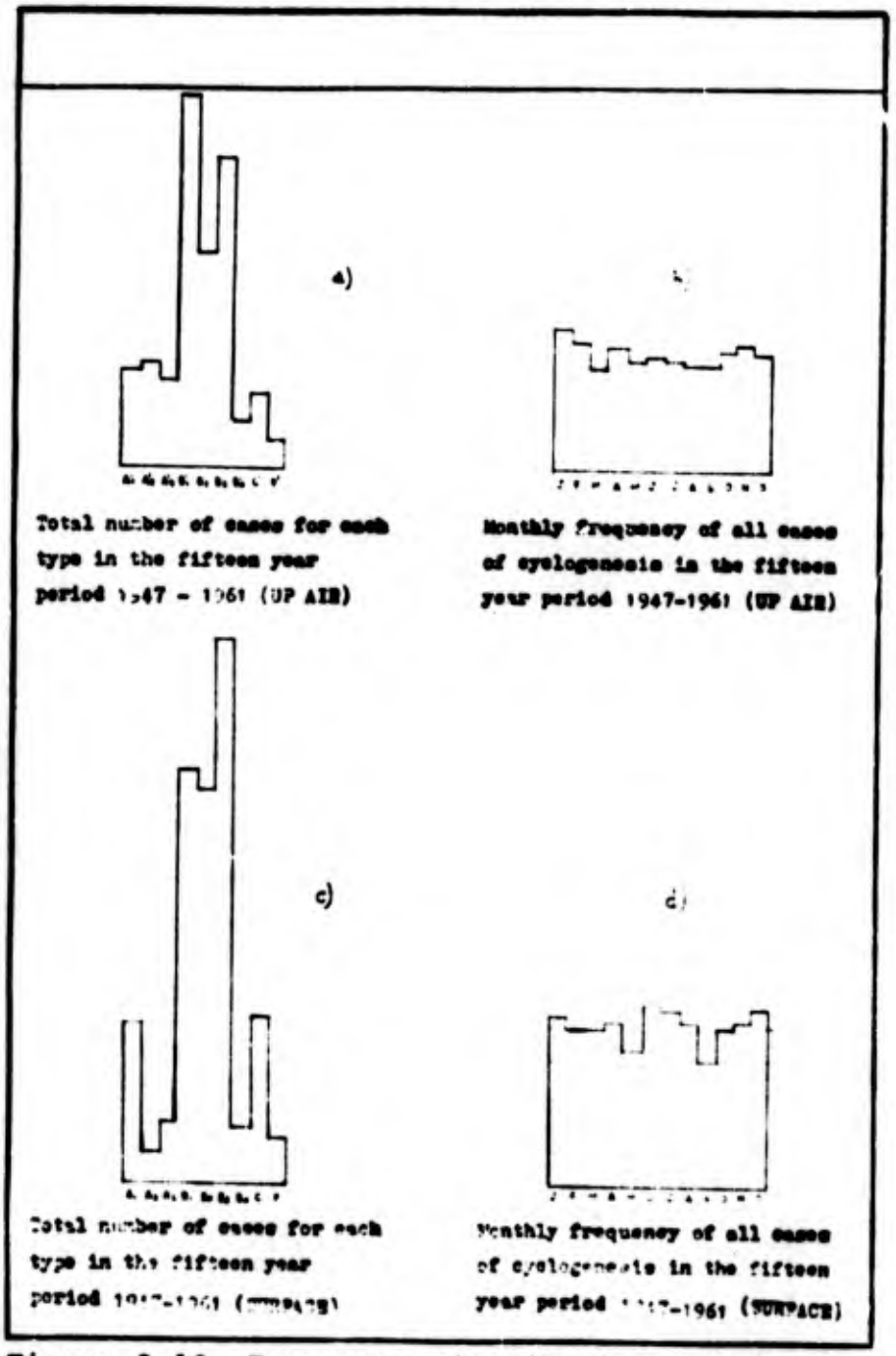

Figure 3.19 Frequency Distributions of the Occurrence of Various Types of Surface Cyclogenesis for (a) the Upper Air Types and (c) the Surface Types During the 15-Year Period 1947-1961; Monthly Frequency Distributions of All Cases of Cyclogenesis for (b) the Combined Upper Air Types and (d) the Combined Surface Types During the Same Time Period. [4]

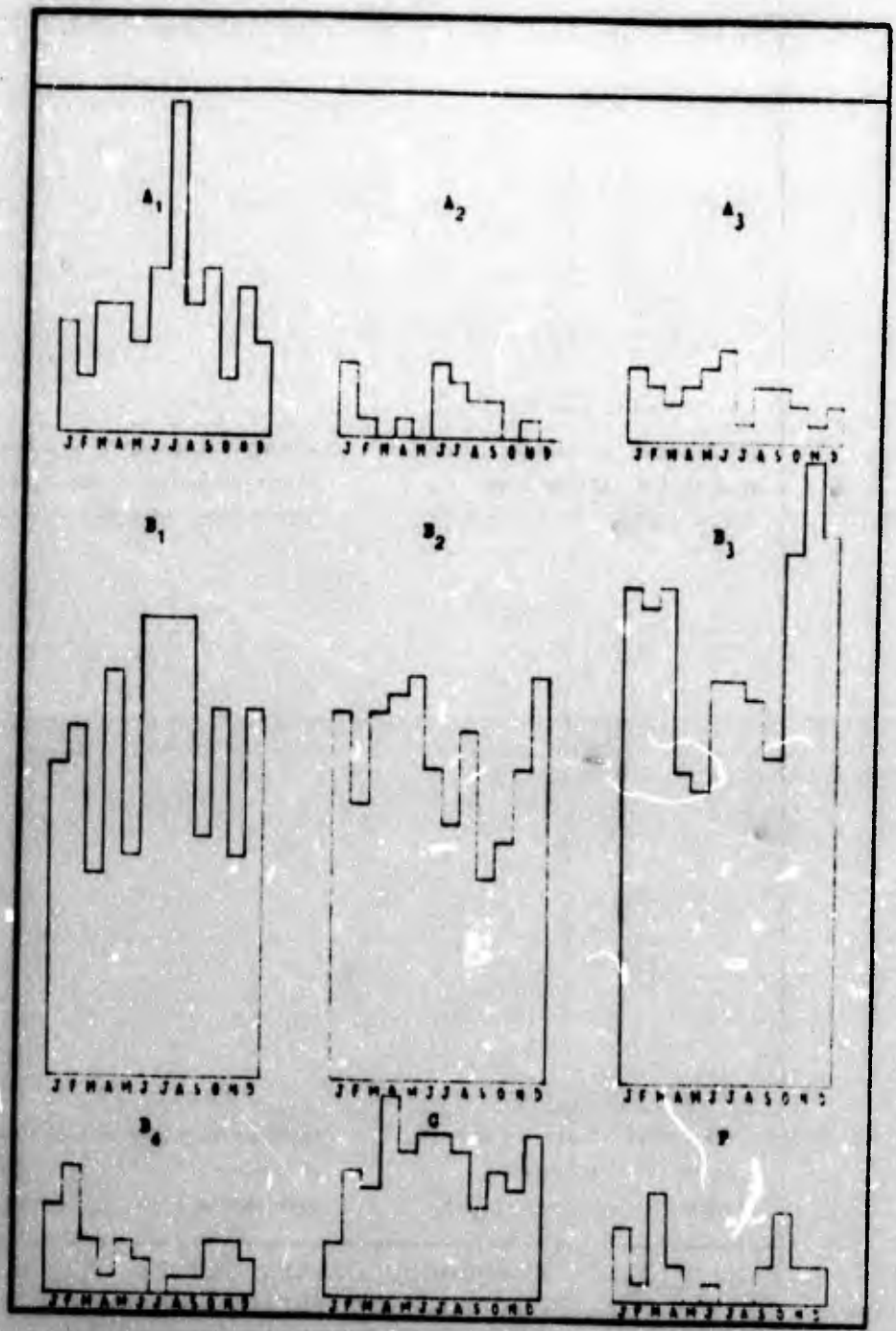

Figure 3.20 Monthly Frequency Distribution of Various Types of Cyclogenesis for Surface Types During the Time Period 1947-1961. [4]

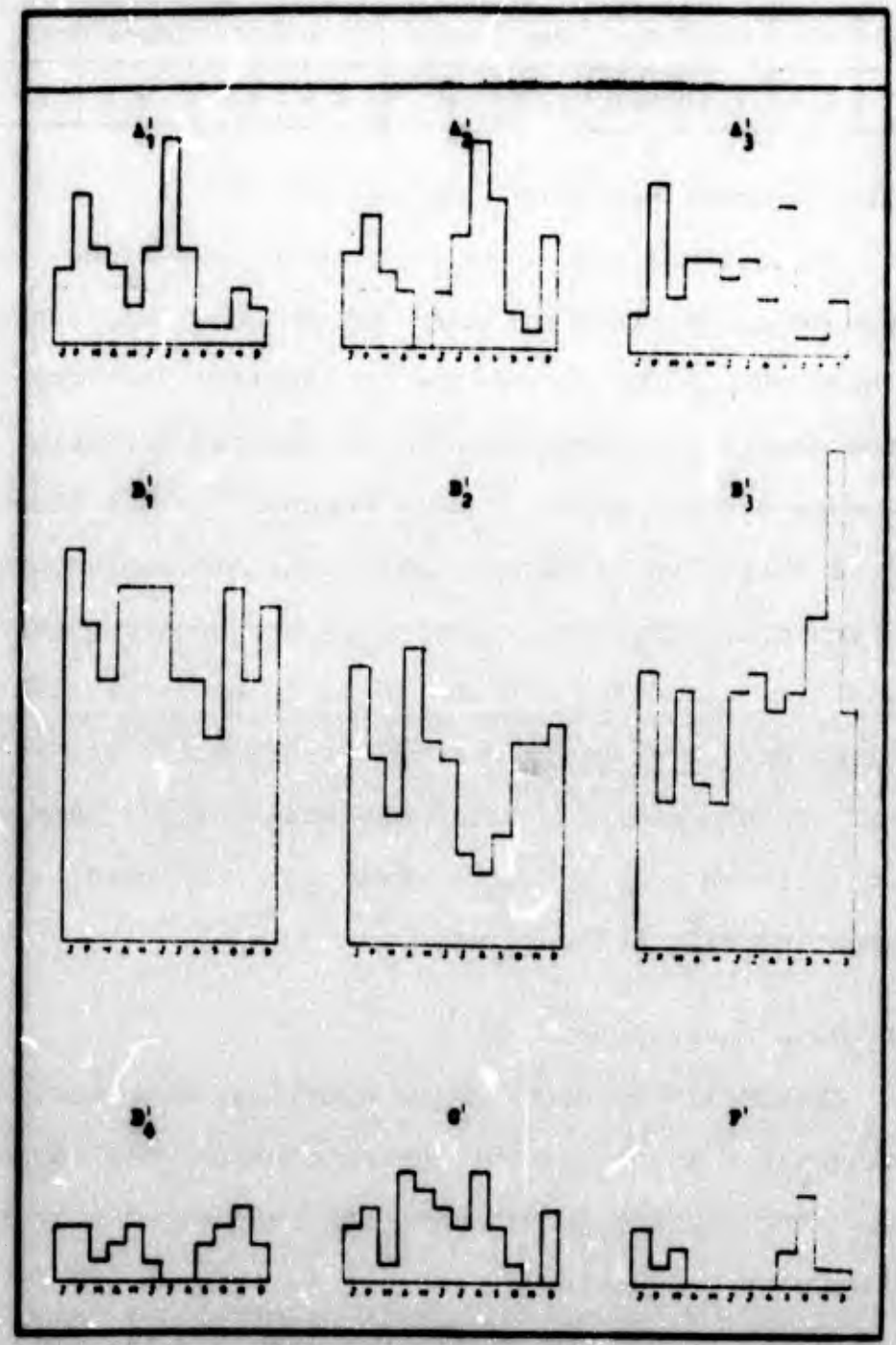

Figure 3.21 Monthly Frequency Distributions of Various Types of Cyclogenesis for the Upper Air Types During the Time Period 1947-1961. [4]

Table 3.1. Average Number of Days Per Month (1952-1961) With Low Over Ligurian Sea.

Jan	Feb	Mar	Apr	May	June	July	Aug	Sept	Oct	Nov	Dec
6.7	5.8	7.1	6.8	5.7	4.5	4.8	4.1	4.8	7.3	10.1	6.5

3.3.3 Diurnal Variation

The diurnal variation of cyclogenesis appears to be related to the diurnal pressure variation. This has been pointed out in the discussion of figure 1.3. Appendix A contains detailed information on the diurnal variation of surface pressure and its seasonal differences. It has been mentioned before that these pressure variations are reflected in land- and sea-breeze systems which are superimposed upon synoptic-scale flow patterns. It should be pointed out that appendix A gives only <u>average</u> values of the diurnal pressure variation. On a day-to-day basis one would expect some modification of these values due to changing cloudiness, tropospheric diurnal heating and cooling, etc.

3.4 Case Description

CENTAM (1963) contains an excellent case analysis of cyclogenesis in the lee of the Alps which will be reproduced here. The surface isobar patterns, and especially the upper-air development patterns, conform to types B_1, B_1' (transition to B_4, B_4') shown in figures 3.7 to 3.14. The present case study thus describes the most frequent type of lee cyclogenesis. It also conforms to the period illustrated in figure 1.3. A blocking ridge over the western Atlantic and a

trough over Scandinavia and eastern Europe at 0000 GMT on 17 February 1958 indicate a low-index flow pattern (fig. 3.22(b)).

It is worth noting that cyclogenesis is already evident between 1200 GMT 17 February and 0000 GMT 18 February, long before the cold front overruns the Alps. At 1200 GMT 18 February, the cold front appears "wrapped around" the arch of the Alps and advances from the east into northern Italy. This advance was probably accompanied by a period of bora winds along the coast of northern Yugoslavia.

Figure 3.23 shows the mean sea-level pressure field of 17 and 18 February 1958. It clearly reveals the double structure of the low, one center lying over the Gulf of Genoa and branching into the upper Po valley (Piedmont), the other over the northern Adriatic Sea. The temperature for the same period, reduced to sea level with an assumed lapse rate of 0.6° C./100 m. is shown in figure 3.24. The advance of the cold air from the northeast rather than from the west is clearly evident from this diagram. Figure 3.25 illustrates the advance of the cold front by hourly positions on 18 and 19 February 1958. Again, this diagram shows that the front advances into northern Italy from the east. Only as the cold front reaches the middle Po valley do we find a rapid advance of the cold air to the west of the Alps into the Ligurian Sea.

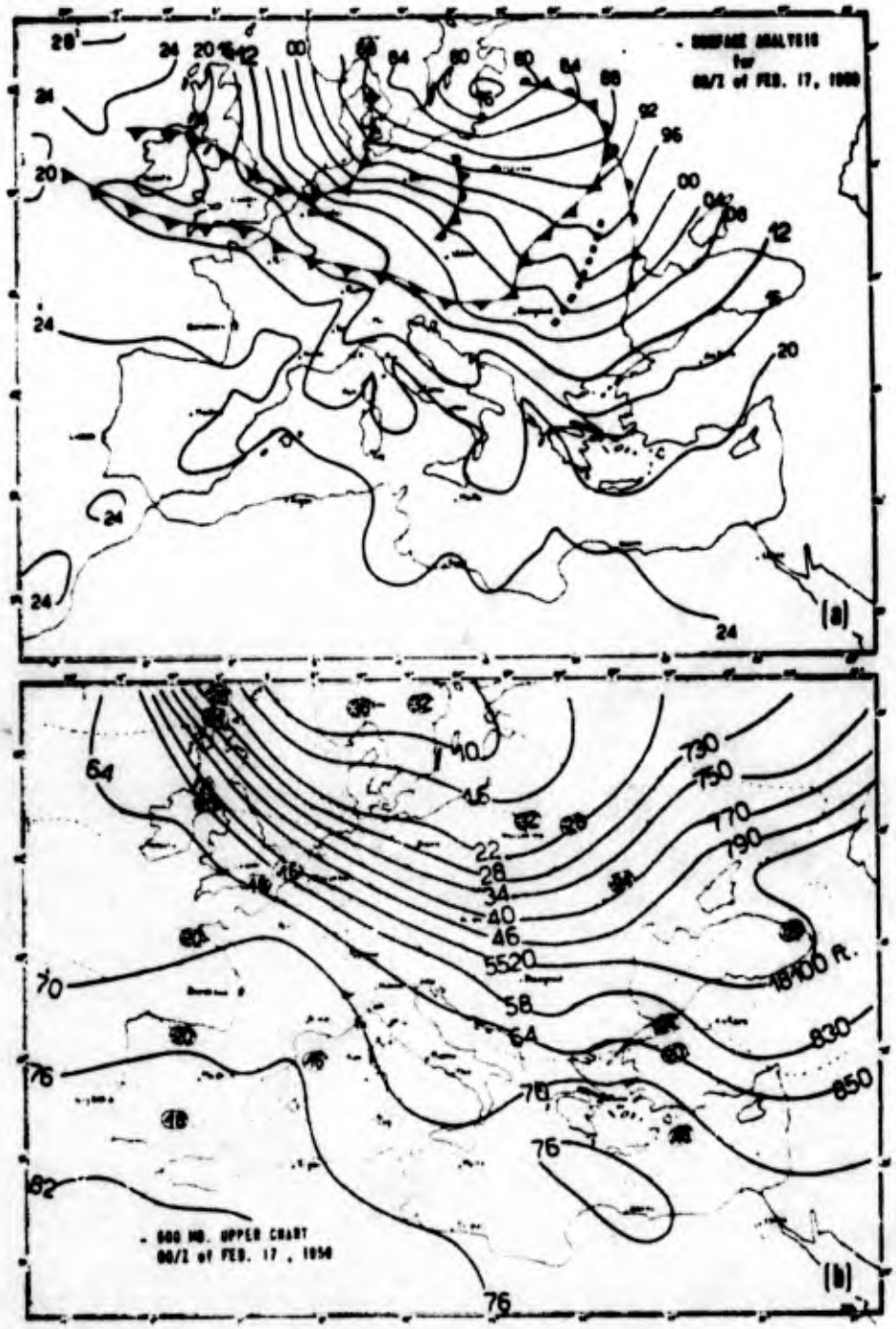

Figure 3.22 Surface and 500-Mb. Analysis for a Case of Genoa Cyclogenesis in February 1958. [4]

trough over Scandinavia and eastern Europe at 0000 GMT on 17 February 1958 indicate a low-index flow pattern (fig. 3.22(b)).

It is worth noting that cyclogenesis is already evident between 1200 GMT 17 February and 0000 GMT 18 February, long before the cold front overruns the Alps. At 1200 GMT 18 February, the cold front appears "wrapped around" the arch of the Alps and advances from the east into northern Italy. This advance was probably accompanied by a period of bora winds along the coast of northern Yugoslavia.

Figure 3.23 shows the mean sea-level pressure field of 17 and 18 February 1958. It clearly reveals the double structure of the low, one center lying over the Gulf of Genoa and branching into the upper Po valley (Piedmont), the other over the northern Adriatic Sea. The temperature for the same period, reduced to sea level with an assumed lapse rate of 0.6° C./100 m. is shown in figure 3.24. The advance of the cold air from the northeast rather than from the west is clearly evident from this diagram. Figure 3.25 illustrates the advance of the cold front by hourly positions on 18 and 19 February 1958. Again, this diagram shows that the front advances into northern Italy from the east. Only as the cold front reaches the middle Po valley do we find a rapid advance of the cold air to the west of the Alps into the Ligurian Sea.

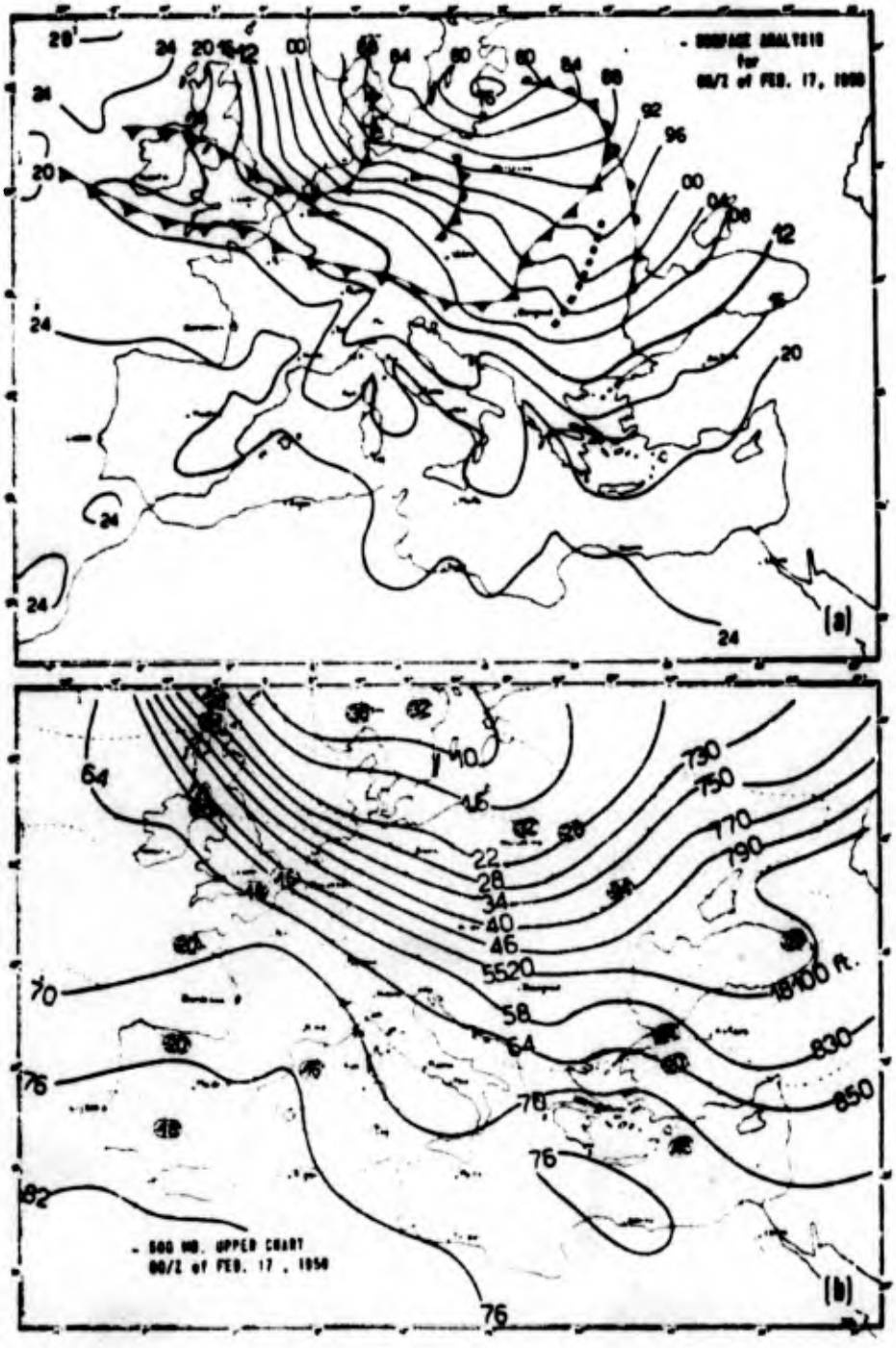

Figure 3.22 Surface and 500-Mb. Analysis for a Case of Genoa Cyclogenesis in February 1958. [4]

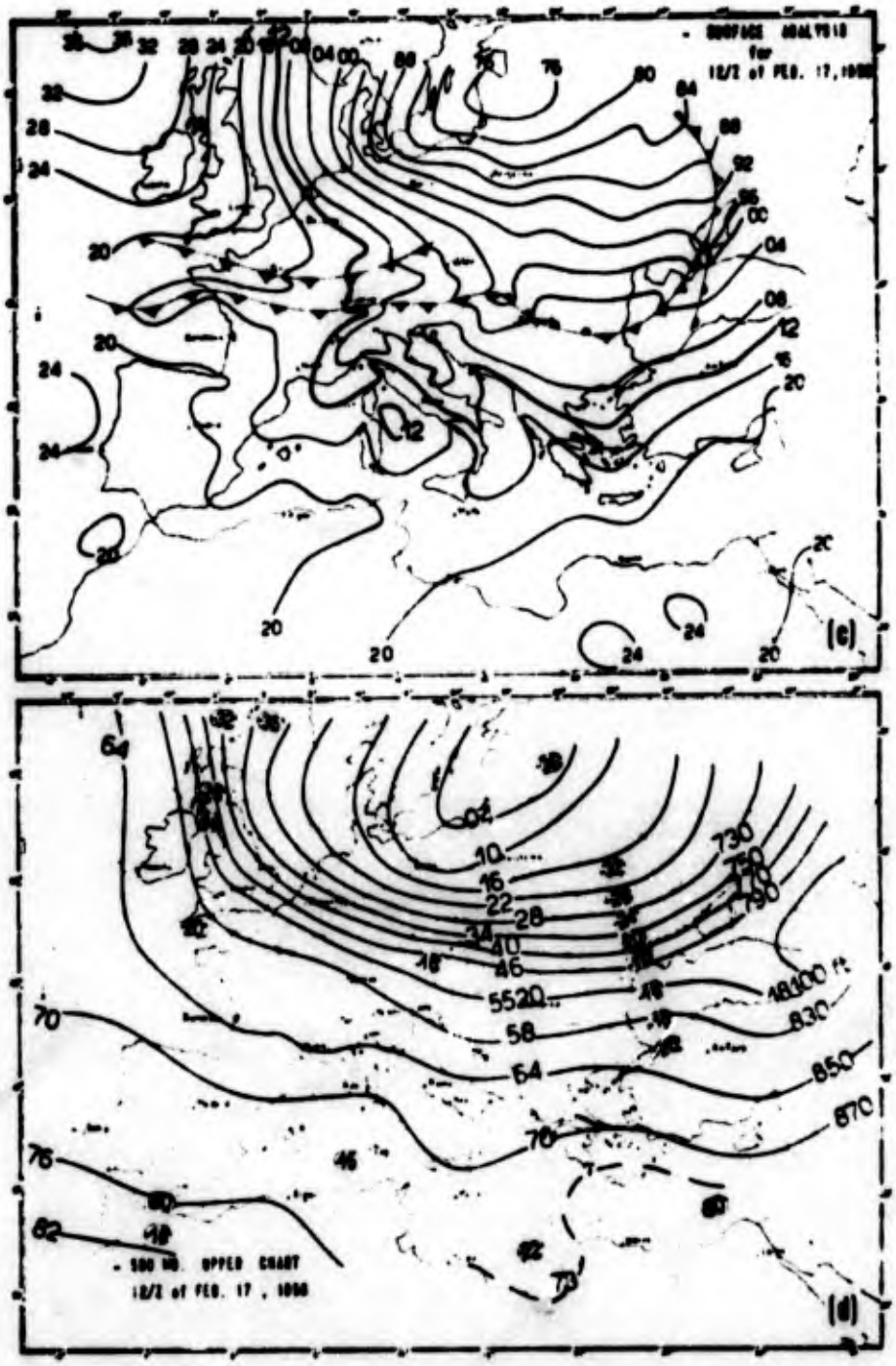

Figure 3.22 (Continued) Surface and 500-Mb. Analysis for a Case of Genoa Cyclogenesis in February 1958. [4]

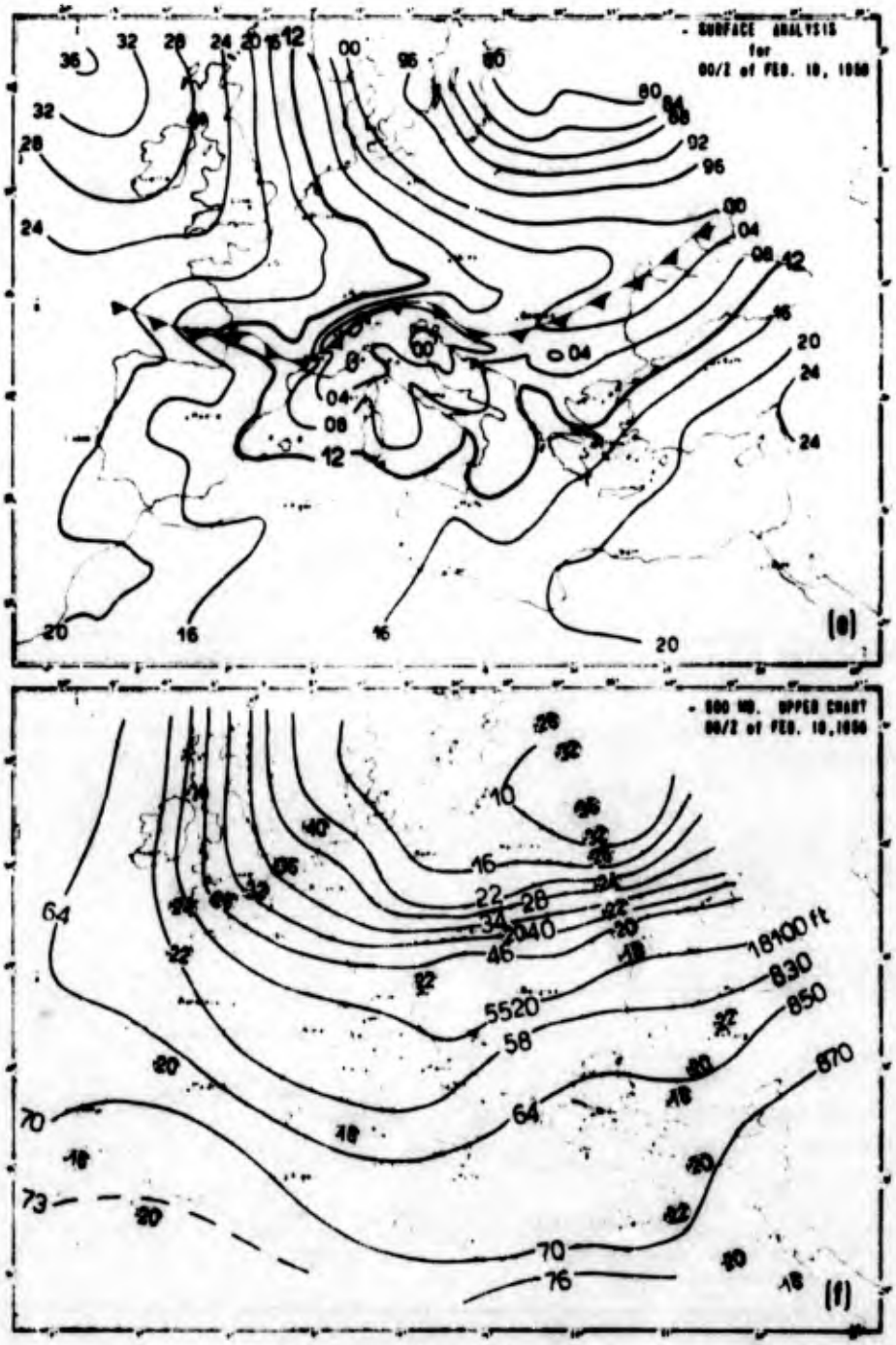

Figure 3.22 (Continued) Surface and 500-Mb. Analysis for a Case of Genoa Cyclogenesis in February 1958. [4]

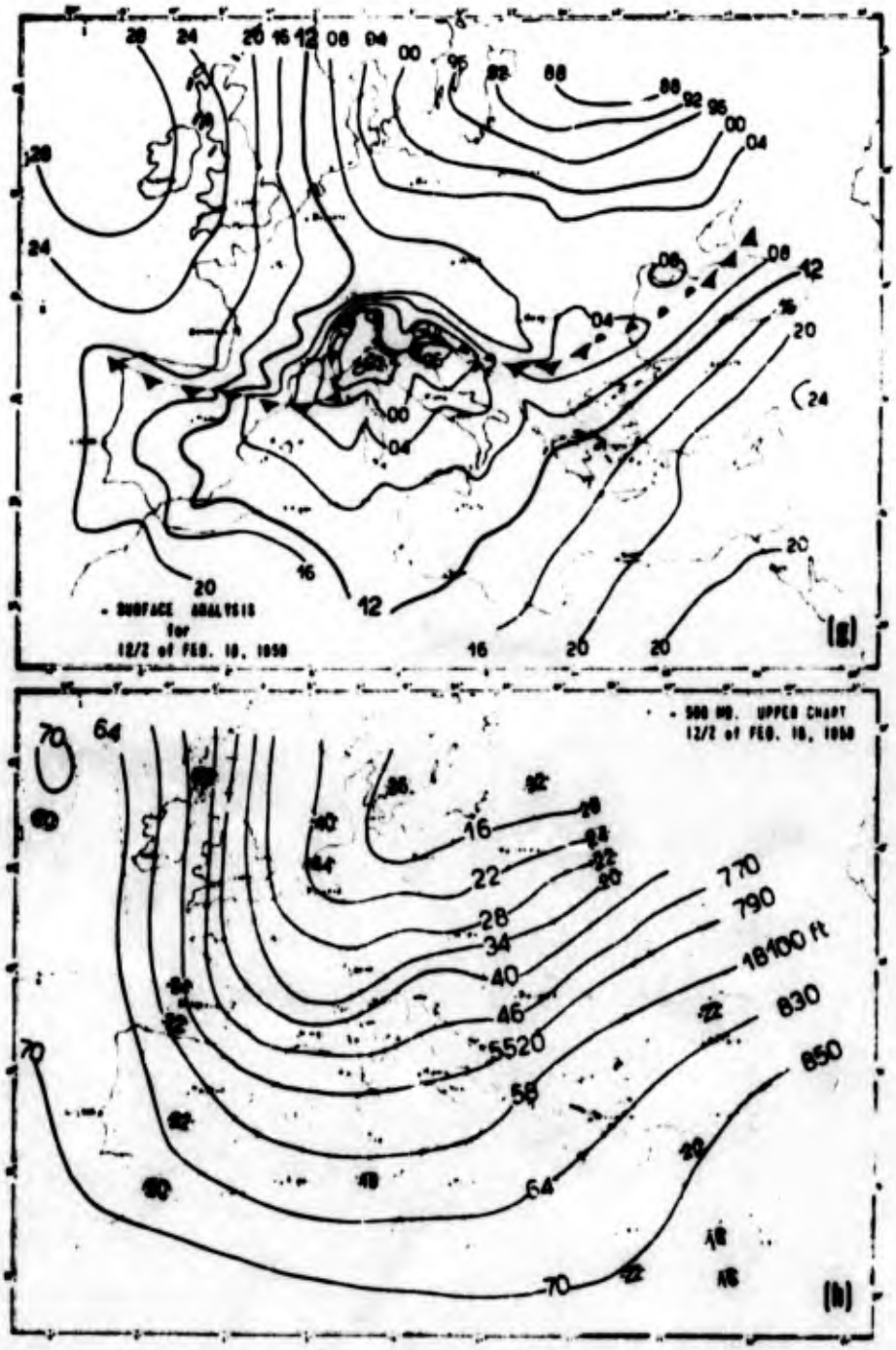

Figure 3.22 (Continued) Surface and 500-Mb. Analysis for a Case of Genoa Cyclogenesis in February 1958. [4]

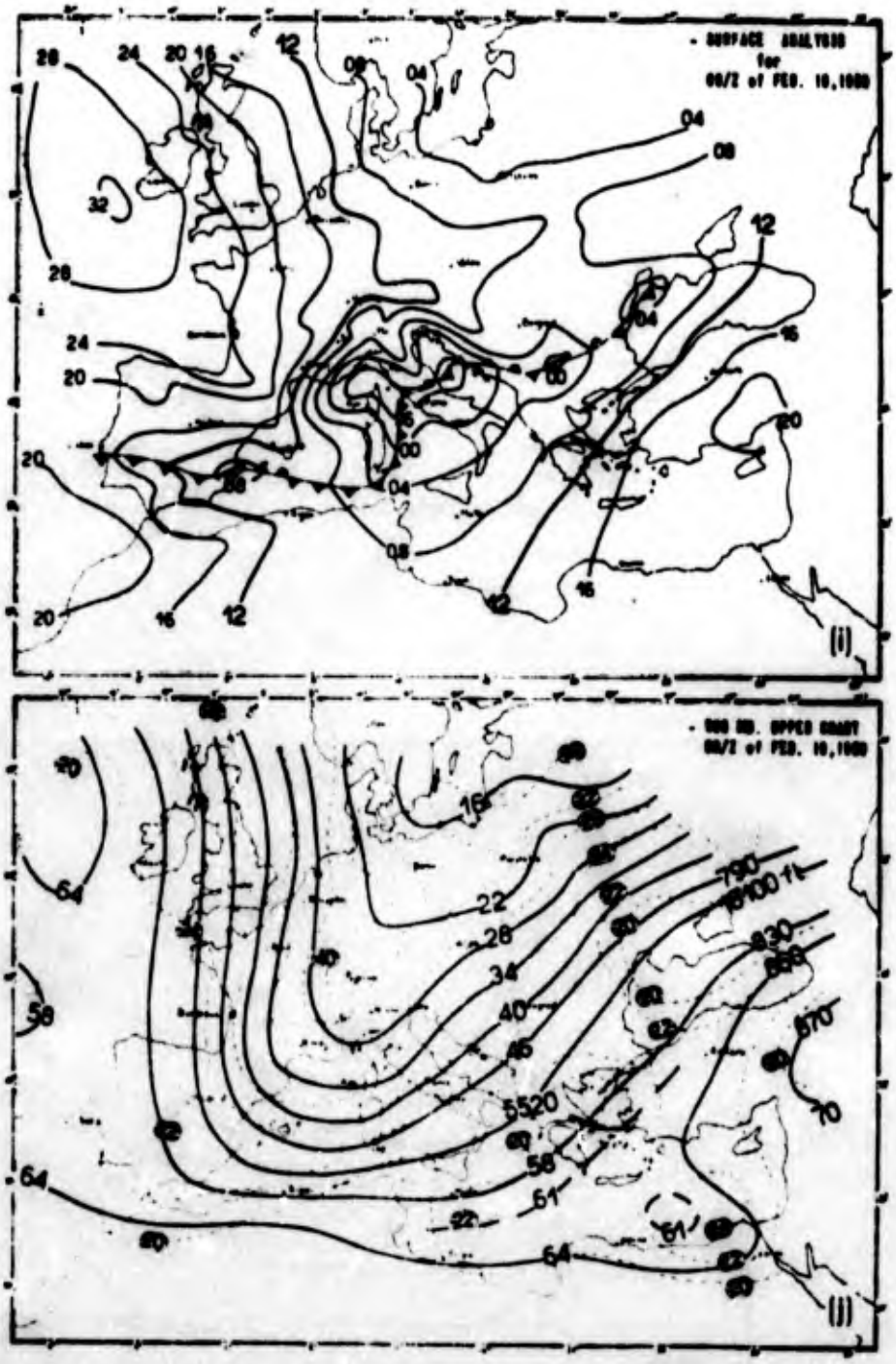

Figure 3.22 (Continued) Surface and 500-Mb. Analysis for a Case of Genoa Cyclogenesis in February 1958. [4]

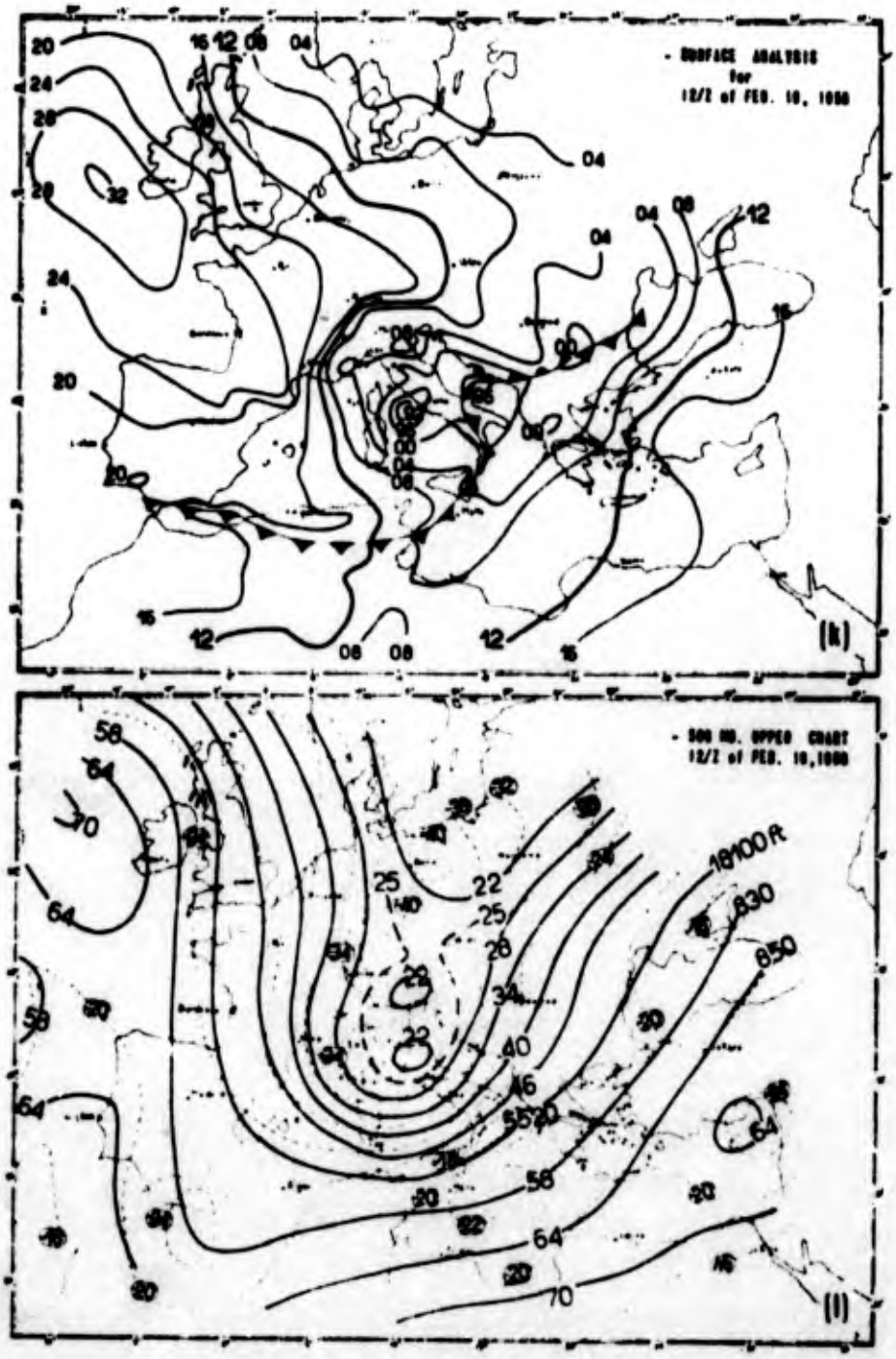

Figure 3.22 (Continued) Surface and 500-Mb. Analysis for a Case of Genoa Cyclogenesis in Feburary 1958. [4]

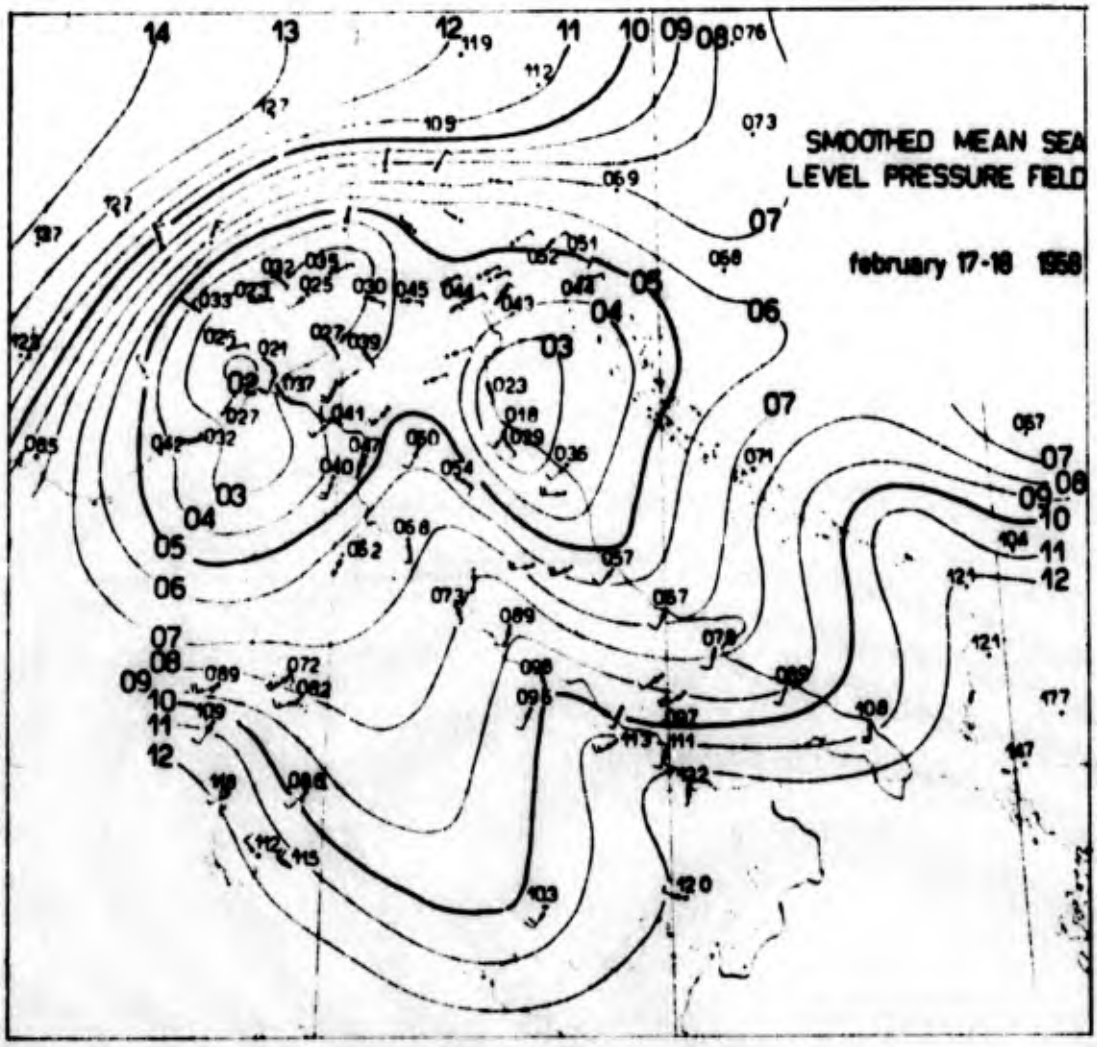

Figure 3.23 Smoothed Mean Sea-Level Pressure Field, 17 to 18 February 1958. [4]

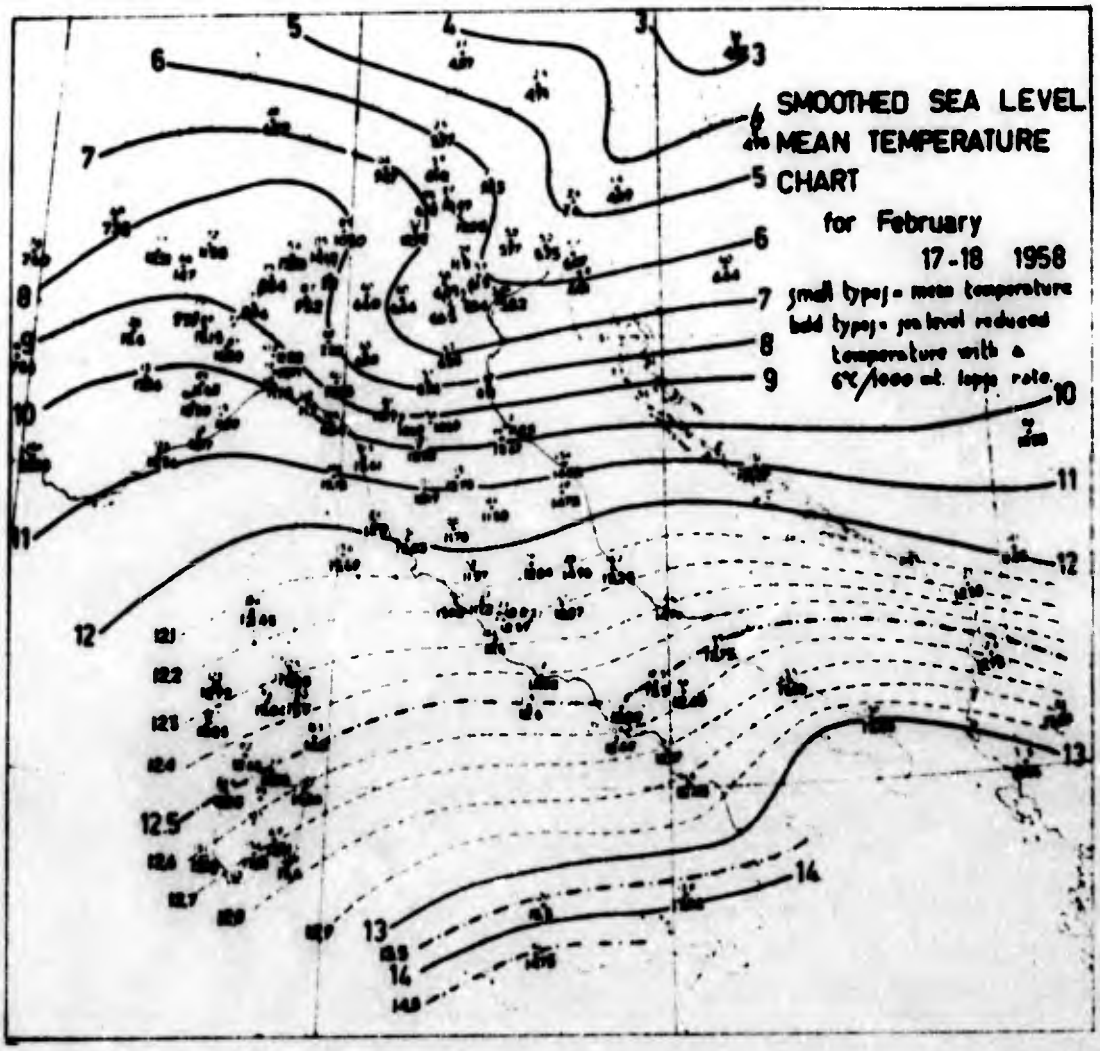

Figure 3.24 Mean Temperature Reduced to Sea Level Under the Assumption of a Lapse Rate of 0.6°C./ 100 M., 17 to 18 Feburary 1958. [4]

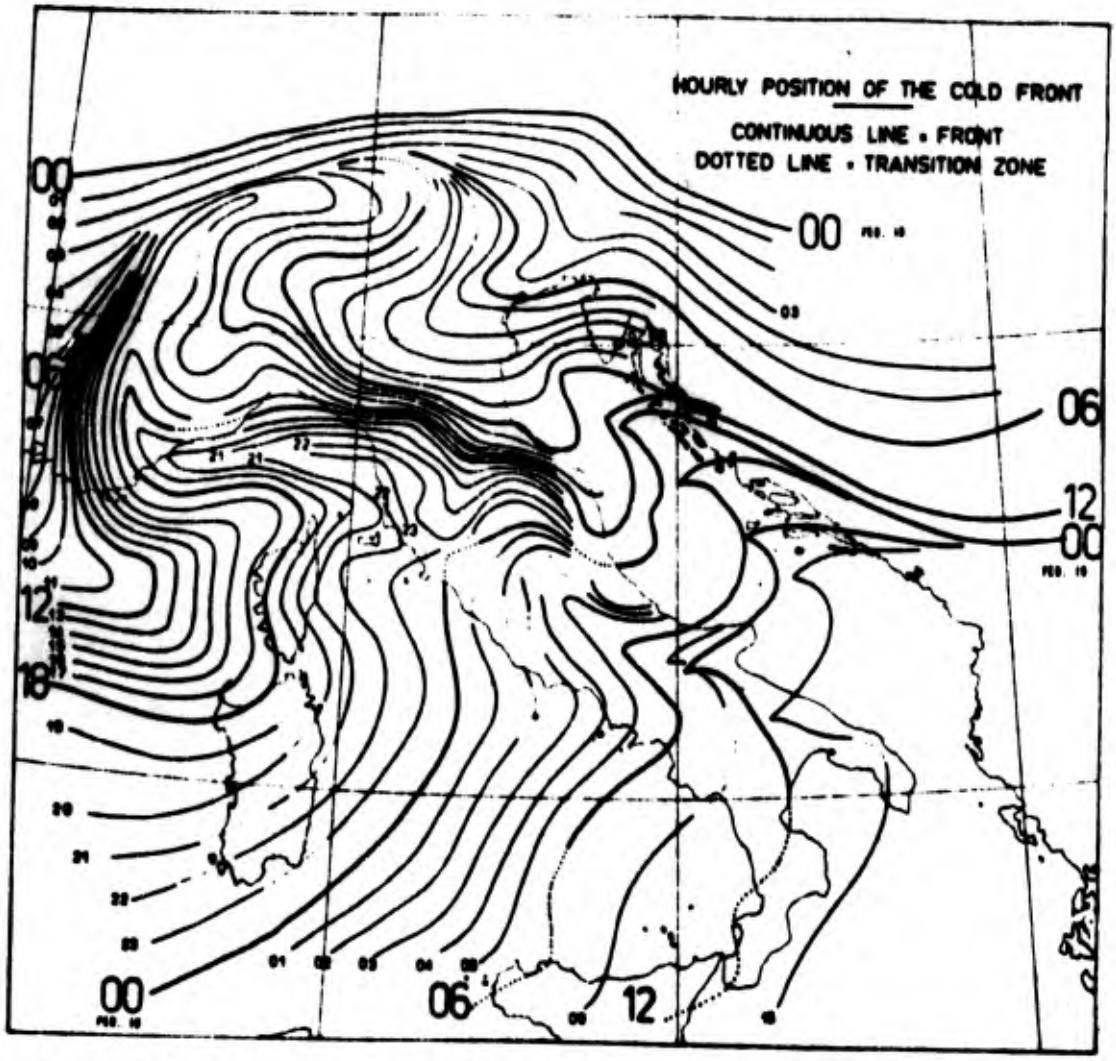

Figure 3.25 Hourly Positions of the Cold Front Between 0000 GMT 18 February 1958 and 1500 GMT 19 February 1958. [4]

3.5 Forecasting of Genoa Cyclogenesis

From the foregoing discussion it appears that Genoa cyclogenesis is intimately linked with the orographic effects of the Alps and, to a lesser degree of importance, with the thermal contrast between land and sea. We should expect, therefore, that numerical forecasting schemes which do not take into account these orographic and thermal effects will fail to predict Genoa cyclogenesis adequately.

George and Wolff [11] investigated surface cyclogenesis in the Mediterranean and found it to be highly dependent on the upper-air flow pattern as given by the contours at 500 mb. Synoptic examples of cyclogenesis following the change from westerly to northwesterly flow and a method for prediction are given in the reference.

From the synoptic example given in section 3.4, it appears that cyclogenesis may occur before the arrival of frontal systems south of the Alps. This differs from the experience of an American forecaster who expects cyclogenesis in the lee of the Rocky Mountains to take place along a frontal system that may have become quasi-stationary over Colorado or northwestern Texas.

Very little in the way of objective forecast techniques is presently available that would supplement numerical prediction models. Therefore, the following should be considered merely as a list of suggestions which will have to undergo critical field tests, and which will be opened to improvement with the help of experienced local forecasters:

(1) The vorticity advection pattern at jet stream level should provide a first clue of upper-divergence occurring over the cyclogenetically active region south of the Alps.

(2) Pressure-fall patterns associated with the movement of upper troughs should be monitored closely. One should keep in mind that a travelling pressure-rise pattern associated with advancing cold air may be blocked along the northern arch of the Alps. This blocking effect may lead to pressure falls on the south side of the Alps which would not normally occur in the absence of mountains.

(3) Genoa cyclogenesis appears to occur readily with deep troughs over Europe. Such troughs are usually the result of the superpostion of long- and short-wave patterns. Continuity diagrams may provide a clue to the establishment of such a wave pattern. Phase velocity as well as group velocity effects will have to be considered in the evaluation of the forecasting applicability of such diagrams. The 500-mb. height distribution along the 45° N. latitude circle appears to be best suited for the construction of such continuity diagrams.

4. NORTH AFRICAN DEPRESSIONS

(Based upon material presented by H. Flohn, D. Pedgley and Cdr. D. ROE and written material by D. Winstanley.)

4.1 Definition

North African lows and Sahara depressions, sometimes also referred to as Atlas lee depressions, usually form to the south of the Atlas Mountains. Poor observational data often prohibit detection of the incipient stages. Figure 4.1 shows the most frequent tracks of these cyclones. (Roe) They often give rise to severe dust storms and sometimes to intensive rainfall over otherwise arid regions. An associated phenomenon is the "sirocco" (or "scirocco") which is a warm south or southeast wind in advance of Atlas lee depressions.

4.2 General Description

It appears that the name "Atlas lee depression" for North African lows is a misnomer. The precipitation observed on occasion over northwest Africa with such depressions, and their tendency to migrate out over the Mediterranean, speaks against a lee effect. (Roe)

The most reliable criterion, according to Roe, for the development of a low to the south of the Atlas range is the presence of an upper trough lying over Spain with its axis oriented approximately NE - SW producing a deep southwesterly flow over northwest Africa (figs. 4.2 and 4.3). Such a trough may be mobile and, for example, associated with a depression moving eastward across Europe and a cold front

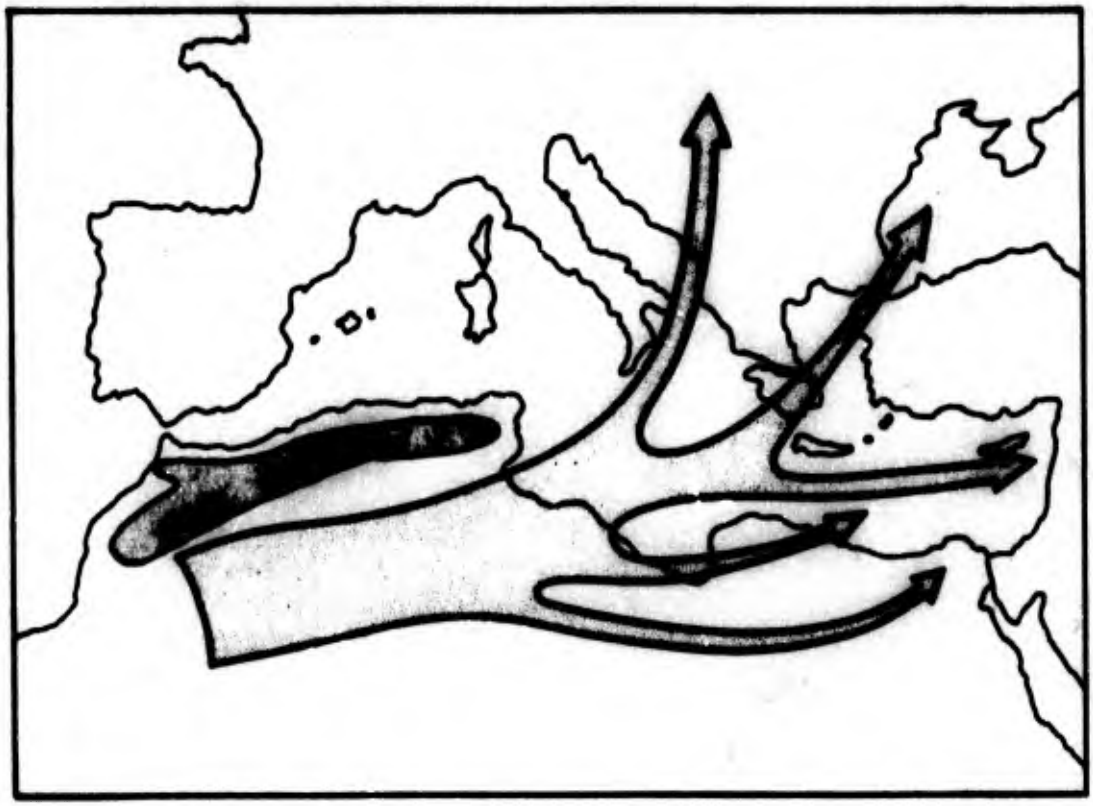

Figure 4.1 Typical Tracks of Northwest Saharan Depressions. (Roe)

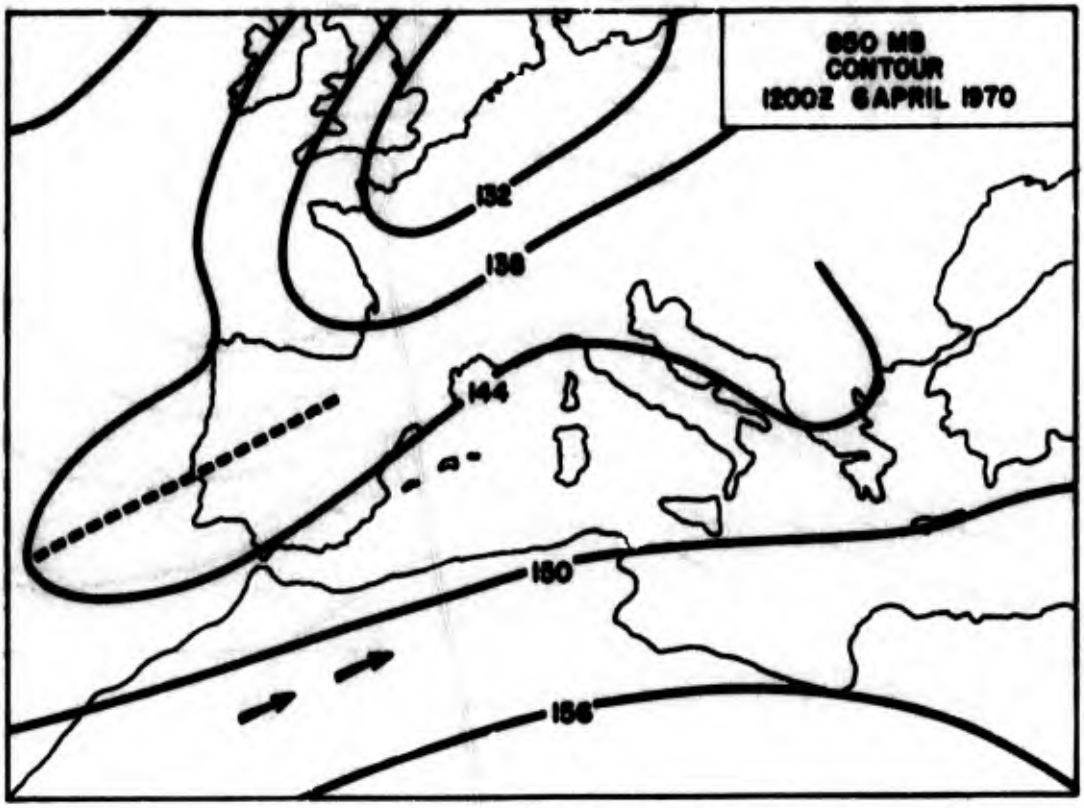

Figure 4.2 850-Mb. Analysis, 1200 GMT 6 April 1970, Typical for the Development of Northwest Saharan Depressions. (Roe)

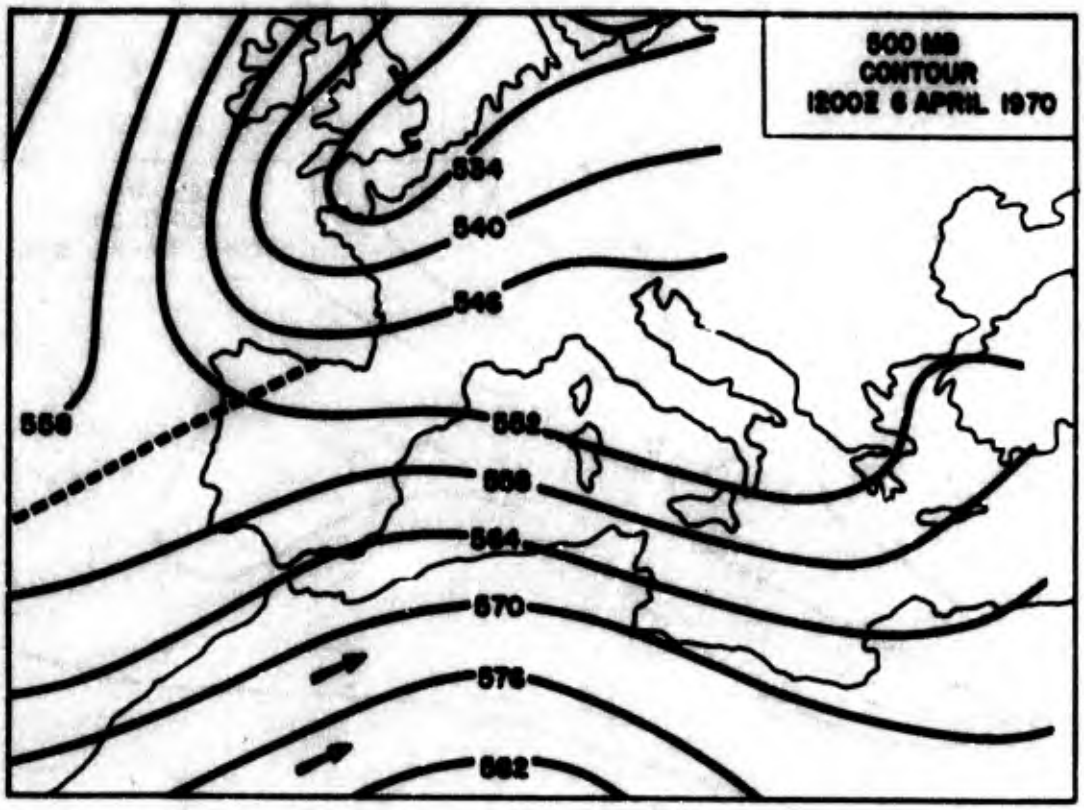

Figure 4.3 500-Mb. Analysis, 1200 GMT 6 April 1970, Typical for the Development of Northwest Saharan Depressions. (Roe)

advancing southeastward towards the Atlas Mountains. Alternatively the upper trough may be nearly stationary. This may be the case when a ridge extends across France from the Atlantic anticyclone. The presence of a cold front is apparently immaterial for the development of a depression and in many cases no front is detectable on the surface chart. When a cold front is present, development of the low usually occurs before the front reaches the Atlas range. A similar sequence of events has been described in section 3 for Genoa cyclones. The surface flow over the Mediterranean also appears to be insignificant, having little bearing on whether or not development occurs in the lee of the Atlas mountains. (Roe)

The lows apparently form in a deep flow from between west and south and they do not seem to be the result of a lee effect. Cdr. ROE does not recall a northwest African low developing in association with a deep northwesterly airstream over the Atlas mountains; on the contrary, presssure usually rises under such conditions. However, a lee trough often may be discerned, particularly over southern Tunisia.

Cyclogenesis is more satisfactorily explained by a combination of potential instability in the southwesterly airstream, coupled with vorticity advection along the leading flank of the upper trough. Should an old frontal zone be present in the area, this then would be a preferred cyclogenetic area (see Reiter [22]), but such fronts are highly

difficult to trace over the Sahara where synoptic information is sparse and irregular. Kirk [14, 15] and El-Tantawy [10] have pointed to the relation between surface disturbances over northern Spain and waves travelling eastward in the upper westerlies. These westerlies, for example shown in figures 4.2 and 4.3, may be identified with the subtropical jet stream. Cloud streaks observed from satellite photographs frequently outline the course of this subtropical jet stream. On occasion they show that the southwesterly current over North Africa may originate in tropical latitudes over the Atlantic ([23]; Flohn, oral communication). It has been shown by Reiter and Nania [24] and by Reiter and Whitney [25, 26] that interactions between the polar front jet and the subtropical jet stream takes place, especially in deep troughs. We have to suspect that the development of north African depressions is a manifestation of such interaction.

4.3 Occurrence

4.3.1 Seasonal and Diurnal Variations

Of all cyclonic disturbances entering the Mediterranean, Sahara and North African depressions are the most frequent in spite of the fact that they form over a continental area. Their average frequency is 14 cases per year, i.e., about 20% of all Mediterranean cyclones; 8 cases on the average are observed during spring (March-May). (Roe, Flohn)

It is observed that a desert depression forming over northwest Africa to the south of the Atlas mountains moves

in a quasi-steady state, with little or no intensification and with a retention of its configuration of isobars and isotherms. This occurs despite persistence in a region favorable to cyclogenesis due to upper positive vorticity advection. It is likely, therefore, that there is a mechanism which prevents the continued distortion of the thermal field that is expected with continued cyclogenesis. Such a mechanism is convective mixing within the northerly winds behind a depression. It is here that the warming of the lower troposphere as air flows from sea to land will reduce the rate of advection of isotherms with the result that the distortion of the isotherms is less than that which might be expected from advection alone, and a brake is placed on the rate of development. This brake is applied diurnally; therefore, a diurnal oscillation in the rate of development is possible but not yet verified. (Pedgley)

4.3.2 Geographic Characteristics

Desert depressions are often observed to form over southern Tunisia or northwestern Libya, or to intensify in the same region having previously moved eastwards as diffuse centers or open troughs close to the southern side of the Atlas mountains. It is in this region of formation or intensification that lower tropospheric air can first stream southwards in the rear of these relatively weak disturbances. Further west, the Atlas mountains are a barrier to such flow and they probably prevent the advective distortion of the thermal field which is observed to occur more freely to the

east. (Pedgley) However, cases of strong cyclogenesis do occur to the south of the Atlas mountains with associated cold air crossing the Atlas range. Two such cases will be described later in section 4.4.

During its passage eastward, as the Atlas barrier becomes ineffective, the Sahara low may deepen considerably if moving in association with a mobile upper trough. When the initiating trough is stationary, the low is not likely to deepen as it moves away from the generating area and if it should track out of the southwesterly flow into a westerly or northwesterly stream on the east side of the upper ridge, it will probably fill. (Roe)

When the upper trough is driven south into the Sahara (perhaps by an anticyclone covering the Mediterranean) the lows may continue to develop further south, namely to the south of the trough axis. In this case they may travel subsequently northeastwards to cross the Mediterranean coast in Cyrenaica or Egypt, causing a freshening of the northeasterlies in the central Mediterranean as the lows pass to the south. (Roe)

A frequent but by no means invariable development, which occurs in conjunction with the appearance of a depression to the south of the Atlas, is for a low to be generated to the north of the Atlas range (fig. 4.4). Such lows are usually formed when the upper flow over northwest Africa is between southwest and south in this case a lee effect is thought to be the initiating factor. (Roe)

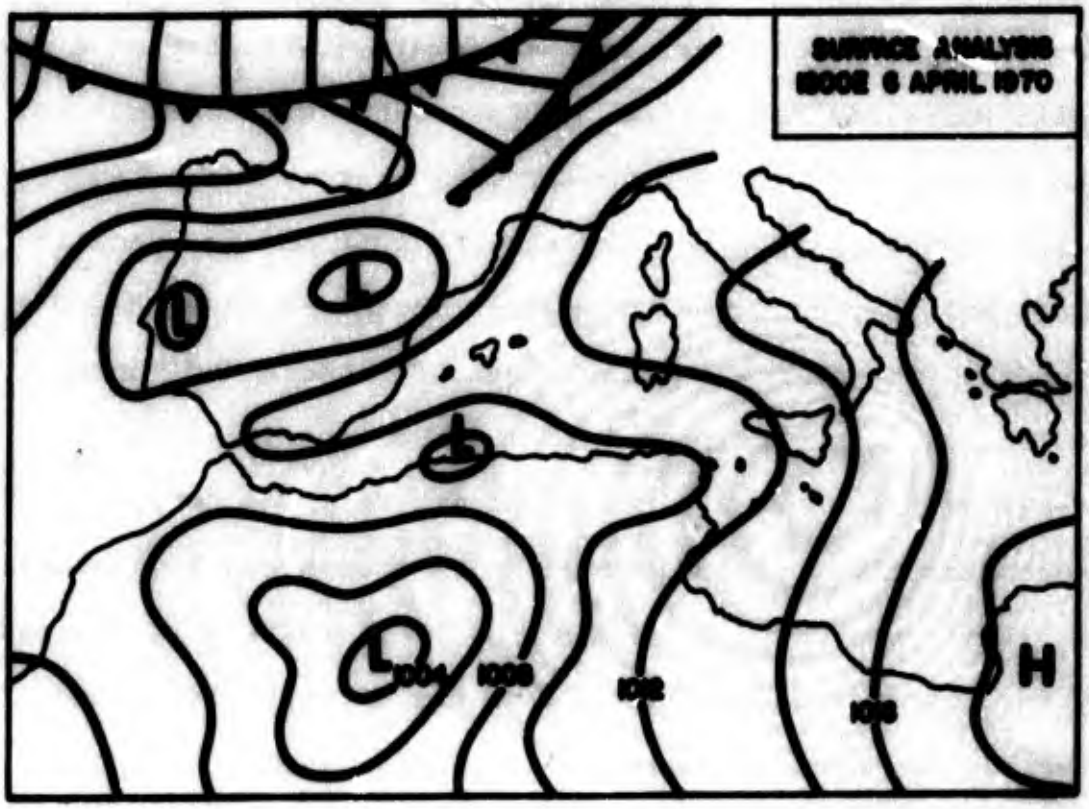

Figure 4.4 Surface Analysis, 1800 GMT 6 April 1970, Example of a Secondary Depression North of the Atlas Mountains. (Roe)

The two lows generally move eastward together, the parent to the south of the Atlas range and the subsidiary along the coast of Algeria and Tunisia. Should the parent low cause the upper flow over the Atlas to back to south-easterly, the subsidiary low may remain stationary or even drift westwards for a time. A keen watch must be kept for the formation of the subsidiary lows as they are often small features which are not easy to spot on the synoptic chart but they can give unexpected increases in wind and thundery outbreaks along the coast of Algeria and Tunisia. Occasionally they develop into major depressions, particularly on the arrival of a cold front from the north, and thereafter may move independently of the parent low. (Roe)

The approach of a low over southern Tunisia is signalled by falling surface pressure, altocumulus castellanus and possibly thundery outbreaks while surface winds over the Gulf of Gabes freshen from the south or southeast. (Roe) Barometeric tendencies in the Mediterranean are often misleading, being masked by diurnal variation which should be allowed for (see appendix A).

A simple depression, which has been tracked past the widely spaced observing stations over the Sahara, usually turns out to be a complex system with several centers by the time it reaches southern Tunisia[1] with its denser synoptic

---

[1] Pedgley disputes this statement, attributing the complexity to observational errors, failure to reduce pressures at sea level, etc. Roe, however, has observed complex centers at Malta.

coverage. A frequent occurrence is for a center to develop in advance of the main complex in the corner of the Gulf of Gabes. (Roe)

When the low emerges over the Mediterranean the upper flow should be inspected to determine the likely subsequent direction of movement, and the 500-mb. chart is a good guide. The subsidiary depression passing to the east of Tunisia usually disappears as a separate entity leaving a frontal trough. (Roe)

In spring the sea is cool and as the hot air moves northward a substantial inversion, which may be as great as 15° to 18° C. in extreme cases, is created between the surface and approximately 3000 ft. (fig. 4.5). A time section of a typical spring depression system moving across Malta is shown in figure 4.6. The shallowness of the low circulation, its warm core, surface stability and upper instability are clearly seen. (Roe)

When winds are light, low stratus clouds form, amounts increasing with the length of sea track; drizzle and sea fog are to be expected in the Ionian and Adriatic Seas. With strong winds, vast quantities of dust trapped beneath the inversion produce a thick haze which can reduce visibility to a few hundred yards at Malta and further north. The dust is raised mainly over the desert during the day, is carried northwards and is often thickest in the Malta area in the late afternoon or evening. Instability persists above the inversion and high based cumulus or cumulonimbus clouds are

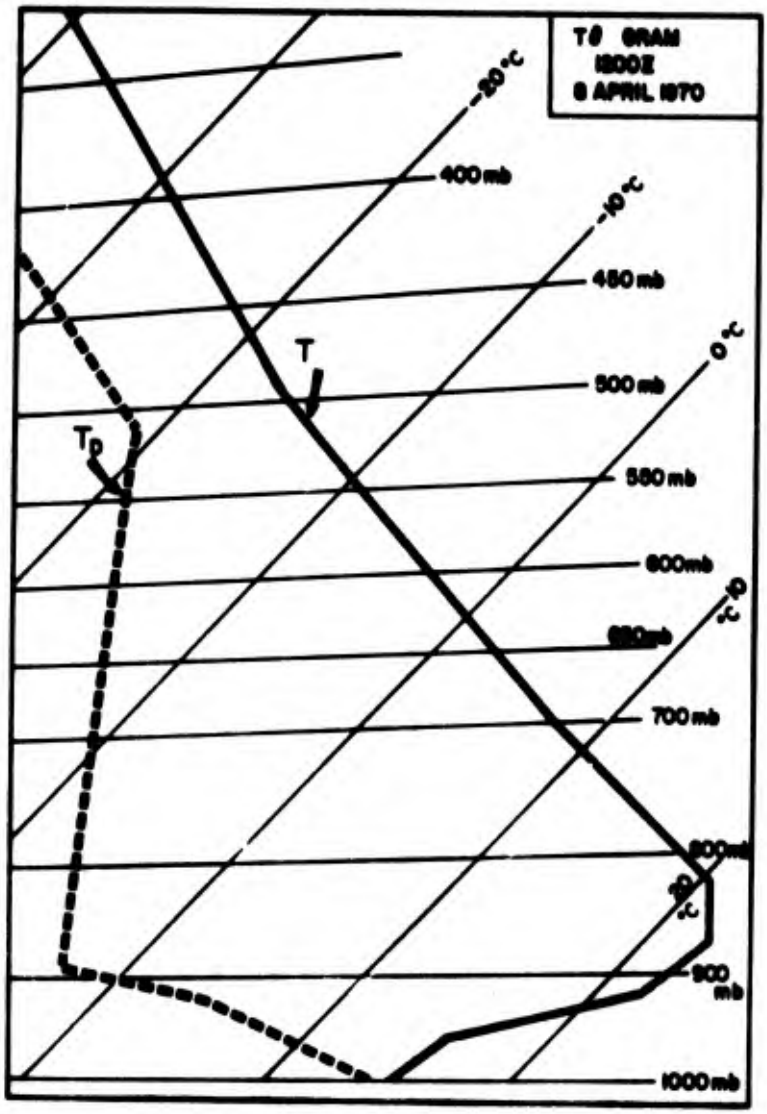

Figure 4.5 Typical Sounding in Southwesterly Flow, Malta, 1200 GMT 8 April 1970. (Roe)

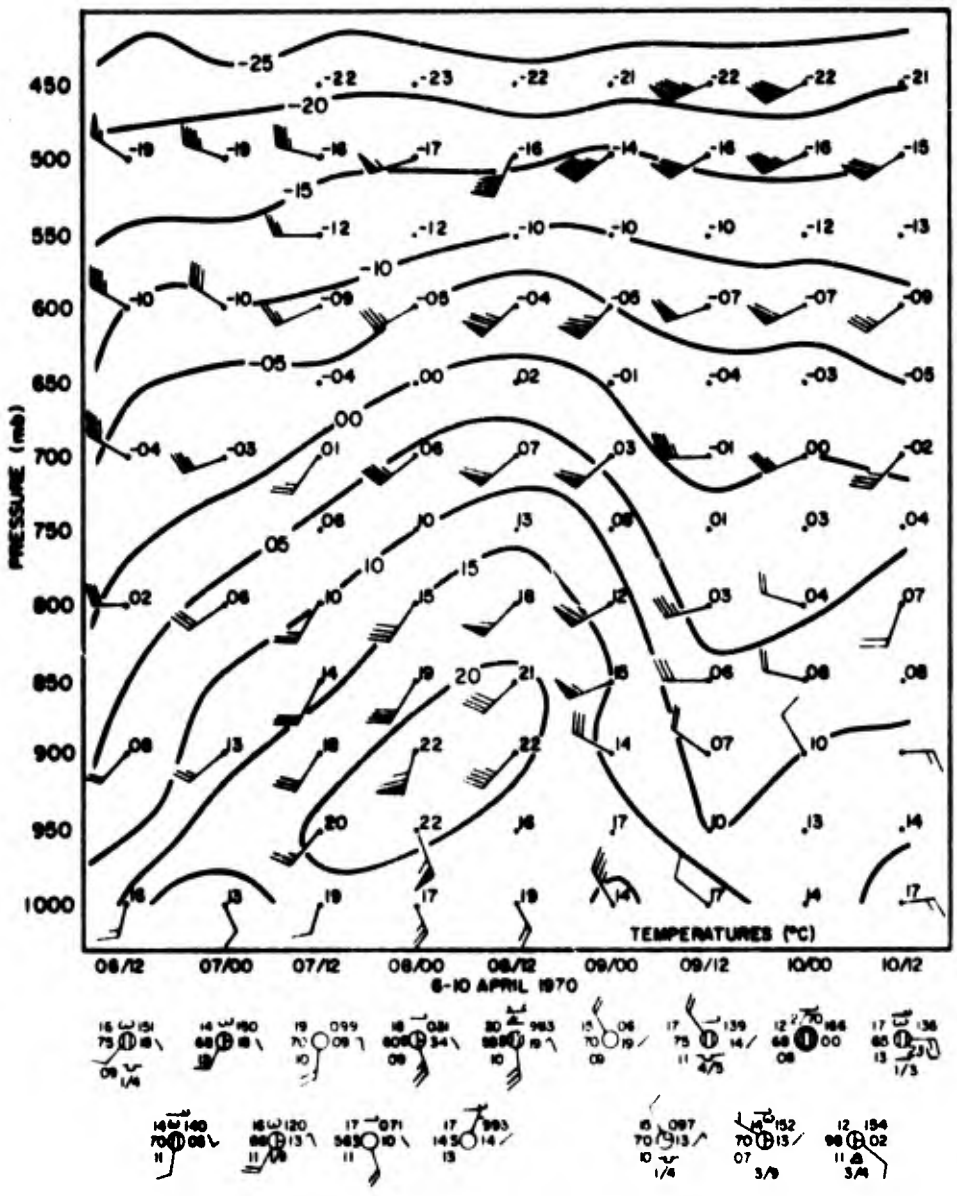

Figure 4.6 Vertical Time Cross-Section of Temperature, Wind and Surface Weather Conditions at Malta, 6 to 10 April 1970. (Roe)

present, though amounts of rainfall are small but very muddy. (Roe)

During all seasons, the operation of aircraft, particularly from carriers, is seriously affected by the scirocco. Dense belts of altocumulus castellanus which approach from the southwest and are probably associated with weak troughs in the upper flow should be treated with caution as they often are associated with radical and sudden changes in surface wind speed and direction. (Roe)

Apart from the reduction in visibility caused by the dust, it clutters the radar screens and penetrates everywhere. Thick deposits in aircraft cockpits have been observed. Turbulence above the inversion is severe particularly if castellanus is present, and pilots report that aircraft are difficult to control. An indication of the turbulence may be deduced from barograph traces which commonly show violent "pumping" underneath regions with serious turbulence conditions. (Roe)

The surface inversion produced in spring gives extremely anomalous radar and radio propagation in the dust-laden atmosphere below the inversion. Helicopters are liable to be out of radio contact at a range of a mile or two. (Roe)

When the scirocco blows over islands with hilly terrain, turbulence may mix the inversion layer on the downwind side and ships running for shelter into the lee of the island can experience a sudden uncomfortable rise in air temperature. (Roe)

As the low and its associated troughs pass to the east, the arrival of the cooler air in the rear gives a rapid amelioration in weather conditions. Visibility improves quickly and the temperature drops abruptly as the wind swings to a northwesterly direction from which it may blow quite strongly for about 24 hours. When a mobile upper trough is following the depression, the weather will remain unsettled, showery and thundery, until the passage of the upper trough. The period of unsettled conditions associated with the whole complex lasts on the average about 4 days. (Roe)

Should the depression take a course towards the eastern Mediterranean, the scirocco conditions will spread progressively eastwards along the northeast African coast, remaining confined to the eastern side of the associated cold front. (Roe)

A characteristic feature of the weather over northeast Africa during the spring, February to June, is the occurrence of spells of southerly winds at a time when climatological charts (e.g. [33]) shows that predominant directions are between north and east. These southerlies bring high temperatures and low dewpoints and sometimes they are strong enough to produce widespread dust storms. This type of weather, called khamsin in the United Arab Republic (from the Arabic for "fifty", and applied to the fifty days following the Coptic Easter) and ghibli in Libya (an Arabic word for "south"), can cause considerable personal discomfort. (Pedgley)

With the setting up of a synoptic network over Egypt at the beginning of this century, a relationship was soon discovered between these spells of southerly winds and the approach of depressions from the west, crossing either the Mediterranean or the desert just south of the coast of north Africa [6]. With the accumulation of synoptic analyses over a number of years, it was possible to discuss the synoptic climatology of these "khamsin depressions" [31]. About half of them were found to be of the "desert" or "Sahara" type, but the fraction was greater in April and May. Desert depressions are not frequent: an average of about six each year can be expected, the latest usually occurring about mid-June. With each depression, khamsin weather lasts a few days, rarely more than four.

Following the development of classical Norwegian ideas on the structure of depressions, frontal structures were given to desert depressions over Egypt (e.g., [3, 8, 34]), but in the absence of data to the west their origin was obscure. When a synoptic network had been established over northwest Africa in the 1920's, it became clear that at least some desert depressions had an origin just south of the Atlas mountains [12]; while others, "Sahara-Soudan" disturbances, developing over the Sahel of West Africa south of the Sahara in the region from Senegal to the Niger Republic, could at times be traced northeastwards as far as Egypt [12, 20, 21]. But the nature of these latter disturbances was still obscure. (Pedgley)

An extension of the frontal concept postulated that desert depressions formed along a front separating cool, polar air over the Mediterranean from warm air over north Africa that had come from Arabia and the Red Sea [9], but Sayed Ahmed [30] pointed out that most khamsin depressions are secondaries to larger depressions over Europe or the northern Mediterranean. However, it was clear that the frontal structure was not always simple because, although the cold front is usually well-marked, the warm front is frequently found to be diffuse [16, 17]. (Pedgley)

At present, although there is general acceptance of a frontal nature of desert depressions [1], their structure, origin and evolution are still poorly understood, no doubt in part a result of the sparseness of data, especially from the middle and upper troposphere. (Pedgley)

4.4 Case Descriptions

Nania gives two typical sequences of surface and 500-mb. weather maps characterizing the development of North African lows (figs. 4.7 and 4.8, 11 to 14 April 1967 and 10 to 15 December 1967). Both sequences are characterized by a blocking high over the Atlantic and a deep trough over western Europe that extends to the African coast. The triggering impulse, although not well-documented by the 500-mb. maps presented here, comes from a jet maximum that travels southward along the east side of the blocking ridge. Cold air spilling over the Atlas mountains (1200 GMT 11 April 1967, and

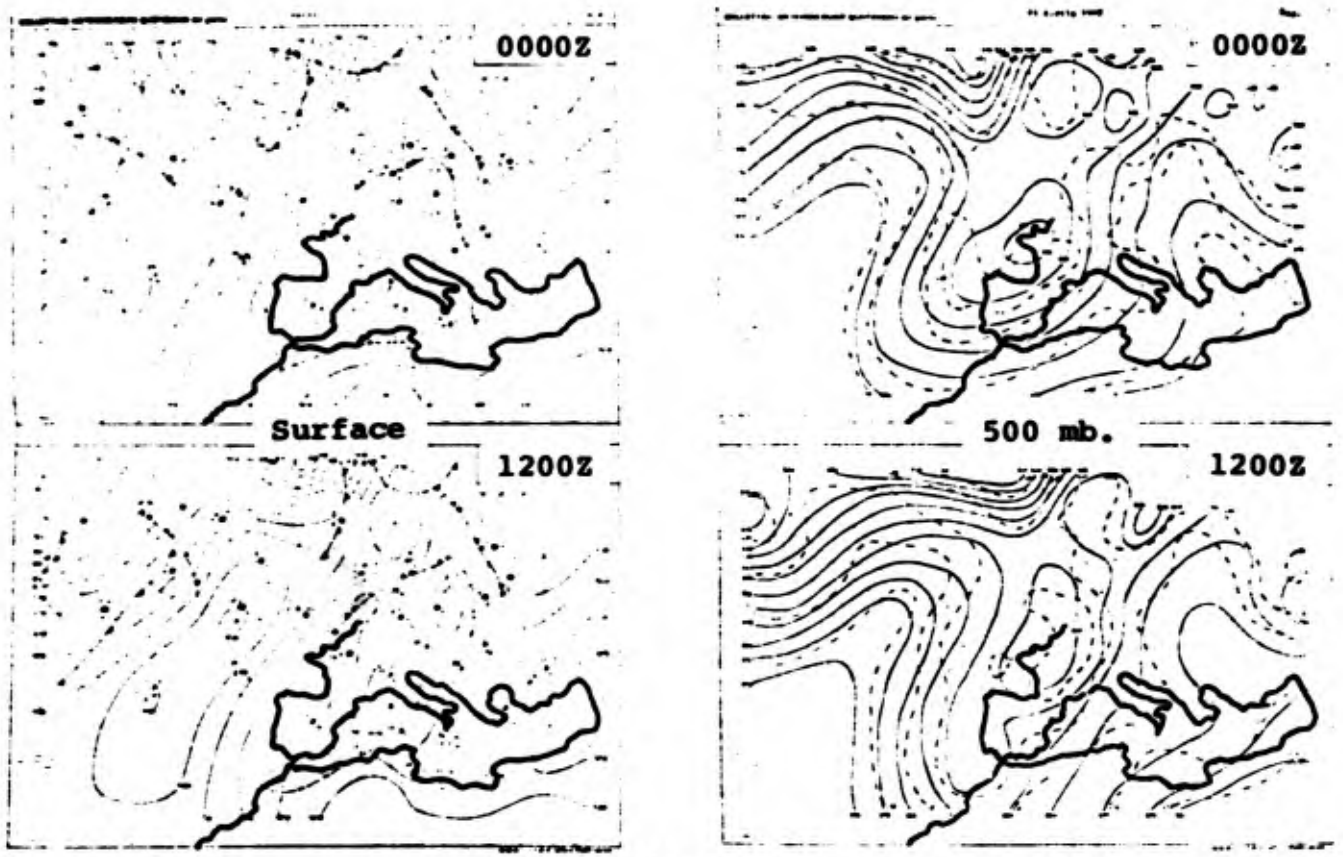

Figure 4.7 Series of Surface and 500-Mb. Analyses, 11 to 14 April 1967, Characteristic for the Development of a North African Depression. (Nania)

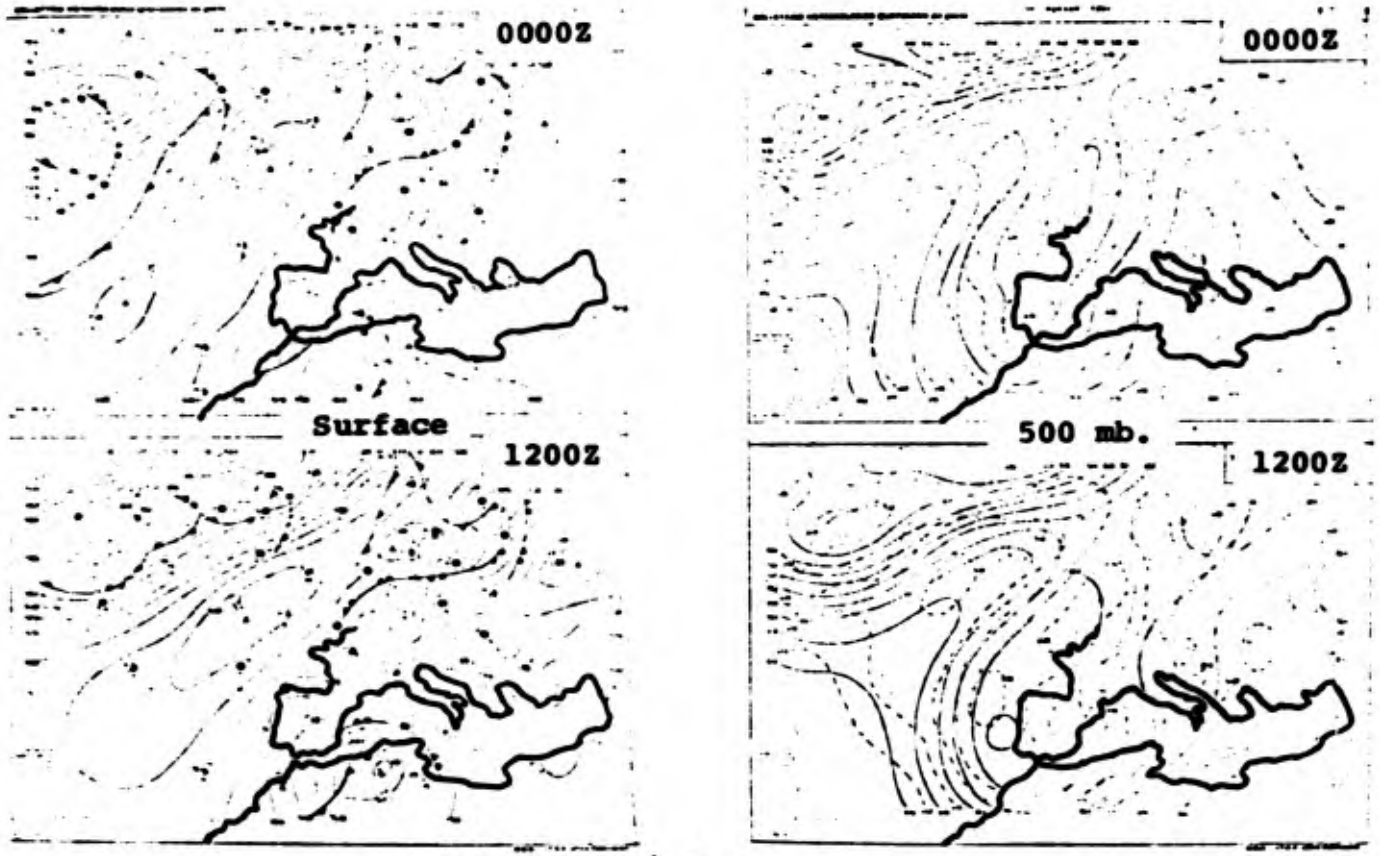

Figure 4.7 (Continued) Series of Surface and 500-Mb. Analyses, 11 to 14 April 1967, Characteristic for the Development of a North African Depression. (Nania)

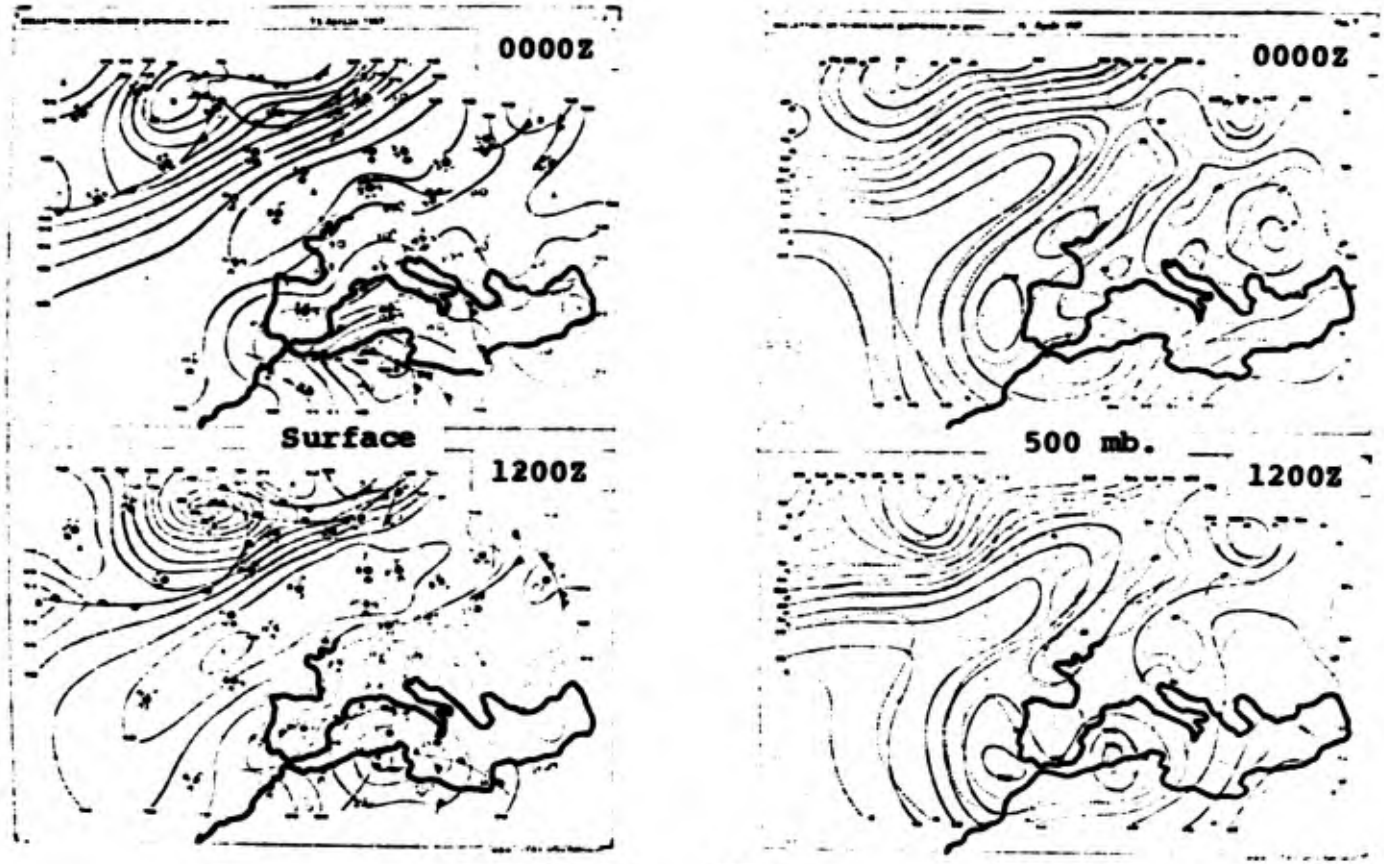

Figure 4.7 (Continued) Series of Surface and 500-Mb. Analyses, 11 to 14 April 1967, Characteristic for the Development of a North African Depression. (Nania)

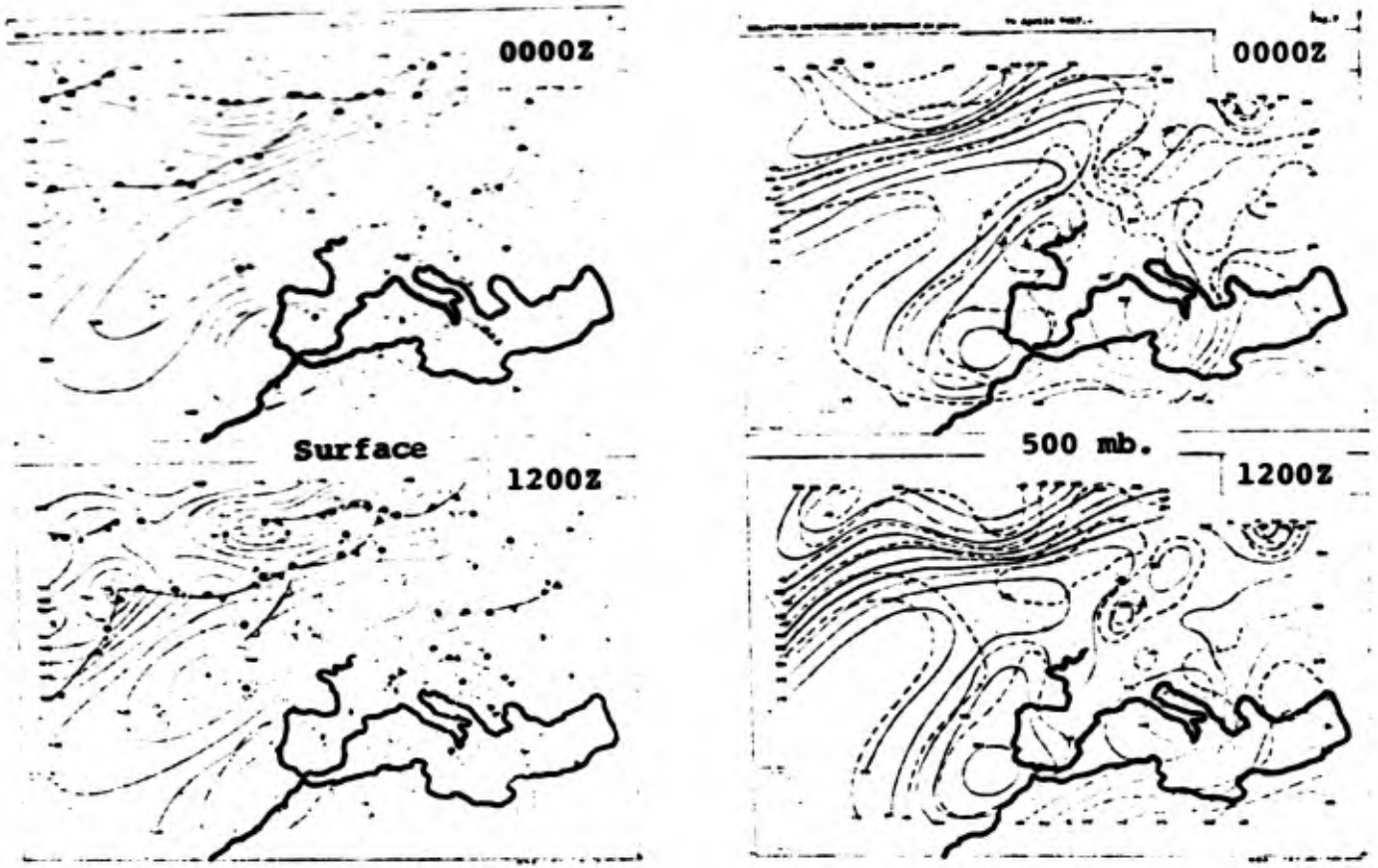

Figure 4.7 (Continued) Series of Surface and 500-Mb. Analyses, 11 to 14 April 1967, Characteristic for the Development of a North African Depression. (Nania)

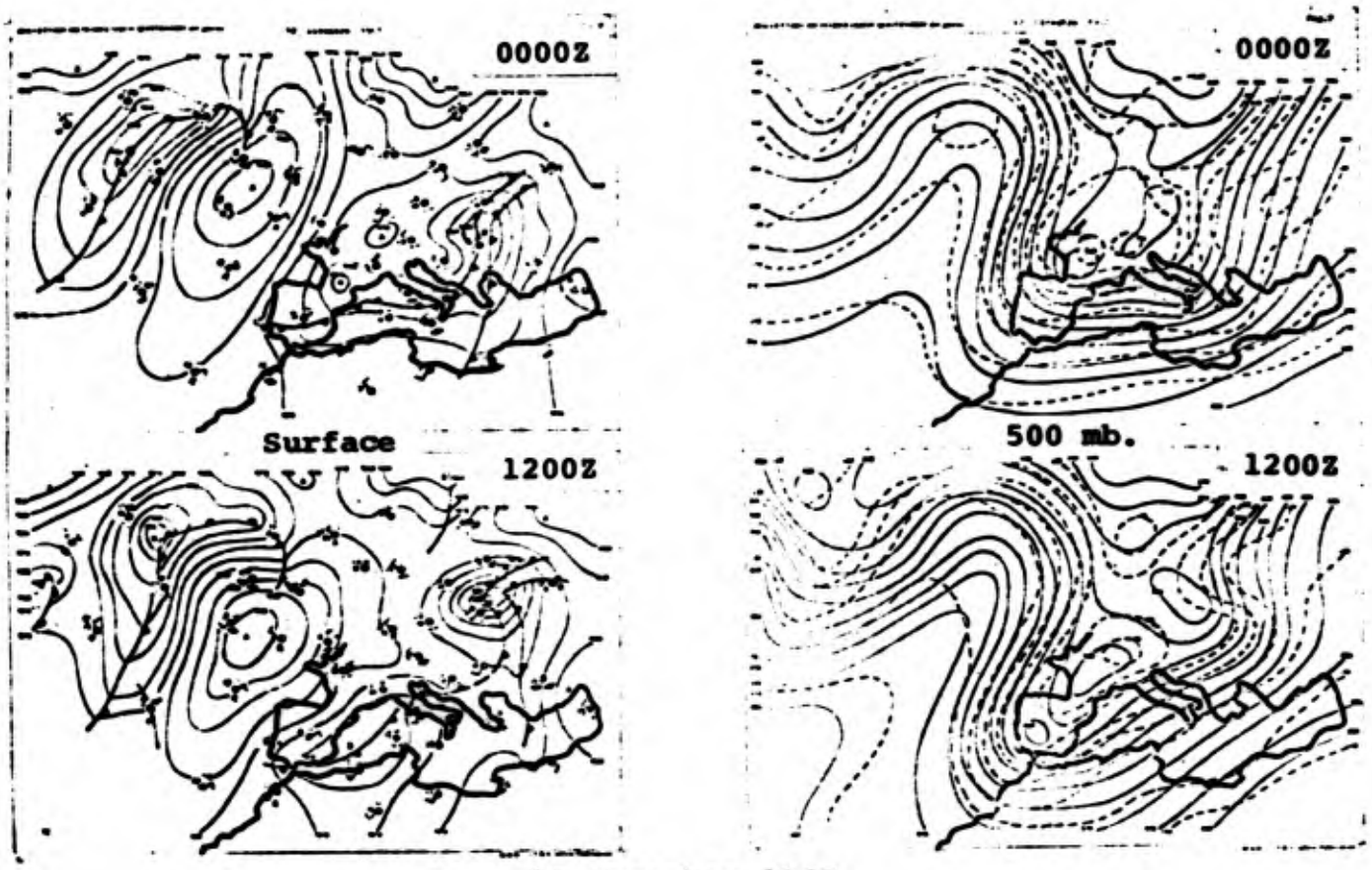

Figure 4.8 Series of Surface and 500-Mb. Analyses, 10 to 15 December 1967, Characteristic for the Development of a North African Depression. (Nania)

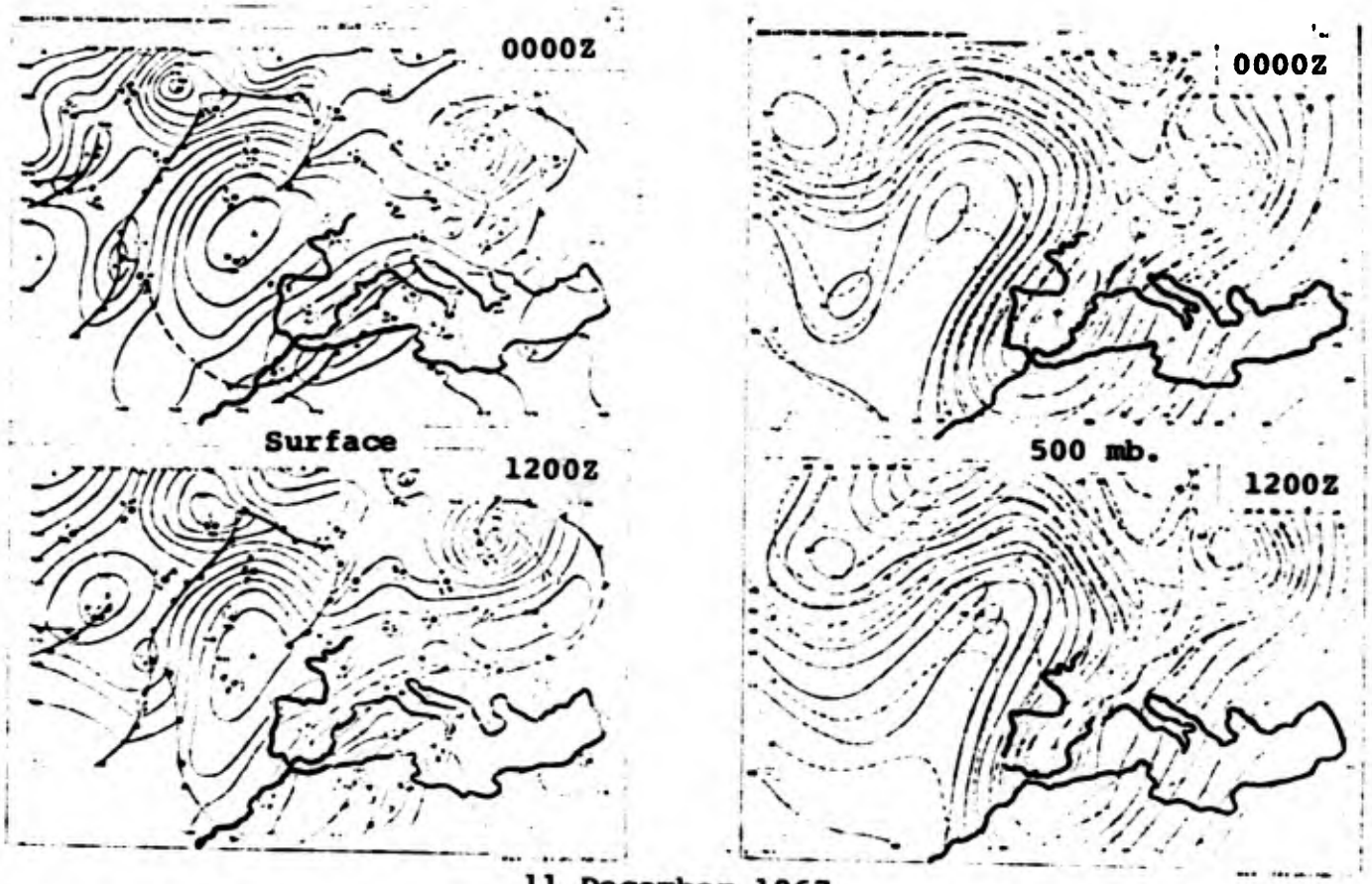

Figure 4.8 (Continued) Series of Surface and 500-Mb. Analyses, 10 to 15 December 1967, Characteristic for the Development of a North African Depression. (Nania)

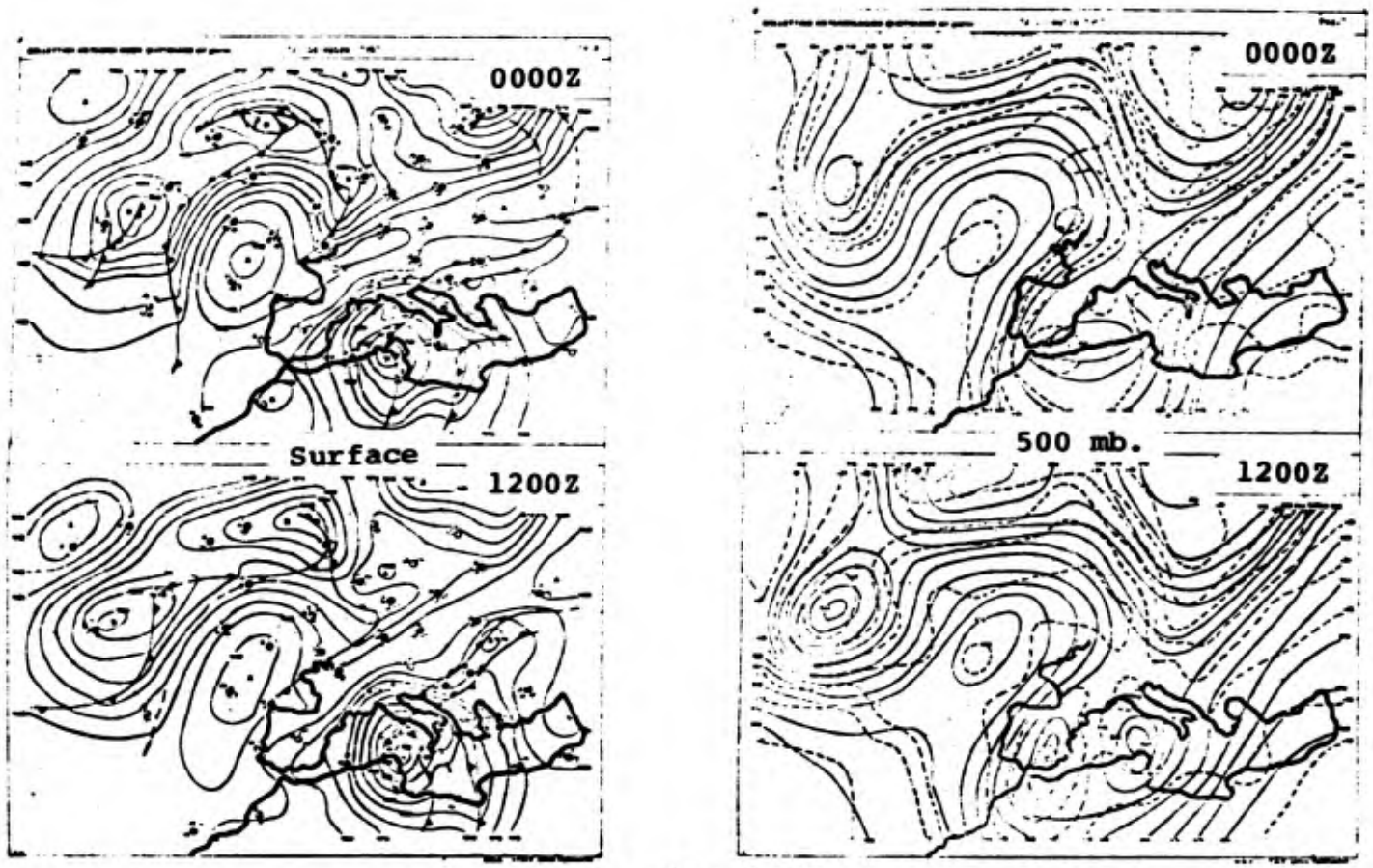

Figure 4.8 (Continued) Series of Surface and 500-Mb. Analyses, 10 to 15 December 1967, Characteristic for the Development of a North African Depression. (Nania)

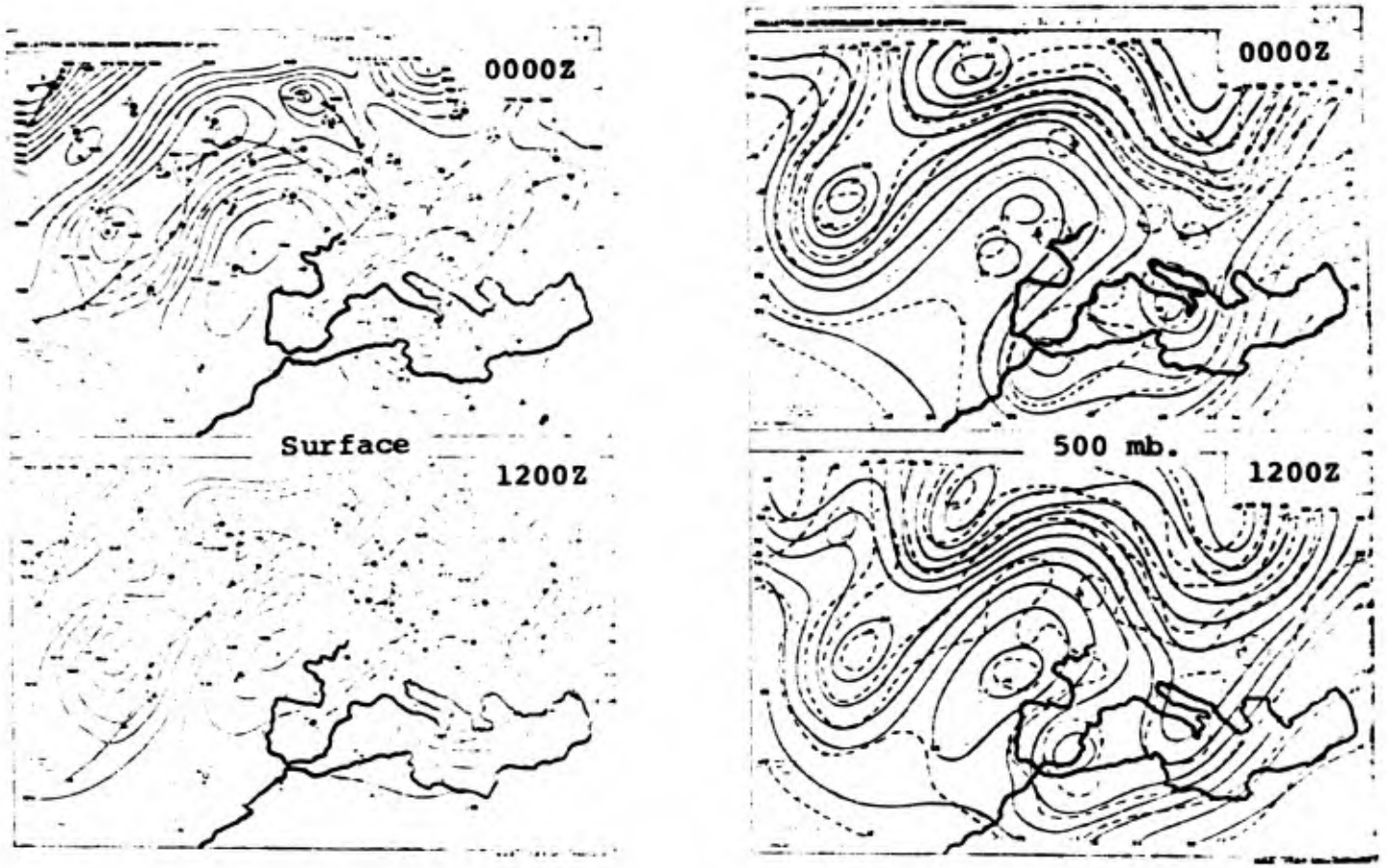

13 December 1967

Figure 4.8 (Continued) Series of Surface and 500-Mb. Analyses, 10 to 15 December 1967, Characteristic for the Development of a North African Depression. (Nania)

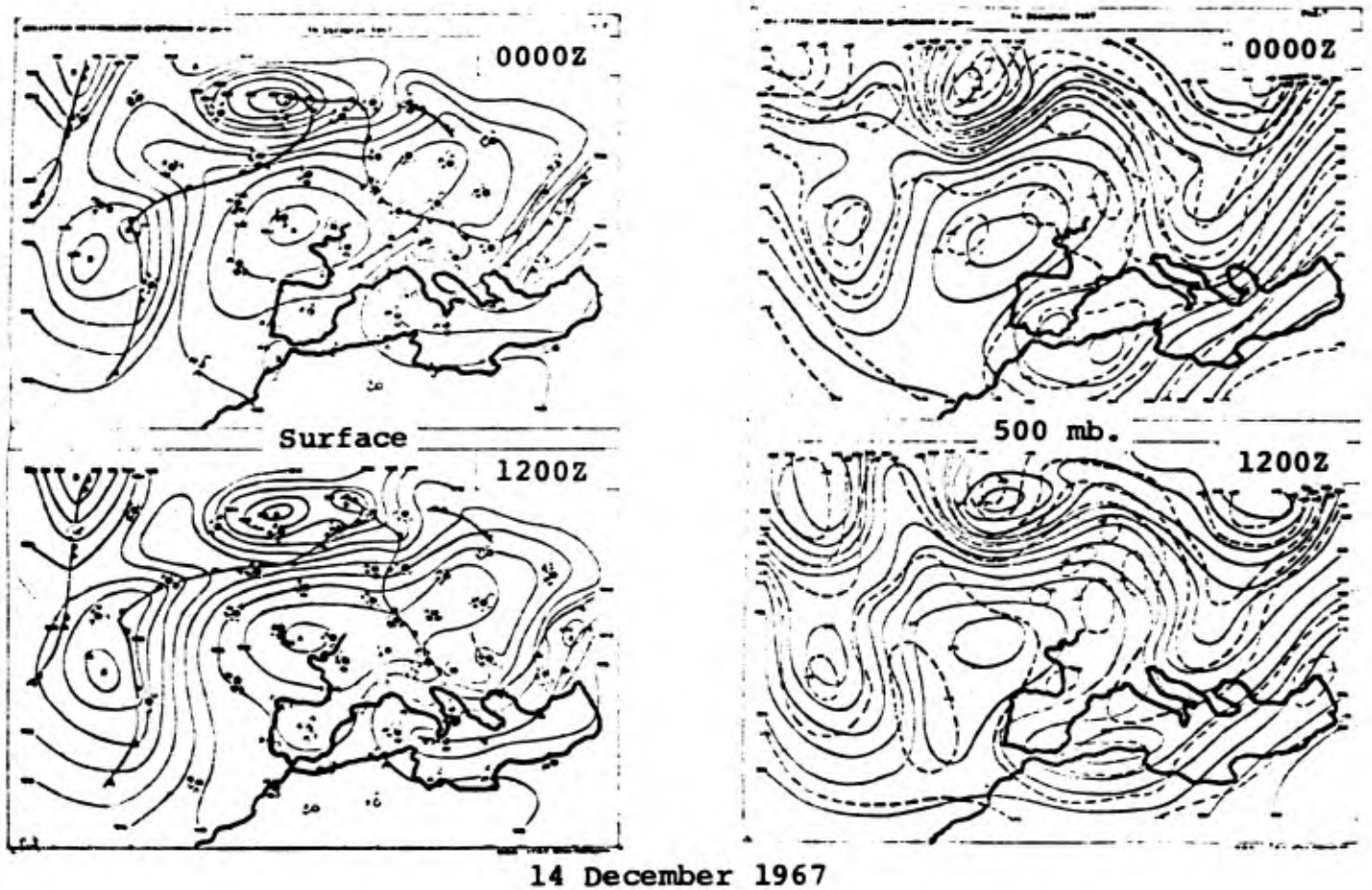

Figure 4.8 (Continued) Series of Surface and 500-Mb. Analyses, 10 to 15 December 1967, Characteristic for the Development of a North African Depression. (Nania)

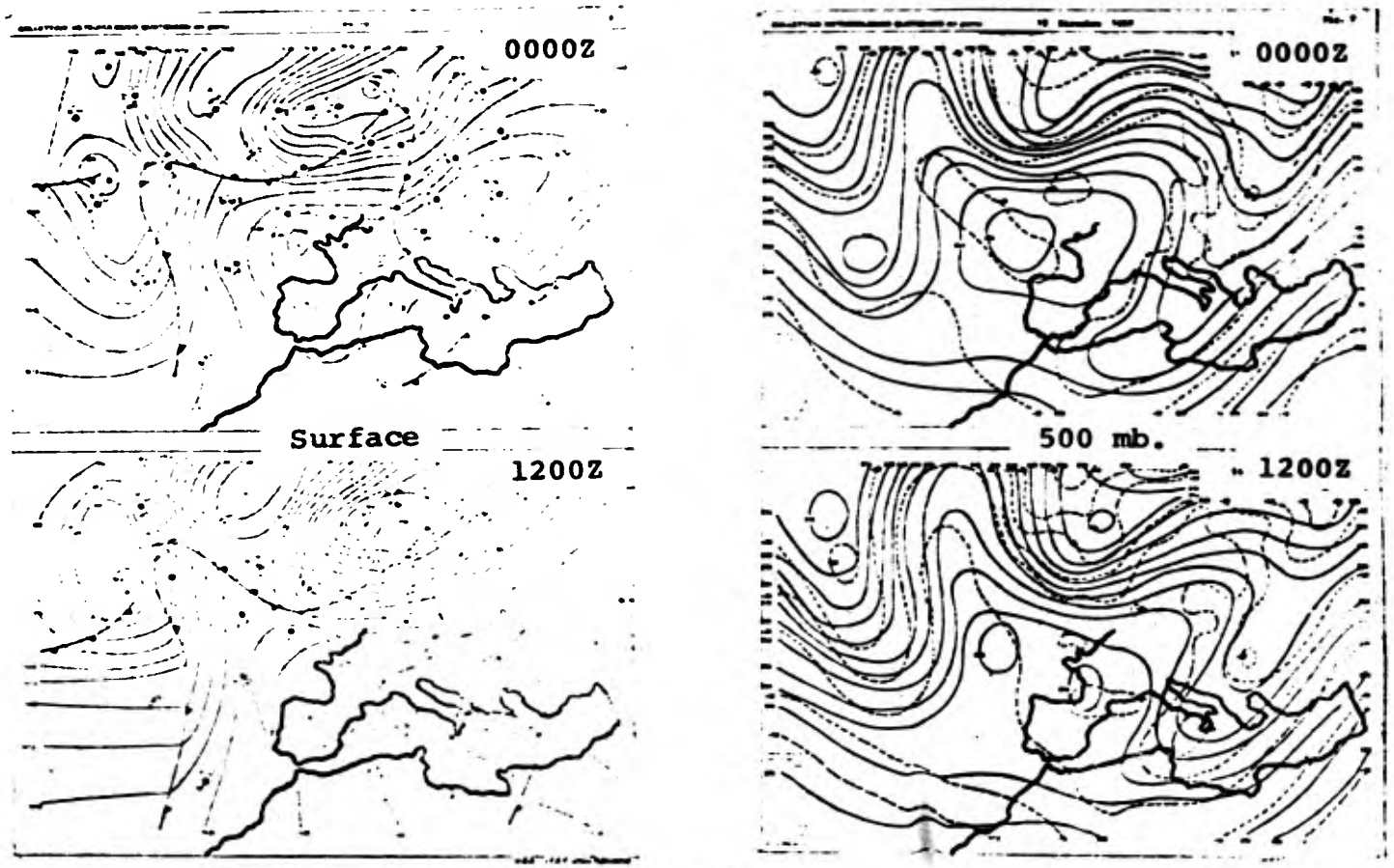

Figure 4.8 (Continued) Series of Surface and 500-Mb. Analyses, 10 to 15 December 1967, Characteristic for the Development of a North African Depression. (Nania)

0000 GMT 11 December) sets off an intensification of the cyclonic disturbances. Winstanley, describing the cause of heavy floods in north Africa during December 1969 that were associated with a Sahara depression, also comments on the spilling of cold air over and around the Atlas mountains.

Strong dust storms have been noted by Pedgley behind cold fronts associated with north African lows. Figure 4.9 shows a time section for Gialo, Libya (21°02' N., 21°34' E., sta. no. 62161) for March 11 to 15, 1962, during the passage of two desert depressions over Libya and the United Arab Republic. (Time runs from right to left.) Winds are strongest during the passage of the cold fronts which are marked by an abrupt shift in wind direction. Winds of 30 knots or more were associated with visibilities below 200 m.

According to Pedgley, the occurrence of extensive precipitation with a Sahara depression is the exception rather than the rule. Most of the observed clouds are at cirrus levels. Middle clouds, with bases usually above 600 mb., even 500 mb., appear chaotic, and are often oriented in bands or sheets parallel to the flow ahead of the depression. These middle clouds are often glaciated and form virga which, however, rarely reach the ground. This is presumably due to the high rate of evaporation in the lowest, dry layers of the desert atmosphere. Cold downdrafts from these virga may lead to gusty surface winds and to erratic surface pressure fluctuations. (Pedgley)

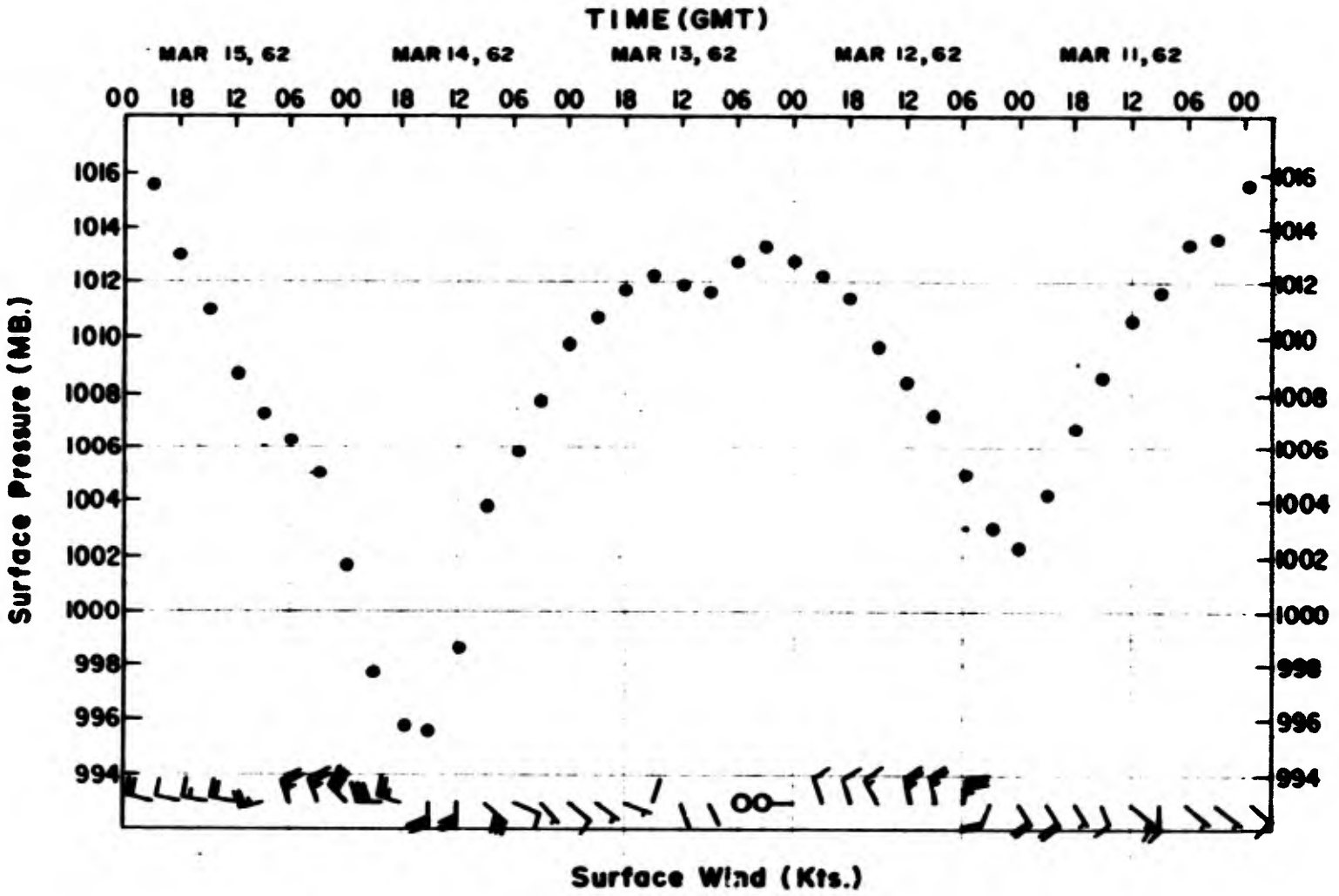

Figure 4.9 Time Cross-Section of Surface Pressures and Winds for Gialo, Libya (29°02' N., 21°34' E., sta. no. 62161), 11 to 15 March 1962. (Pedgley)

The upper-air maps of both cases of north African lows presented here suggest the existence of a southwesterly jet stream over, or to the south of, the Atlas mountains as the depressions develop. This jet stream obviously interacts with the impulse that comes from the north and travels along the east side of the Atlantic high-pressure ridge.

4.5 Forecasting North African Depressions

The forecasting of cyclonic developments south of the Atlas mountains at the present is severely restricted by the sparsity of data in this region. An augmentation of upper-air data from satellite photographs is advocated. The presence of cirrus streaks often reveals the axis of the subtropical jet stream near 200 mb. (remarks by Flohn, Reiter; [23]). There also is a data source not yet tapped in the form of Doppler wind measurements by commerical aircraft flying between European and African cities. (Pedgley, Winstanley)

If a southwesterly jet stream is present along the south side of an elongated trough line, such as shown in figures 4.7 and 4.8, a close watch should be kept on the movement of cold fronts in the vicinity of the Atlas mountains, and on jet maxima in the northerly current over the Atlantic that might push these fronts across the mountains.

Unfortunately none of the presently used numerical forecastings techniques predicts the formation and movement of the North African depressions adequately. This is due partly

to the poor input data from these data-sparse regions into objective analysis program and partly to local effects from mountain ranges and air-sea differences.

5. THE ETESIAN

(Based almost exclusively upon material supplied by D. Metaxas, supplemented by a study by Cdr. N. ÖNÜR.)

5.1 Definition

The etesian is a northerly wind, prevailing during the summer in the eastern Mediterranean and in the Aegean Sea.

5.2 General Description

"Etesian" in Greek stands for "yearly", indicating the regularity with which these winds appear each summer. The Turkish word for these winds is "meltem". These winds, because of their frequency during the warm season, constitute a major factor in the climate of the eastern Mediterranean. The prevailing period is May to October-November with maximum frequency and strength occurring in July and August.

Winds are generally northerly along the Greek coast even during winter when they may reach speeds exceeding those of the etesian. In May and November the frequency of northerly winds is minimum (fig. 5.1) and only those northerly winds

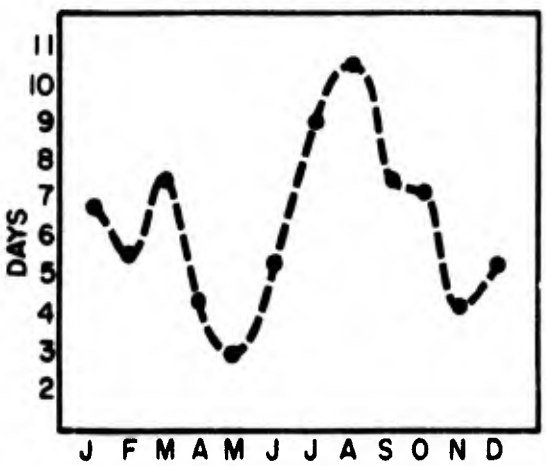

Figure 5.1 Mean Number of Days With Northwest, North and Northeast Winds ≥ Beaufort Force 4 (11 kts.) at 1400 LT, Hellenikon Airport, Athens (1949-1968). (Metaxas)

between May and November are considered as etesian winds, the remainder forming part of the winter season.

The term "etesian" is usually attached to a north wind that exceeds a certain minimum speed. Since the sea breeze in Athens is of a southerly direction and counteracts the etesian, those days for which Athens reports a northwind at noontime and apparently has a general pressure gradient of considerable strength, also qualify as "etesian days". (Carapiperis)

The pressure gradients necessary to drive the etesian winds are provided by a low pressure region along the southern coast of Turkey, and a high-pressure region over the Balkans. This is evident from the mean sea-level pressure charts for summer and winter (figs. 5.2 and 5.3). With such a characteristic pressure pattern the cause of the etesian winds must be sought partly from the monsoonal character of the circulation between the warm land masses of Asia Minor and the cool Mediterranean, and partly from synoptic disturbances that lead to anticyclogenesis over the Balkans.

The strong winds in an etesian situation may be enhanced by channeling effects between islands. Such effects also render wind reports from certain locations unrepresentative.

5.3 Occurrence

5.3.1 Seasonal and Interannual Variations

It has been stated above that the etesian winds are a typical summer phenomenon. Following the definition of an

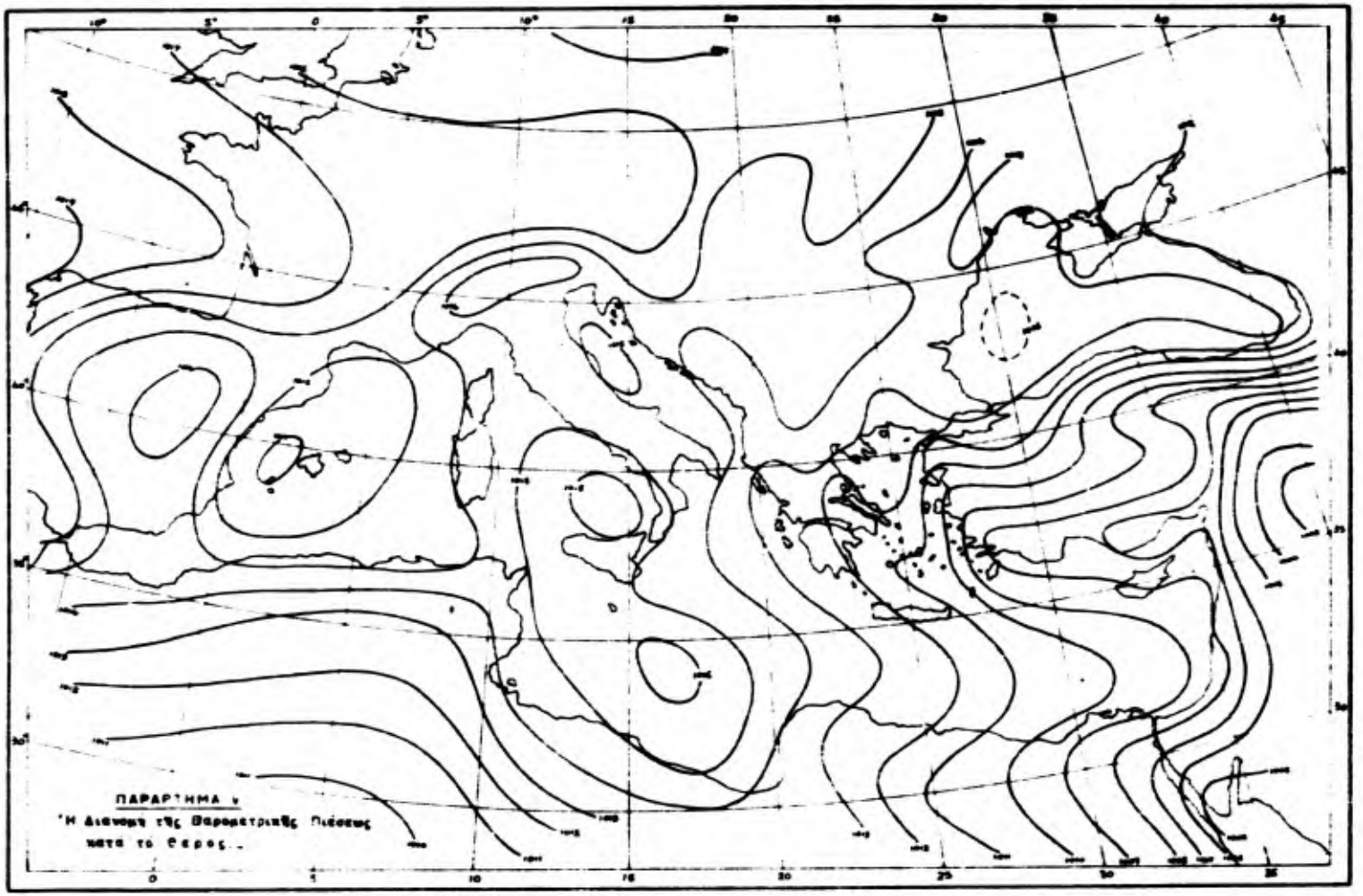

Figure 5.2 Mean Sea-Level Pressure (mb.) During Summer. (Metaxas)

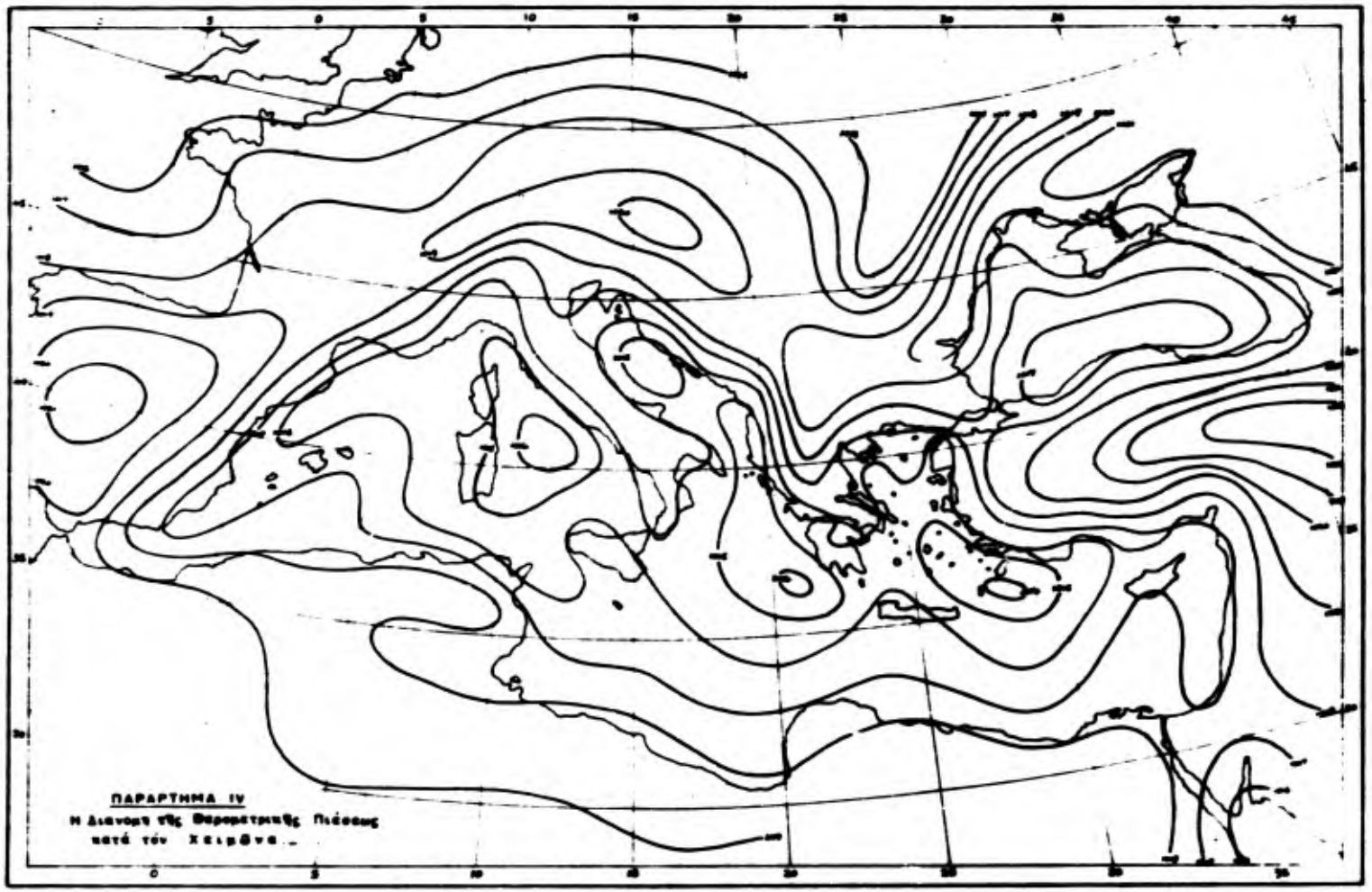

Figure 5.3 Mean Sea-Level Pressure (mb.) During Winter. (Metaxas)

etesian day from the sea-breeze behavior at Athens, Carapiperis found the mean number of etesian days, based upon records between 1893 and 1952 (table 5.1).

Table 5.1. Mean Number of Etesian Days During the Period 1893-1952 at Athens. (Metaxas from Carapiperis)

Month	May	Jun	Jul	Aug	Sep	Oct
No. of Etesian Days	4.3	6.0	13.0	13.6	11.1	5.7

The mean number of days with north or northeast winds at the National Observatory (sta. no. 16714, 5 km. (3 n. mi.) inland), at Nea Philadelphia (sta. no. 16701, 10 km. (6 n. mi.) inland), and at Hellenikon Airport (sta. no. 16716 on the south coast near Athens) is shown in table 5.2.

Table 5.2. Number of Days With North or Northeast Winds ≥1 Beaufort Force (≥1 kt.) and ≥4 Beaufort (11 kts.). (Metaxas)

Station		May	Jun	Jul	Aug	Sep	Oct
Nea Philadelphia	≥1	6.8	9.5	16.1	16.0	13.6	12.5
	≥4	3.2	4.0	9.0	8.7	5.8	6.6
Athens Nat. Observatory	≥1	5.3	7.5	13.3	14.0	12.3	11.6
	≥4	2.3	4.0	8.4	9.1	7.1	6.5
Hellenikon Airport	≥1	4.1	6.6	11.1	12.9	11.1	11.1
	≥4	2.8	4.7	8.9	10.2	7.4	7.2

The number of etesian days per year varies considerably; Carapiperis has found a correlation of the yearly number of etesian days with the 11-year sunspot cycle. For the Hellenikon Airport (1947-1969 data) the standard deviation of the monthly number of etesian days varies from 3.2 in June to 4.2 in August. Thus there is a good chance that no

etesians occur during any given May or June. Some of this variability is expressed in table 5.3.

Table 5.3. Maximum and Minimum Number of Etesian Days Occurring Monthly and Yearly During Period 1947-1969 at Hellenikon Airport. (Metaxas)

	May	Jun	Jul	Aug	Sep	Oct	Year Jun-Sep
Max. no. year	13 1950	15 1957	23 1967	23 1949	18 1964	24 1969	60 1961
Min. no. year	0 1959	0 1948	6 1966	2 1968	5 1952	1 1960	27 1968

Table 5.4 shows the mean number of continuous etesian days for each month (May to October) and the number of cases, in a 60-year period, where the etesian lasted 5 days or more and 10 days or more. It will be noted that etesian periods of 5 days or more are not uncommon, occurring on the average about once per month in July and August.

Table 5.4. Monthly Mean Number of Continuous Etesian Days and the Number of Cases Where Duration of Etesian Was ≥5 Days and ≥10 Days (60-year period). (Metaxas)

	May	Jun	Jul	Aug	Sep	Oct
Mean no. of continuous days	2.2	2.2	3.7	3.6	3.1	2.4
No. of cases ≥5 days	10	18	63	66	46	18
No. of cases ≥10 days	1	2	16	13	10	1

5.3.2 Variations Within the Aegean Sea

Metaxas provided a thorough statistical treatment of wind observations (taken at 0800, 1400 and 2000 local time) of 40 island and coastal stations. This material, classified

into four classes of Beaufort scale and into three etesian wind directions, is given in appendix C. The high frequency of strong winds at Naxos (sta. no. 16732) should be pointed out as a remarkable feature.

The streamlines for winds ≥6 Beaufort and the frequency of such winds is given in figure 5.4. It appears that the Cyclades Islands, to which Naxos belongs, bear the brunt of the etesian throughout the season. In the interpretation of figure 5.4, allowance should be made for a bias in the wind measurements used in this analysis due to the channeling effects by islands mentioned in section 5.2. Even though it appears from figure 5.4 that the island of Crete lies outside the main reach of the etesian, strong or gale force winds are frequent along the south coast of this island during the etesian season. This is also observed elsewhere where mountains are oriented perpendicular to the etesian. Katabatic flow on the "lee side" of these mountains generate gusty wind conditions similar to the föhn of the Alps and the chinook of the Rocky mountains. In the case of Crete, gaps in the island mountain range exercise an additional channeling effect that tends to increase wind speeds locally.

5.3.3 Diurnal Variation of the Etesian

The large diurnal variation in the intensity of the etesian is caused mainly by the differential heating of land and sea. This differential heating would normally supply the pressure gradients that drive the land- and sea-breeze system. An additional influence upon the diurnal variation

of the etesian is the turbulent mixing in an adiabatic to superadiabatic planetary boundary layer that extends to a height of approximately 1000 m. over land and provides increased momentum transport towards the ground during daytime hours.

Along the west coast of Turkey the sea breeze supports the etesian, as may be seen from figure 5.4. The maximum wind force along this coast, therefore, appears near 1700 local time, and the minimum near 0500. The percent variation between maximum and minimum (expressed as a percent of the mean wind) is large, due to the superimposed land and sea breeze effect of Asia Minor. Table 5.5 gives this percent variation for the airport at Rhodos (or Rhodes, sta. no. 16749).

Table 5.5. Variation Between the Maximum and the Minimum Wind, Expressed as a Percent of the Mean, at Rhodes Airport (1955-1964). (Metaxas)

May	Jun	Jul	Aug	Sep	Oct
92	95	117	104	96	75

In Athens, on the other hand, the sea breeze opposes the etesian. Hence the frequency of northerly winds has a minimum near noon because there are days when the sea breeze is stronger than the etesian. If one examines only the days at Athens when the wind at 1400 local time is $\geq$4 Beaufort, one still obtains strongest winds during the daytime. The summer months have a tendency for a secondary minimum in the early afternoon when the opposing effect of the sea breeze is

strongest. This secondary minimum is not present during the winter (fig. 5.5). The percent variation between maximum and minimum winds at Athens is also largest during the etesian season (fig. 5.6).

Metaxas also examined the diurnal variation of winds ≥4 Beaufort at Limnos (or Lemnos, sta. no. 16651) in the northern part of the Aegean Sea, and at Naxos in the southern part. At Limnos the wind maximum occurs before 1400, whereas at Naxos it is found between 1400 and 1700 LT. At Limnos

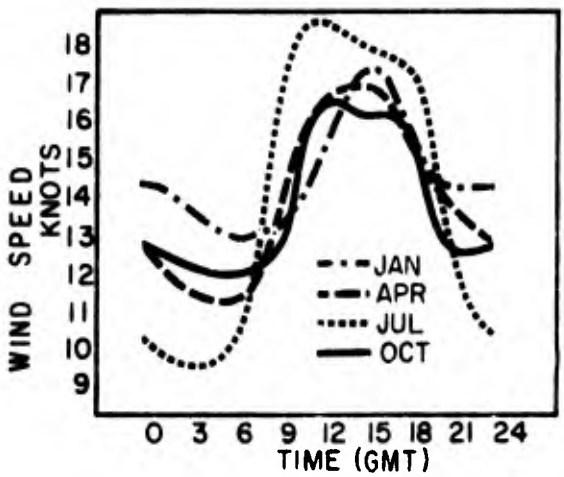

Figure 5.5 Diurnal Variation of Mean Wind Speed (kts.) at Athens for Those Days on Which the Wind at 1400 LT Is > Beaufort Force 4 (11 kts.). (Metaxas)

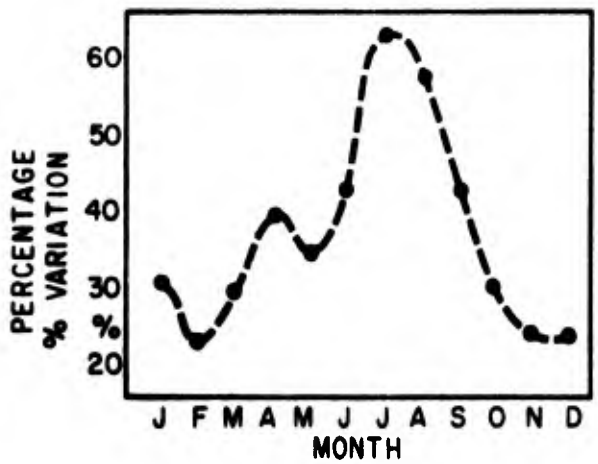

Figure 5.6 Percentage Variation Between Maximum and Minimum Winds at Athens. (Metaxas)

the mean wind force at 1600 is even less than that 0500 LT. The variability between maximum and minimum at Naxos is about one half of that at Hellenikon. At Limnos it is still less.

From the foregoing it would appear that the low-pressure trough shown along the south coast of Turkey undergoes diurnal pulsations of intensity, so that the etesians are reinforced by the sea-breeze effect in the southern Aegean. In the northern Aegean and near the Macedonian and the Thracean coasts this reinforcement by the sea breeze is absent. The heating of the land during the daytime and its influence upon the pressure gradient even opposes the etesian regime.

5.3.4 Etesian Weather

The surface flow in the etesian seems to be generally divergent (fig. 5.4). This agrees with the traditional concept that etesian weather is dry with clear skies. Metaxas reports, however, that the months of May-June and October-November show maxima of instability over Greece, and consequently a maximum of thunderstorm days. Thunderstorms and lightning frequently occur on the day preceding the outbreak of the etesian, as well as on the first day of the etesian. This holds especially for May-June and September-October, less so for July and August. In the Aegean Sea during July and August scattered clouds, mostly altocumulus, announce the establishment of an etesian-wind period the following day. This fact is well-known to local fishermen. Orographic clouds may form on some islands during the etesian, especially if winds are strong.

5.4 Case Description

Northerly winds in the Aegean are established by one of the following two processes:

(a) The eastward passage of a surface depression, with an associated cold front, over central or southern Greece. The winds then veer to north and northwest.

(b) The passage of a cold front moving towards the south or southeast. Anticyclogenesis follows over the Balkans and the wind over the Aegean veers to north to northeast. Greece is then covered by cold air.

Condition (a) prevails in the establishment of winter northerlies, condition (b) during the summer etesian regime. It is rare that a surface depression reaches Greece during summer. In winter a thermally-produced ridge of cold air over the Balkans is quite frequent. In summer the thermal trough along the Turkish south coast dominates the weather situation. This persistent thermal trough causes the high frequency of the etesians. The moving winter depressions, however, cause the higher frequency of gale or near gale force winds in the open Aegean during that season.

During strong etesian winds the thermal trough south of Turkey extends relatively far to the west, towards and beyond Rhodos. It may even form a closed low there, so that winds at Rhodos itself are almost calm.

Metaxas studied 35 cases between 1960 and 1969 in which the etesian lasted for at least 3 consecutive days. The mean 500-mb. chart for the starting days of the etesian period is shown in figure 5.7. A sharp ridge prevails over France and a trough line is located over the Ionian Sea,

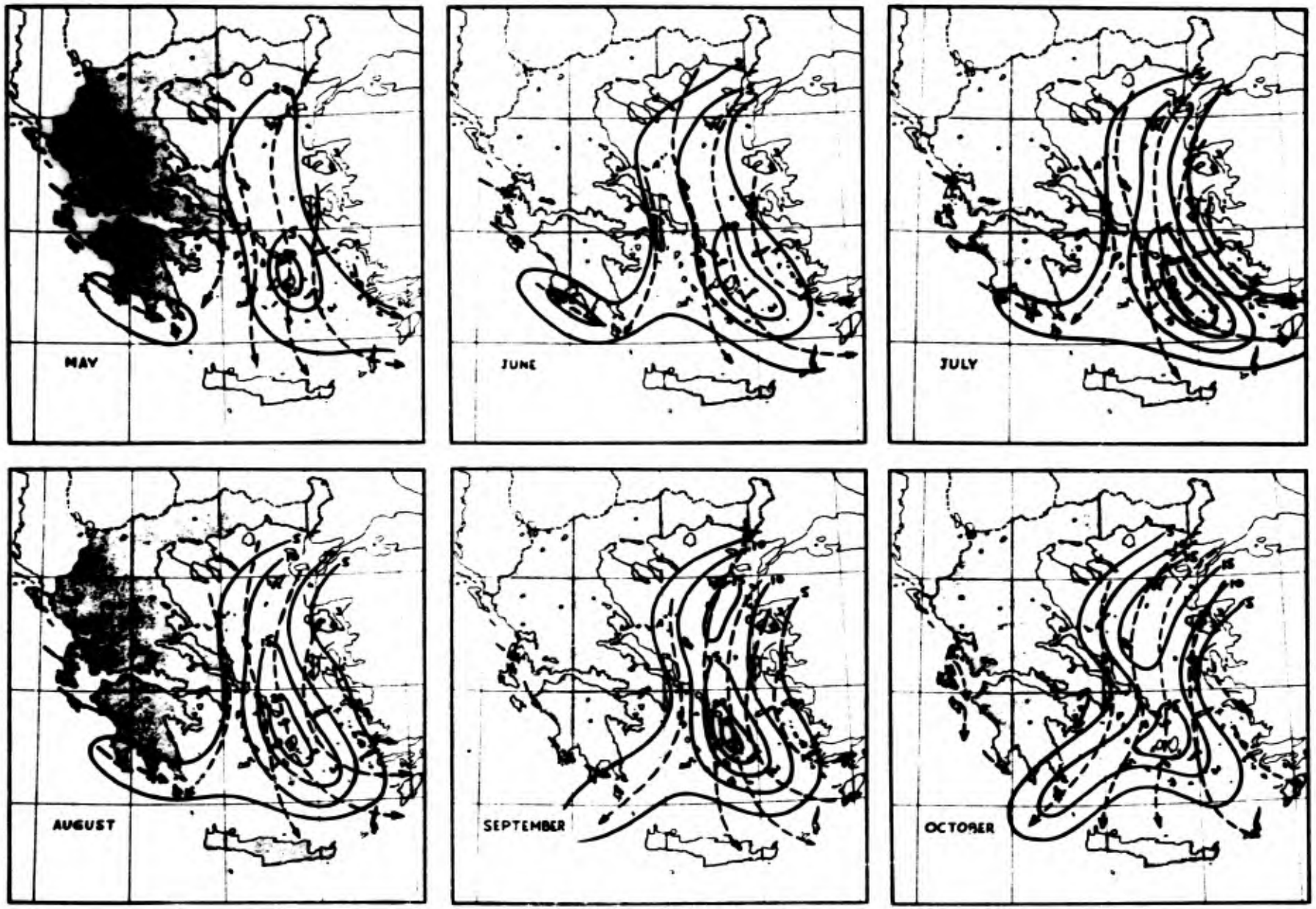

Figure 5.4 Streamlines (dashed) for Winds ≥ Beaufort Force 6 (22 kts.) and Frequency (solid lines, %) of Such Winds. (Metaxas)

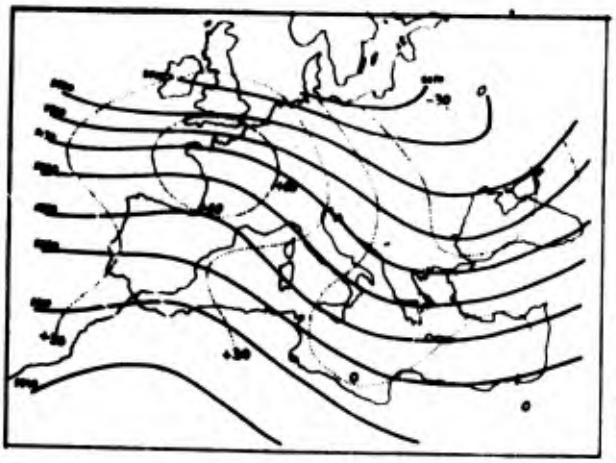

Figure 5.7 Mean 500-Mb. Chart During the First Day of an Etesian Period in July and and August Lasting for Three or More Days (35 cases from 1960-1969), Dotted Lines Are the Anomalies From the Climatological Mean. (Metaxas)

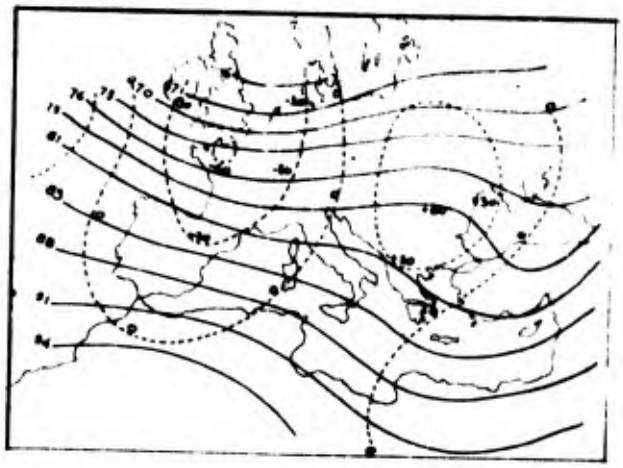

Figure 5.8 Mean 500-Mb. Chart at the Cessation of an Etesian Period in July and August Lasting for Three or More Days (35 cases from 1960-1969), Dashed Lines Are the Height Changes From the Chart in Figure 5.7. (Metaxas)

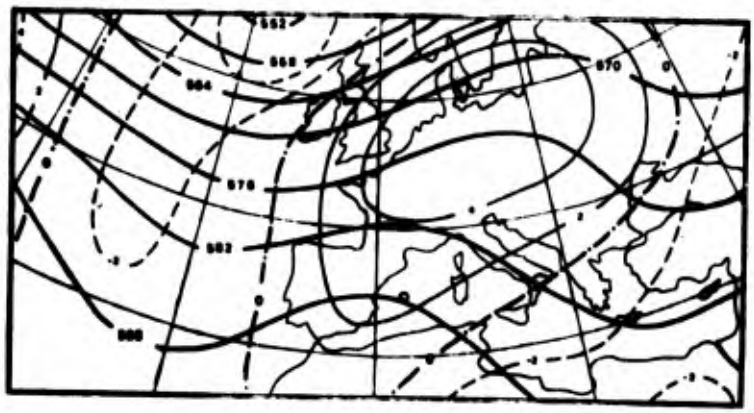

Figure 5.9 Mean 500-Mb. Chart (heavy solid lines) and Height Anomalies From the Climatological Mean, July 1967 (23 Etesian days, much above normal). (Metaxas from A. Gazzola)

northern Greece and the eastern Balkans. Judging from the vorticity advection, this pattern is conducive to cyclogenesis over Asia Minor and to anticyclogenesis over the Balkans.

Figure 5.8 shows the mean conditions for the cessation of the etesian. The trough has moved eastward. Its former position over the south Ionian Sea has now been taken up by a ridge. A trough prevails over France.

Comparison of these two charts with evidence given in section 2.4 leads to the conclusion that the mistral and the etesian occur out of phase: if one prevails the other is suppressed.

The surface weather conditions in the cases studied by Metaxas always showed a cold front moving towards the south or southeast over Greece during the establishment of the etesian regime. The day preceding the etesian is usually characterized by thunderstorms over the Balkans, often also in northern Greece, and sometimes spreading as far south as Athens. These thunderstorms are either triggered by the frontal passage or by the instability induced by vorticity advection in the trough.

The speeds of progression of the system causing the etesian may differ greatly:

(a) With fast-moving systems the subsequent etesian period usually is short, ≤ 5 days. The passing trough-ridge pattern is shallow, with westerlies prevailing above. Another etesian period frequently follows within a short time.

(b) Slow-moving systems are characterized by deep surface depressions in the Black Sea region, associated with a cut-off low at 500 mb. Strong northerly winds prevail at upper levels. An extended etesian period follows with strong and gusty winds at the surface. Thunderstorms in the eastern Balkans and over northeastern Greece and northern Turkey often continue for several days.

The influence of the synoptic pattern upon the establishment of the etesian becomes strikingly evident on comparison of the mean 500-mb. flow patterns of July 1967 (23 etesian days) and August 1968 (2 etesian days) (figs. 5.9 and 5.10).

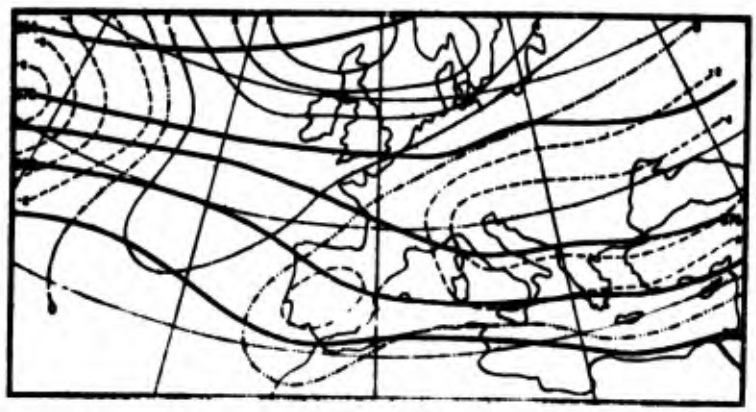

Figure 5.10 Mean 500-Mb. Chart (heavy solid lines) and Height Anomalies From the Climatological Mean, August 1968 (2 Etesian days, much below normal). (Metaxas from A. Gazzola)

The ridge and trough shown in figure 5.9 lie slightly farther to the east than in figure 5.7. The latter figure characterizes conditions during the outbreak of the etesian, whereas figure 5.9 holds during a persistent etesian regime. One should expect, therefore, that the ridge-trough pattern of figure 5.9 should lie halfway between that of figures 5.7 and 5.8.

The establishment and cessation of a short etesian period is illustrated in figures 5.11 and 5.12 (7 September 1969 and 11 September 1969). Anticyclogenesis over the Balkans behind a cold front, and thunderstorm activity as far south as Athens heralded the arrival of the etesian. The movement of the upper low over Italy and a warm frontal system moving northeastward into Greece terminated the etesian period.

The establishment of an extended etesian period with a blocking ridge over France is illustrated in figure 5.13. Short-wave disturbances moving into the long-wave trough produced surges in the etesian, the first one appearing on 15 July 1969, in association with a cold front moving southward over Greece and Turkey. The persistent long-wave ridge-trough pattern caused the month of July 1969 to be of the coldest on record. The etesian period continued until

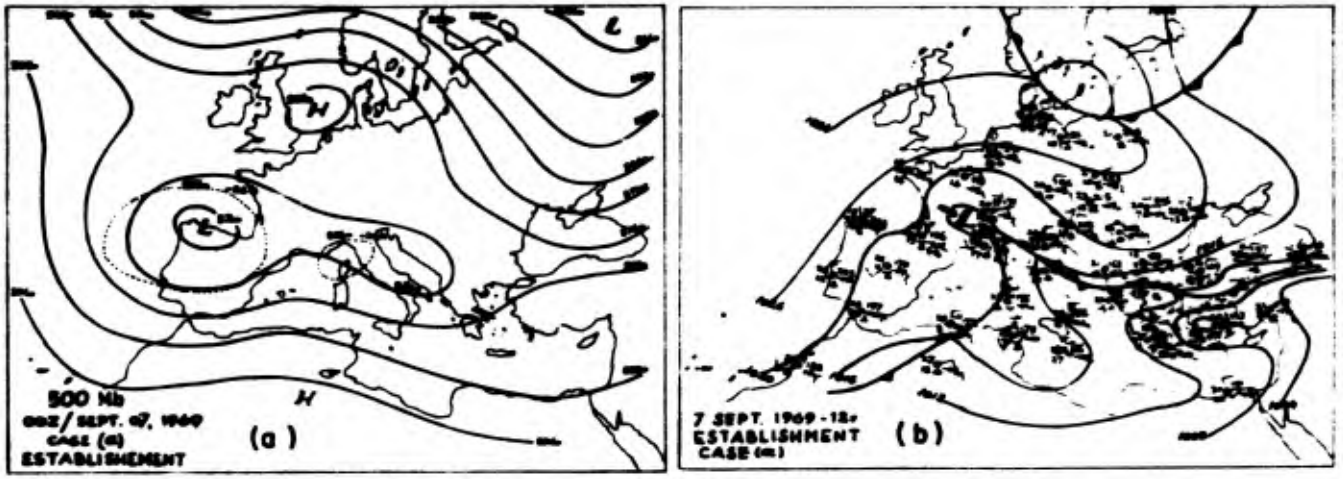

Figure 5.11 (a) 500-Mb. 0000 GMT and (b) Surface Analysis 1200 GMT, 7 September 1969 (establishment of a short Etesian period). (Metaxas)

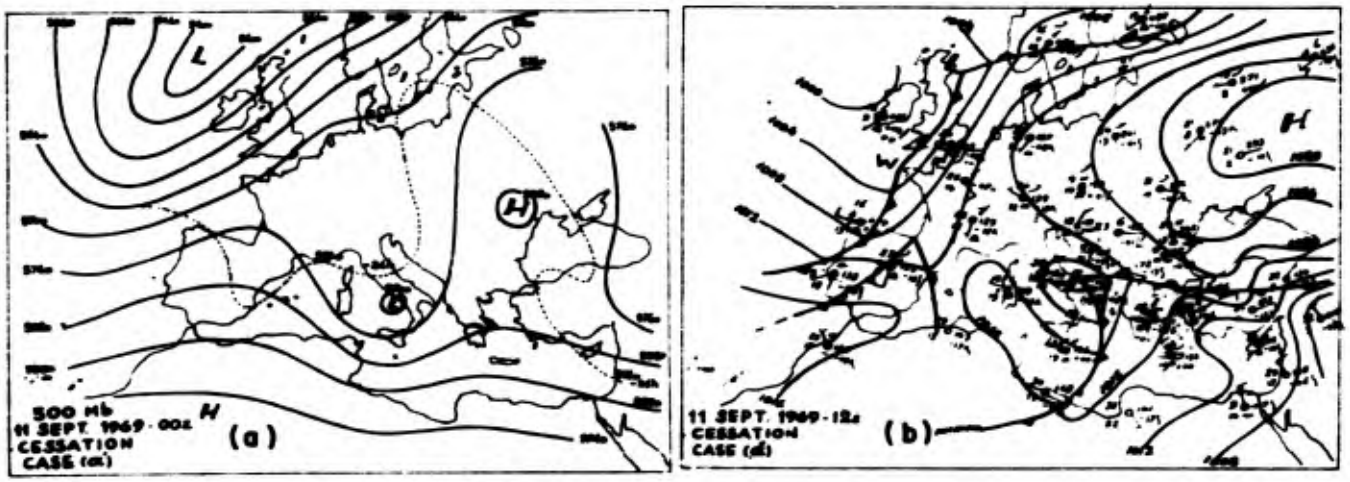

Figure 5.12 (a) 500-Mb. 0000 GMT and (b) Surface Analysis 1200 GMT, 11 September 1969 (cessation of a short Etesian period). (Metaxas)

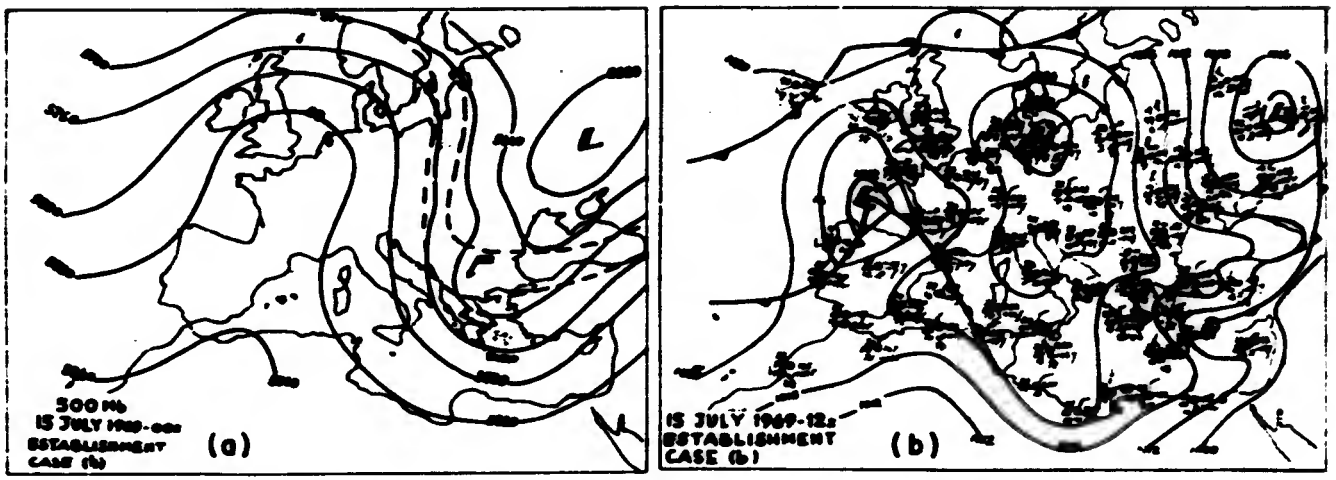

Figure 5.13 (a) 500-Mb. 0000 GMT and (b) Surface Analysis 1200 GMT, 15 July 1969 (establishment of a long Etesian period). (Metaxas)

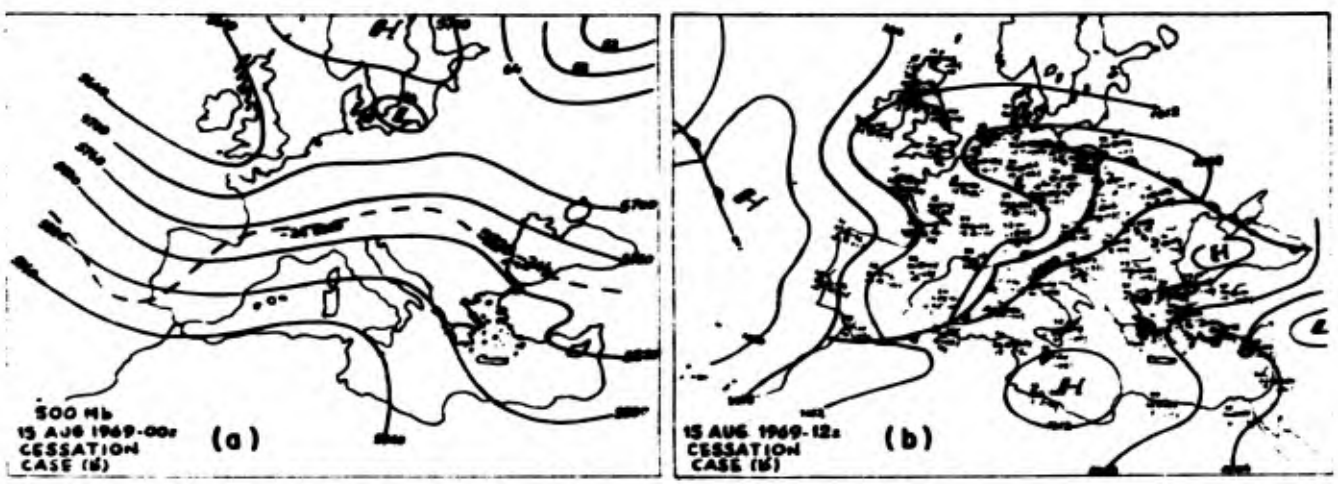

Figure 5.14 (a) 500-Mb. 0000 GMT and (b) Surface Analysis 1200 GMT, 15 August 1969 (cessation of a long Etesian Period). (Metaxas)

26 July, and reestablished itself after only short interruptions. Finally, on 13 August, the cut-off low over eastern Europe started to move and with the farther eastward movement of the ridge, the etesian surges terminated on 15 August 1969 (fig. 5.14). Short-wave disturbances moving in the now established westerly current from Italy into Greece affected only the western part of the country and no longer gave rise to etesian winds.

5.5 Forecasting the Etesian

The main tool in forecasting the etesian, its outbreak and its cessation, is the 500-mb. chart. The passage of troughs and ridges, as described in section 5.4, provides the clue to successful forecasting. Again, the numerical forecasting product presently available is not the complete answer. The use of additional forecasting tools, such as continuity diagrams (trough-ridge diagrams) centered at 40° N. latitude, is advocated.

A blocking long-wave ridge over France and western Germany, located farther to the east than its normal position (see fig. 2.2), heralds extended etesian periods. Under more zonal ("high-index") flow conditions (figs. 5.11 and 5.12), transient etesian episodes may be expected.

In terms of its establishment, and its forecasting problems, the etesian bears a certain similarity to the mistral. It appears, therefore, that similar forecasting techniques should apply.

6. THE RED SEA CONVERGENCE

(Based upon material supplied by D. Pedgley, H. Flohn and Cdr. ROE.)

6.1 Definition

During the cool season (October to May) a low-level convergence zone between northerly and southerly flow forms over the Red Sea. This zone is characterized by light and variable winds.

6.2 General Description

From about October to May, a northwesterly air stream from the Mediterranean blows across the northern part of the Red Sea; whereas coming from the Gulf of Aden across the plains of Afar and through the narrow southern entrance to the Red Sea (the Bab el Mandeb), there is a stream blowing from the southeast (fig. 6.1). These two streams meet in a region of calm or light and variable winds known as the Red Sea Convergence Zone. During the northern winter, the average position of this convergence zone is relatively far to the north, near Port Sudan, but subsequently it moves southward into the latitude of Massawa (sta. no. 63203). Cloudiness with heavy rains may occur along this convergence zone, at time spreading into the normally arid regions of Arabia. (Pedgley)

6.3 Occurrence

Detailed synoptic maps of the southern Red Sea are extremely difficult to draw because of lack of observations from

Figure 6.1 Locator Map of the Southern Red Sea Area. [18]

both land stations and ships. In addition, the land stations are situated near the coast with diurnal variations especially affected by a sea breeze.

During February 1964, time cross-sections of ship data indicated the average position of the convergence zone was at approximately 17° N. (fig. 6.2). The zone was characterized by day-to-day variations in position, with significant pulses separated by a period of approximately 5 days. This movement is typical during the months October to May. The southerly stream of air extended at least as far north as 22° N. and

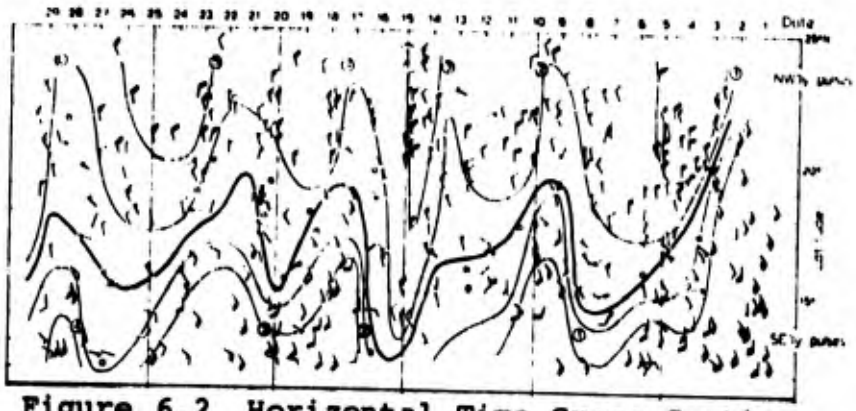

Figure 6.2 Horizontal Time Cross-Section Along the Mid-Line of the Southern Red Sea Showing Winds Reported by Ships During February 1964. [18]

the northerly winds at times reached as far south as 13° N. The winds were remarkedly confined to preferred directions, either northwest to north or southeast to south. When the wind speed was less than 10 knots, there was a tendency for stronger fluctuations in direction. These fluctuations may be an indication of weak mesoscale circulations. One must be aware of the large number of errors which occur in computing light winds onboard moving ships. (Pedgley)

As may be noted from figure 6.2, the winds blowing through the narrow strait of Bab el Mandeb may at times be quite strong; winds of 20 to 30 knots are common and they may reach gale force. These winds are connected with the northeast monsoon over the Arabian Sea that extends into the Gulf of Aden. Roe related his experiences with a freak tropical storm in the Gulf of Aden during November 1967, which could be detected only from satellite pictures. Easterly winds of 40 to 45 knots were encountered over the middle of the Gulf of Aden, reaching possibly 60 to 70 knots along the north

coast of the Somalian Republic. Channeling of these winds through Bab el Mandeb could produce severe hazards to naval operations. However, such incidents appear to be rare.

6.4 Case Description

When the northerly and southerly air streams remain in contact with the sea for at least a few hours, the turbulent and radiative exchange of heat tends to produce a maritime layer that has a potential temperature comparable to the sea surface temperature, and a depth which may be as great as a few thousand feet. The surface of the southern Red Sea has a remarkedly uniform average temperature -- in February it is about 26° C. -- so it is not surprising that both southerly and northerly flows have maritime layers with similar temperatures. However, from a large number of soundings it seems that the maritime layer associated with the southerly flow is just slightly warmer. Where the two streams meet, the resulting convergence deepens the maritime layer, and the lifting produces clouds which appear as a sheet with its top sharply defined by the base of the inversion. The resulting release of latent heat increases the potential temperature of the rising air which is thus able to return northwards above the lower, northwesterly winds (fig. 6.3). (Pedgley)

Cloud tops cannot greatly exceed the level of the neighboring plateau because once this altitude is passed, the potentially much cooler maritime layer spills onto the plateau. The soundings indicate the presence of a lower, cool and moist,

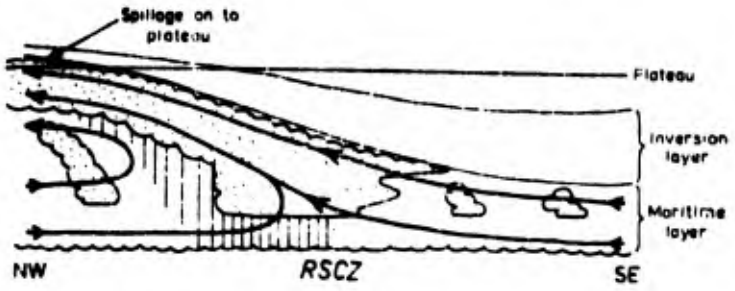

Figure 6.3 Schematic Diagram Showing the Formation of Stratiform Cloud Within the Returning Maritime Layer of the Southeasterly Flow Along the Red Sea Convergence Zone (RSCZ). [18]

maritime layer sometimes consisting of northwesterlies surmounted by southeasterlies, and separated by a very stable layer (often an inversion) from a land-derived, warm and dry layer aloft. This great stability strongly inhibits vertical motion. Consequently, over the Red Sea, flow is parallel to the walls of the deep rift in the earth's surface within which the Red Sea lies.

It is clear from the limited vertical depth of the maritime layer that cumulus clouds must be shallow, unless daytime heating over land is able to destroy the inversion. Thus, over the sea and adjacent coastal plains one would expect the highest possible cumulus tops to be at about 8,000 feet. With a typical base around 2,000 feet, such clouds are deep enough to produce at most only moderate showers of short duration. Heavy thundershowers, supported by a sea-breeze effect, are likely to occur over the escarpment of the rift valley only south of the convergence zone. (Pedgley, Flohn)

An episode of torrential rains over the Red Sea between 15 and 20 April 1968, has been described by Pedgley. Although such rainfalls are very rare indeed, a short description of the pertinent weather pattern is given here because it shows

the involvement of the subtropical jet stream over Africa. Unfortunately, at this time we know only little about the behavior of this jet.

Rainfall totals for the period in question are given in figure 6.4. They were associated with a deep trough aloft (fig. 6.5) and a cold front which penetrated unusually far south (fig. 6.6). The development was probably triggered by a jet maximum over North Africa (fig. 6.7), whose existence could be established reliably only by the use of aircraft Doppler wind information. Such data usually are difficult, if not impossible, to obtain on a routine basis.

6.5 Forecasting Problems

It is felt that the Red Sea convergence itself presents no great hazards to traffic, either at sea or in the air. High winds in the strait of Bab al Mandeb are a different matter. There, however, one is faced with the lack of adequate data upon which to base reliable forecasts. Roe discussed frustrating experiences in trying to predict squalls that move in the northeasterly winter monsoon from the Persian Gulf into the Arabian Sea.

During the southwest monsoon (summer season) traffic proceeding eastward in the Gulf of Aden becomes fully exposed to strong winds when rounding Cape Guardafui, the most easterly point of the Somali Republic. There a low-level jet stream blows along the coast of east Africa. A shear line and eddies may develop downstream (towards the northeast) of the Cape during this season.

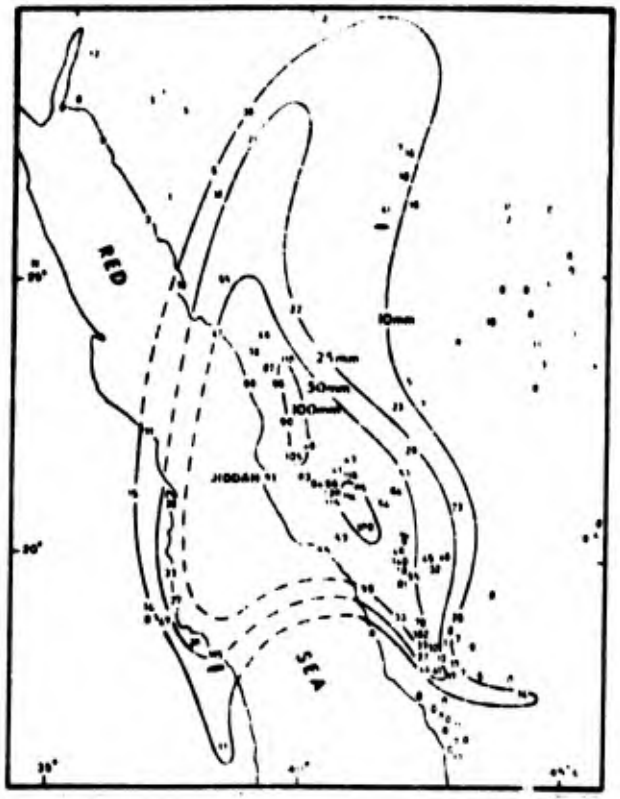

Figure 6.4 5-Day Rainfall Totals (mm.) Over Northwest Arabia, 0900 LT 15 April to 0900 LT 20 April 1968. [18]

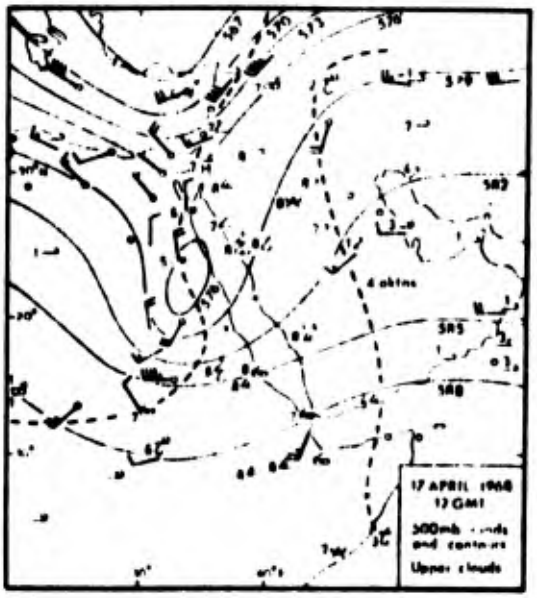

Figure 6.5 500-Mb. Analysis and Upper Cloud Observations, 1200 GMT 17 April 1968 (areas between dashed lines >4 okta of upper clouds). [18]

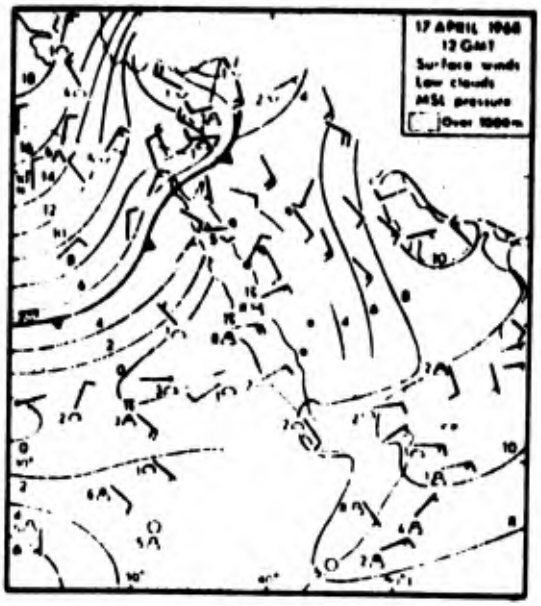

Figure 6.6 Mean Sea-Level Pressure (mb.) Surface Winds and Low Clouds, 1200 GMT 17 April 1968. [18]

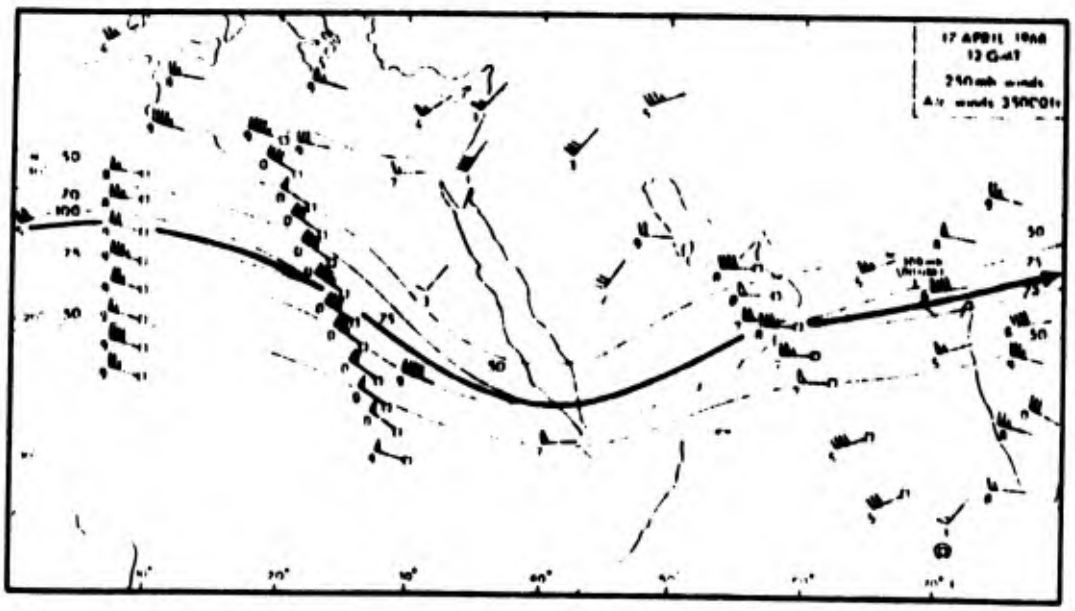

Figure 6.7 250-Mb. Winds and 35,000 Ft. Aircraft Winds, 1200 GMT 17 April 1968. [18]

The effect of the subtropical jet stream on thunderstorm activity and precipitation over the Red Sea area during the cool season is difficult to forecast because of lack of data. Satellite cloud photos and time sections of the few reporting radiosonde stations should be used to locate the jet stream and any long- or short-wave patterns.

Climatological and synoptic analyses have shown that the jet axis over Arabia in April occurs most frequently near 30° N. A similar latitude has been found over India and northeastern Africa, but at 0° E. over northwest Africa it is nearer 25° N. These latitudes agree reasonably with the trough-and-ridge pattern found by Krishnamurti based on data for three mid-winter months. No observations have been published on the extent and frequency of daily departures from this mean position. (Flohn)

We have to suspect that when the jet stream is displaced far to the south of its normal position, abnormal weather should be expected over the Red Sea and the Arabian Peninsula. In particular, the southwesterly current ahead of a deep trough which penetrates into tropical latitudes may harbor considerable thunderstorm and precipitation activity. In the absence of radiosonde or Doppler wind data, satellite photographs may provide the only clues to such rare but hazardous weather patterns. (Flohn, Reiter)

REFERENCES

1. AIR MINISTRY, METEOROLOGICAL OFFICE, "Weather in the Mediterranean." London, Her Majesity's Stationery Office, Vol. I, 362 pp., Vol. II, 372 pp., 1962.

2. BEAN, B. R., B. A. CAHOON, C. A. SAMSON, and G. D. THAYER, "A World Atlas of Atmospheric Radio Refractivity." U.S. Government Printing Office, ESSA Monograph 1, 130 pp., 1966.

3. BIRTWISTLE, A., Geog., 31, pp. 59-62, 1946.

4. CENFAM, "Research Work on the Project 'Cyclonge Development in the Lee of the Alps'." Second General Report, Centro Nazionale per la Fisica dell'Atmosfera e la Meteorologia, Rome, 1963.

5. _____, "Research Work on the Project 'Cyclone Development in the Lee of the Alps'." Fourth General Report, Centro Nazionale per la Fisica dell'Atmosfera e la Meteorologia, Rome, 1964.

6. CRAIG, J. I., Cario Sci. J., 3, pp. 70-72, 1969.

7. DUBIEF, J. and P. QUENEY, La Met., 11, pp. 80-91, 1935.

8. DURWARD, J., Met. Mag., 63, pp. 57-61, 1928.

9. EL-FANDY, M. G., Quart. J. R. Met. Soc., 66, pp. 323-335, 1940.

10. EL-TANTAWY, A. H. I., W.M.O. Tech. Note No. 64, pp. 159-171, 1964.

11. GEORGE, J. J. and P. M. WOLFF, "Cyclogenesis Over Southern Europe and Mediterranean Waters." AROWA 13-1152-038, 82 pp., 1952.

12. HARE, F. K., Met. Off., SDTM No. 43, 1943.

13. HUSCHKE, R. E. (editor), Glossary of Meteorology. American Meteorological Society, Boston, 638 pp., 1959.

14. KIRK, T. H., W.M.O. Tech. Note No. 64, pp. 35-48, 1964.

15. _____, Quart. J. R. Met. Soc., 92, pp. 374-381, 1966.

16. LUNSON, E. A., Met. Off., Prof. Notes 7, No. 102, 1950.

17. METEOROLOGICAL OFFICE, Met. Rep. No. 5, 1950.

18. PEDGLEY, D. E., "The Red Sea Convergence Zone." Weather 21(10):350-358, 1966a.

19. _____, "The Red Sea Convergence Zone." Weather 21(11):394-406, 1966b.

20. QUENEY, P., Trav. Inst. Rech. Sah., 3, 1945.

21. _____, Ann. Geoph., 2, pp. 309-314, 1946.

22. REITER, E. R., "Jet Stream Meteorology." Univ. of Chicago Press, 515 pp., 1963.

23. _____, "Atmospheric Transport Processes. Part III: Hydrodynamic Tracers." U.S. Atomic Energy Commission, Div. of Tech. Information (in preparation), 1971.

24. REITER, E. R. and A. NANIA, "Jet-Stream Structure and Clear-Air Turbulence (CAT)." J. Applied Meteorol. 3(3):247-260, 1964.

25. REITER, E. R. and L. F. WHITNEY, "Subtropical or Polar-Front Jet Stream." Colorado State University, Atmos. Sci. Tech. Paper No. 66, 11 pp., 1965.

26. _____, "Interaction Between Subtropical and Polar-Front Jet Stream." Monthly Weather Review, 97(6):432-438, 1969.

27. REX, D. F., "Blocking Action in the Middle Troposphere and Its Effects Upon Regional Climate. I. Aerological Study of Blocking Action." Tellus 2(3):196-211, 1950a.

28. _____, "Blocking Action in the Middle Troposphere and Its Effects Upon Regional Climate. II. Climatology of Blocking Action." Tellus 2(4):275-301, 1950b.

29. _____, "The Effect of Atlantic Blocking Upon European Climate." Tellus 3(2):1000-111, 1951.

30. SAYED AHMED, M. M., U.A.R., Met. Dept., Pap. No. 1, 1949.

31. SUTTON, L. J., Cario Phys. Dept. Pap. No. 10, pp. 1-8, 1923.

REFERENCES (CONTINUED)

32. SUTTON, O. G., Micrometeorology, McGraw Hill, 1953.

33. THOMPSON, B. W., "The Climate of Africa." Oxford Univ. Press, Oxford, 1965.

34. TWIST, T. F., Met. Mag., 71, pp. 214-215, 1936.

35. U.S. NAVAL OCEANOGRAPHIC OFFICE, "Sailing Directions for the Mediterranean and Western Africa." H.O. Pubs. 50-56.

APPENDIX A

NORMAL PRESSURE TENDENCIES AT SYNOPTIC HOURS IN THE MEDITERRANEAN.

The information contained in Appendix A was provided by the Director of Meteorology and Oceanographic Services (Naval), Royal Navy, London. ["NWS/35/60/179a"]

The analysis of synoptic charts and the estimation of movement of isobaric forms and features is complicated in the Mediterranean and lower latitudes by the pronounced diurnal variation of pressure. This variation has been analysed into diurnal and semi-diurnal components which have been studied in detail by various authorities. The semi-diurnal component has been shown to be fairly regular at or near sea level; its amplitude decreases with increase of latitude and with altitude above m.s.l. The diurnal component is more pronounced inland and at high altitudes, but is also irregular and is sensitive to diurnal variations of temperature, and hence to local variations of cloudiness, rain belts and other weather factors. Over the sea, however, both components are regular, though in landlocked waters even as extensive as the Mediterranean, seasonal fluctuations are observed.

The need has long been felt for tables or charts of representative normals of the pressure tendency at synoptic hours as an aid to forecasting. The attached maps are designed to show representative normals of pressure tendency at all the current synoptic hours between latitudes 30° N. and 45° N. There are four sets of eight charts, one for each season: Spring (March-May), Summer (June-August), Autumn (September-November) and Winter (December-February). Isopleths are drawn at intervals of 0.2 mb., as dashed lines for falling tendencies and as continuous lines for rising ones.

General Notes.

The following notes give some of the principles used in the construction of the charts and explain some of the dominant features:

(a) As a result of the large diurnal amplitude of temperature which produces a large amplitude of pressure tendency in inland areas (especially over N. Africa) the isopleths, notably on the mid-day and evening charts, tend to follow the coast. The modifying influence of the sea is thus clearly apparent.

(b) Where the coverage of observations over high ground (e.g. over N. Africa) was obviously inadequate, no attempt was made to allow for the effect of the high ground on the pressure tendency.

(c) Inland daily tendencies are likely to be greater than normal in cloudless weather and less than normal when clouds and precipitation prevail. When using the charts for these regions, therefore, interpolation between isopleths must be carefully done.

(d) Two stations in the Azores for which data were available are tabled in the left hand margin of the charts.

Sources of Data.

The following sources of data have been used:

(a)	Gibraltar	Met. Mag. Vol. 87, p. 294, 1958.
(b)	Algerian Stations	Weather in the Med., Vol. III.
(c)	Marseilles, Malta	Weather in the Med., Vol. I. (New Edition).
(d)	Italian Stations, Sardinia	Rivista di Met. Aero., XVII, No. 3, p. 3, Rome 1957.
(e)	Spanish Stations, including Mahon. Egyptian, Turkish and Levantine Stations.	Data worked up from Hofmeyr, W.J., Notes, Vol. 7, p. 6, Pretoria, 1958.

(f)	Sea Areas	Jameson, H., M.O. Prof. Note No. 105, 1952 and Netherlands Atlas (Mediterranean)
(g)	General	S.D.T.M. No. 47

Inconsistencies have inevitably arisen between these reports and in some cases have been difficult to resolve. It has been necessary to ignore almost completely the Dutch observations; those from Malta were supplemented by two other sets of observations recorded in manuscript notes, but it has been difficult to fit them all into certain charts. The coverage of observations is fairly good except over the Balkans and Libya. Supplementary values for Nicosia and Tobruk have been obtained by averaging the daily tendencies recorded in Daily Weather Reports by these stations over a period of about four years. Reference (g) has been used extensively to provide data over the Balkans.

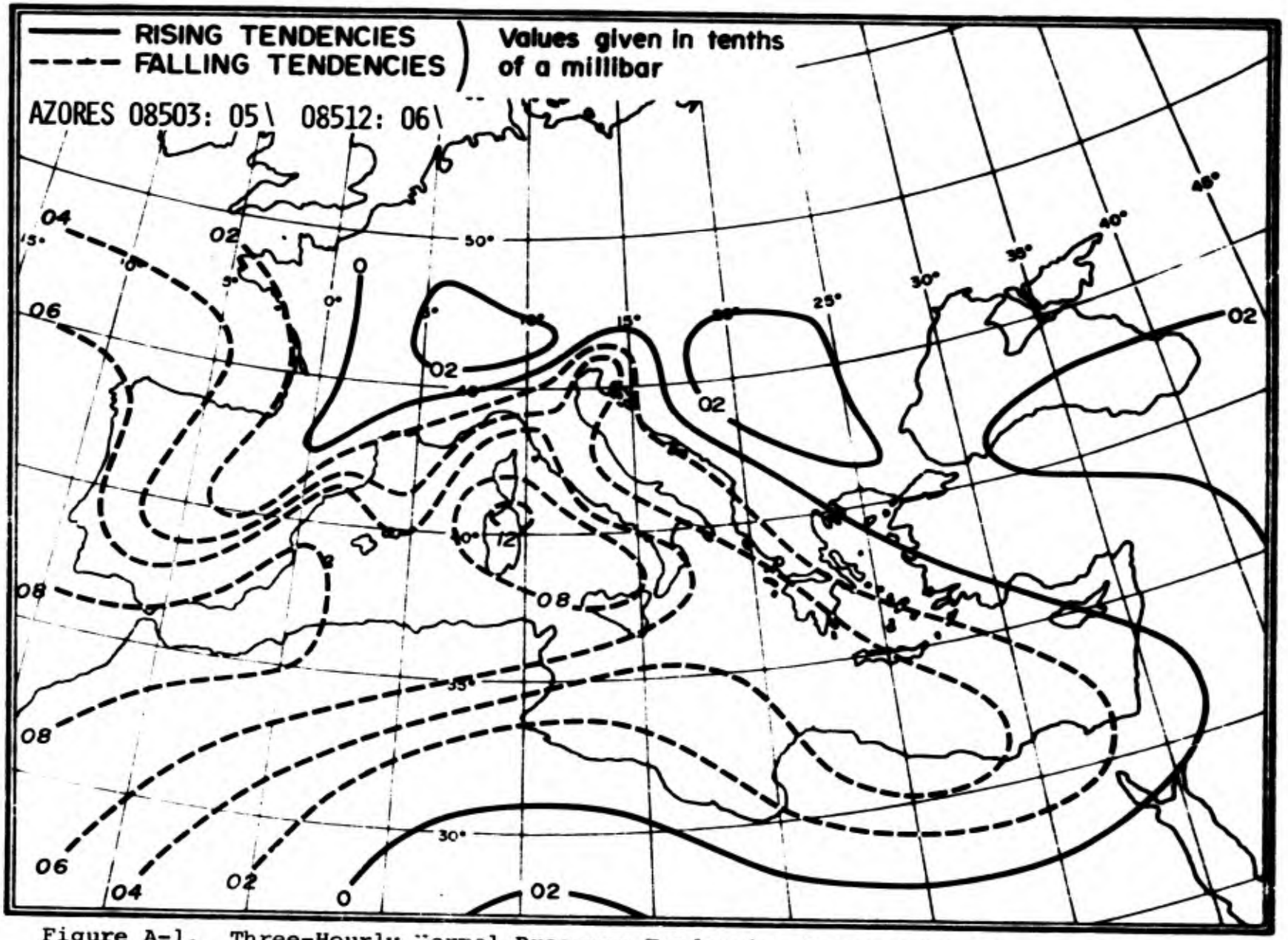

Figure A-1. Three-Hourly Normal Pressure Tendencies Between 0000 GMT and 0300 GMT (valid at 0300 GMT) Spring.

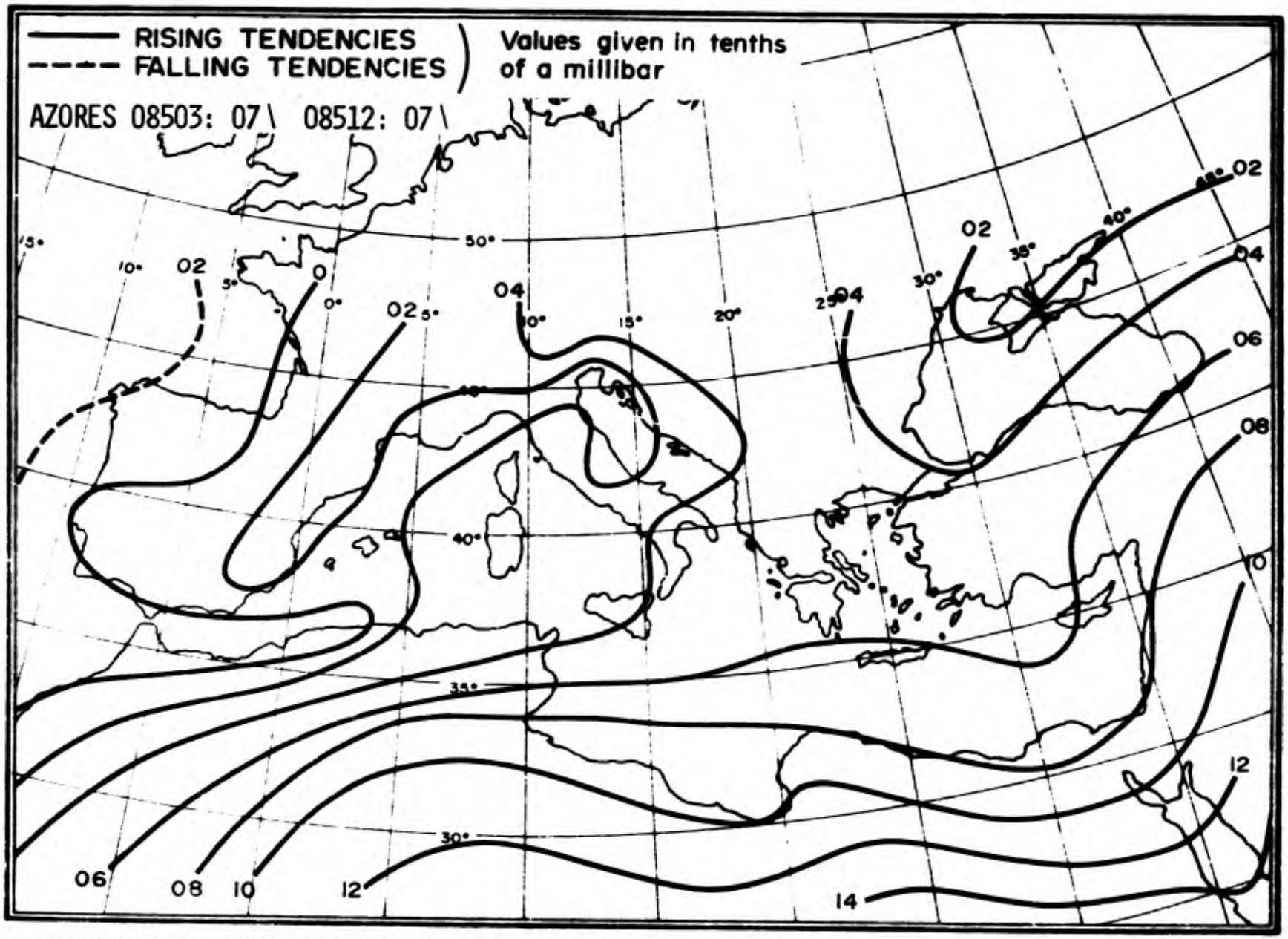

Figure A-2. Three-Hourly Normal Pressure Tendencies Between 0300 GMT and 0600 GMT (valid at 0600 GMT) Spring.

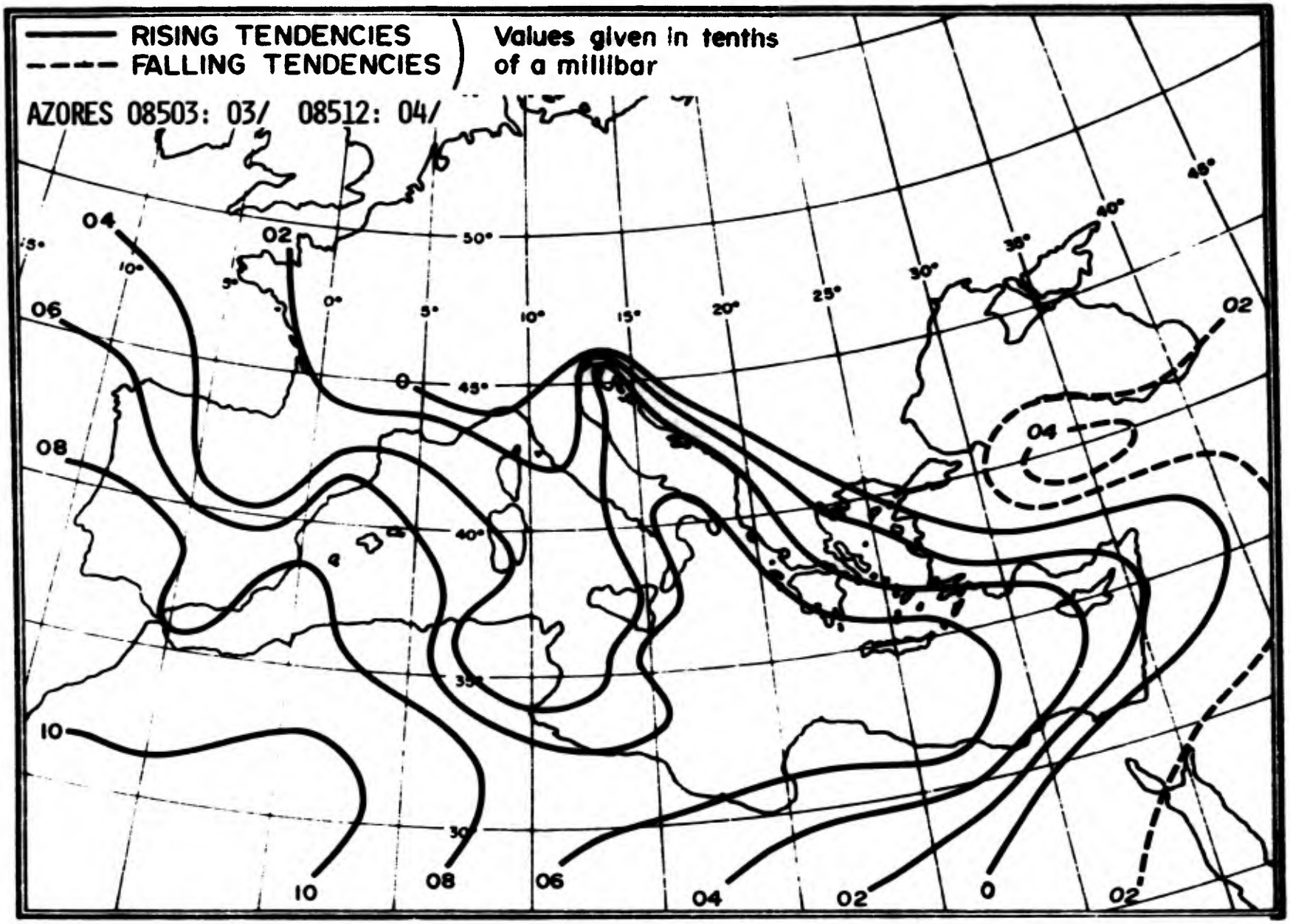

Figure A-3. Three-Hourly Normal Pressure Tendencies Between 0600 GMT and 0900 GMT (valid at 0900 GMT) Spring.

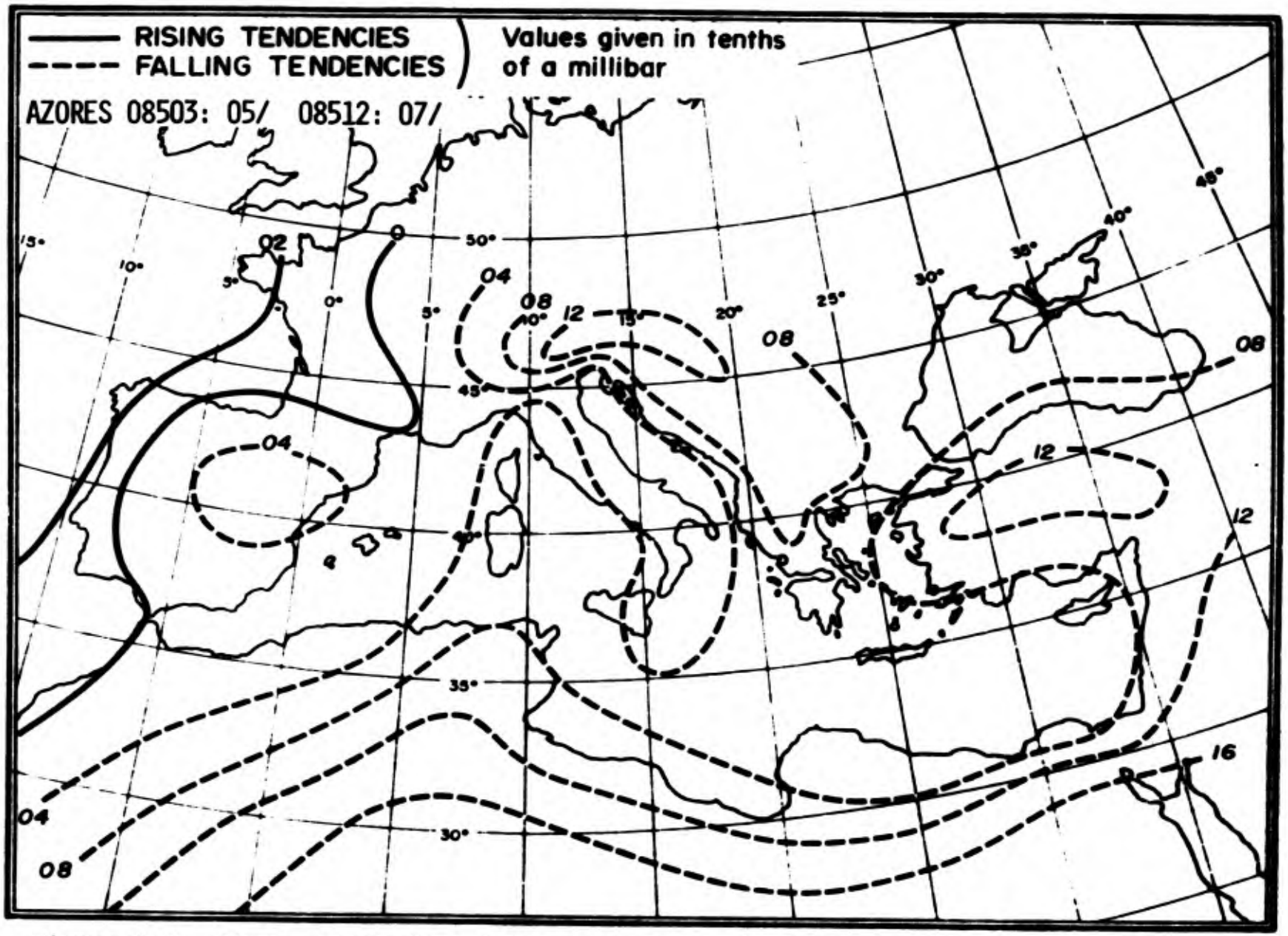

Figure A-4. Three-Hourly Normal Pressure Tendencies Between 0900 GMT and 1200 GMT (valid at 1200 GMT) Spring.

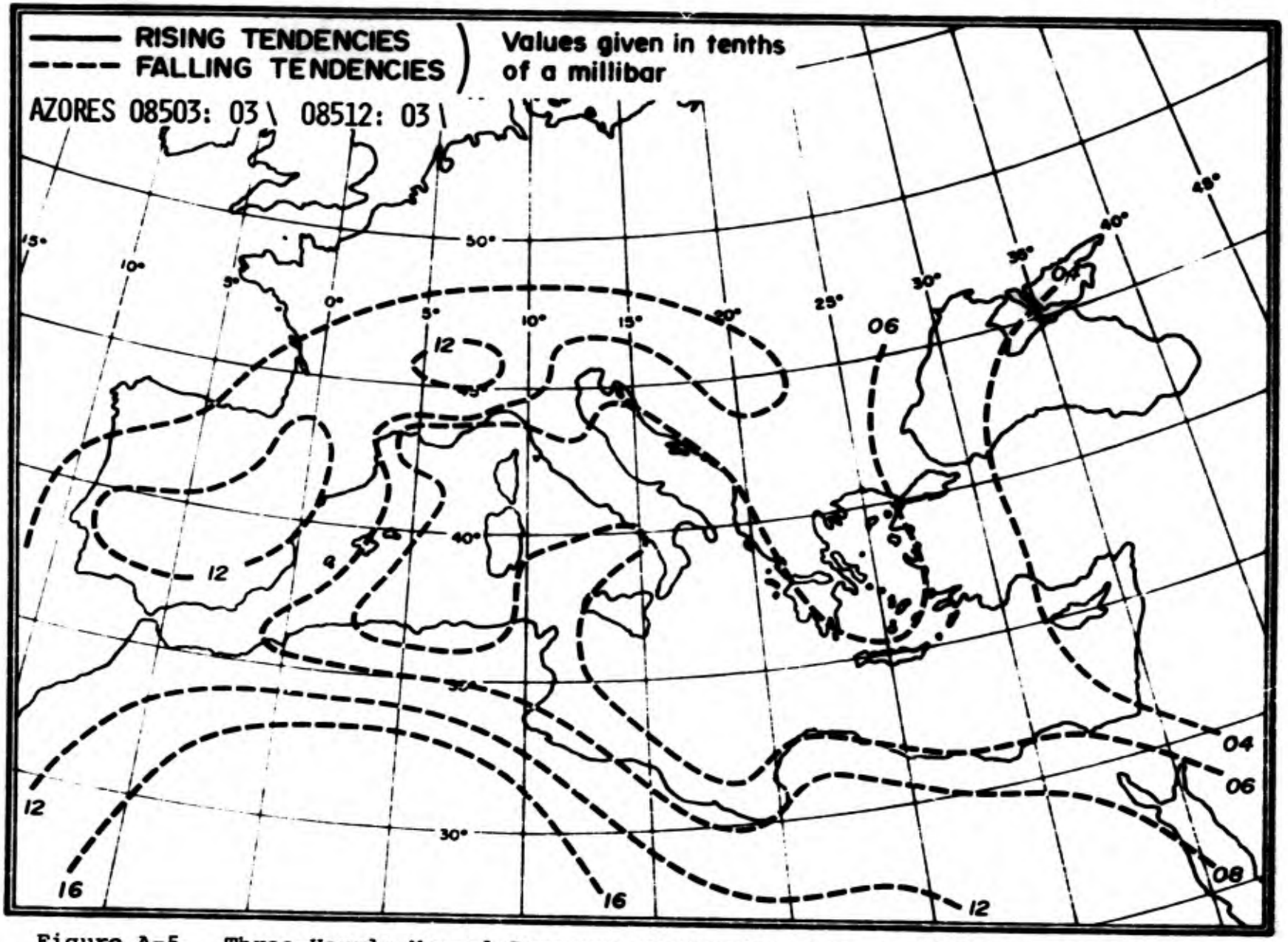

Figure A-5. Three-Hourly Normal Pressure Tendencies Between 1200 GMT and 1500 GMT (valid at 1500 GMT) Spring.

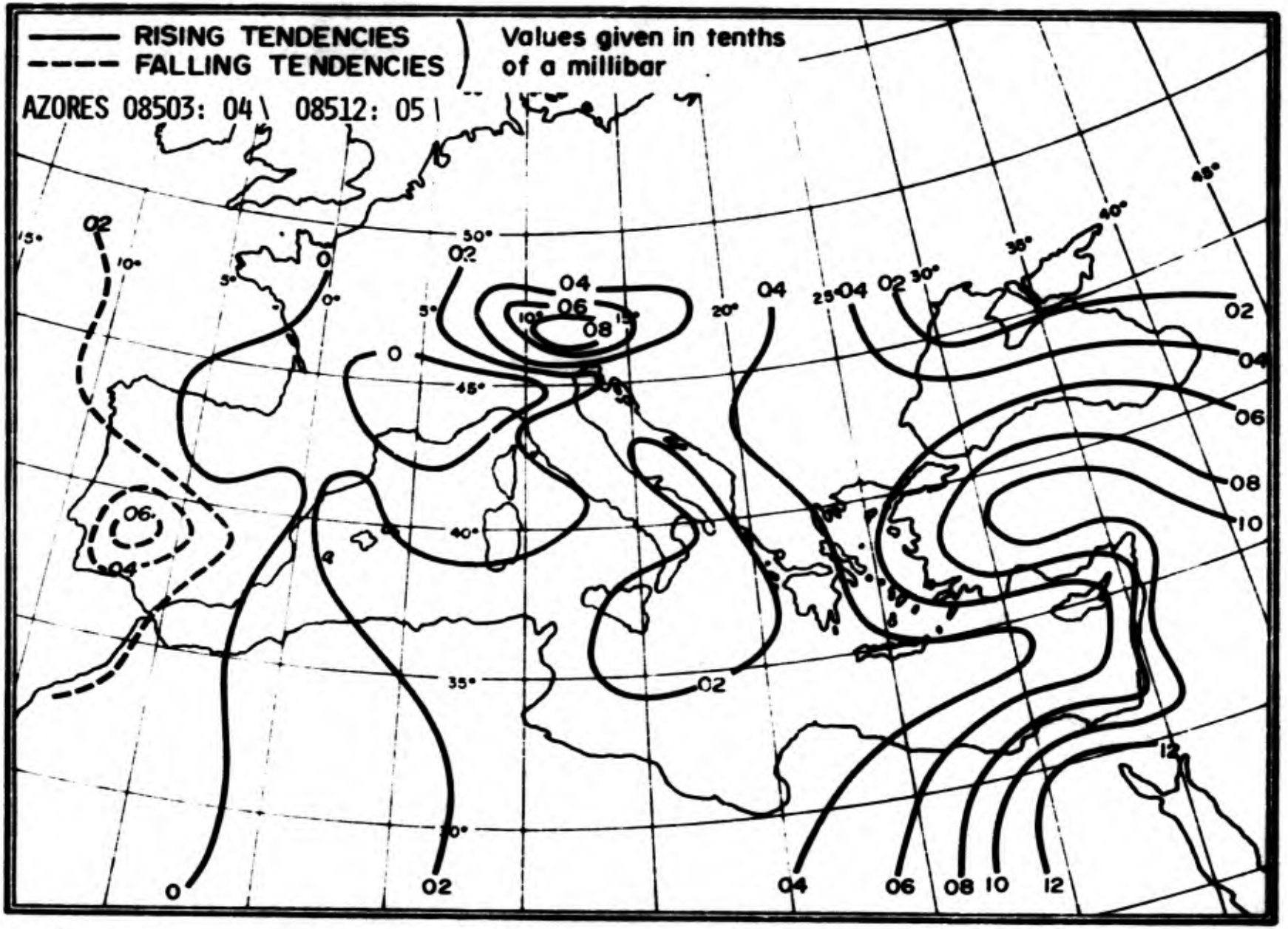

Figure A-6. Three-Hourly Normal Pressure Tendencies Between 1500 GMT and 1800 GMT (valid at 1800 GMT) Spring.

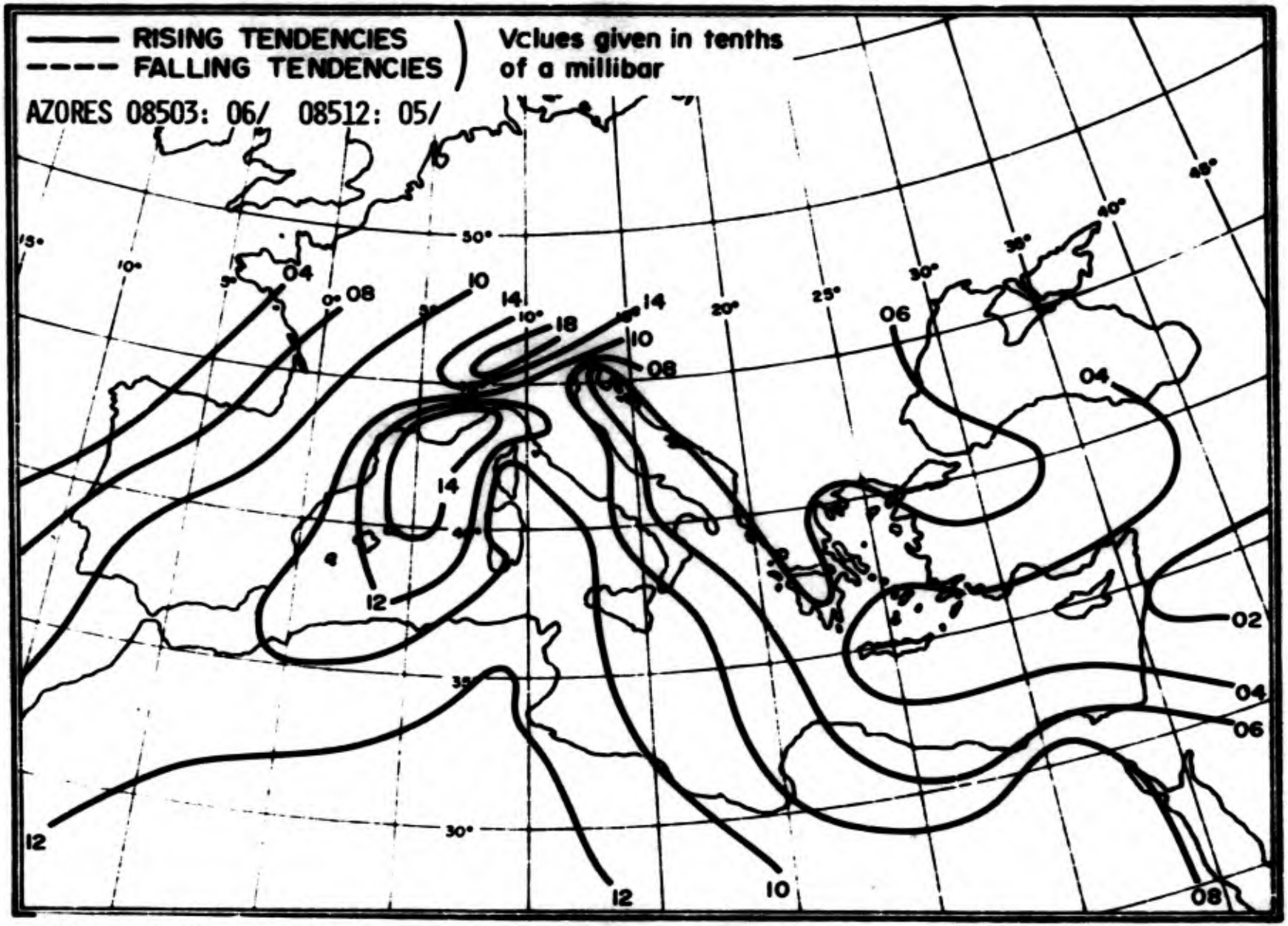

Figure A-7. Three-Hourly Normal Pressure Tendencies Between 1800 GMT and 2100 GMT (valid at 2100 GMT) Spring.

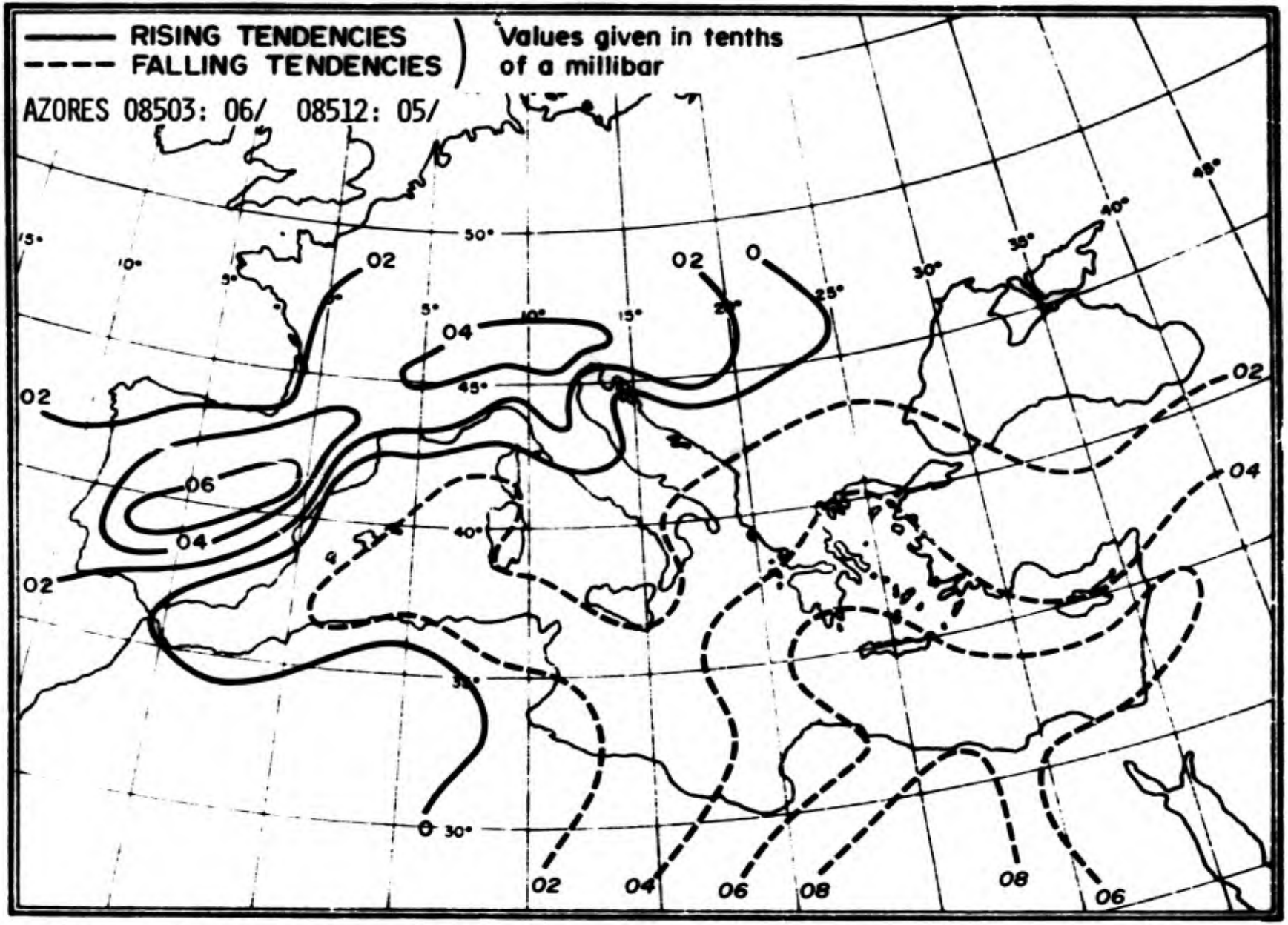

Figure A-8. Three-Hourly Normal Pressure Tendencies Between 2100 GMT and 0000 GMT (valid at 0000 GMT) Spring.

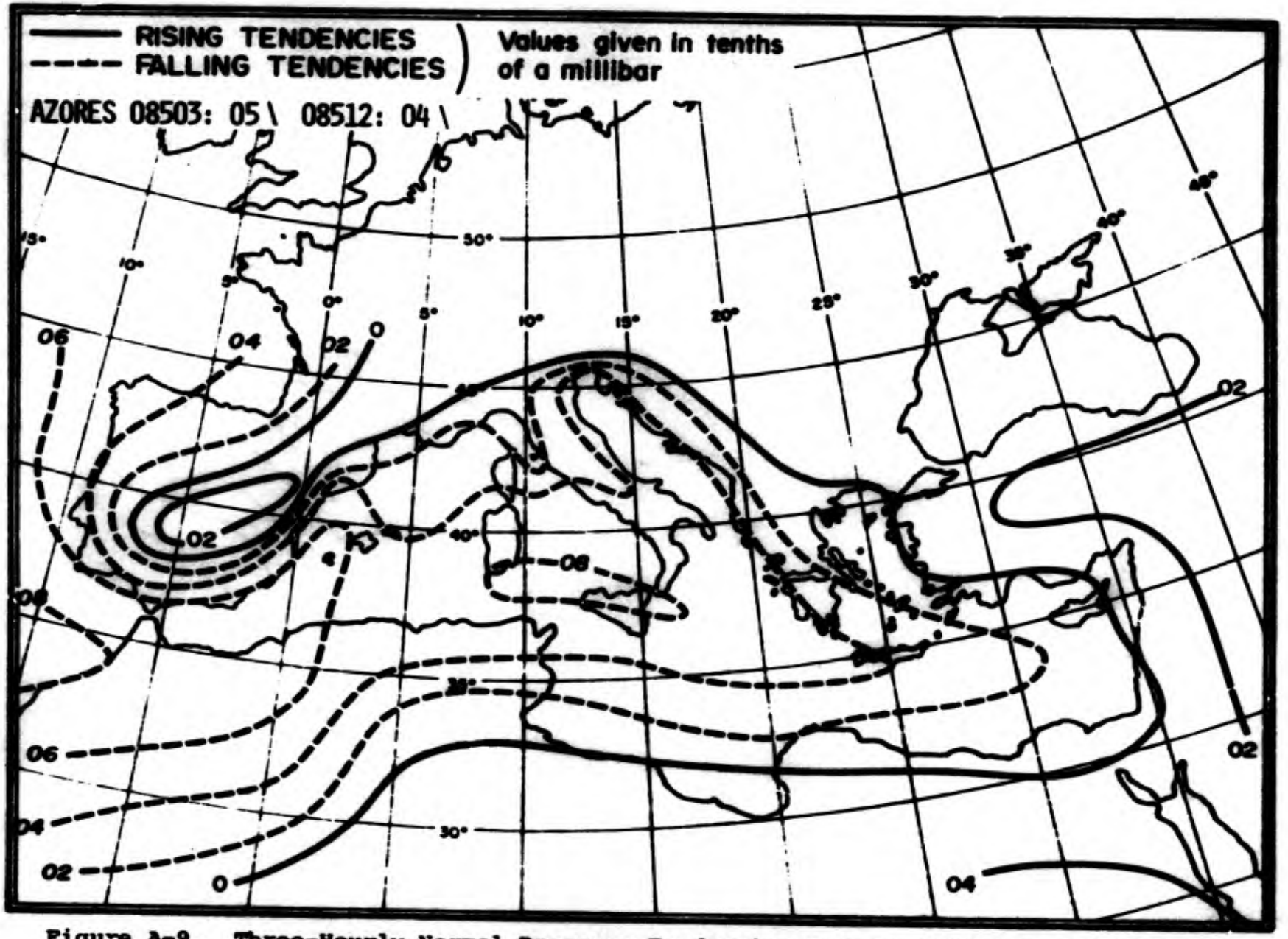

Figure A-9. Three-Hourly Normal Pressure Tendencies Between 0000 GMT and 0300 GMT (valid at 0300 GMT) Summer.

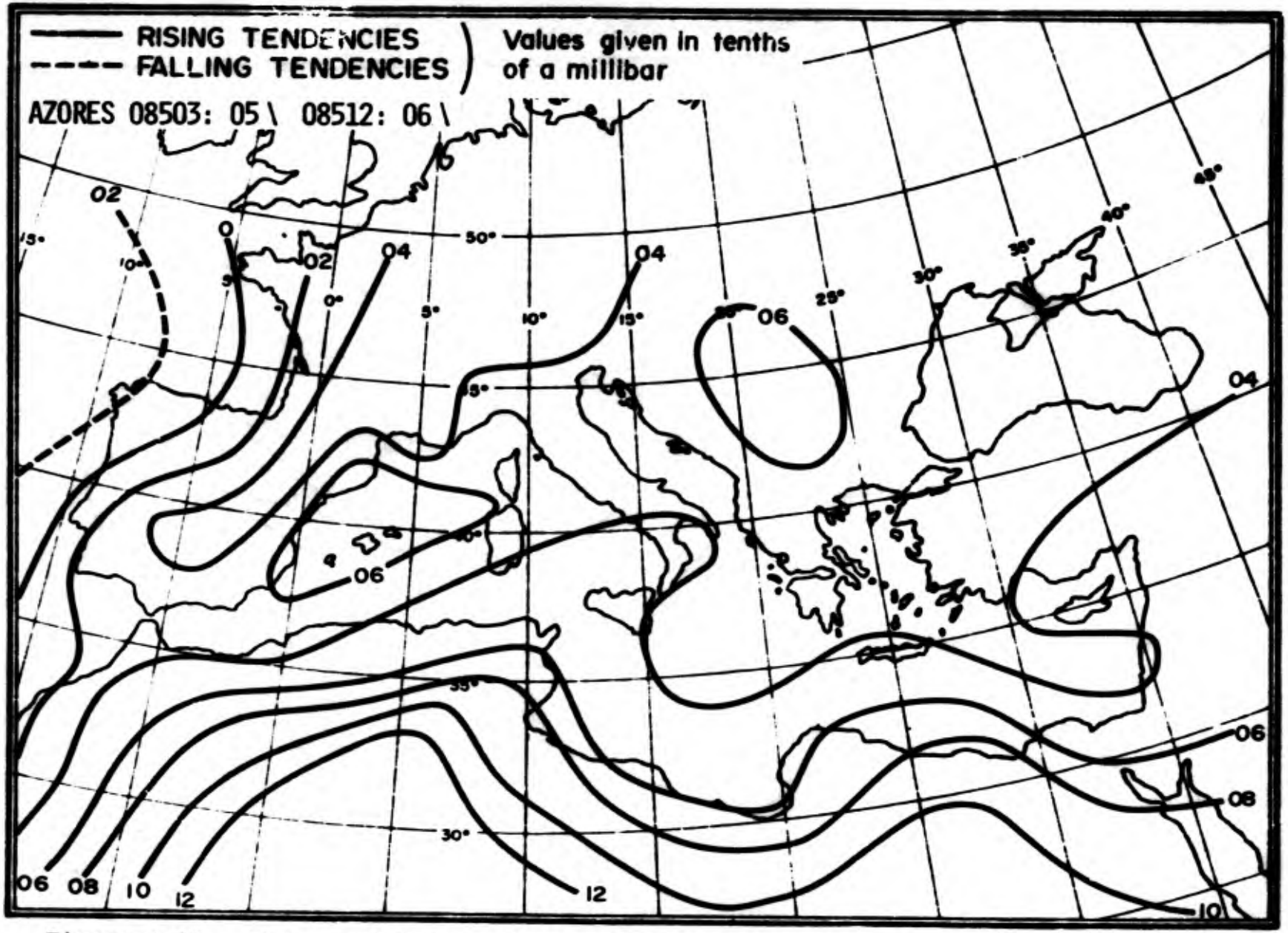

Figure A-10. Three-Hourly Normal Pressure Tendencies Between 0300 GMT and 0600 GMT (valid at 0600 GMT) Summer.

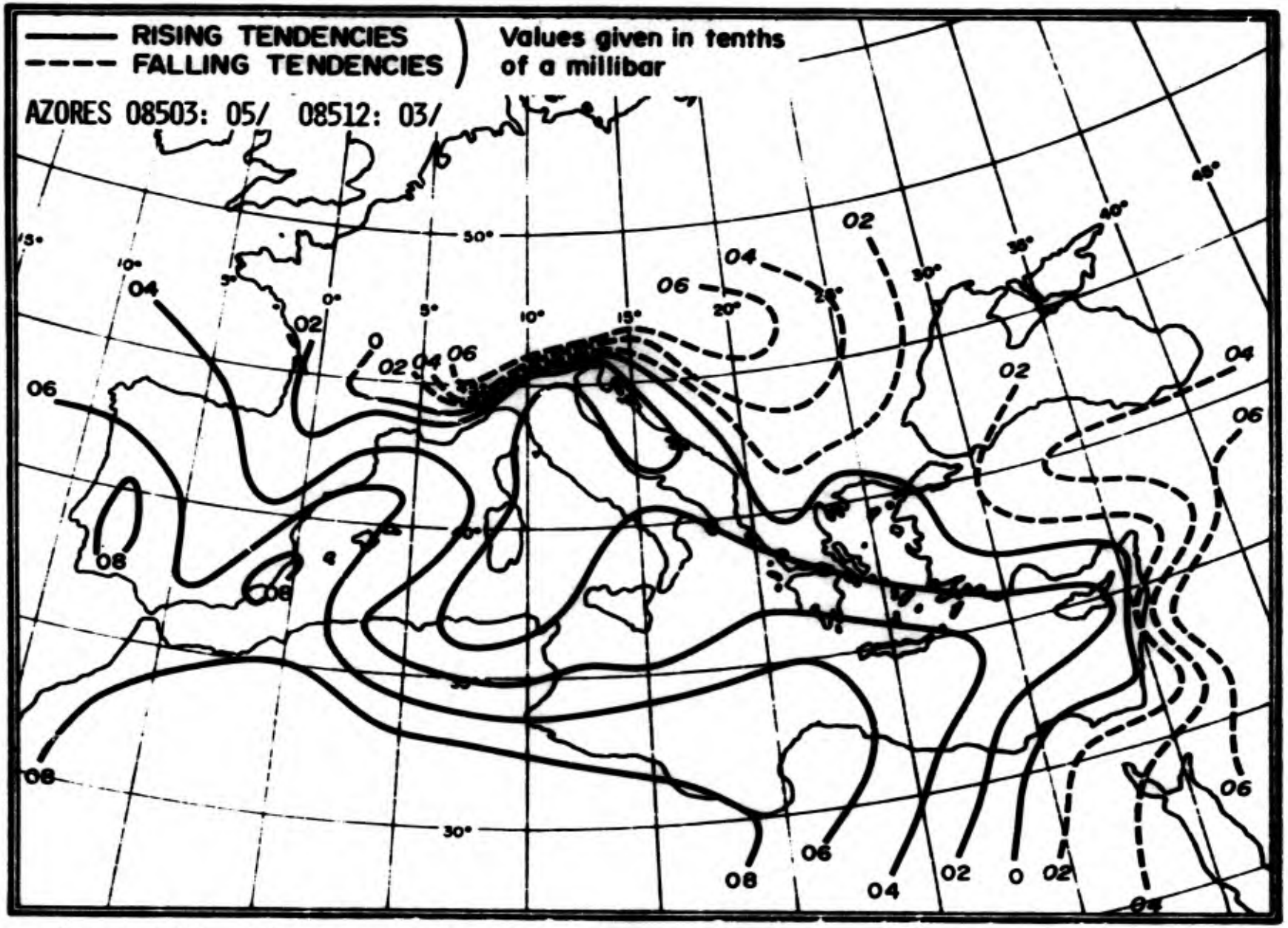

Figure A-11. Three-Hourly Normal Pressure Tendencies Between 0600 GMT and 0900 GMT (valid at 0900 GMT) Summer.

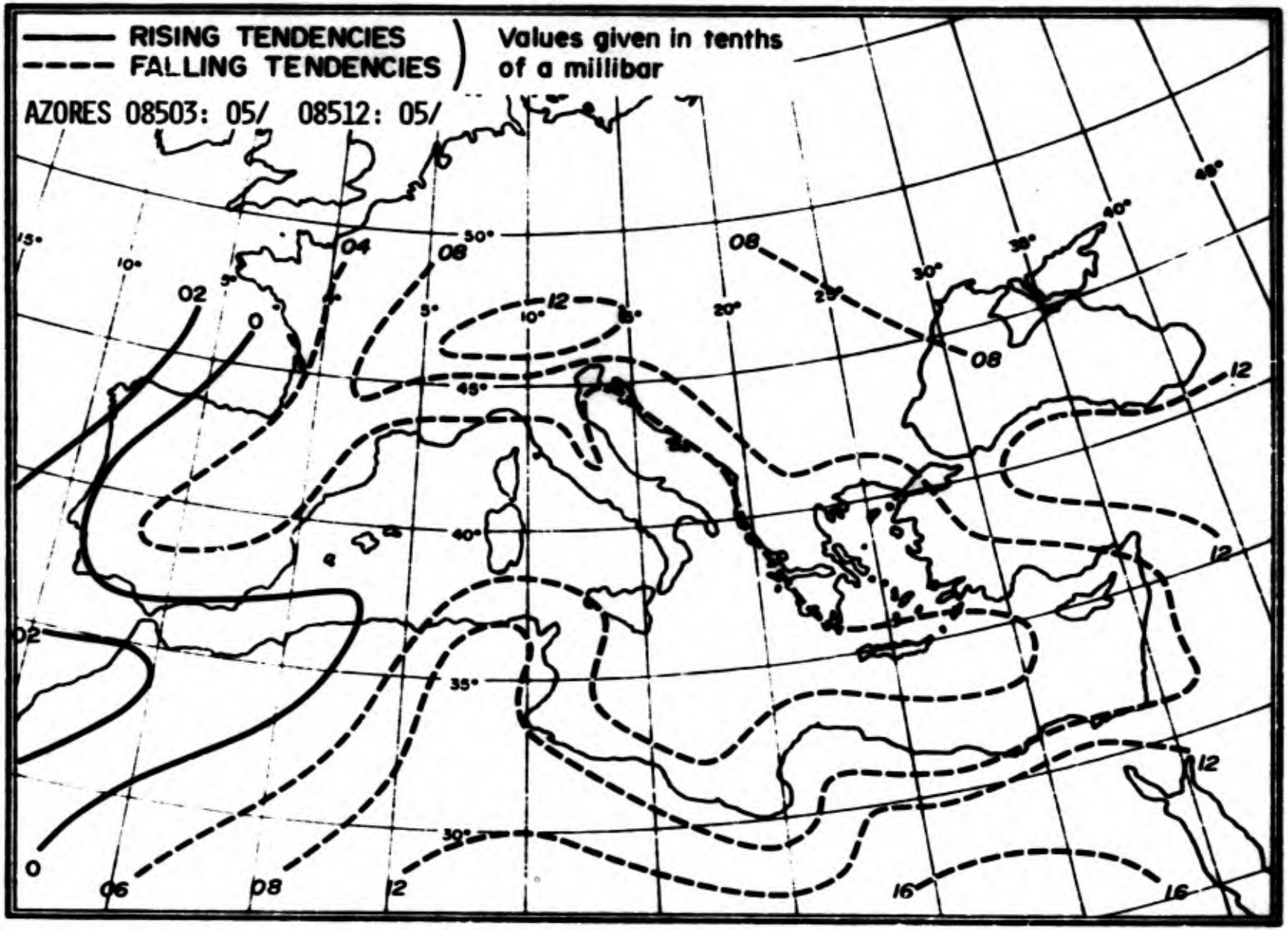

Figure A-12. Three-Hourly Normal Pressure Tendencies Between 0900 GMT and 1200 GMT (valid at 1200 GMT) Summer.

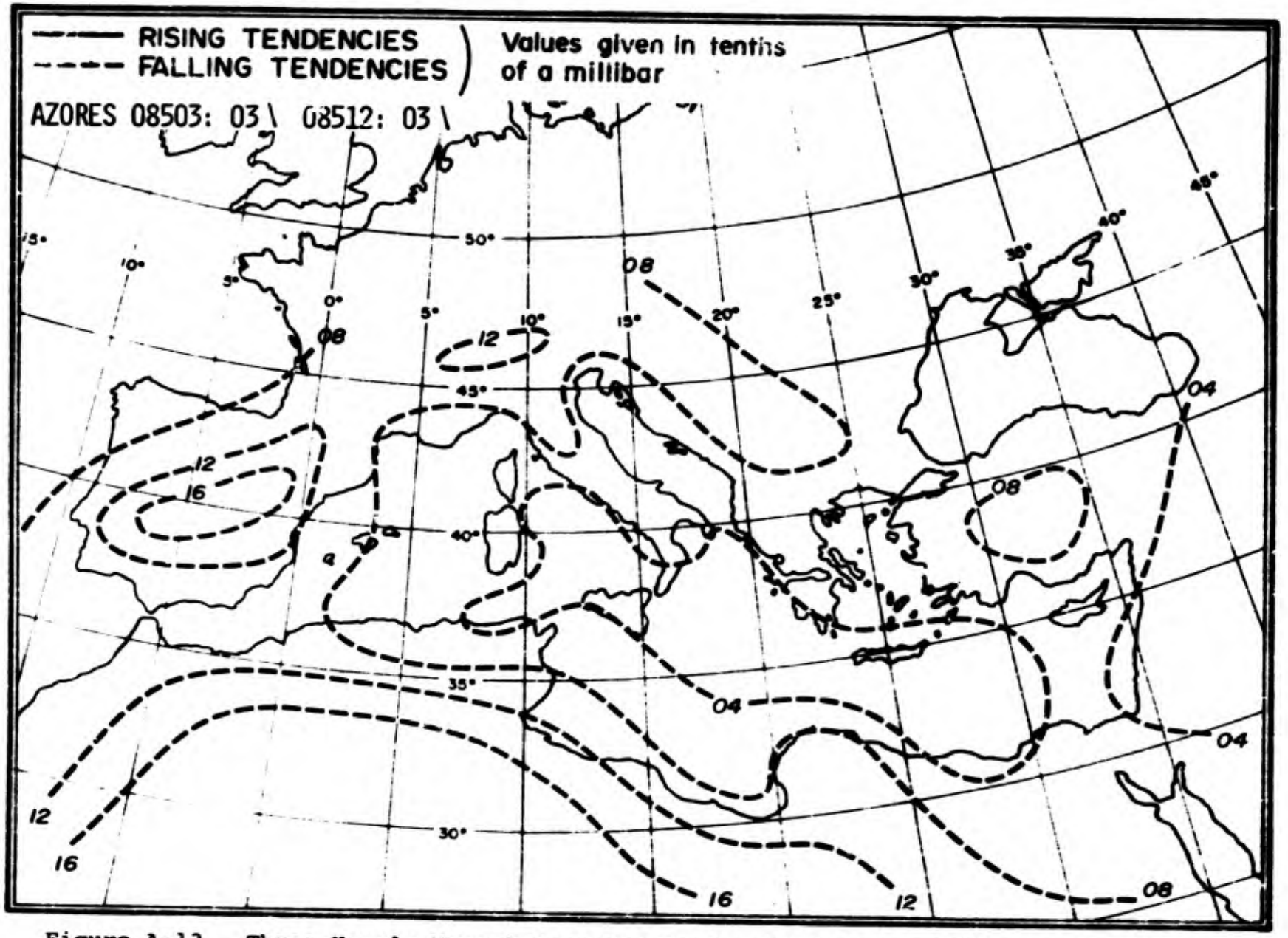

Figure A-13. Three-Hourly Normal Pressure Tendencies Between 1200 GMT and 1500 GMT (valid at 1500 GMT) Summer.

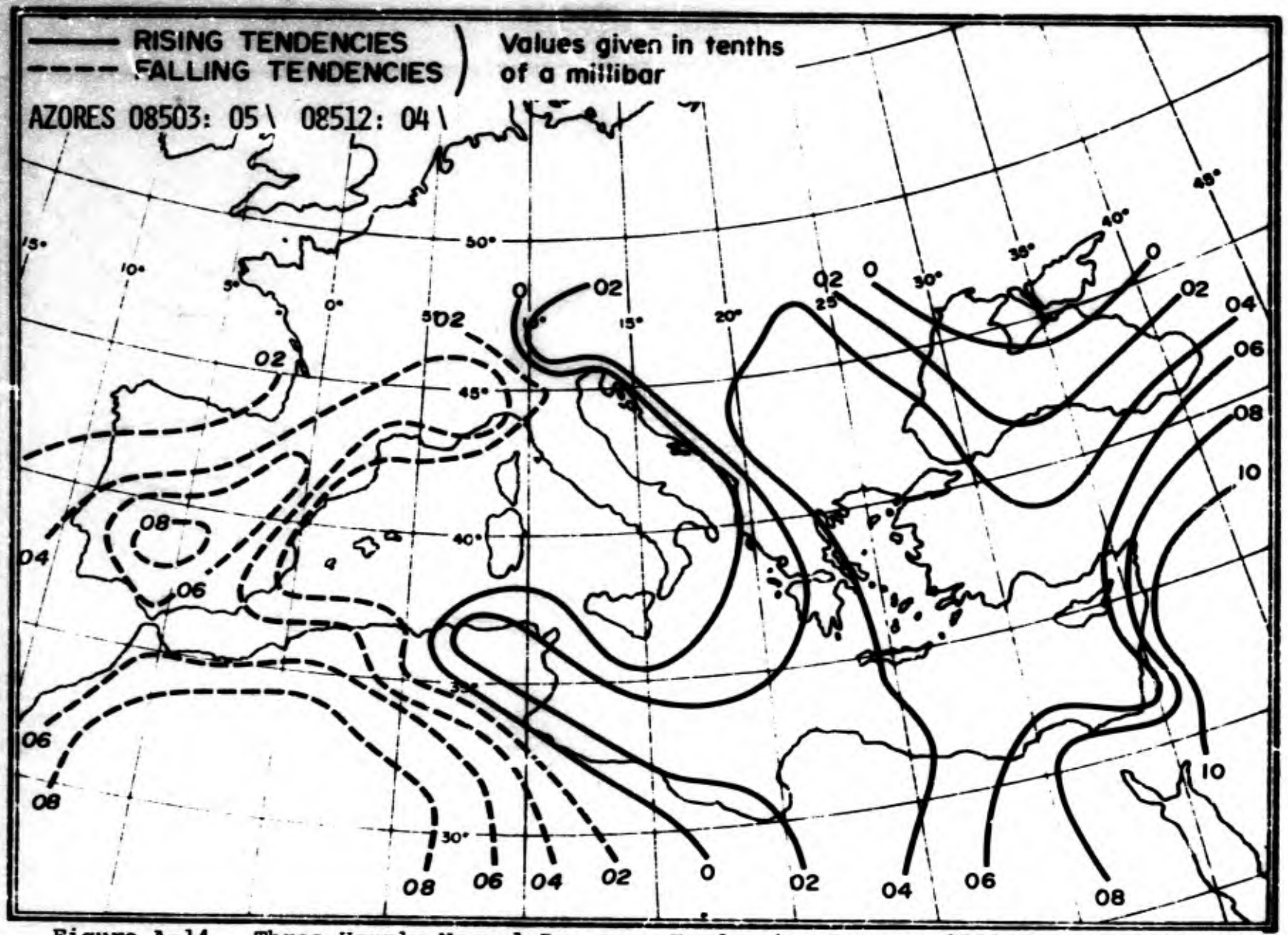

Figure A-14. Three-Hourly Normal Pressure Tendencies Between 1500 GMT and 1800 GMT (valid at 1800 GMT) Summer.

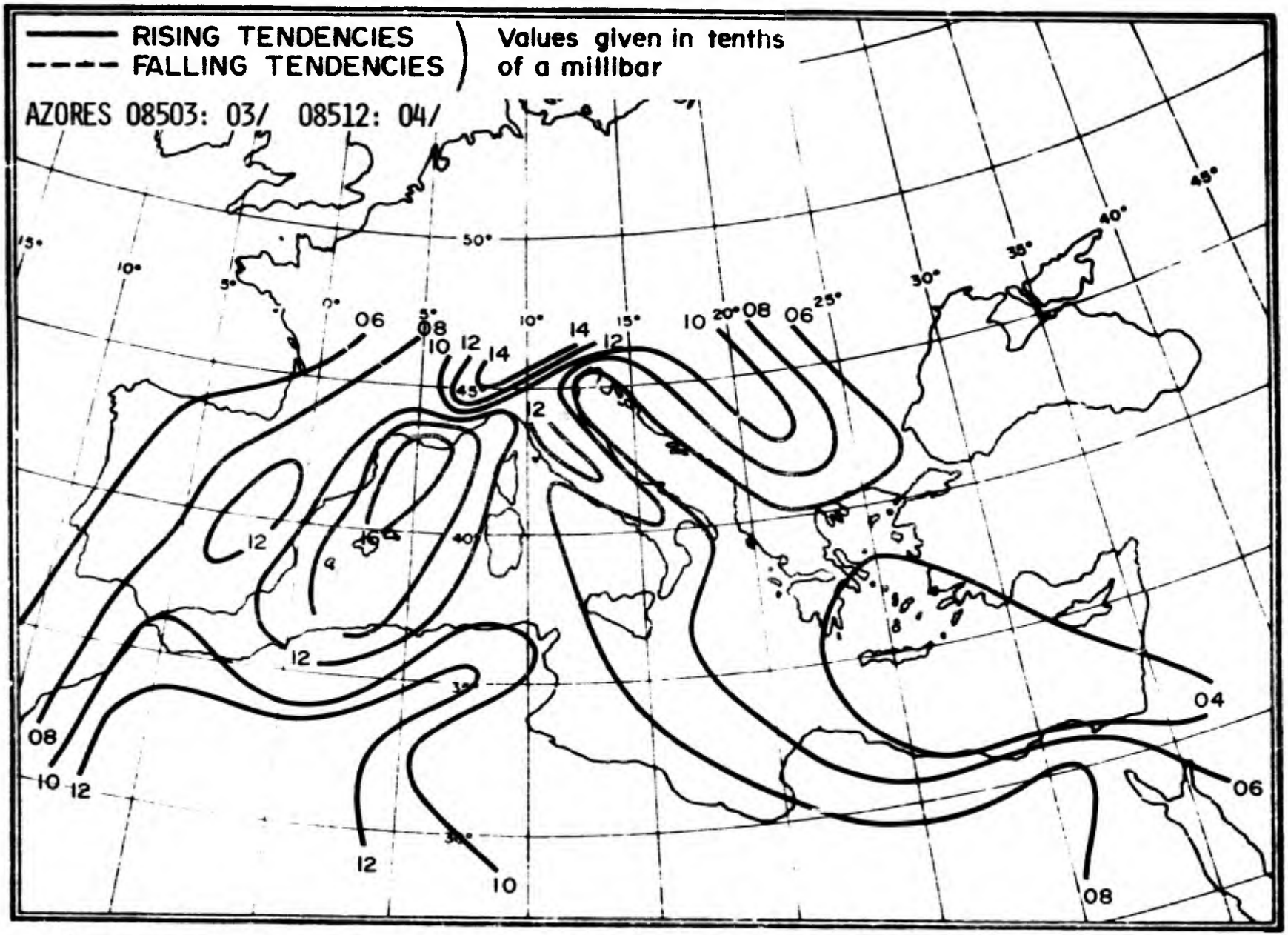

Figure A-15. Three-Hourly Normal Pressure Tendencies Between 1800 GMT and 2100 GMT (valid at 2100 GMT) Summer.

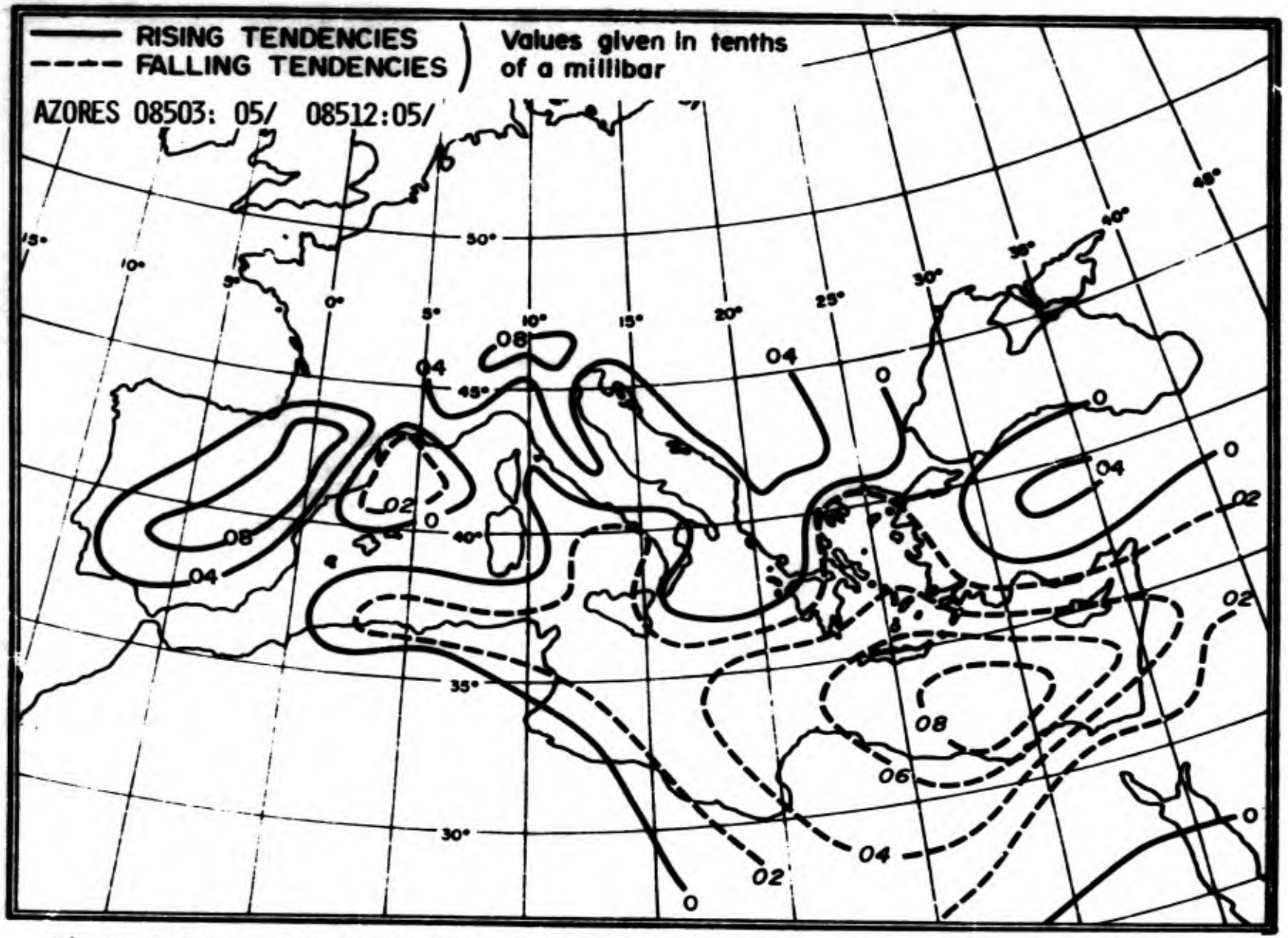

Figure A-16. Three-Hourly Normal Pressure Tendencies Between 2100 GMT and 0000 GMT (valid at 0000 GMT) Summer.

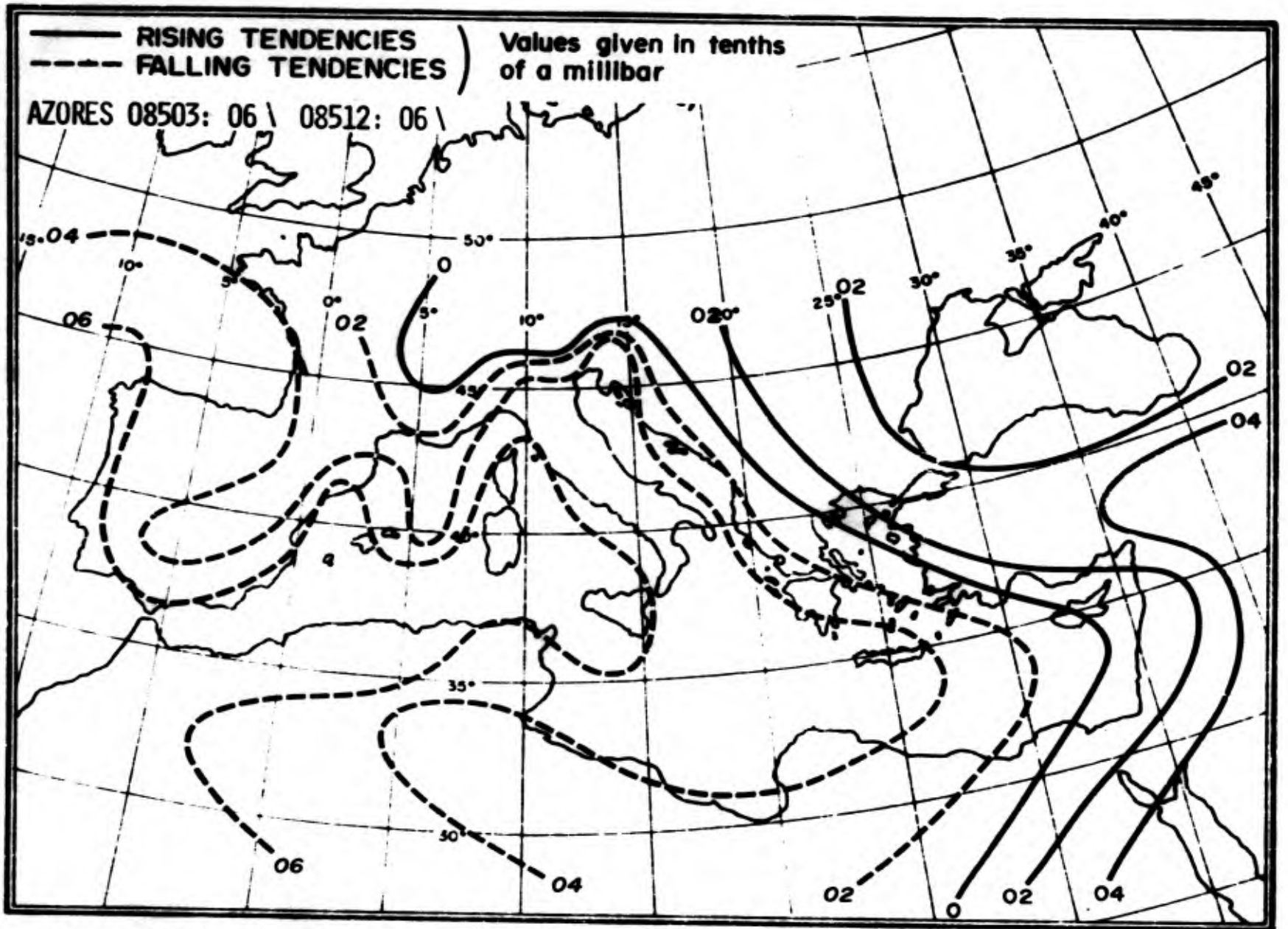

Figure A-17. Three-Hourly Normal Pressure Tendencies Between 0000 GMT and 0300 GMT (valid at 0300 GMT) Autumn.

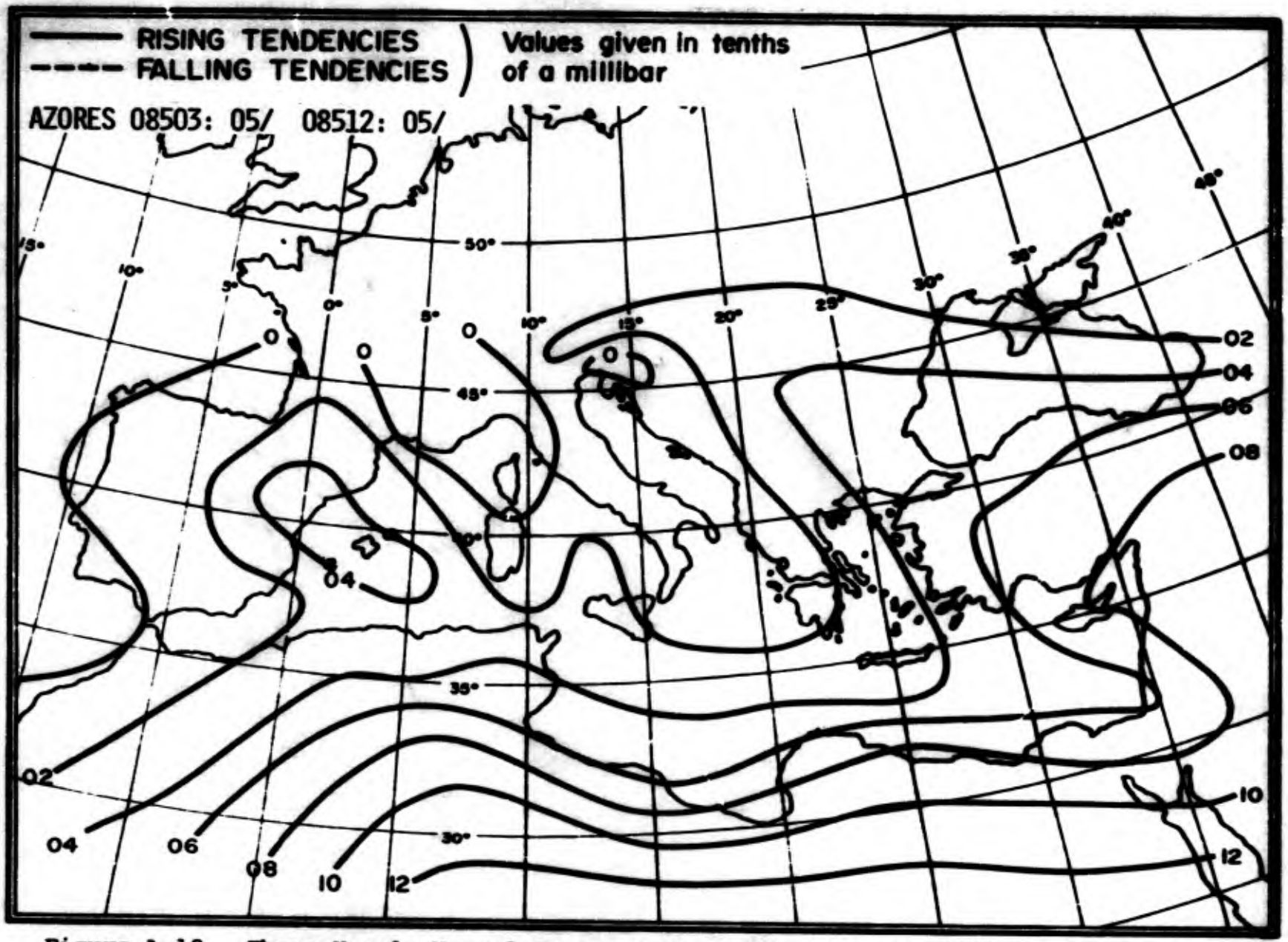

Figure A-18. Three-Hourly Normal Pressure Tendencies Between 0300 GMT and 0600 GMT (valid at 0600 GMT) Autumn.

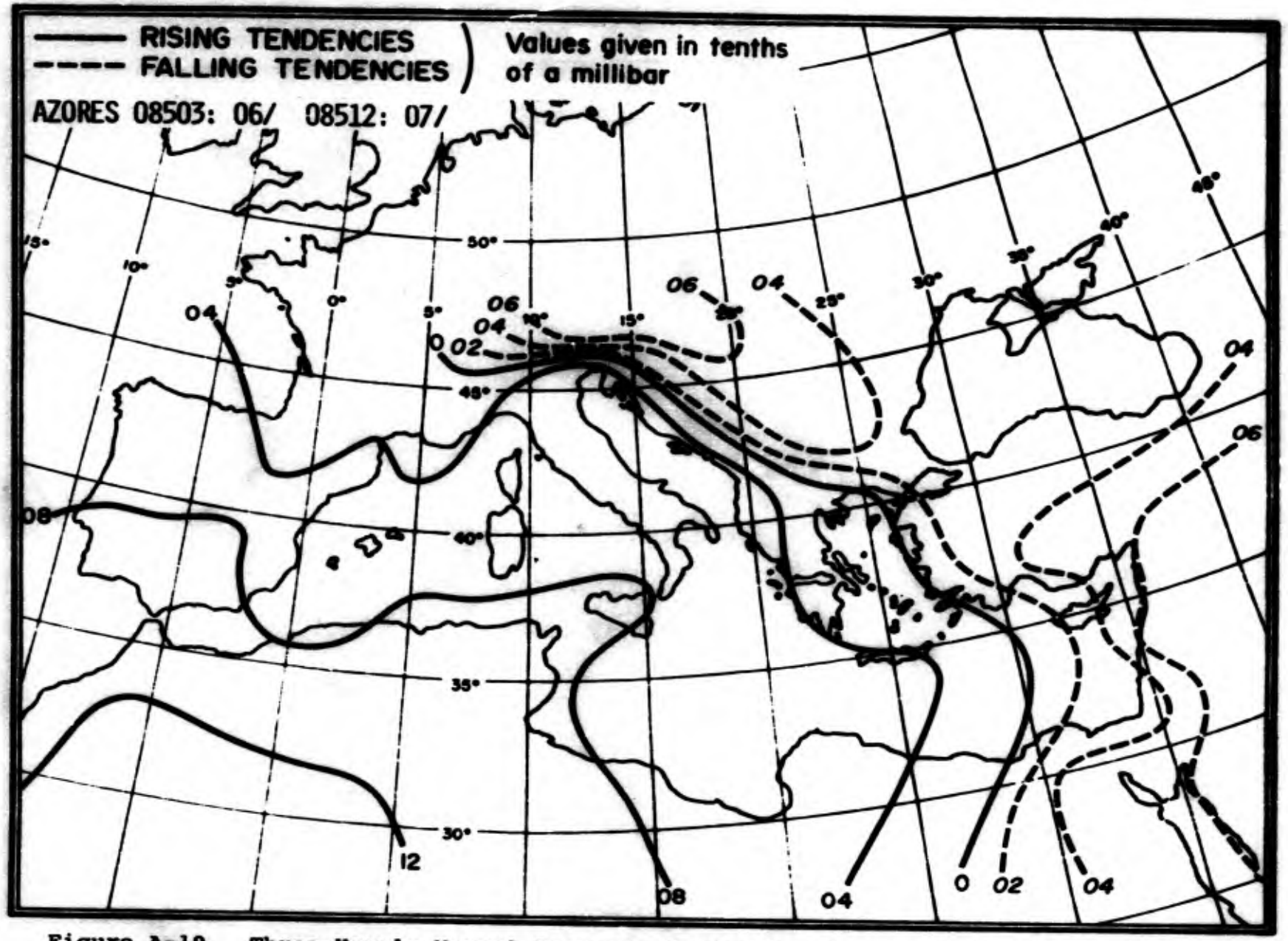

Figure A-19. Three-Hourly Normal Pressure Tendencies Between 0600 GMT and 0900 GMT (valid at 0900 GMT) Autumn.

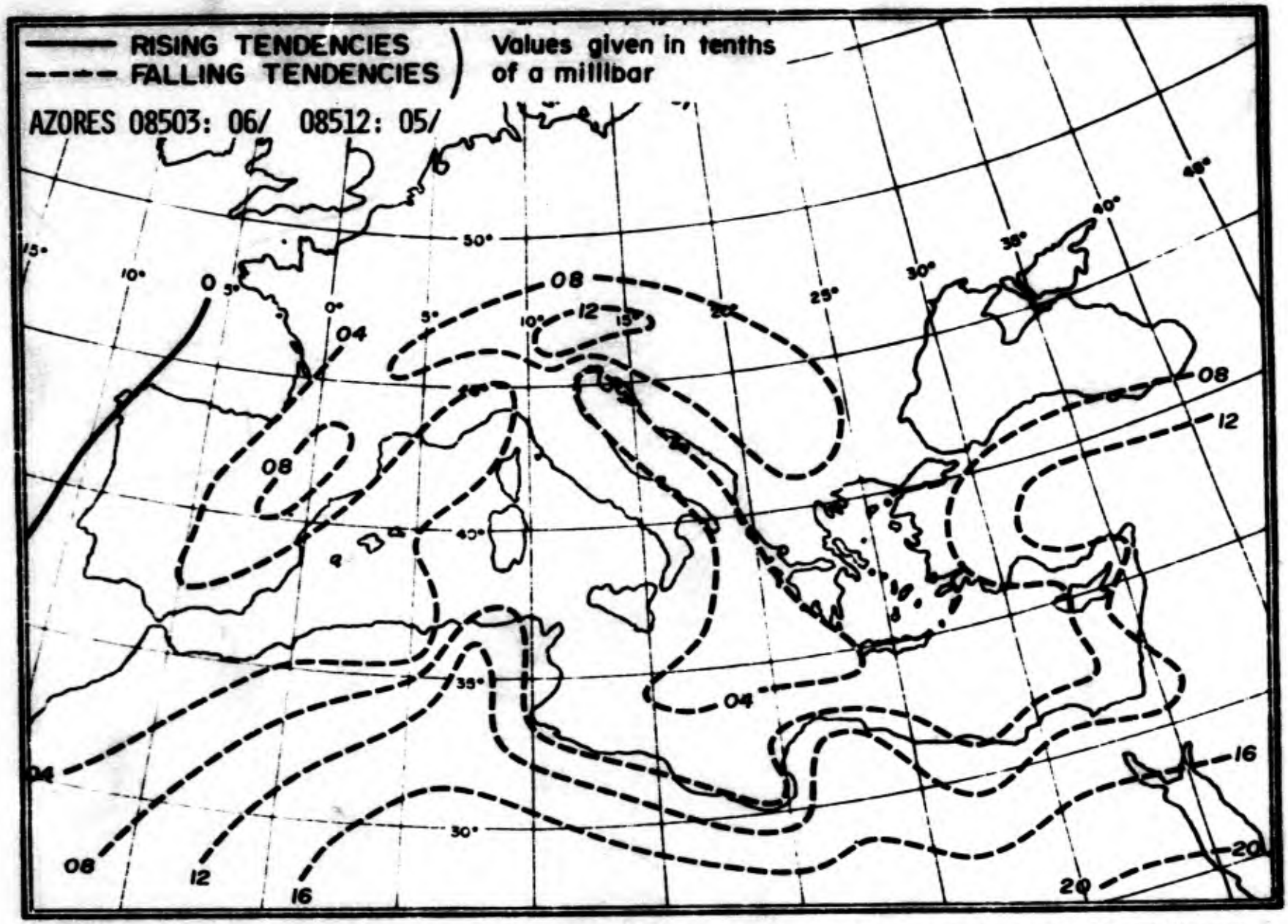

Figure A-20. Three-Hourly Normal Pressure Tendencies Between 0900 GMT and 1200 GMT (valid at 1200 GMT) Autumn.

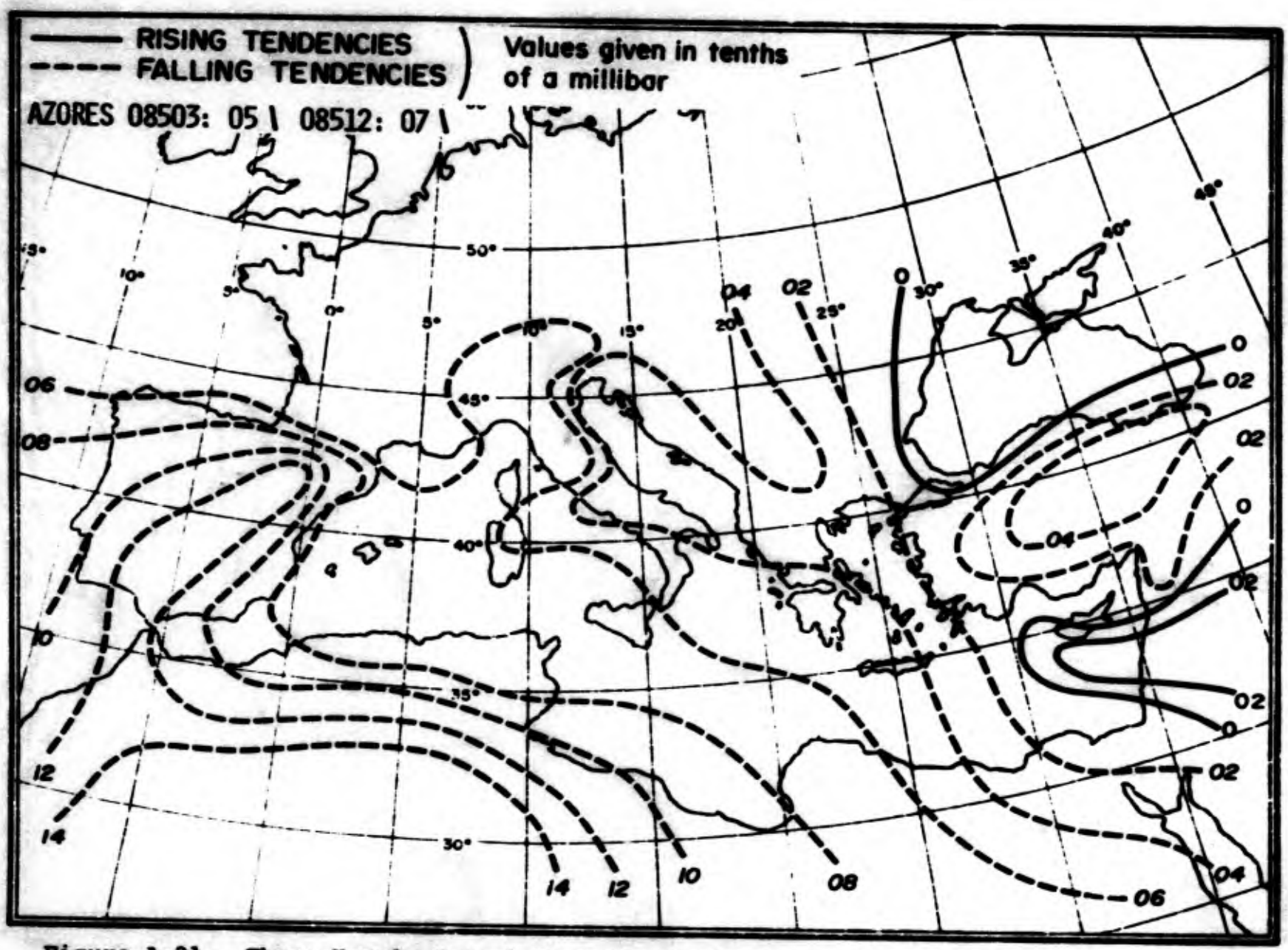

Figure A-21. Three-Hourly Normal Pressure Tendencies Between 1200 GMT and 1500 GMT (valid at 1500 GMT) Autumn.

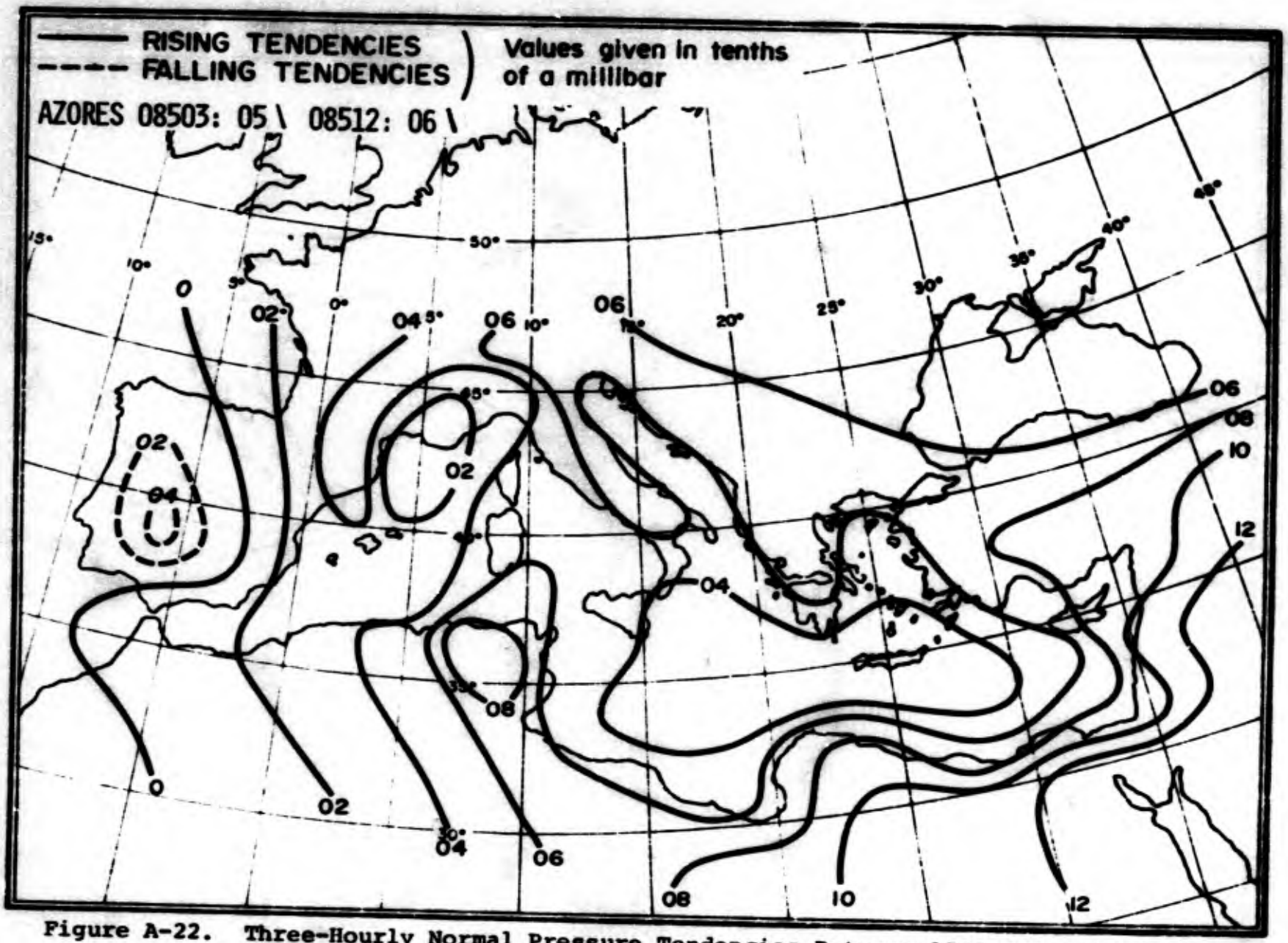

Figure A-22. Three-Hourly Normal Pressure Tendencies Between 1500 GMT and 1800 GMT (valid at 1800 GMT) Autumn.

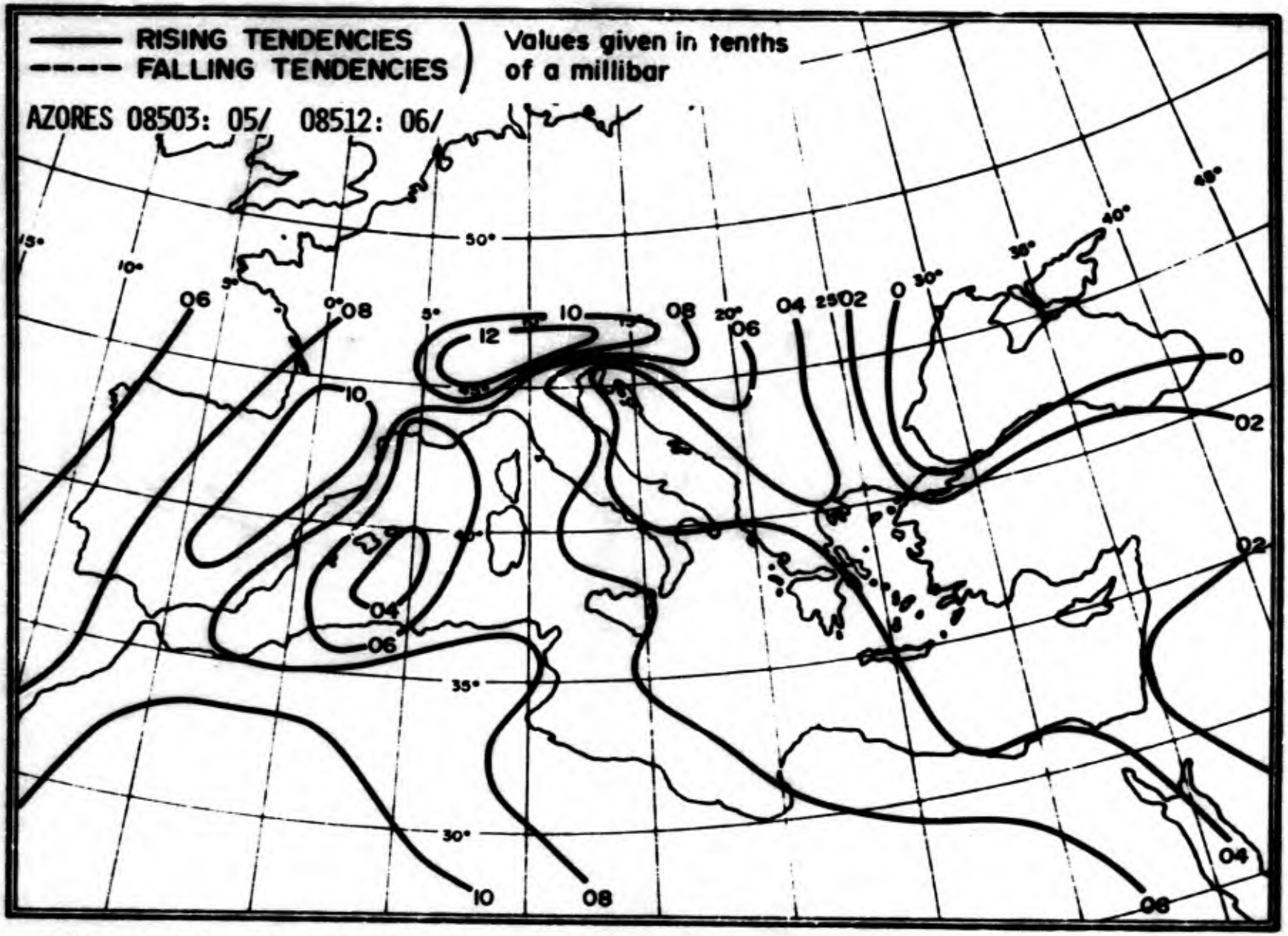

Figure A-23. Three-Hourly Normal Pressure Tendencies Between 1800 GMT and 2100 GMT (valid at 2100 GMT) Autumn.

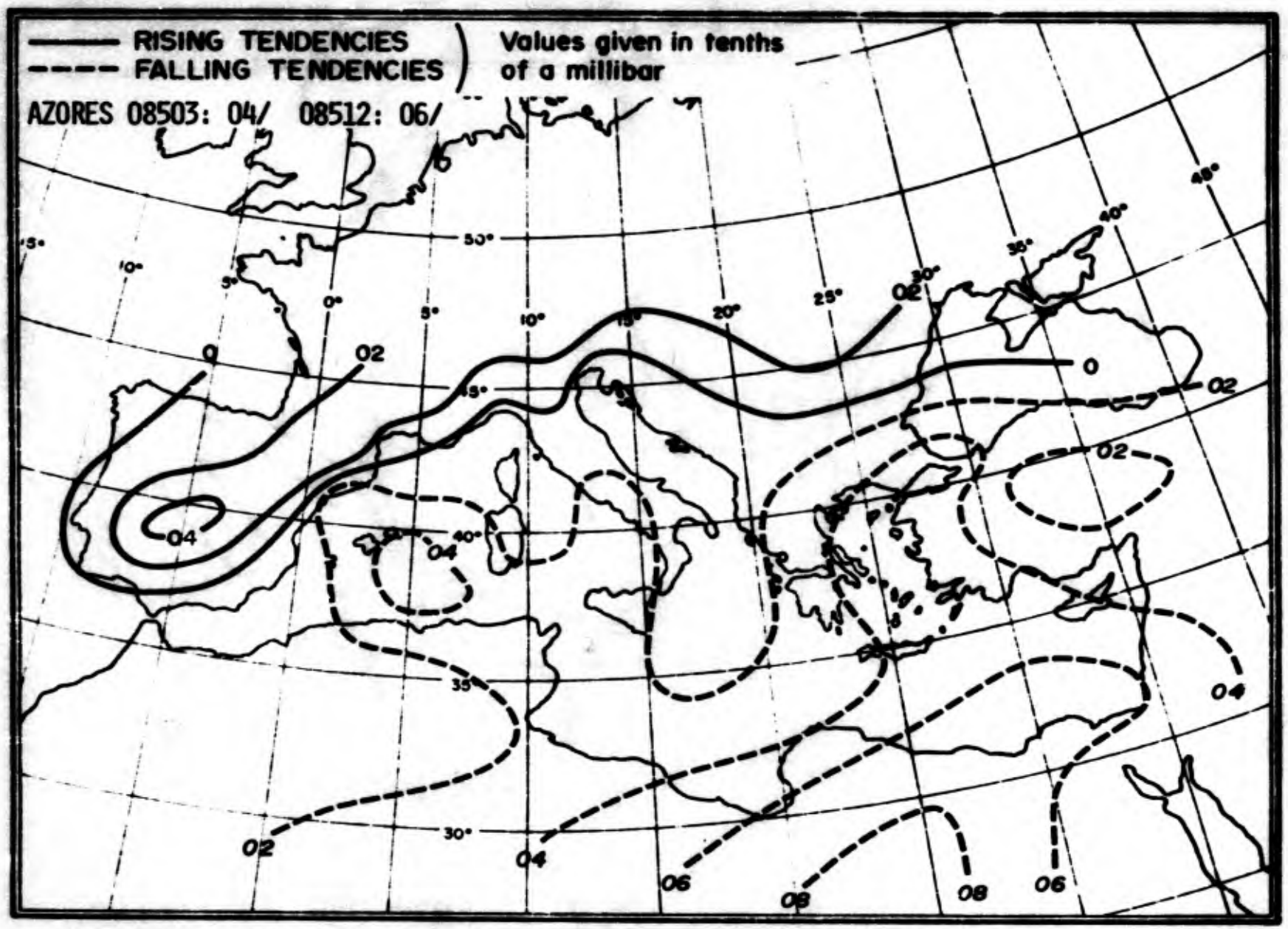

Figure A-24. Three-Hourly Normal Pressure Tendencies Between 2100 GMT and 0000 GMT (valid at 0000 GMT) Autumn.

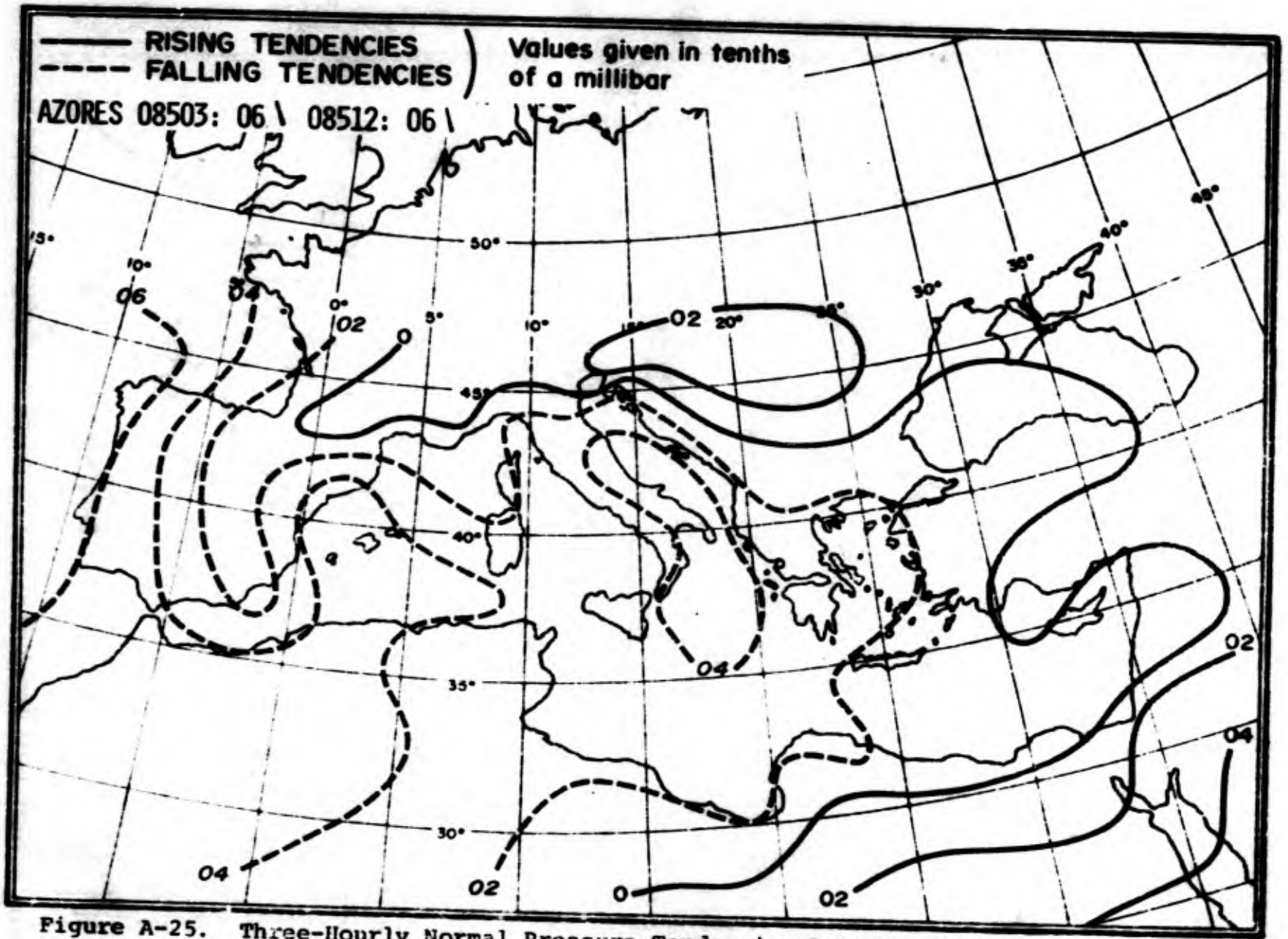

Figure A-25. Three-Hourly Normal Pressure Tendencies Between 0000 GMT and 0300 GMT (valid at 0300 GMT) Winter.

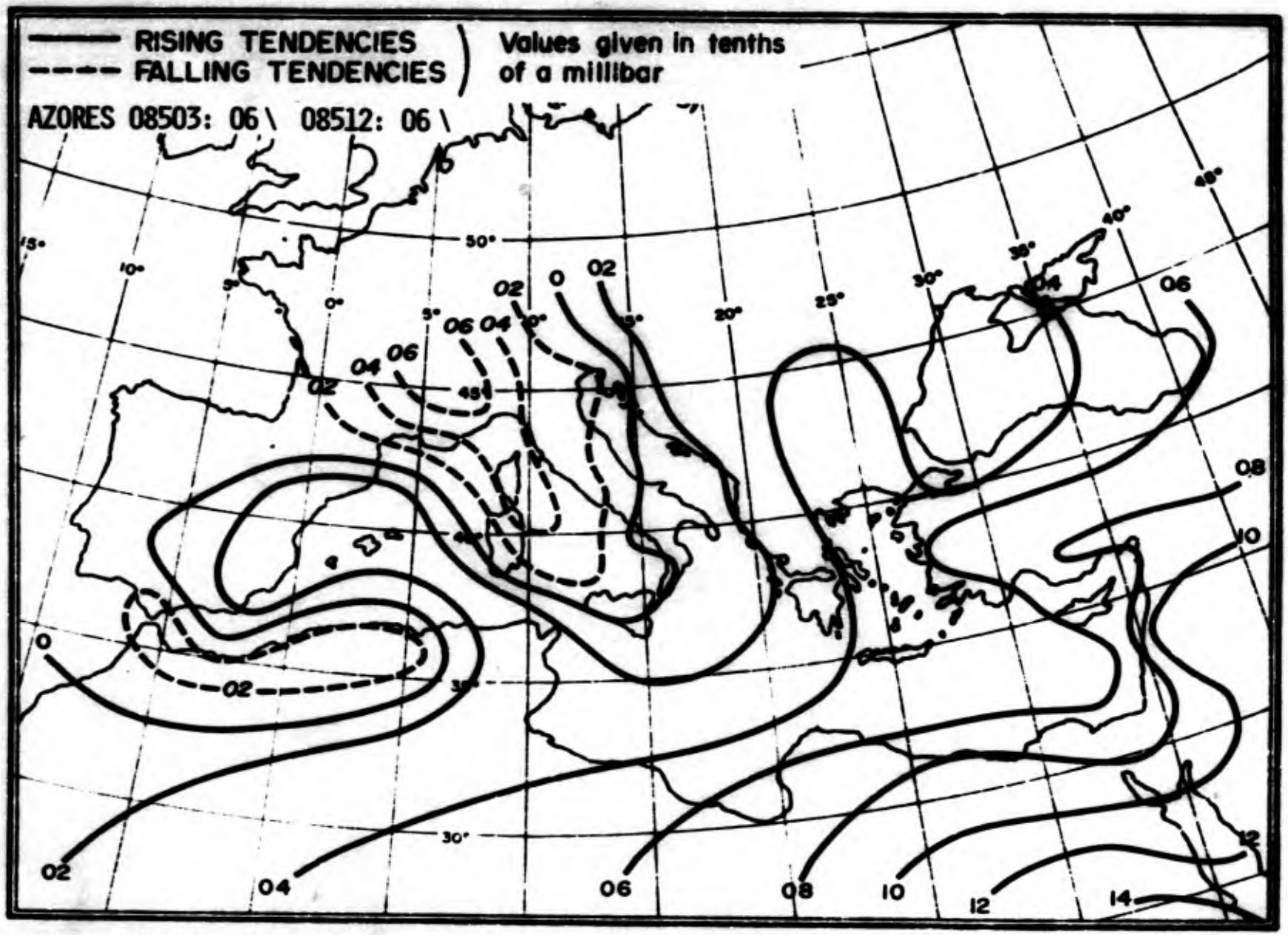

Figure A-26. Three-Hourly Normal Pressure Tendencies Between 0300 GMT and 0600 GMT (valid at 0600 GMT) Winter.

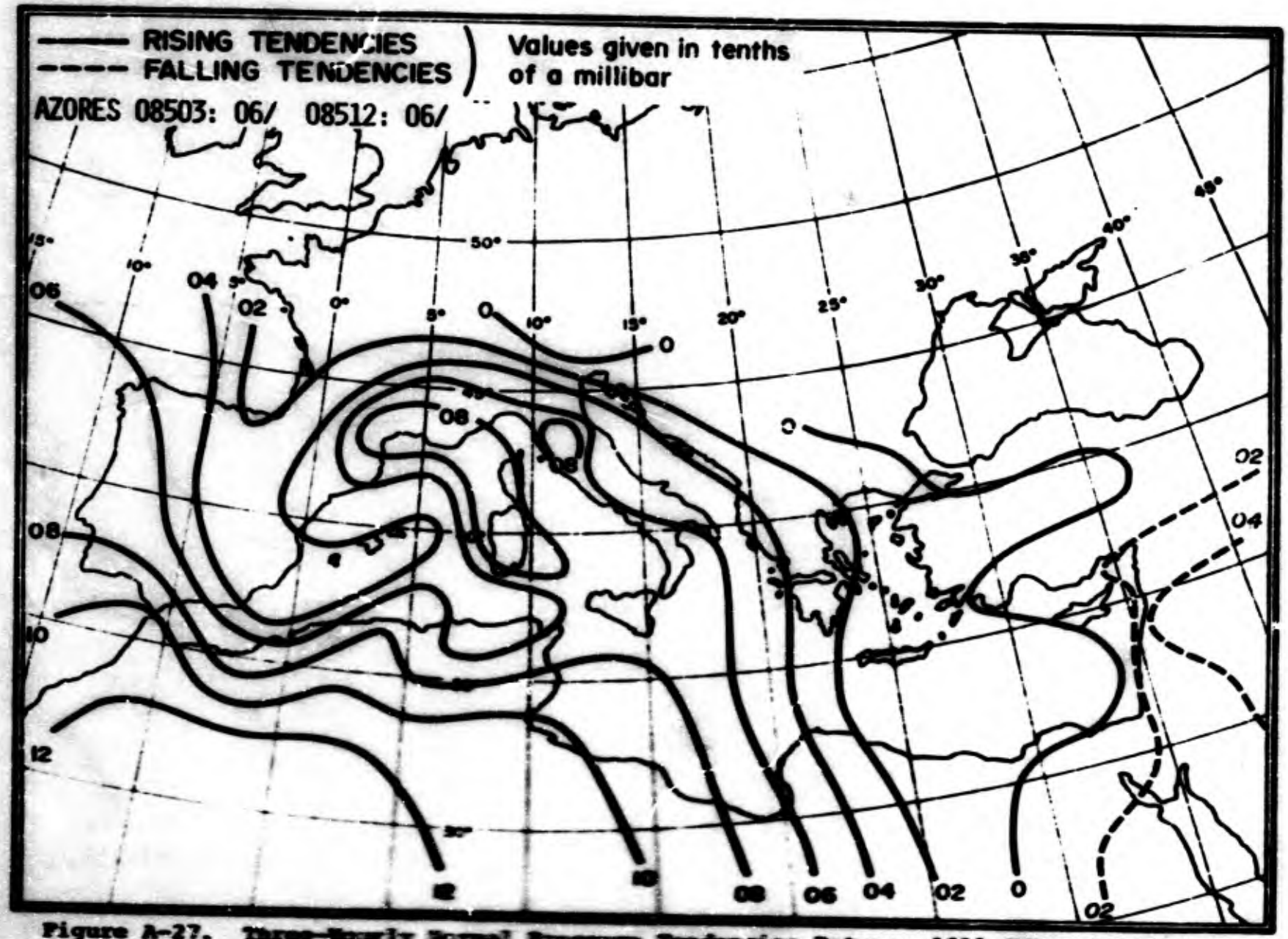

Figure A-27. Three-Hourly Normal Pressure Tendencies Between 0600 GMT and 0900 GMT (valid at 0900 GMT) October.

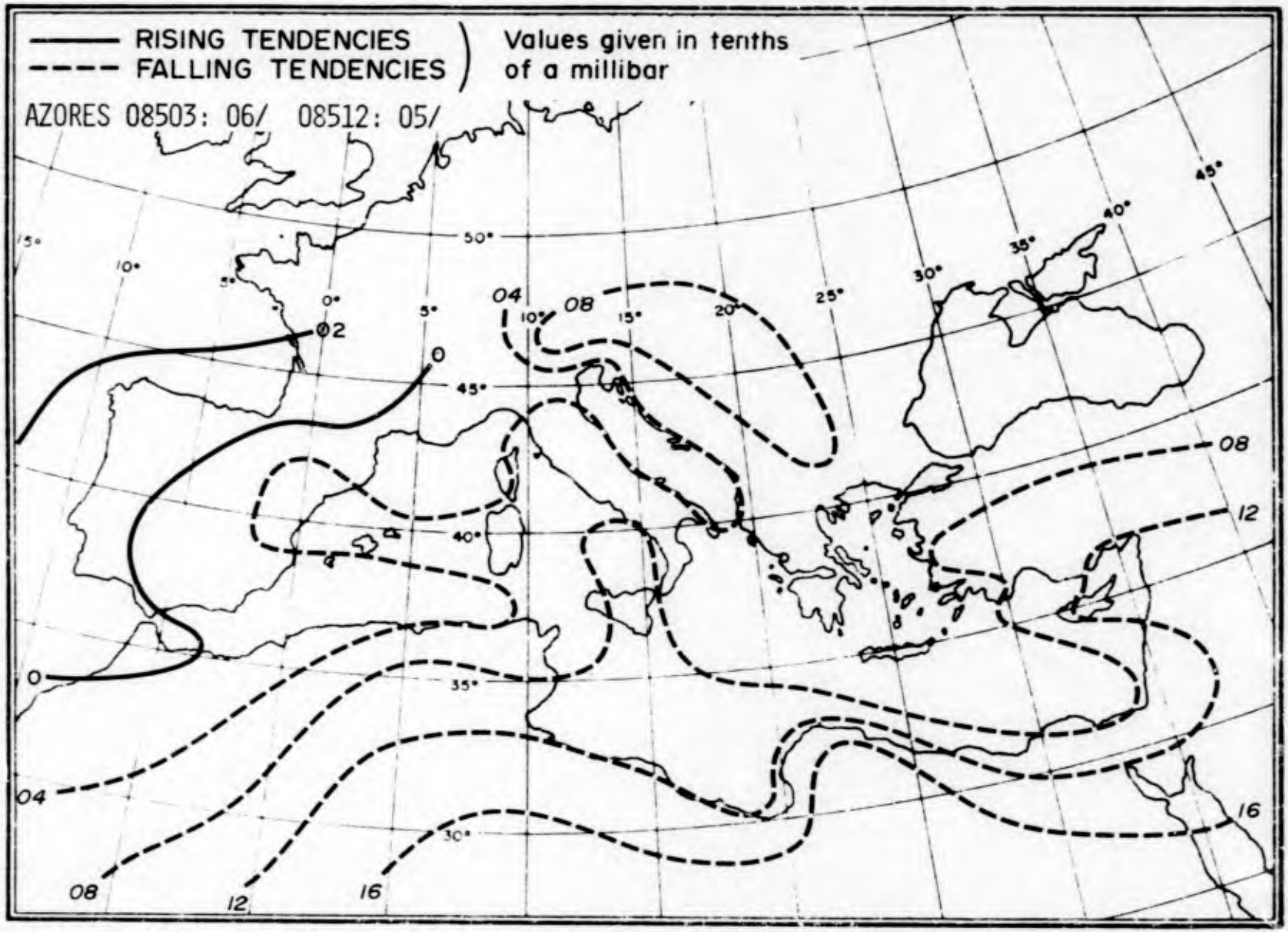

Figure A-28. Three-Hourly Normal Pressure Tendencies Between 0900 GMT and 1200 GMT (valid at 1200 GMT) Winter.

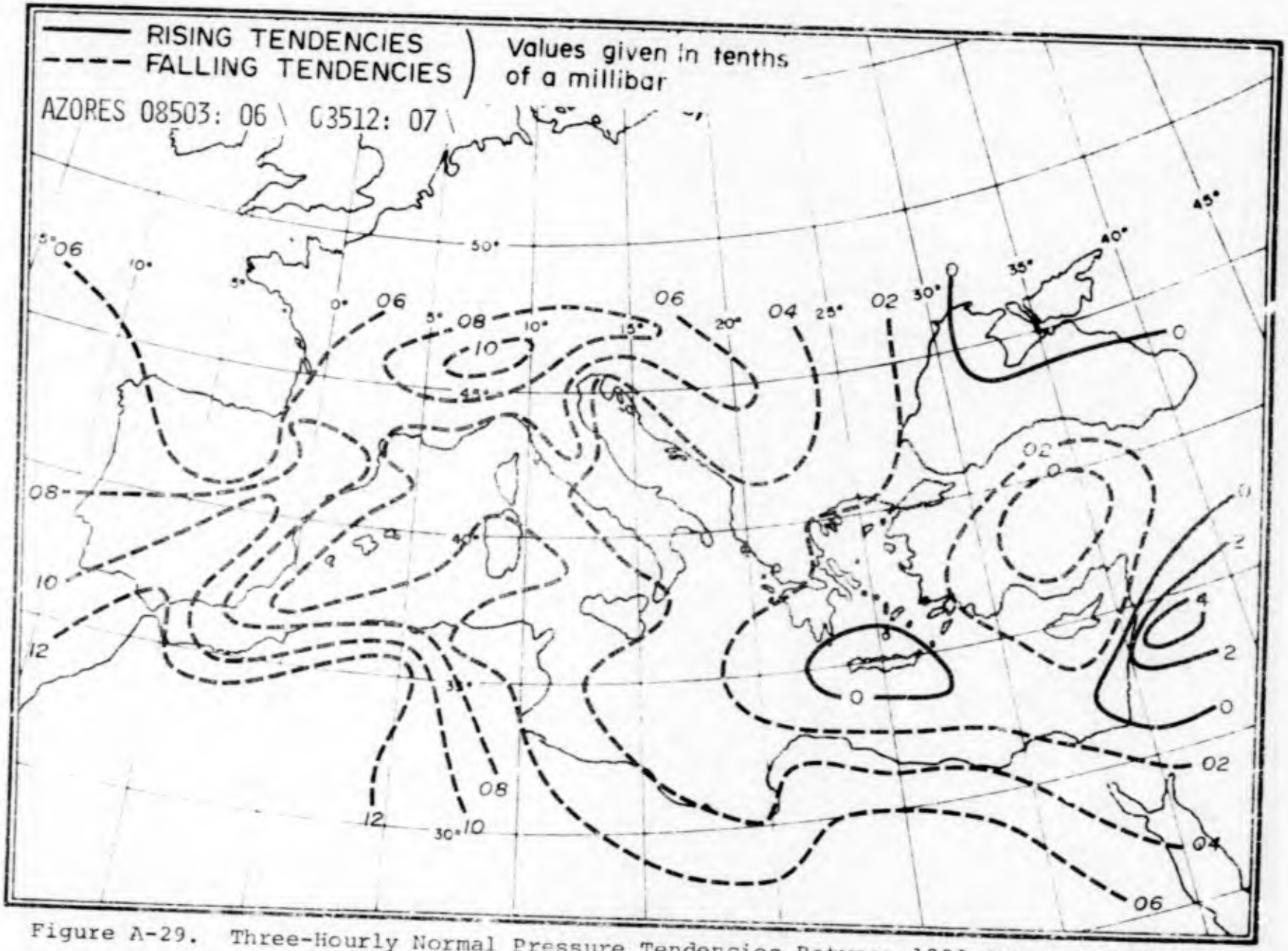

Figure A-29. Three-Hourly Normal Pressure Tendencies Between 1200 GMT and 1500 GMT (valid at 1500 GMT) Winter.

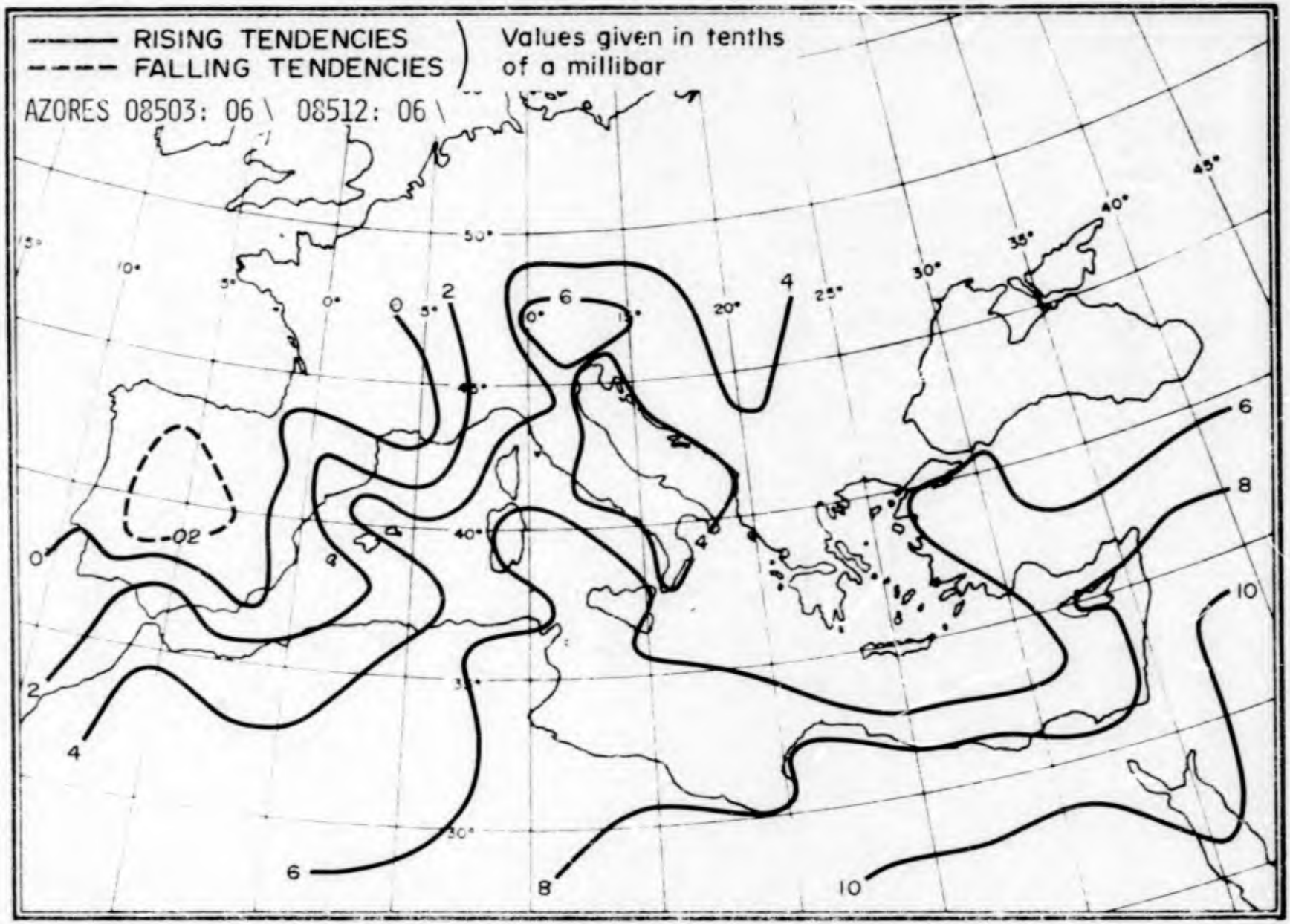

Figure A-30. Three-Hourly Normal Pressure Tendencies Between 1500 GMT and 1800 GMT (valid at 1800 GMT) Winter.

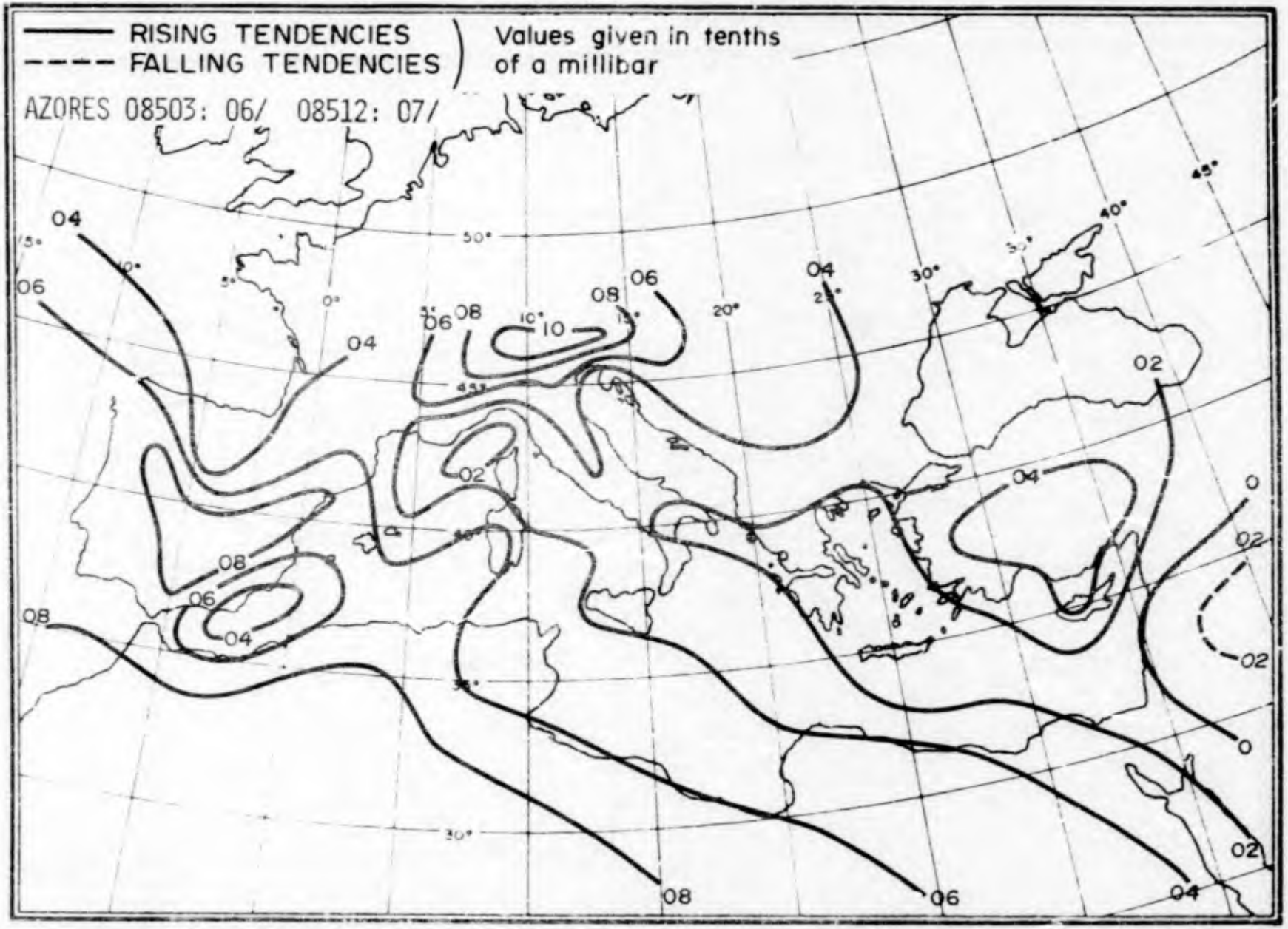

Figure A-31. Three-Hourly Normal Pressure Tendencies Between 1800 GMT and 2100 GMT (valid at 2100 GMT) Winter.

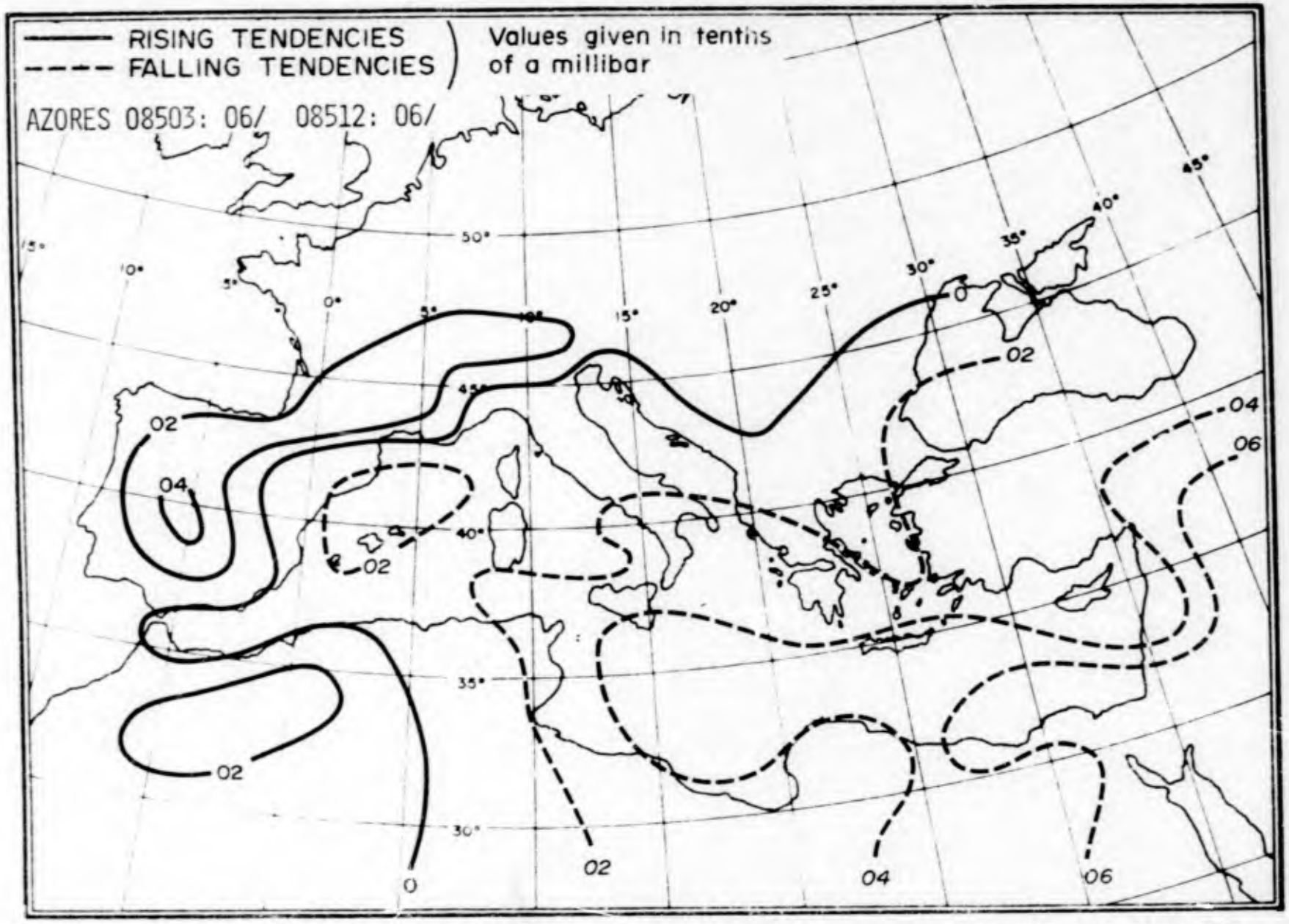

Figure A-32. Three-Hourly Normal Pressure Tendencies Between 2100 GMT and 0000 GMT (valid at 0000 GMT) Winter.

APPENDIX B

MEAN AND STANDARD DEVIATION CHARTS OF THE SURFACE AND 500-MB. LEVELS AT VARIOUS INTERVALS PRECEDING THE OCCURRENCE OF A MISTRAL.

To determine the variability of surface and 500-mb. patterns just prior to the onset of a mistral, mean surface and 500-mb. charts for 11 cases of incipient mistrals were prepared; these mistrals were Air Ministry Type A ([1] Vol. 1, pg. 46) and covered the period January 1969 to March 1970 (excluding May through September). The standard deviations were also calculated. In order to reduce seasonal variations, the mean patterns and standard deviation charts were normalized with respect to the mean conditions at 45° N. between 30° W. and 20° E. These normalized mean charts are shown in figures B-1 and B-2. (Brody, Reiter and Godfrey) The normalized standard deviations shown in figures B-3 and B-4 reveal a minimum in the blocking ridge south of Iceland and in the upper trough (fig. B-4) over France. Standard deviations are relatively large in the baroclinic zone over England where small changes in frontal positions, as well as travelling disturbances, contribute to large pressure changes. It is also interesting to note that the trough over the western Atlantic and the eastern U.S. is subject to great variability as indicated by the large standard deviation values of both the surface and the 500-mb. patterns.

In a similar manner, 13 incipient Air Ministry Type C mistral cases ([1] Vol. 1, pg. 49) between January 1969 and March 1970 (excluding May through September) are summarized in figures B-5 to B-8. (Brody, Reiter and Godfrey) The mean 500-mb. pattern (fig. B-6) shows the arrival of a short-wave

trough over France in a northwesterly jet stream heralding the outbreak of the mistral.

In figures B-2 and B-4, the blocking ridge over the eastern Atlantic and the trough over Europe are the most stable features with the least standard deviation. However, for the Type C mistral, it is now the northwesterly jet stream over the Bay of Biscay that appears to control the start of the mistral. Minimum standard deviations (fig. B-8) occur in the northwesterly jet stream (fig. B-6), in contrast to the Type A mistral, which showed the maximum variability within the jet stream.

Figures B-9 and B-12 show mean and standard deviation charts at 24 hours prior to the mistral development, for the surface and the 500-mb. level for the same eleven Type A mistral cases in figures B-1 to B-4. Whereas figures B-1 and B-2 (at t = 0 h., start of the mistral) show the surface frontal trough and the upper-level short-wave trough within the long-wave pattern to be barely off the French Mediterranean coast, figures B-9 and B-10 (t = -24 h.) show the same frontal trough and upper short-wave trough extending across southern England and into the Bay of Biscay. Additional information on the upper short-wave position may be gained from 24-hour isallobaric analyses (not presented here). The long-wave pattern in figure B-10 is nearly the same as in figure B-2. This is due to the bias of the eleven mistrals forming the sample towards established rather than transitory mistral periods.

Judging from the standard deviation chart (fig. B-11), the warm sector over Spain ahead of the frontal trough extending into the Bay of Biscay is the most reliable characteristic surface feature. Here we find the smallest standard-deviation values. There are slight differences from case to case in the exact positions of the surface frontal trough over southern England and of the pressure rise behind the frontal trough over England and Ireland. Hence, slightly higher standard deviations occur there.

Based on minimum values of standard deviations at 500 mb., figure B-4 (t = 0 h.) revealed the short-wave trough position over southern France and the blocking ridge as the most reliable indicators for the start of the Type A mistral. However figure B-12 (t = -24 h.) shows the minimum standard deviation to be over Spain and France ahead of the 500-mb. short-wave trough shown in figure B-10. On a particular 500-mb. chart this position in advance of this short-wave trough should correspond to the short-wave ridge. Hence this ridge will provide the most reliable indicator for a mistral to occur 24 hours later.

A comparison of figures B-13 to B-16 with figures B-5 to B-8 shows the development of a Type C mistral during the 24 hours preceding its eruption. The long-wave pattern is indicative of a high-index situation. The pattern is rather poorly defined and subject to rapid variations as baroclinic short waves become unstable and increase their amplitudes. The surface frontal trough and upper short-wave trough that

produce the mistral 24 hours later, are found between England and Ireland and over Portugal (figs. B-13 and B-14). Judging from the standard deviation patterns (figs. B-15 and B-16), it is mainly the short-wave upper trough and surface frontal trough over the Bay of Biscay, Spain and Portugal, together with the preceding short-wave ridge and warm sector over southern France, that typify the weather situation 24 hours before the outbreak of the mistral.

Forty-eight hours prior to the Type A mistral (figs. B-17 to B-20), the surface frontal trough is located to the south of Iceland (fig. B-17). It is backed by an extremely strong surge of cold air to the east of Greenland which provides the energy for the fast southward progress of the frontal system during the next 24 hours (see fig. B-9). The short-wave trough in figure B-18 has just rounded the long-wave blocking ridge. Again it is the warm sector preceding the frontal trough that provides the least variation (minimum standard deviation) from case to case (fig. B-19). The upper-flow pattern is considerably more variable. As a relatively stable indicator we may, however, identify the trough in the North Sea (fig. B-20).

In its progress from Iceland into southern France, the frontal trough experiences deceleration, as may be seen by comparing figures B-1, B-9 and B-17. This must be kept in mind by the novice forecaster who might be tempted to move the frontal trough over the North Atlantic south of Iceland

too slowly on the first day, and too rapidly on the following day in an attempt to correct his previous miscalculation.

Frontal movement occurs more steadily during the high-index conditions of Air Ministry Type C (figs. B-21 to B-24). At t = -48 h., the surface frontal trough and the upper short-wave trough are over the eastern Atlantic, making nearly uniform progress of about 12° longitude per day during the next 48 hours. The standard deviation patterns (figs. B-23 and B-24) mark the characteristic positions of the warm sector preceding the frontal zone, and the flat subtropical high-pressure cell.

It should be mentioned that figure B-21 (t = -48 h.) shows some indication of a weak frontal trough over France, similar to that in figure B-5 (t = 0). This is in agreement with the "rule of thumb" that short-wave high and low pressure regions travelling in a nearly zonal current replace each other within 24 hours. In other words, there is a tendency towards a 48-hour periodicity of frontal systems to move into France as long as the high-index circulation is maintained. This fact may be helpful in forecasting recurrent mistral surges. A similar tendency is not apparent for the Type A mistral (figs. B-1 and B-17).

Figures B-25 to B-28 show surface and 500-mb. mean and standard deviation charts three days prior to the outbreak of the Type A mistral. The surface frontal trough and short-wave pattern responsible for the mistral three days later are difficult to identify because they are masked by the high-pressure

ridge over the central Atlantic. An analysis of pressure rise and fall patterns, not attempted here, may be more successful in identifying the short-wave position. In any case it appears difficult to isolate reliable indicators from synoptic weather maps as much as three days ahead of the mistral occurrence. There are, however, several interesting points that should be noted.

First of all, figures B-25 (t = -72 h.) and B-1 (t = 0) bear a certain resemblance over France and the western Mediterranean. This would suggest that the Type A mistral has a tendency to recur with approximately a three-day periodicity. Figure B-25 still shows a marked reservoir of cold air over the Denmark Strait. This reservoir has been strongly depleted at t = 0 (fig. B.-1). The two-day periodicity suggested for the Type C mistral does not seem to hold for Type A as figure B-25 is markedly dissimilar to figure B-9 (t = -24 h.). However, figure B-25 is similar to figure B-1 (t = 0). The same holds for the 500-mb. pattern except that the long-wave trough over central Europe underwent strong deepening within 72 hours.

The standard deviation field of surface pressures (fig. B-27) also gives no reliable indicator of the suspected position of the frontal system which ultimately caused the mistral three days later. The low values over France, however, lend support to the hypothesis that there is a three-day recurrence tendency for mistral surges of Type A.

In the case of the Type C mistral, mean and standard deviation charts for t = -72 h. are not reproduced here as they provide no meaningful forecasting clues.

In addition to the mean and standard deviation charts discussed above, Reiter explored the possibility of extended-range forecasting using 500-mb. continuity diagrams along 55° N. From his diagrams the position of the quasi-stationary long-wave troughs and ridges, and their occasional rapid adjustments, could clearly be seen, as could the short-wave disturbances which, on the average, moved about 10° to 12° longitude per day. He suggested that such a diagram constructed along 50° N. or 45° N. might be better for predicting conditions in the mistral region. These extended-range forecasting techniques, involving the interplay between quasi-stationary long waves and the faster-moving short waves, are to be investigated with a view to developing methods for extended forecasts of mistral surges.

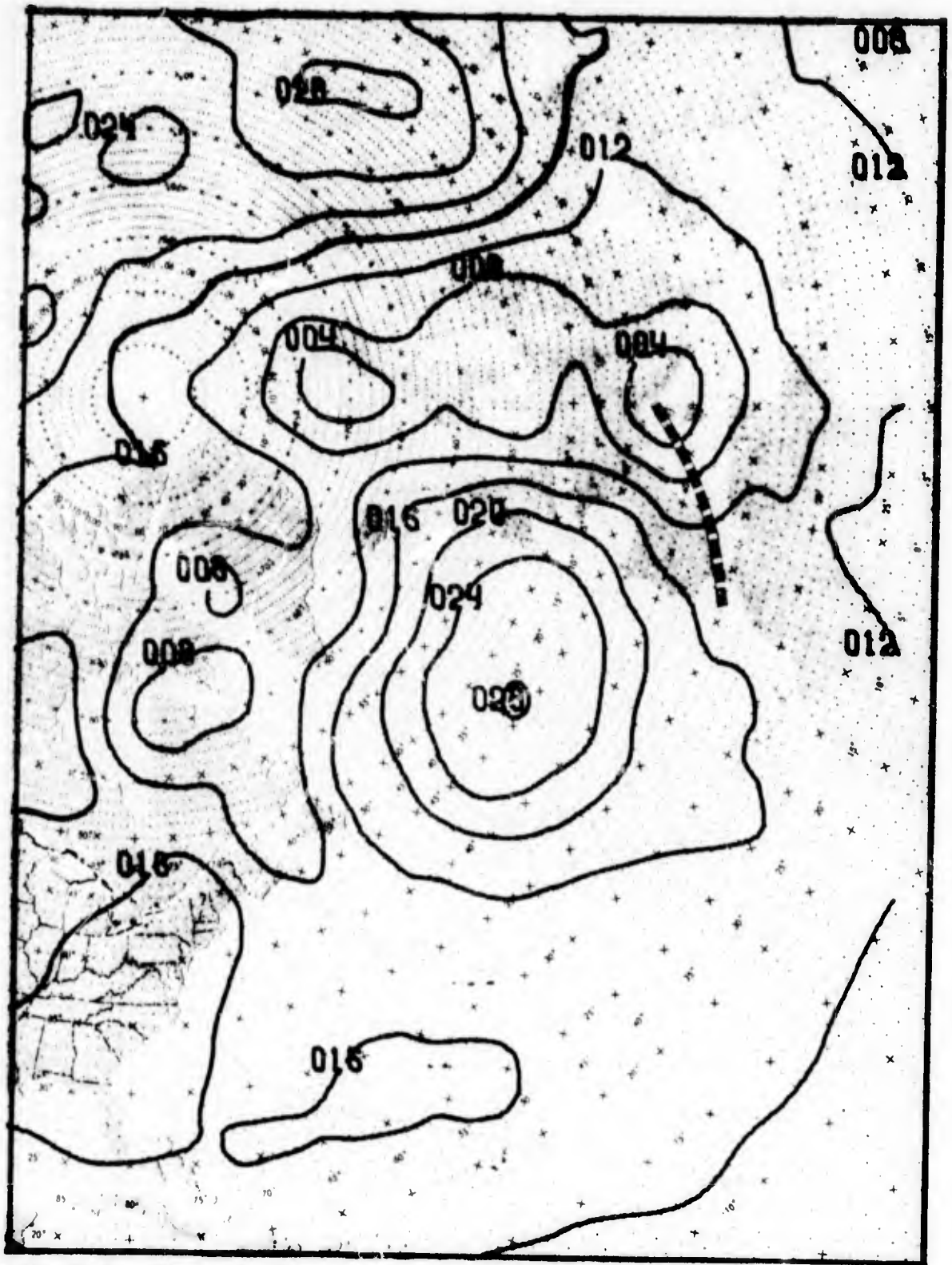

Figure B-1. Mean Hemispheric Surface Pressure (mb.) for Incipient Mistrals, Air Ministry Type A. (Brody, Reiter and Godfrey)

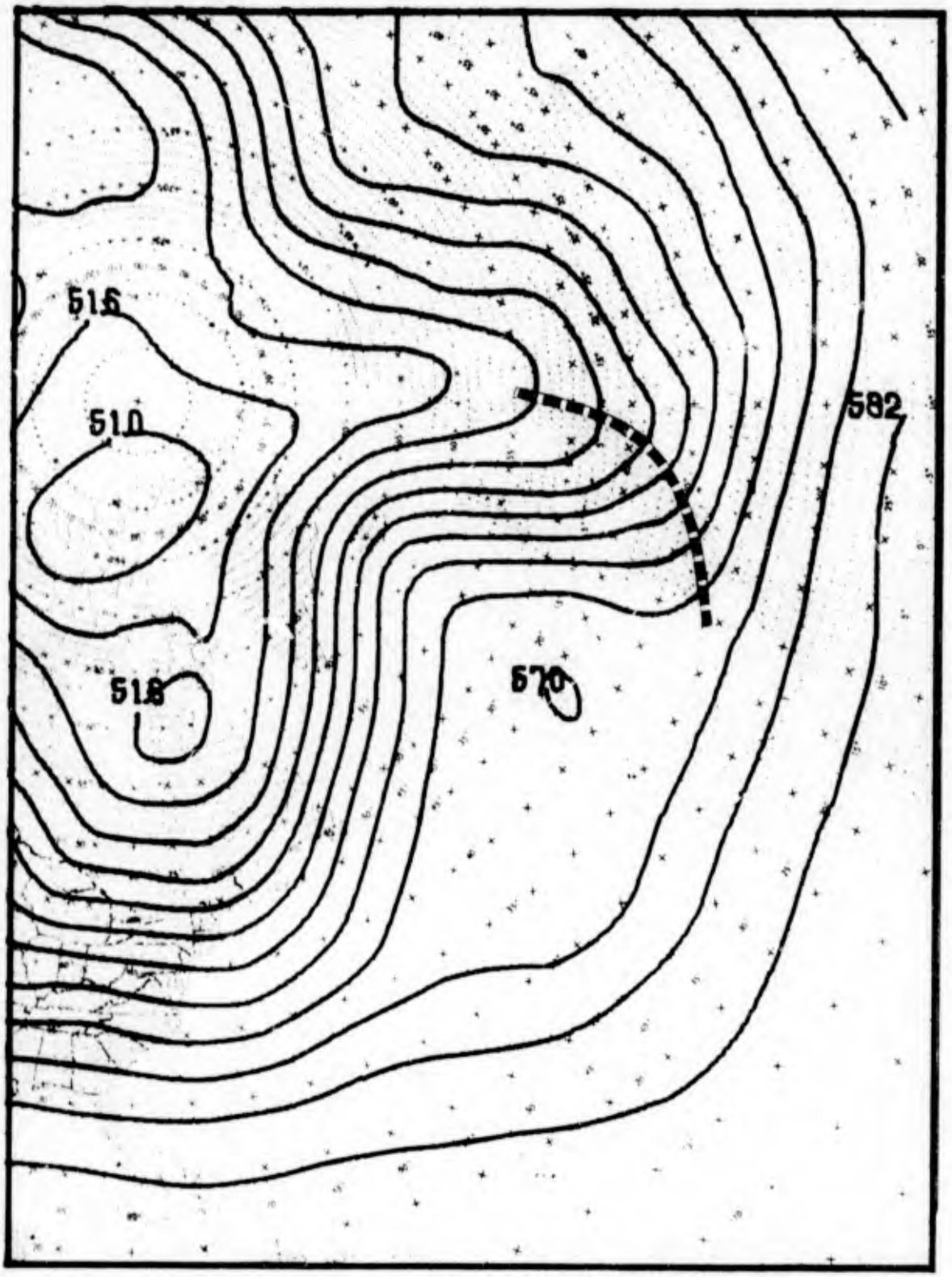

Figure B-2. Mean Hemispheric 500-Mb. Pattern (tens of geopotential meters) for Incipient Mistrals, Air Ministry Type A. (Brody, Reiter and Godfrey)

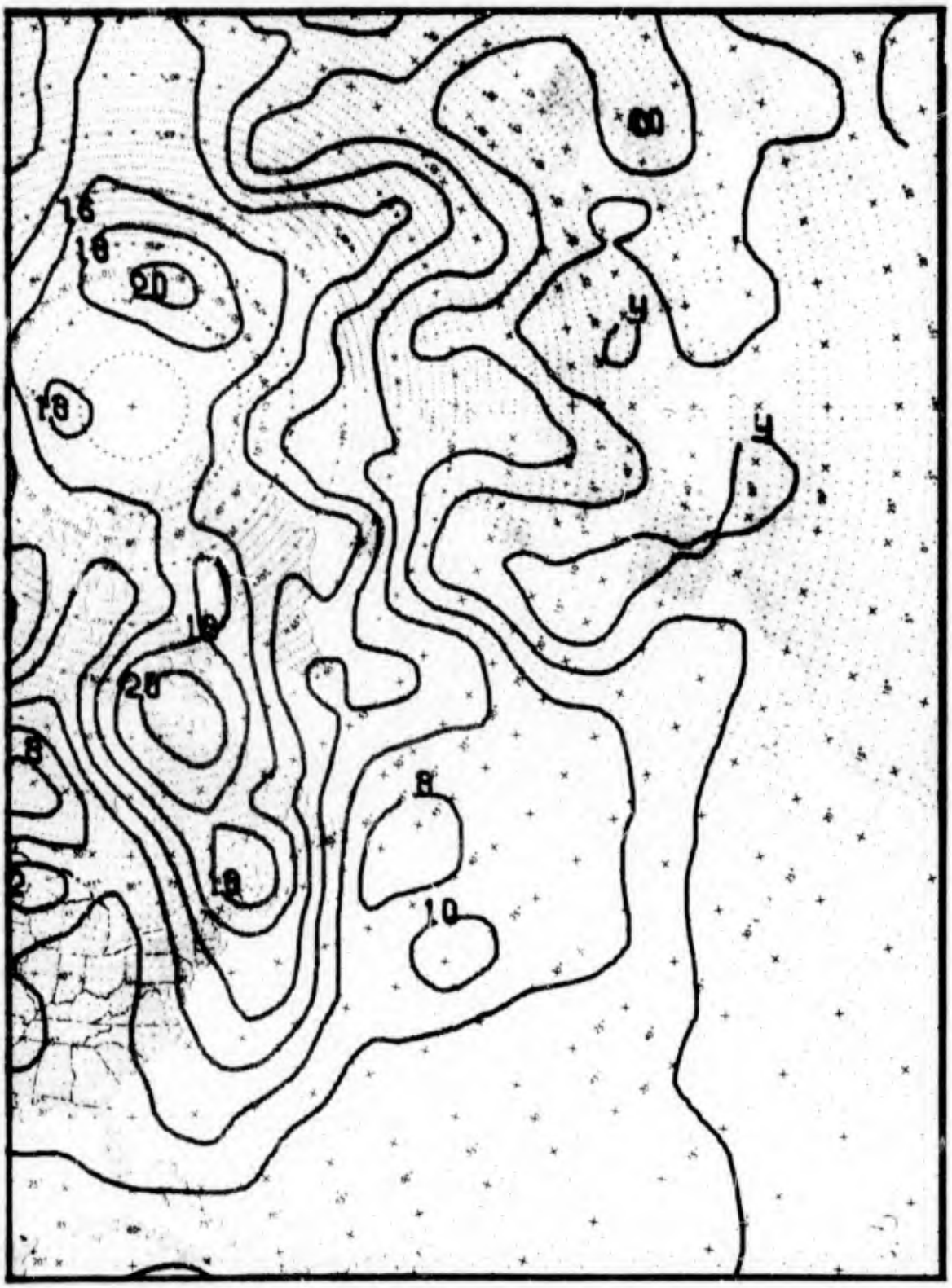

Figure B-3. Standard Deviations of Surface Pressure (mb.) for Incipient Mistrals, Air Ministry Type A. (Brody, Reiter and Godfrey)

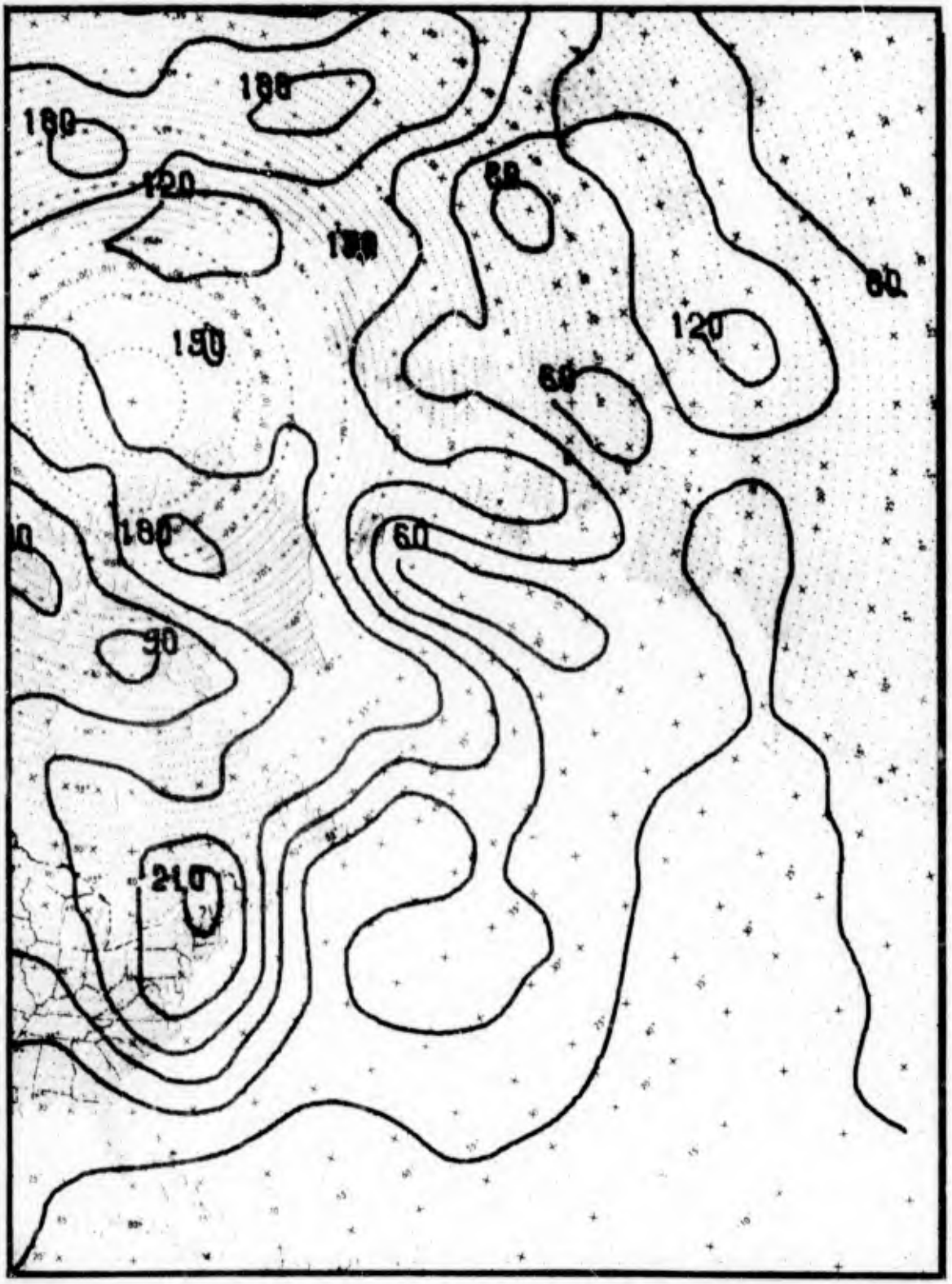

Figure B-4. Standard Deviations of 500-Mb. Heights (geopotential meters) for Incipient Mistrals, Air Ministry Type A. (Brody, Reiter and Godfrey)

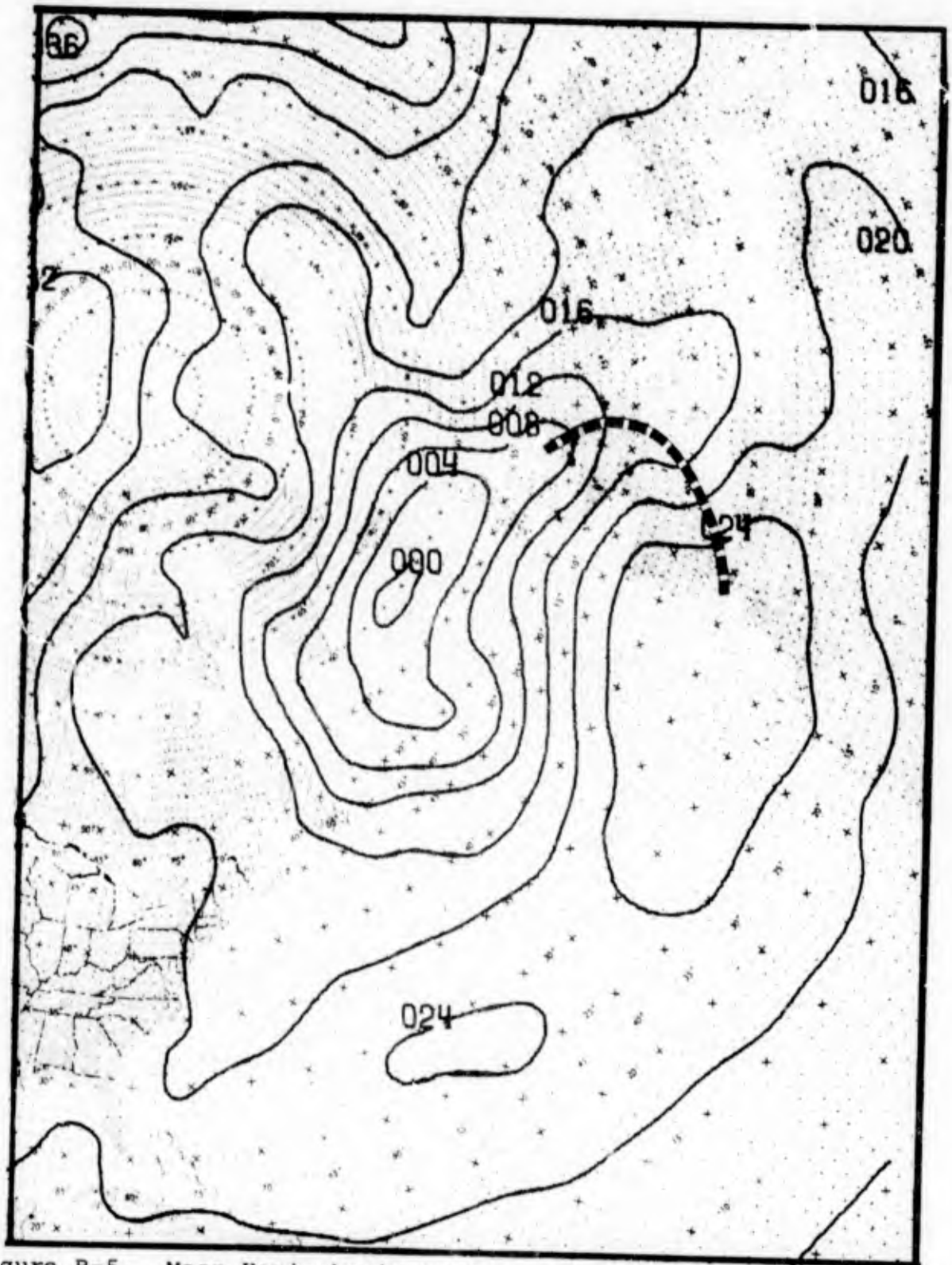

Figure B-5. Mean Hemispheric Surface Pressure (mb.) for Incipient Mistrals, Air Ministry Type C. (Brody, Reiter and Godfrey)

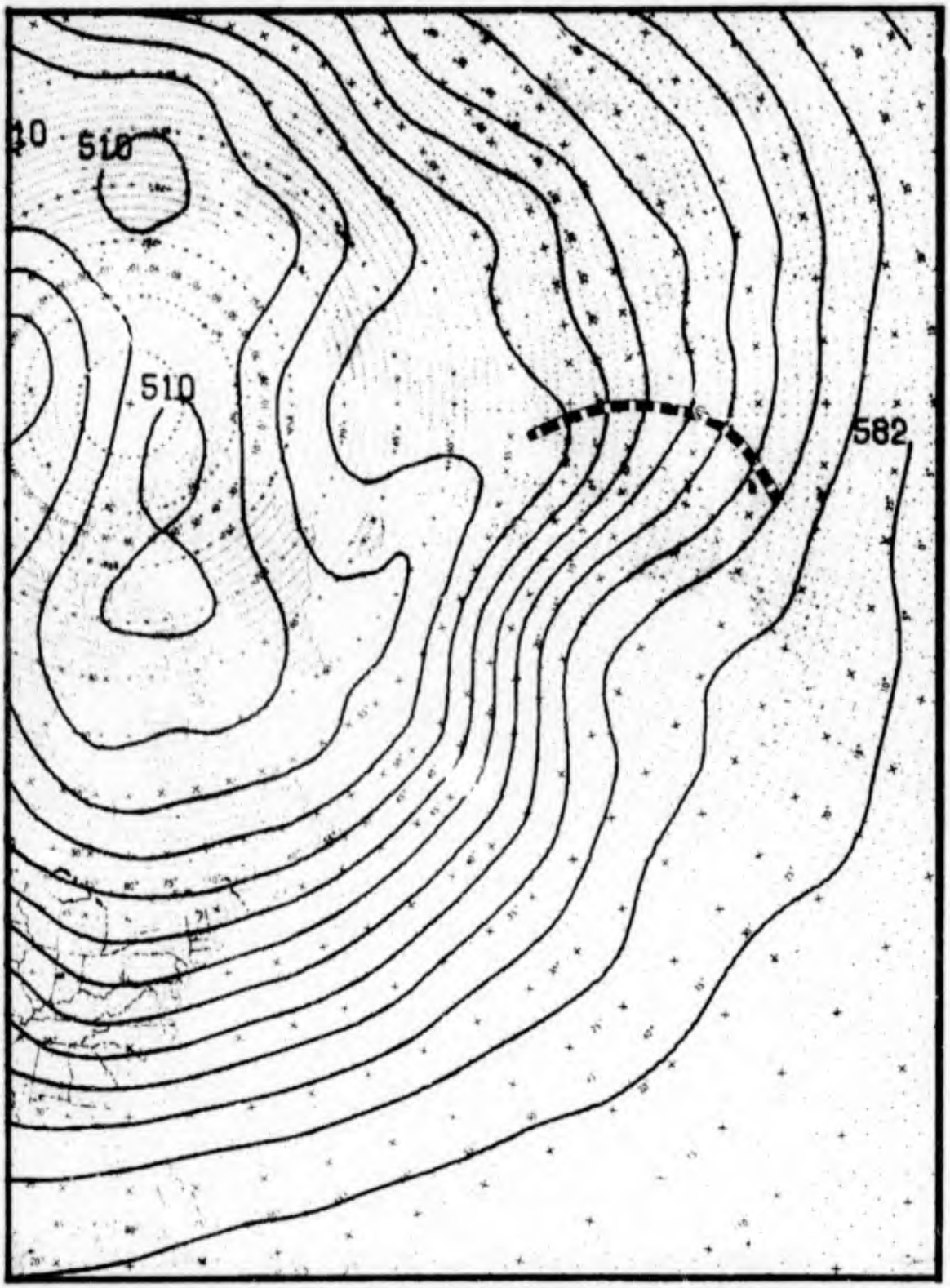

Figure B-6. Mean Hemispheric 500-Mb. Pattern (tens of geopotential meters) for Incipient Mistrals, Air Ministry Type C. (Brody, Reiter and Godfrey)

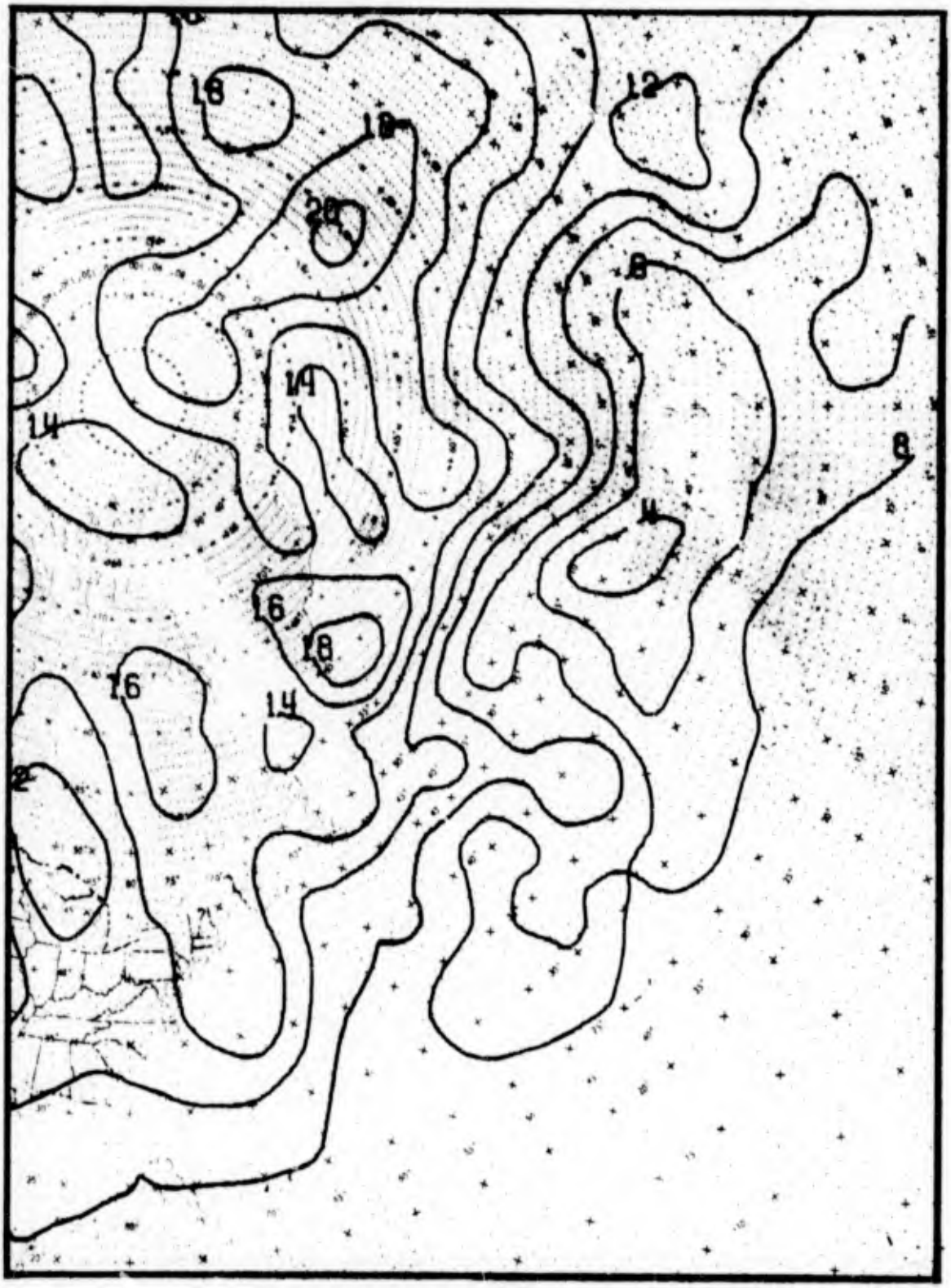

Figure B-7. Standard Deviations of Surface Pressure (mb.) for Incipient Mistrals, Air Ministry Type C. (Brody, Reiter and Godfrey)

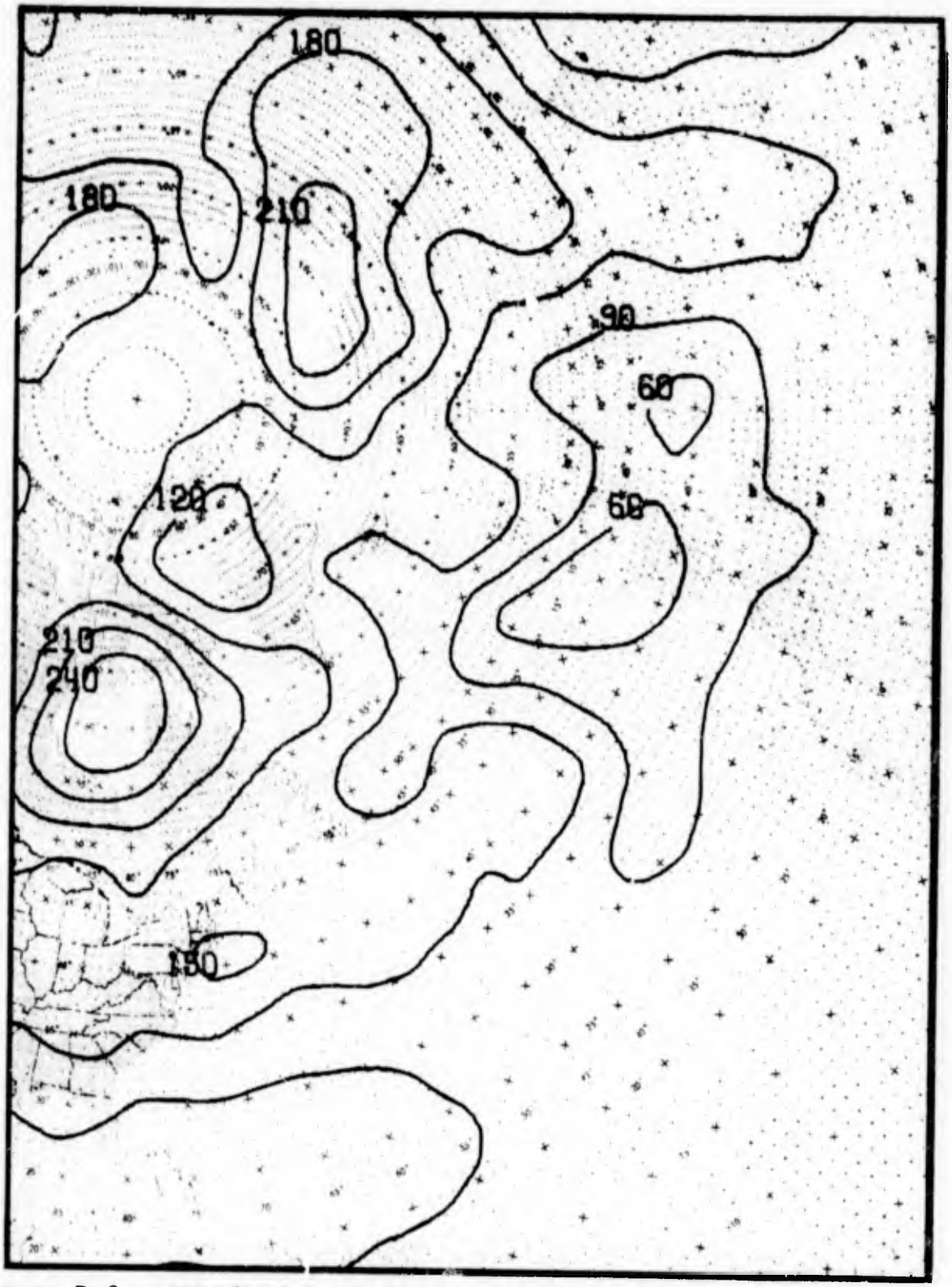

Figure B-8. Standard Deviations of 500-Mb. Heights (geopotential meters) for Incipient Mistrals, Air Ministry Type C. (Brody, Reiter and Godfrey)

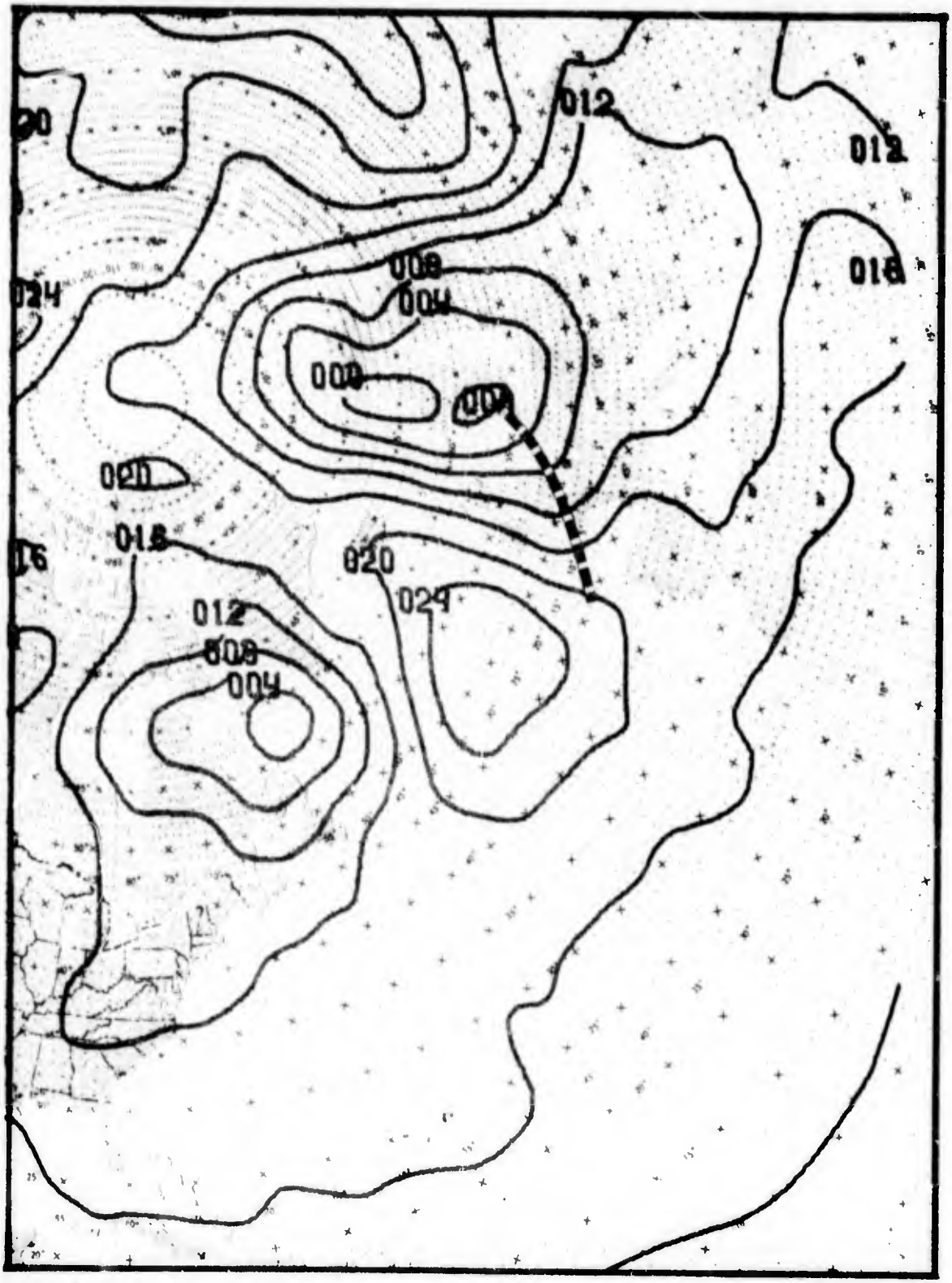

Figure B-9. Mean Hemispheric Surface Pressure (mb.) 24 Hours Before Onset of Mistral, Air Ministry Type A. (Brody, Reiter and Godfrey)

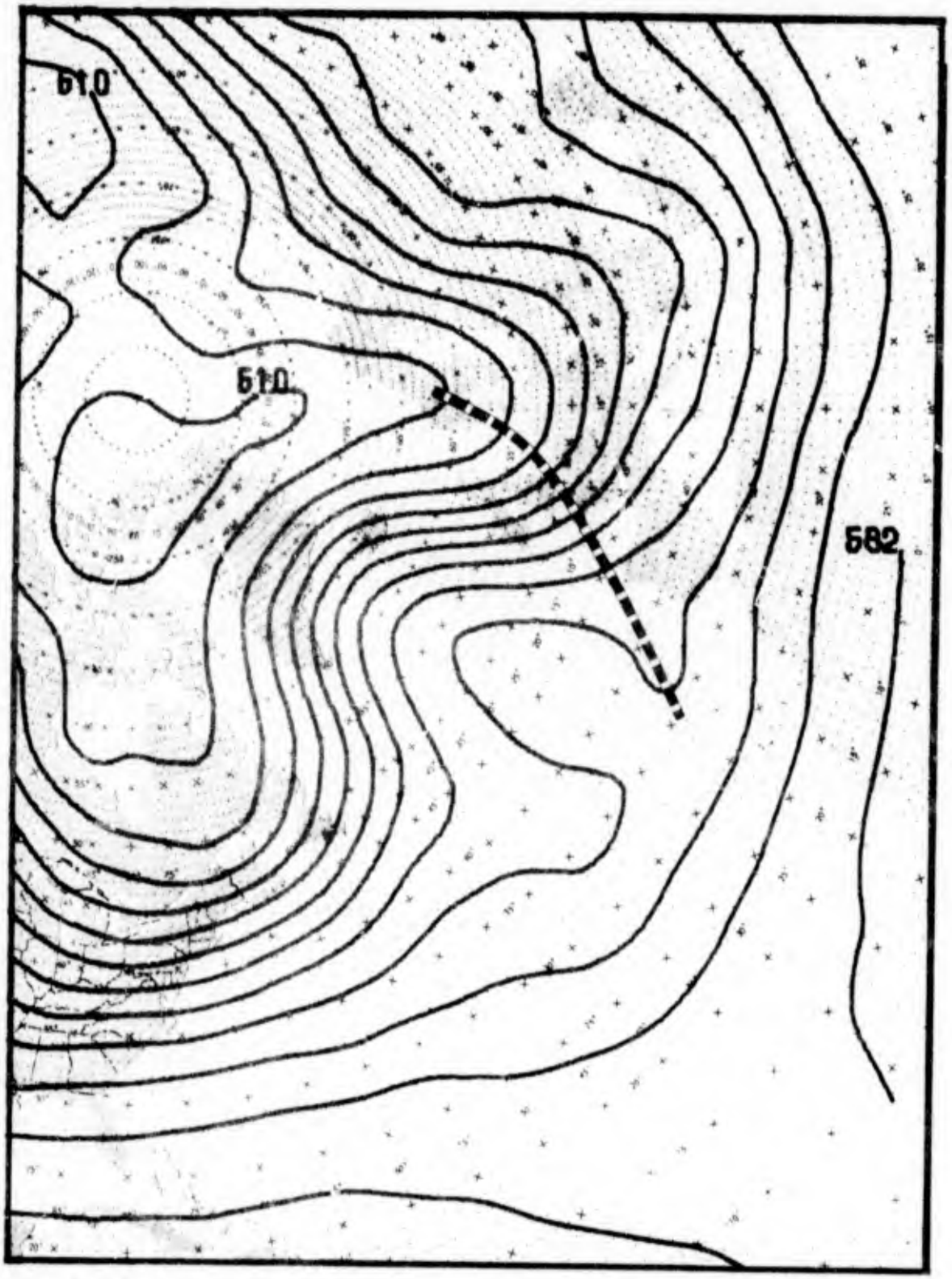

Figure B-10. Mean Hemispheric 500-Mb. Pattern (tens of geopotential meters) 24 Hours Before Onset of Mistral, Air Ministry Type A. (Brody, Reiter and Godfrey)

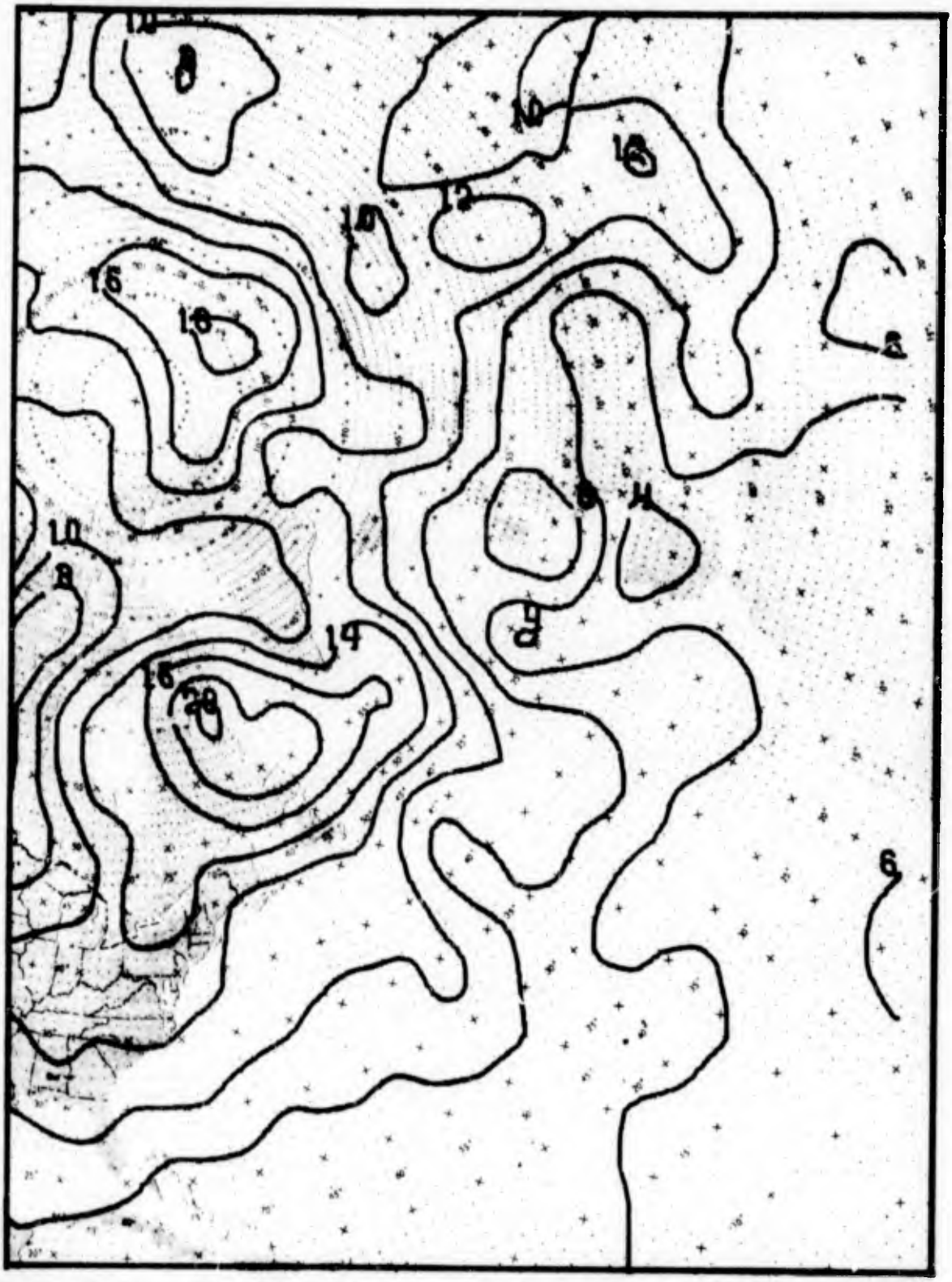

Figure B-11. Standard Deviations of Surface Pressure (mb.) 24 Hours Before Onset of Mistral, Air Ministry Type A. (Brody, Reiter and Godfrey)

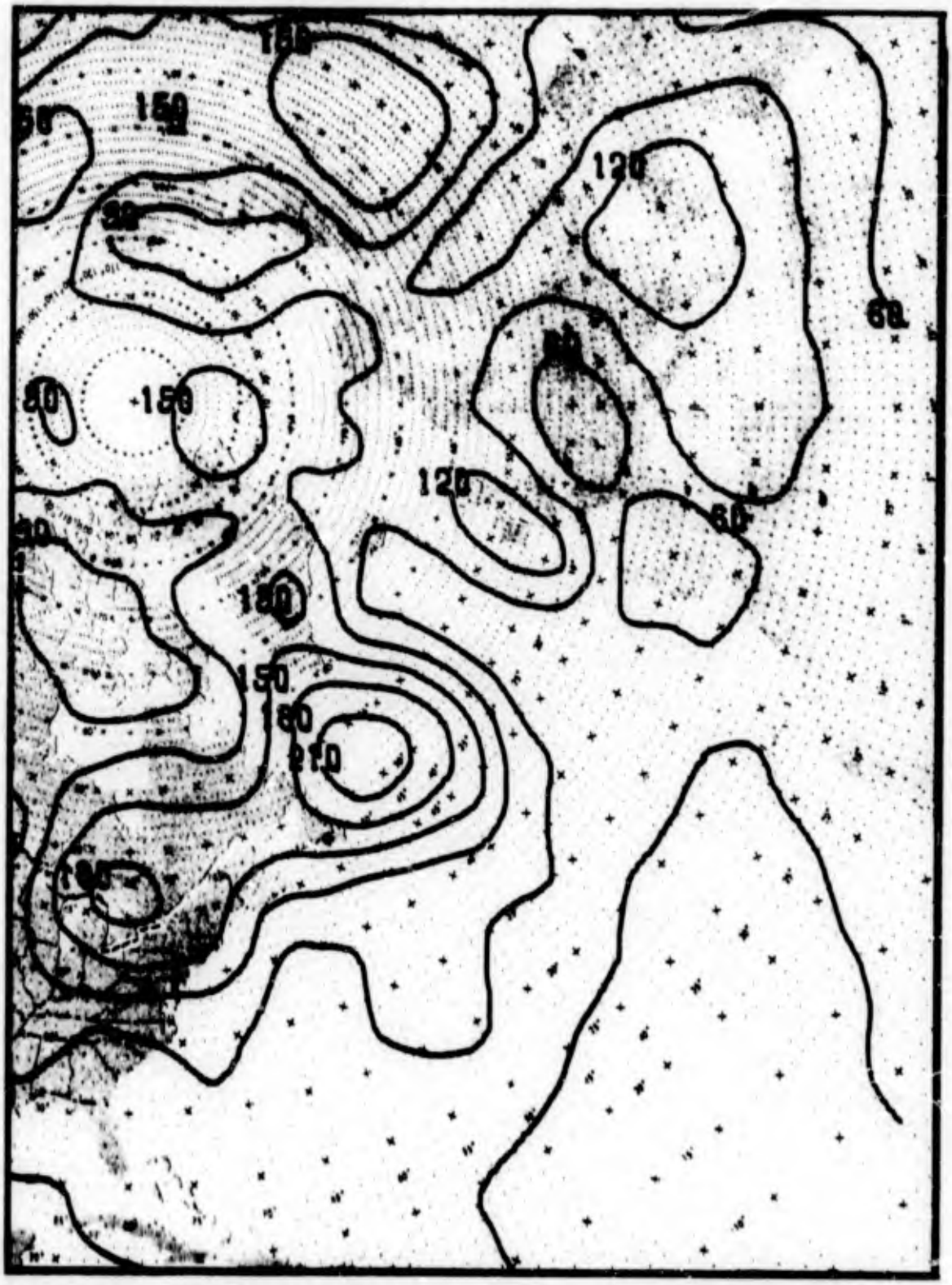

Figure B-12. Standard Deviations of 500-Mb. Heights (geopotential meters) 24 Hours Before Onset of Mistral, Air Ministry Type A. (Brody, Reiter and Godfrey)

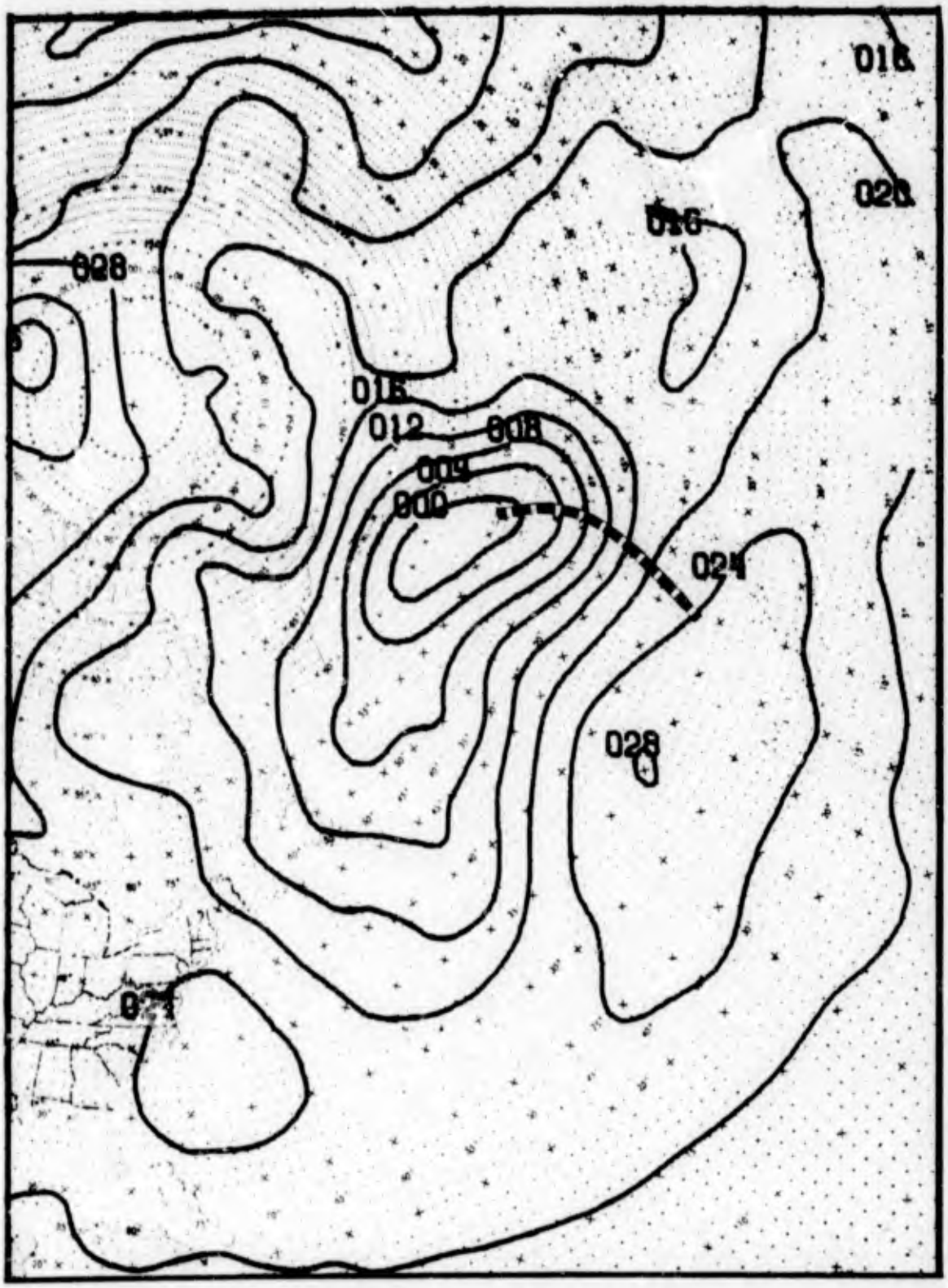

Figure B-13. Mean Hemispheric Surface Pressure (mb.) 24 Hours Before Onset of Mistral, Air Ministry Type C. (Brody, Reiter and Godfrey)

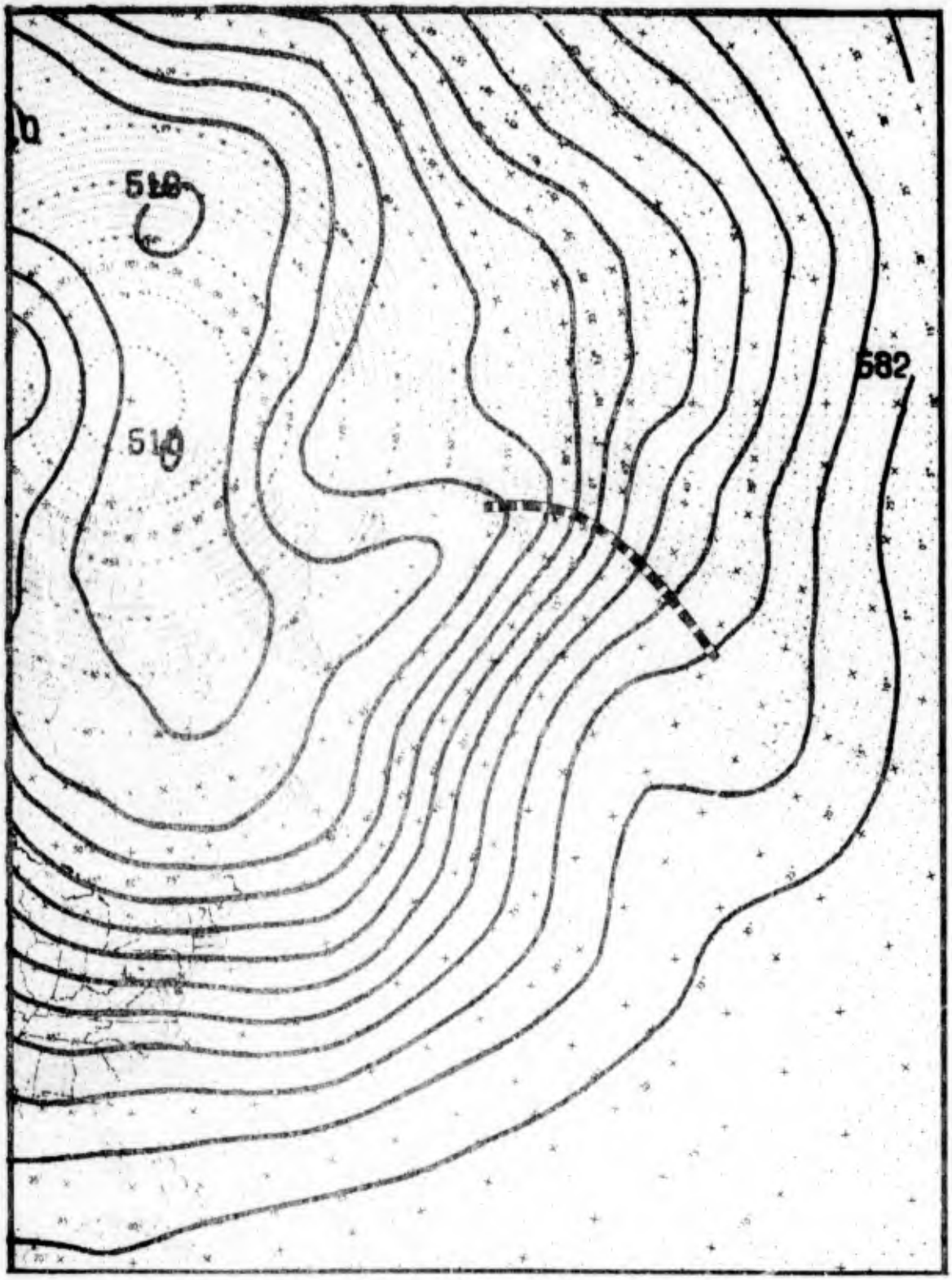

Figure B-14. Mean Hemispheric 500-Mb. Pattern (tens of geopotential meters) 24 Hours Before Onset of Mistral, Air Ministry Type C. (Brody, Reiter and Godfrey)

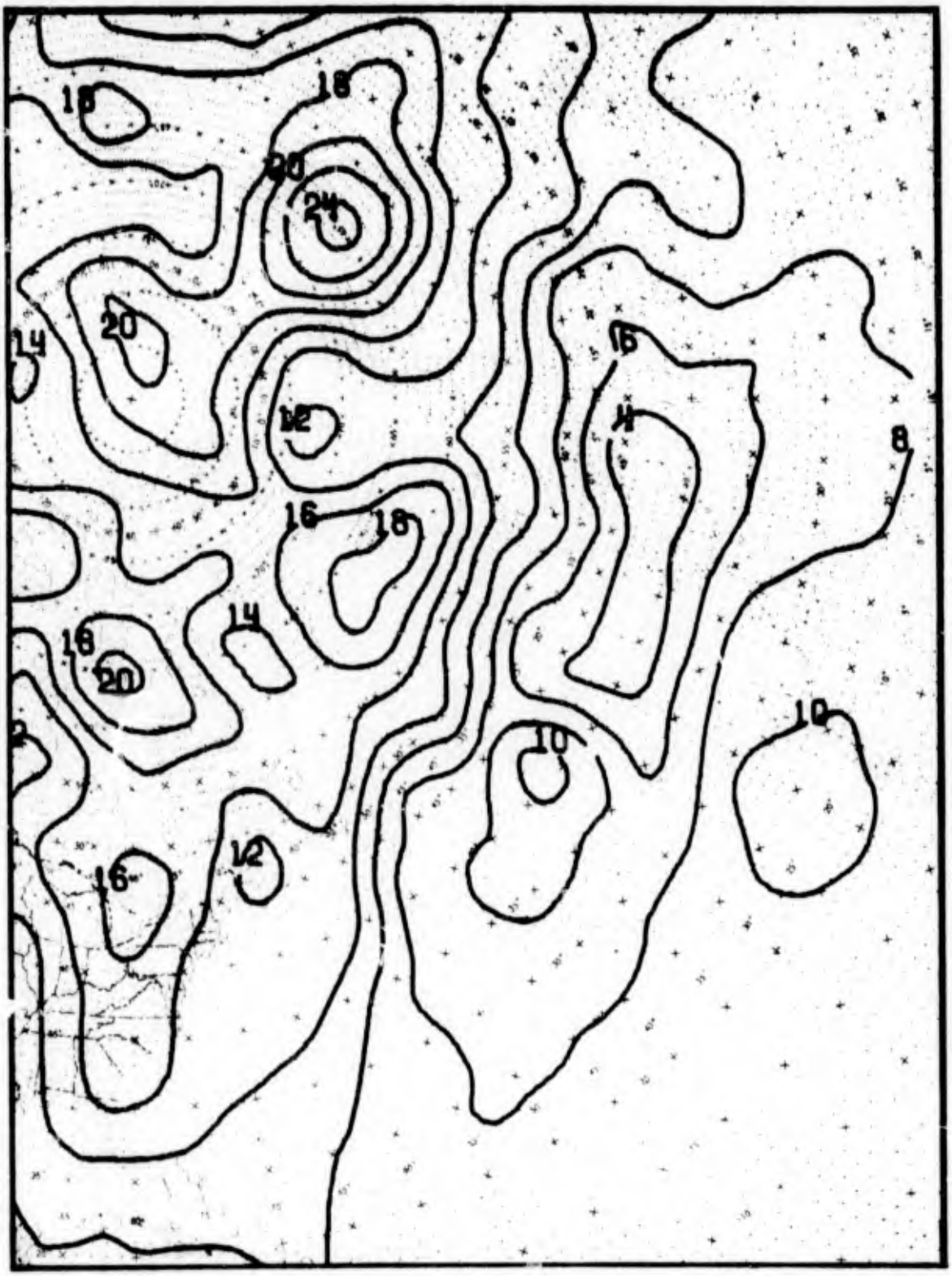

Figure B-15. Standard Deviations of Surface Pressure (mb.) 24 Hours Before Onset of Mistral, Air Ministry Type C. (Brody, Reiter and Godfrey)

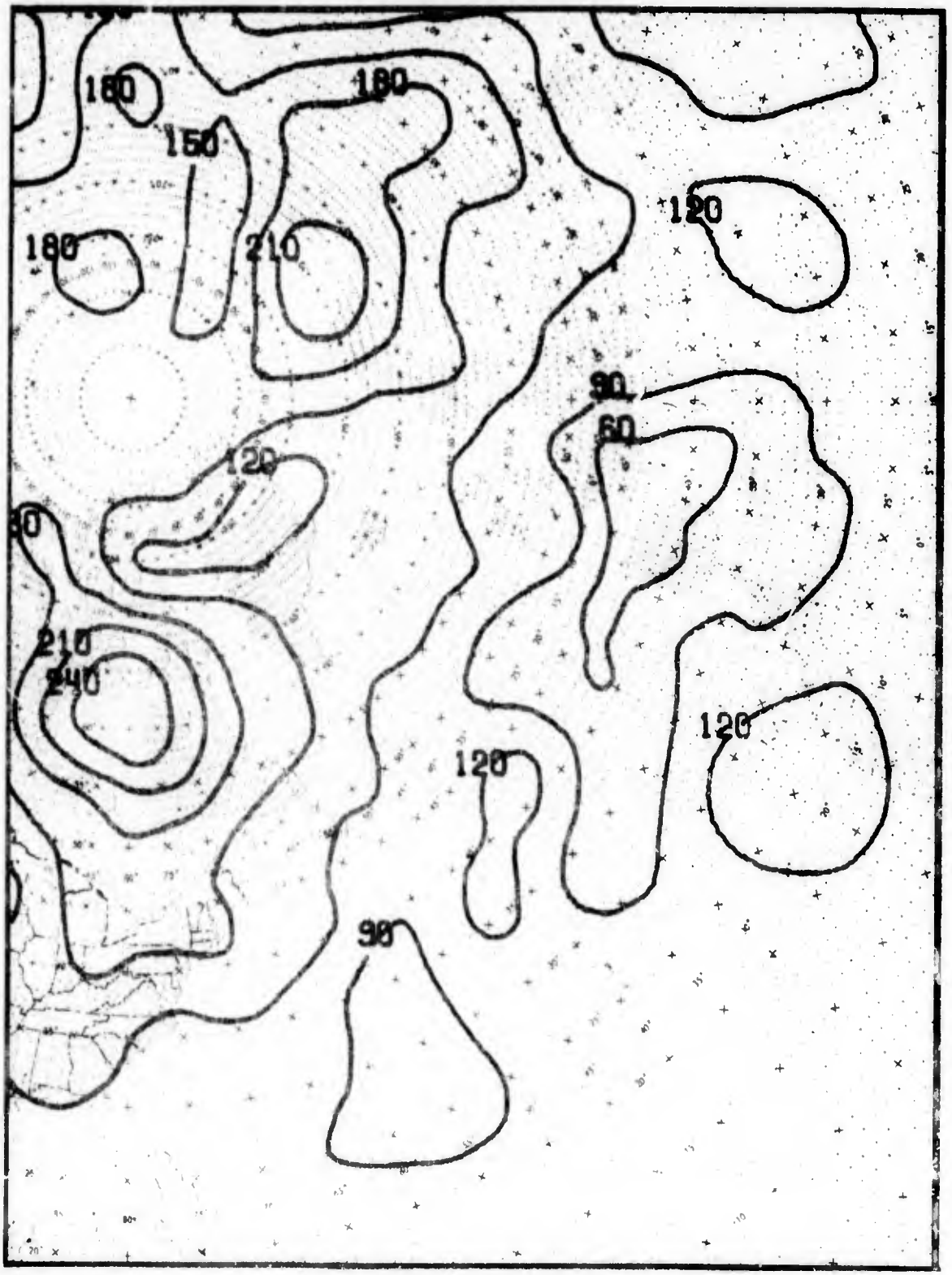

Figure B-16. Standard Deviations of 500-Mb. Heights (geopotential meters) 24 Hours Before Onset of Mistral, Air Ministry Type C. (Brody, Reiter and Godfrey)

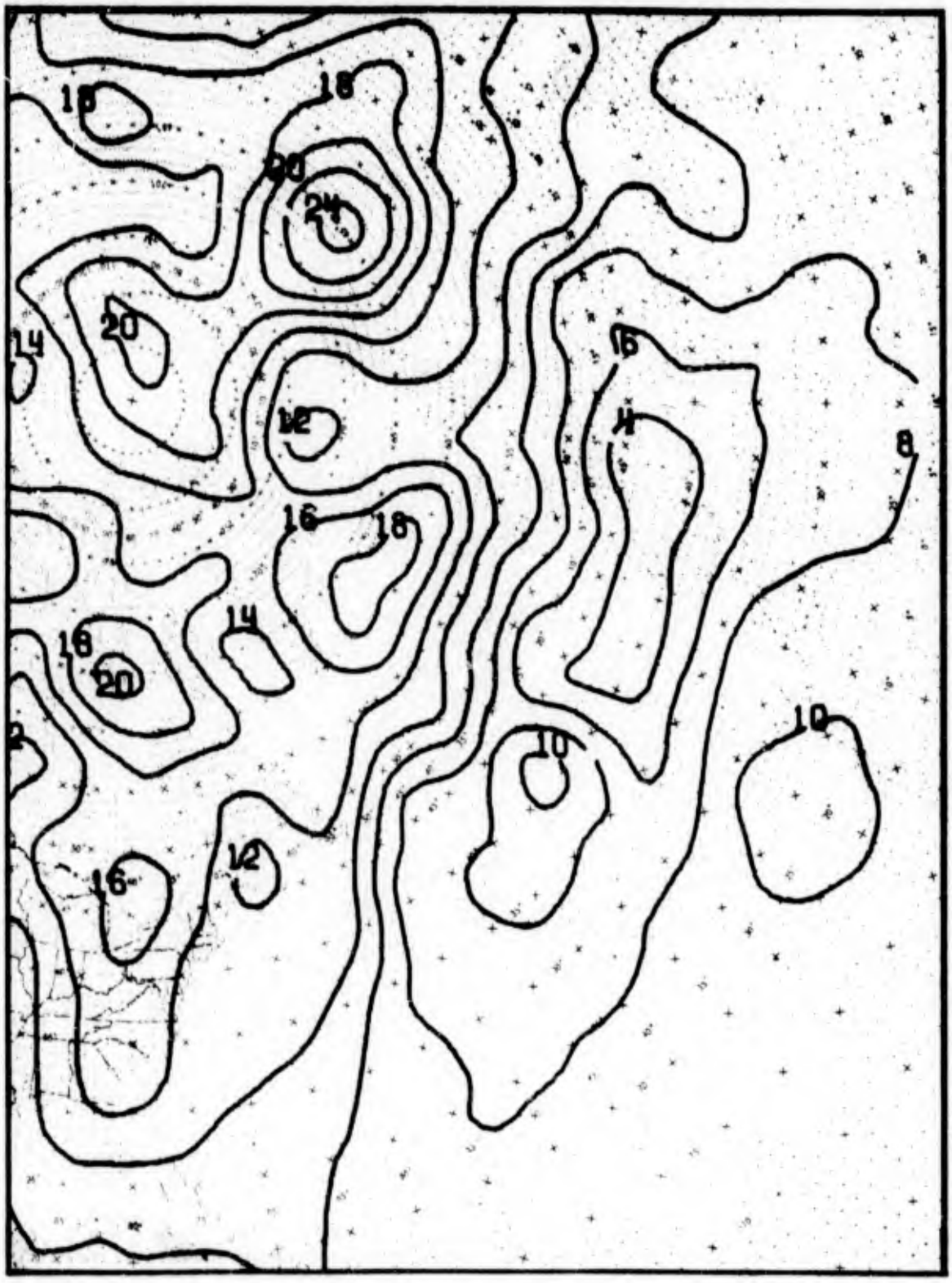

Figure B-15. Standard Deviations of Surface Pressure (mb.) 24 Hours Before Onset of Mistral, Air Ministry Type C. (Brody, Reiter and Godfrey)

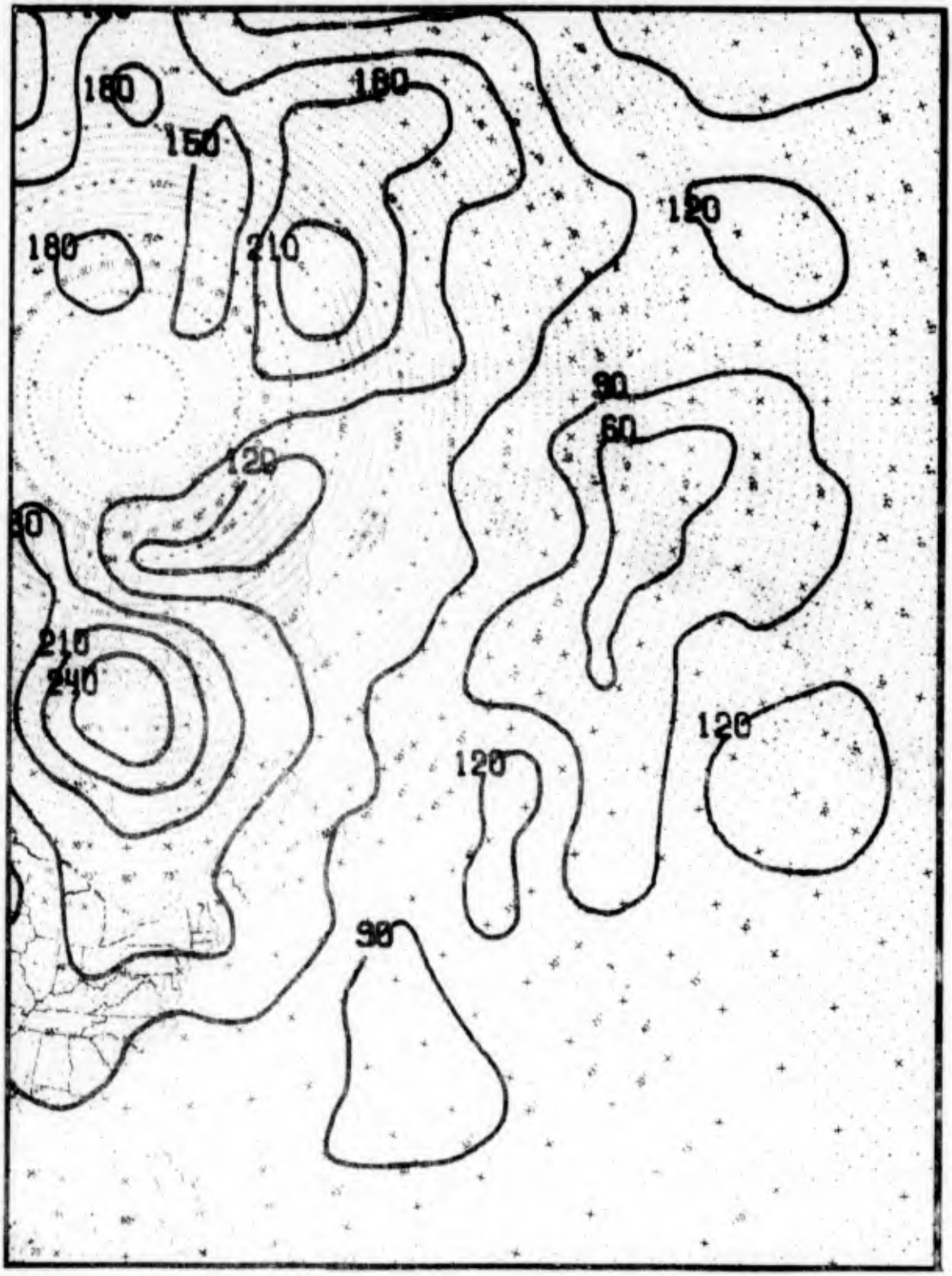

Figure B-16. Standard Deviations of 500-Mb. Heights (geopotential meters) 24 Hours Before Onset of Mistral, Air Ministry Type C. (Brody, Reiter and Godfrey)

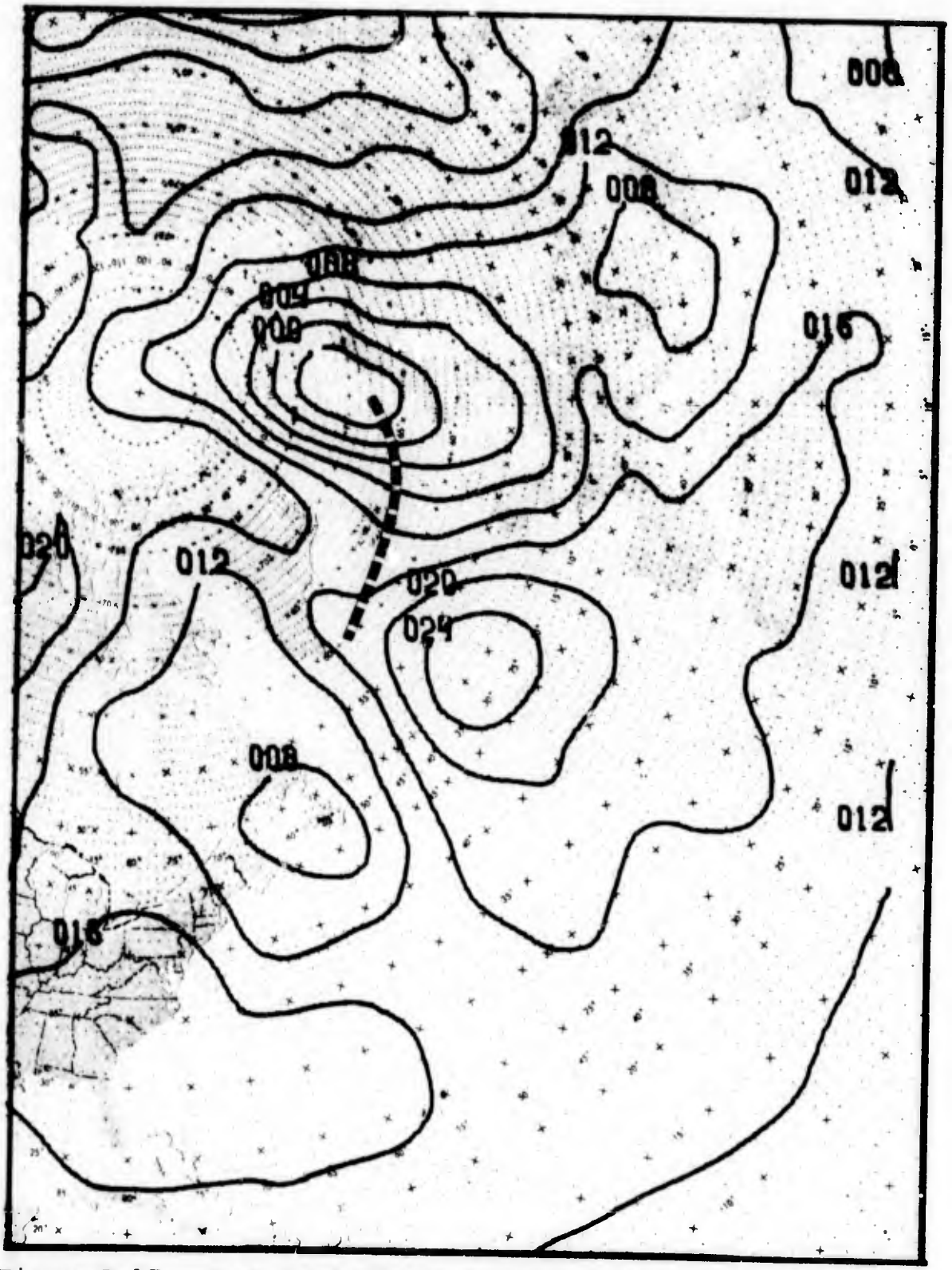

Figure B-17. Mean Hemispheric Surface Pressure (mb.) 48 hours Before Onset of Mistral, Air Ministry Type A. (Brody, Reiter and Godfrey)

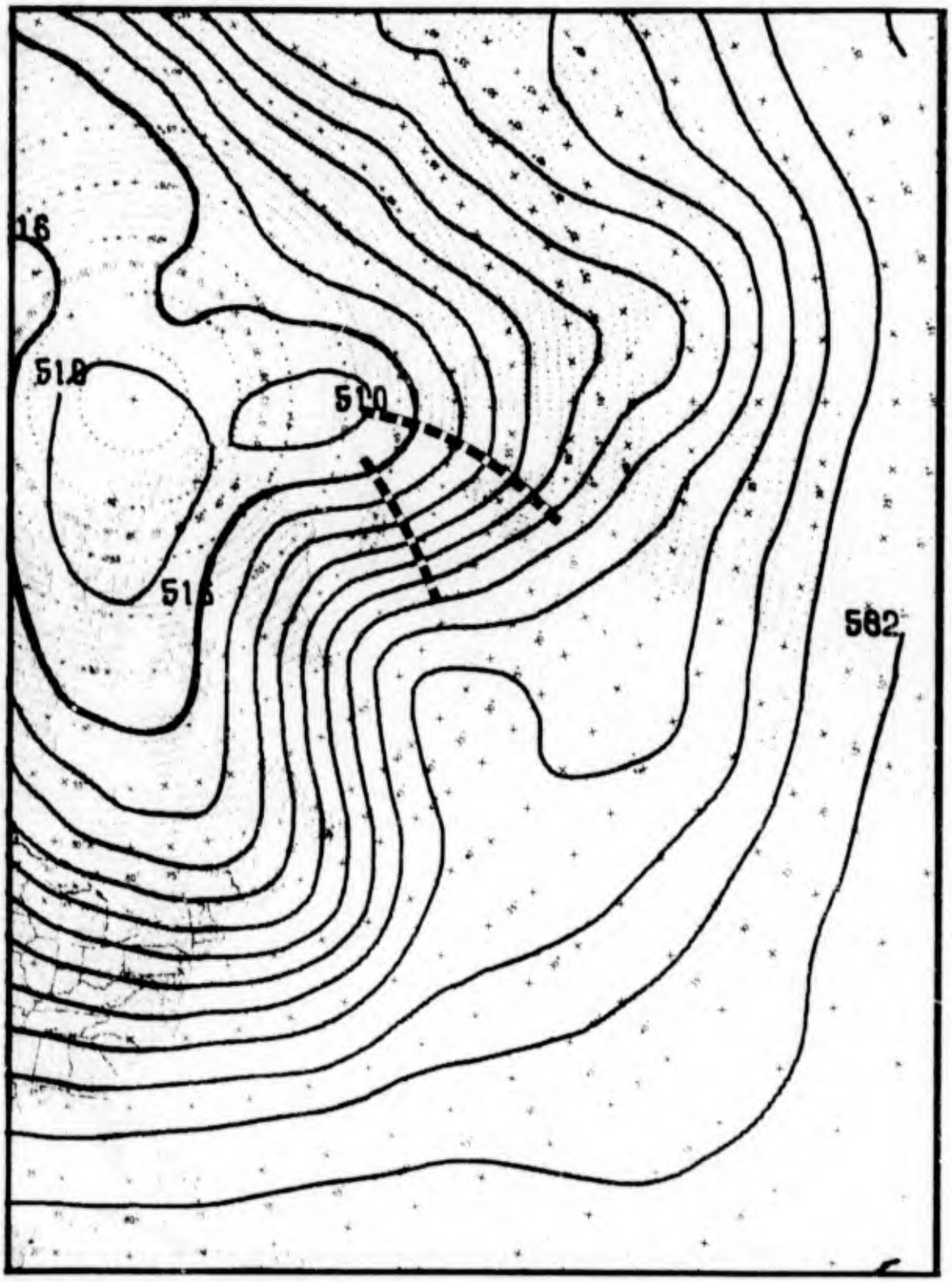

Figure B-18. Mean Hemispheric 500-Mb. Pattern (tens of geopotential meters) 48 Hours Before Onset of Mistral, Air Ministry Type A. (Brody, Reiter and Godfrey)

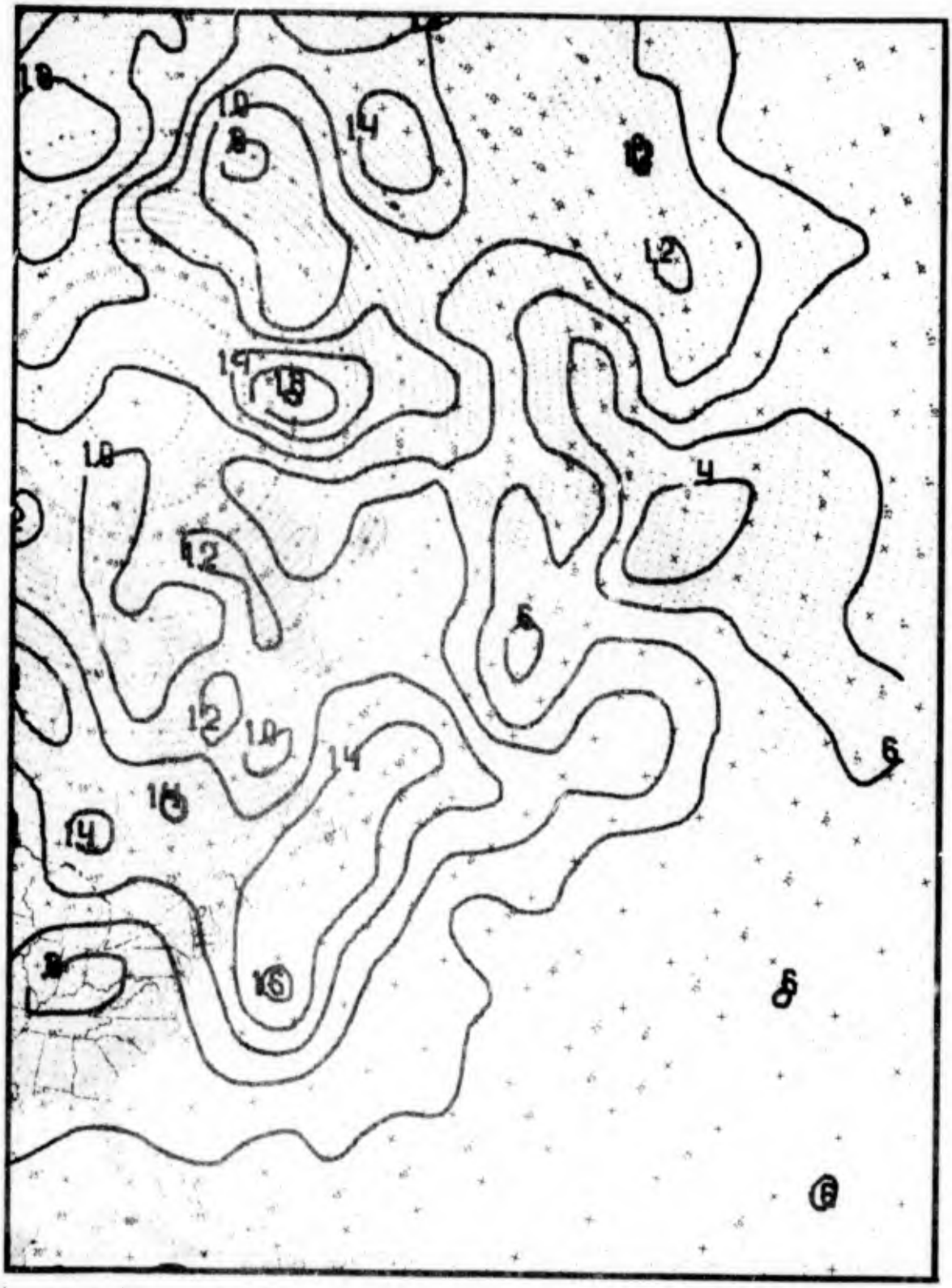

Figure B-19. Standard Deviations of Surface Pressure (mb.) 48 Hours Before Onset of Mistral, Air Ministry Type A. (Brody, Reiter and Godfrey)

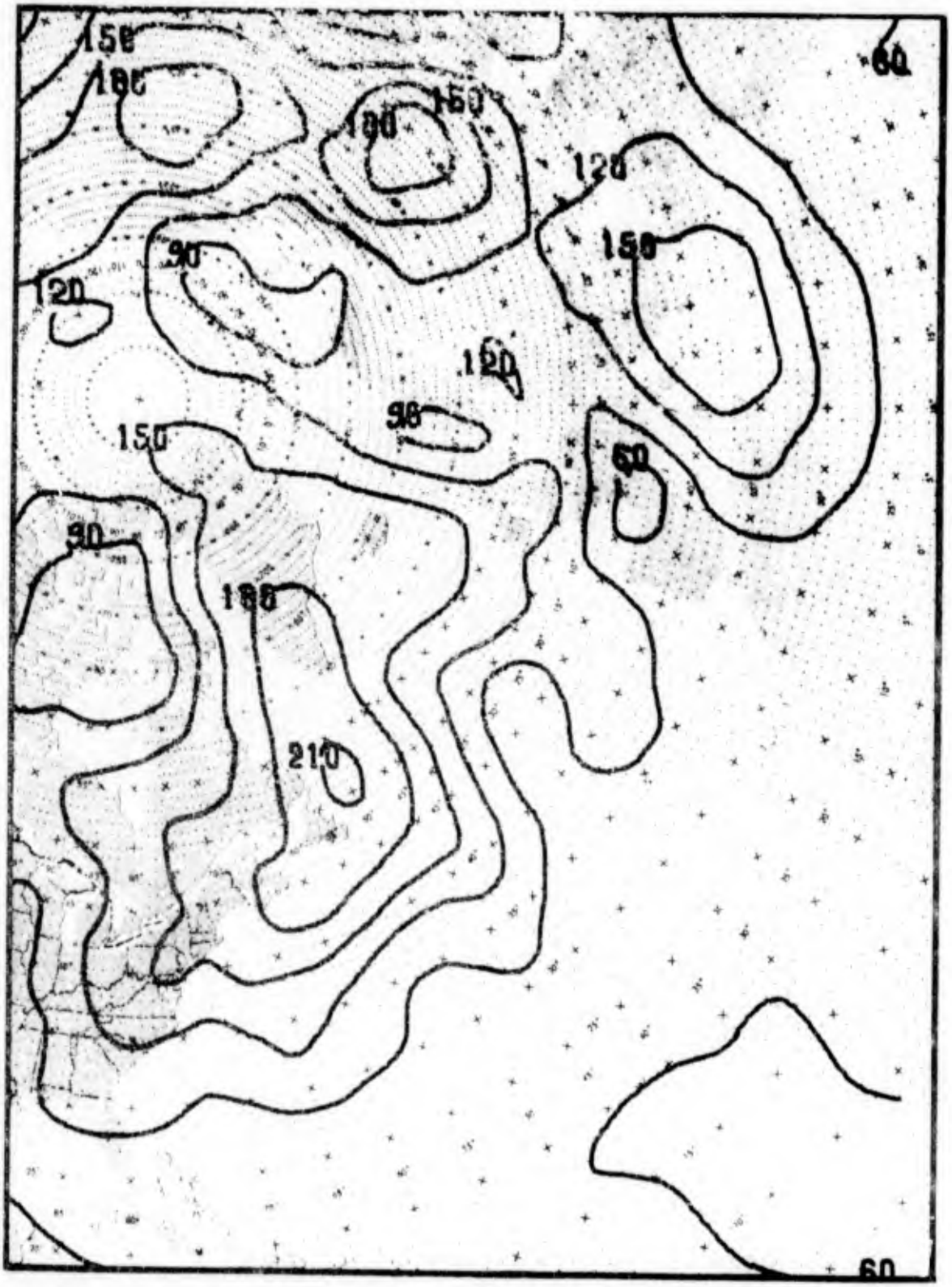

Figure B-20. Standard Deviations of 500-Mb. Heights (geopotential meters) 48 Hours Before Onset of Mistral, Air Ministry Type A. (Brody, Reiter and Godfrey)

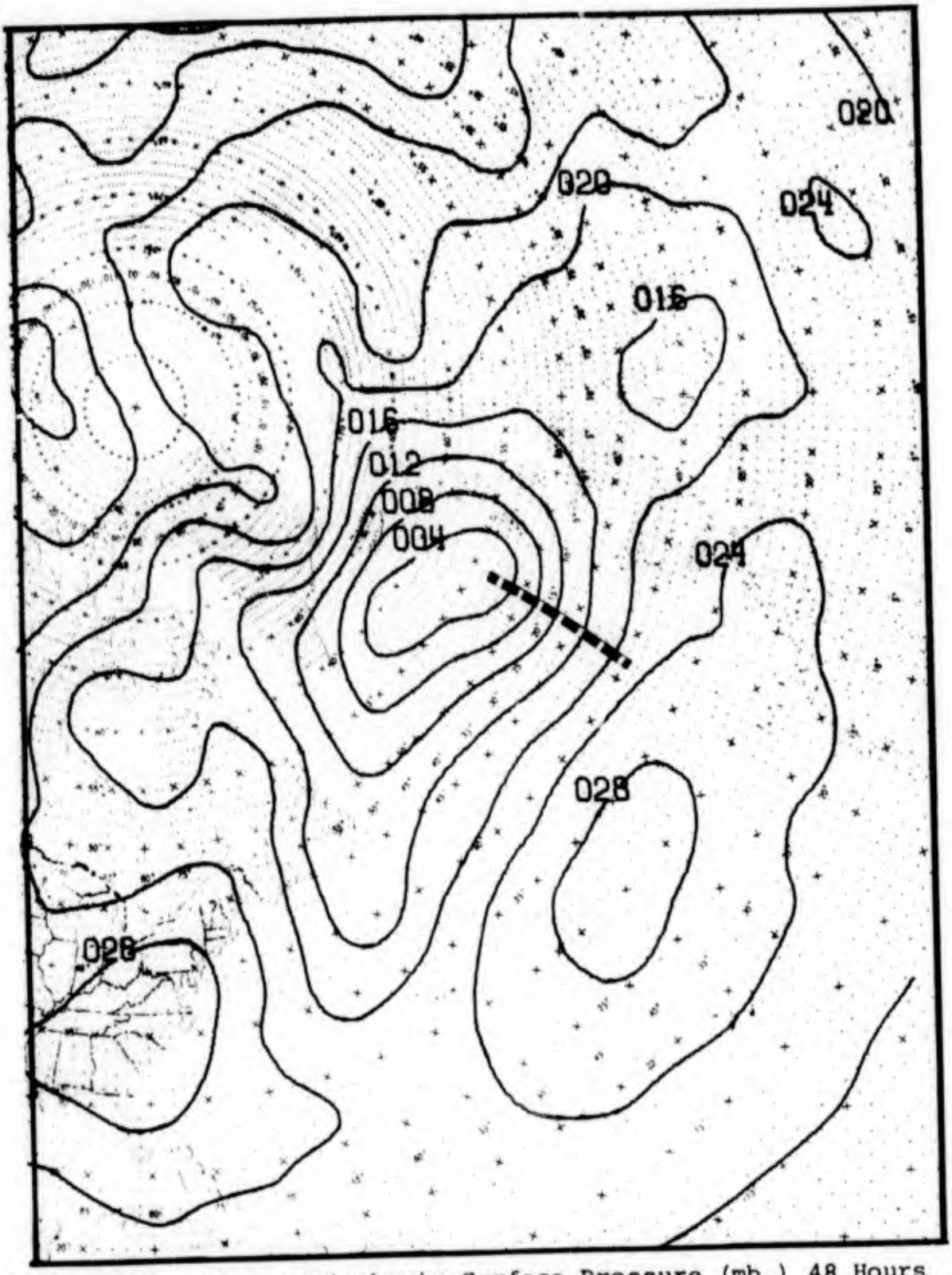

Figure B-21. Mean Hemispheric Surface Pressure (mb.) 48 Hours Before Onset of Mistral, Air Ministry Type C. (Brody, Reiter and Godfrey)

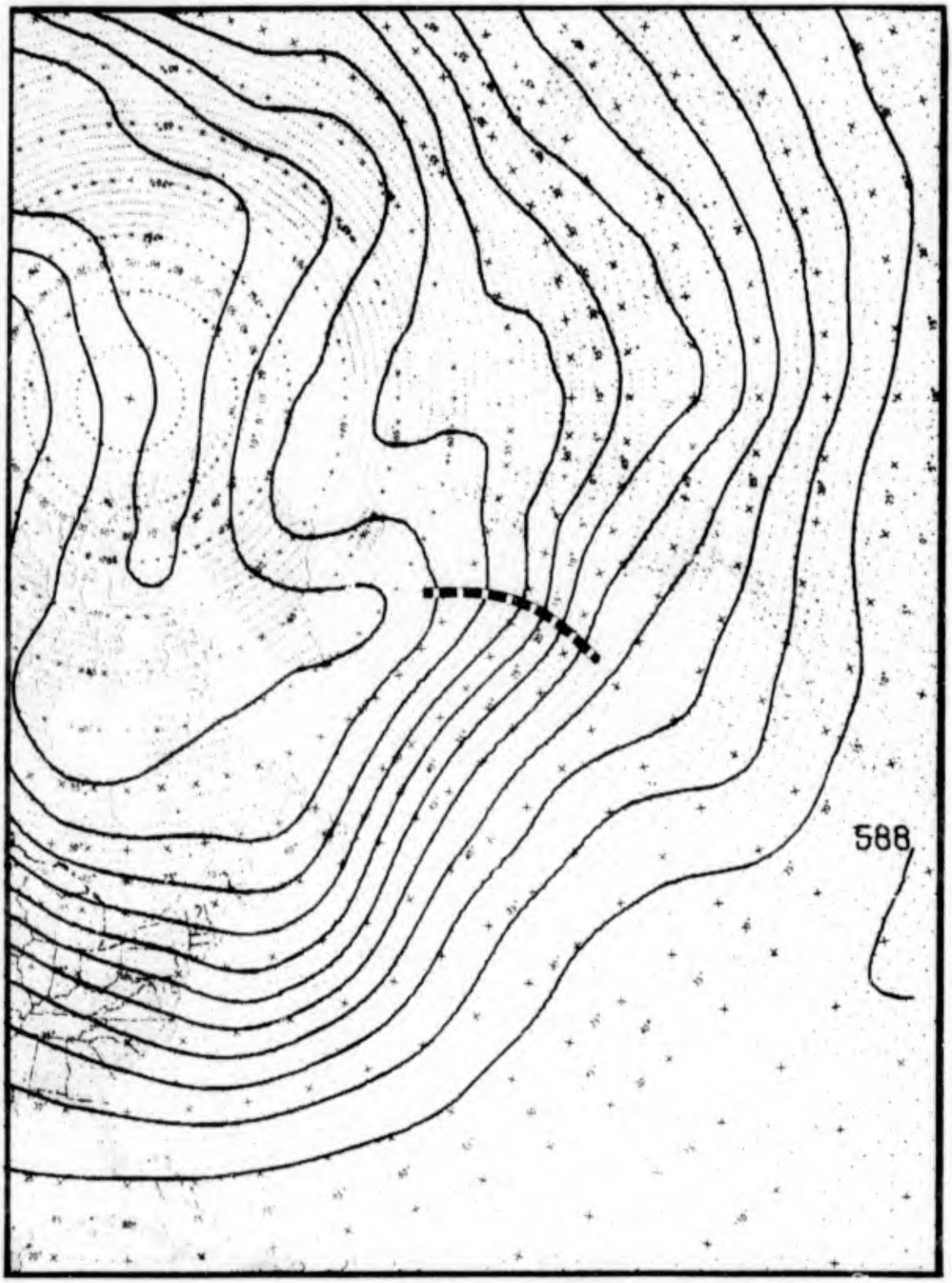

Figure B-22. Mean Hemispheric 500-Mb. Pattern (tens of geopotential meters) 48 Hours Before Onset of Mistral, Air Ministry Type C. (Brody, Reiter and Godfrey)

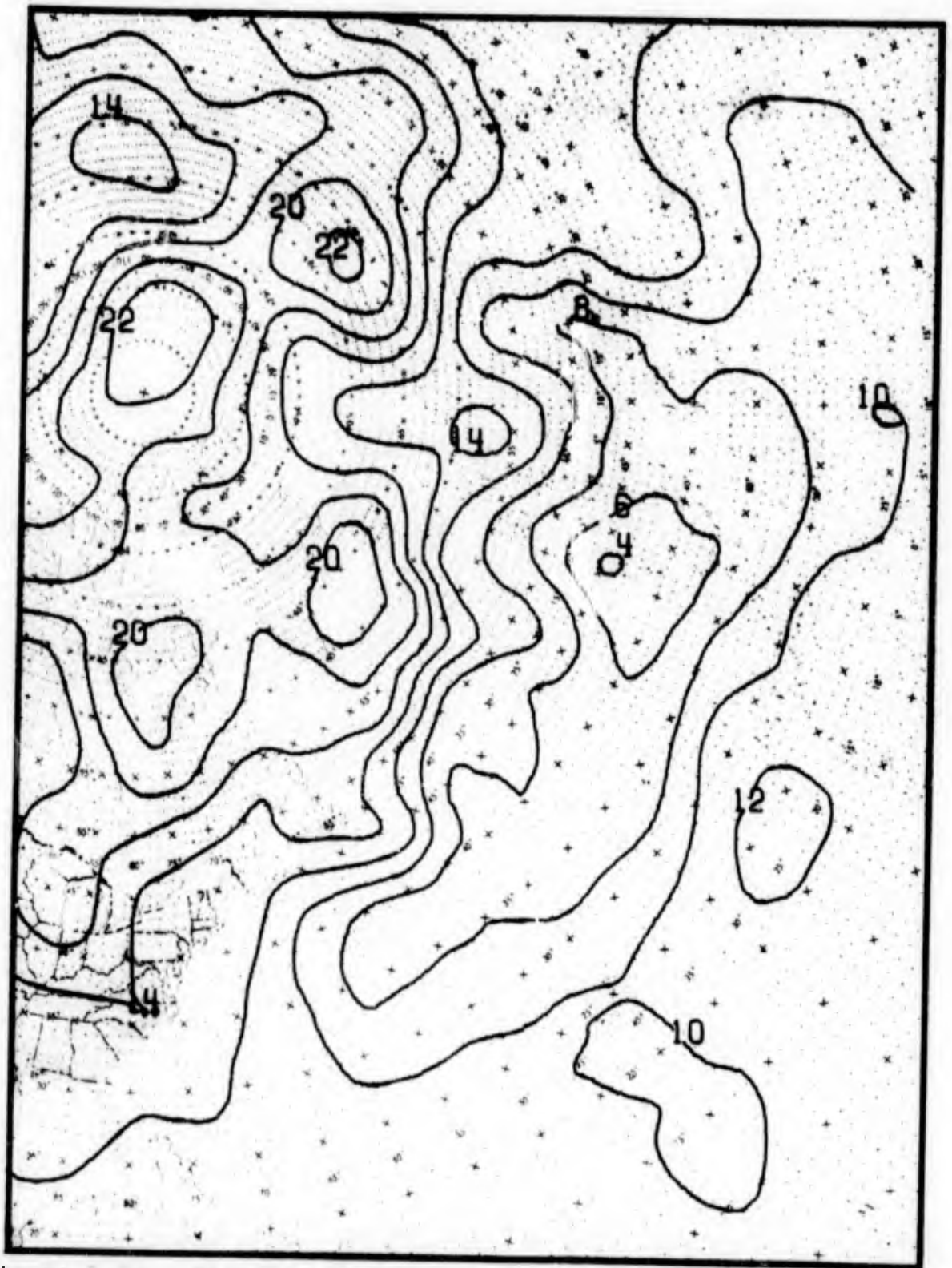

Figure B-23. Standard Deviation of Surface Pressure (mb.) 48 Hours Before Onset of Mistral, Air Ministry Type C. (Brody, Reiter and Godfrey)

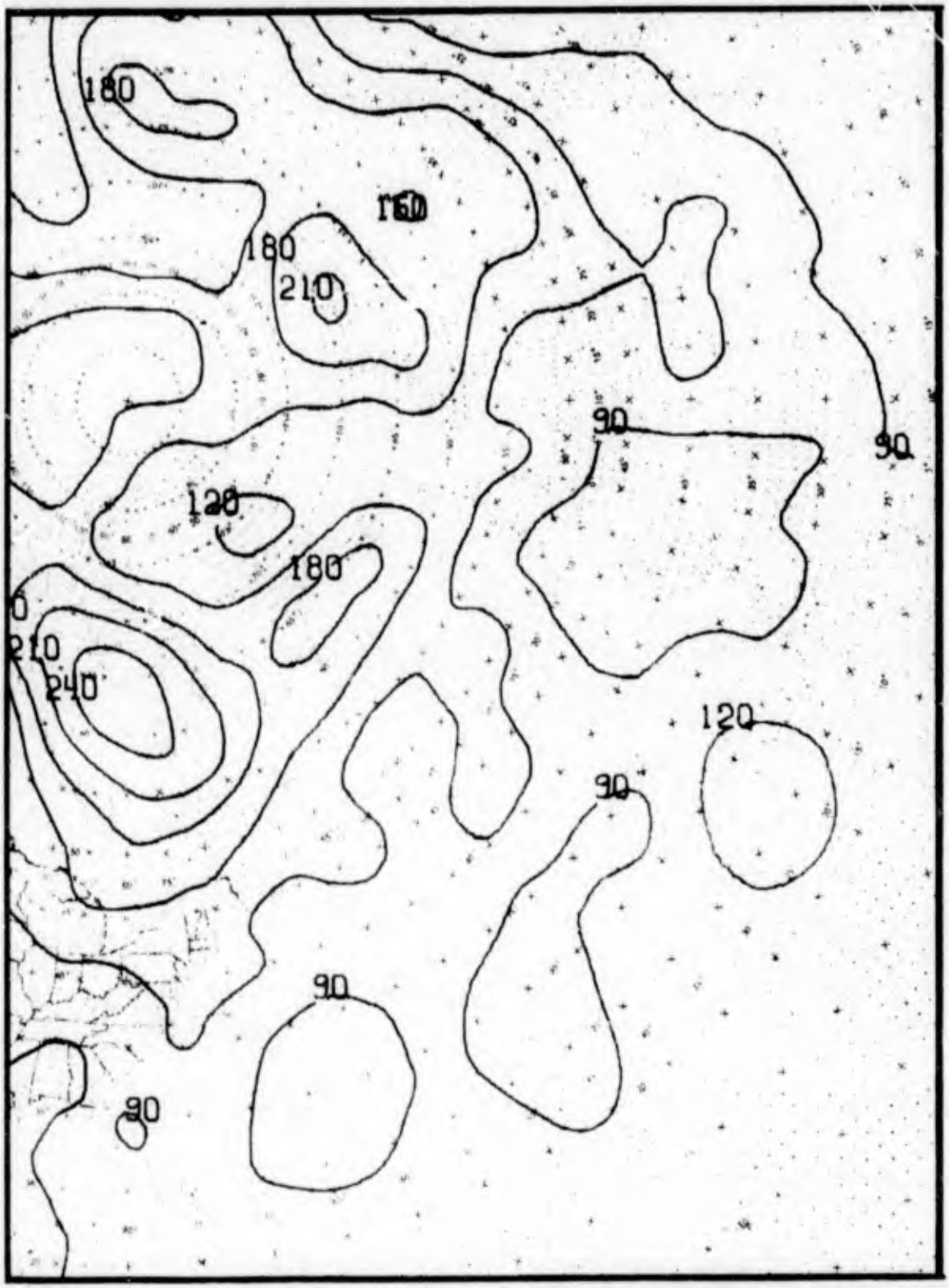

Figure B-24. Standard Deviations of 500-Mb. Heights (geopotential meters) 48 Hours Before Onset of Mistral, Air Ministry Type C. (Brody, Reiter and Godfrey)

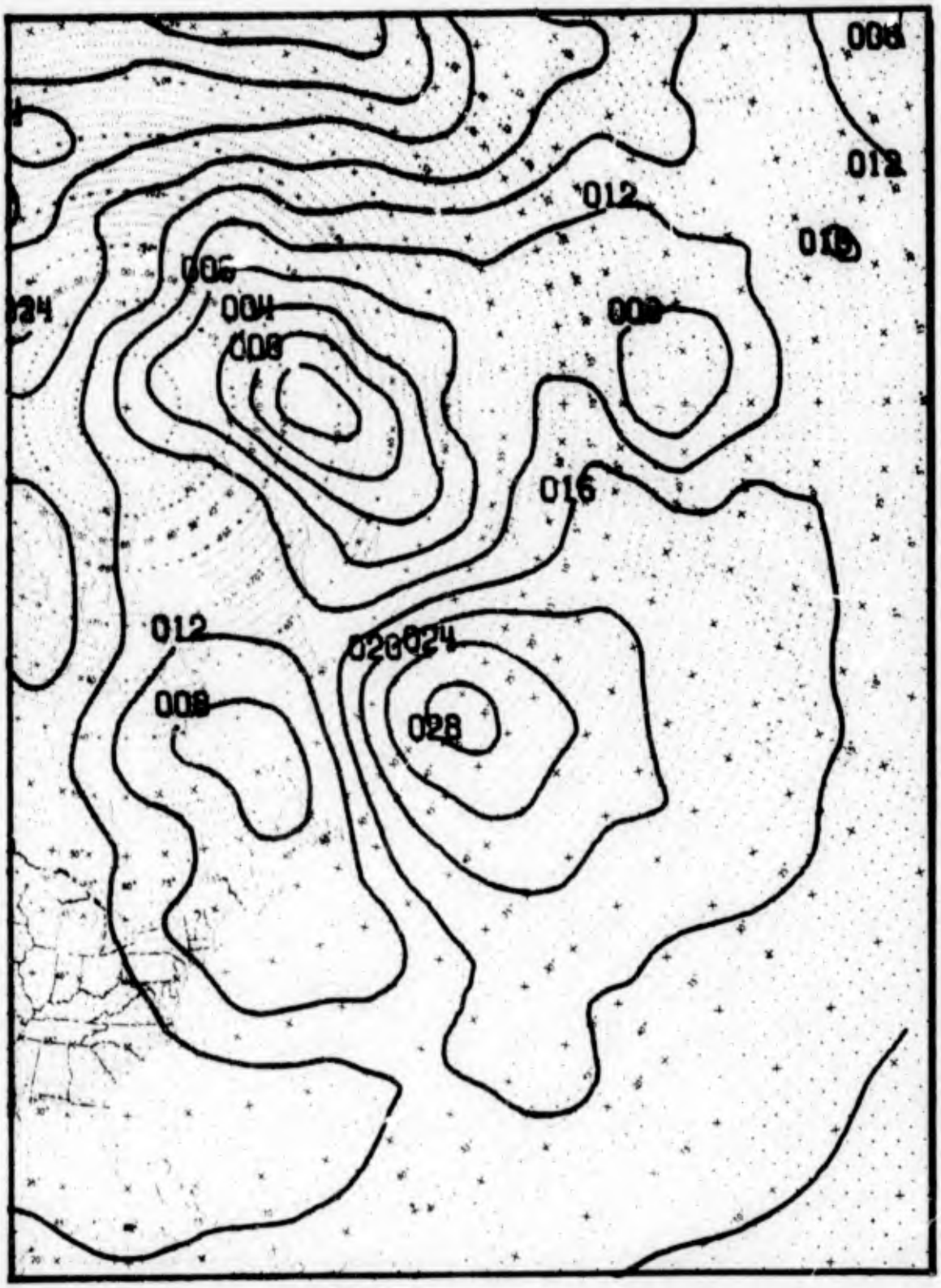

Figure B-25. Mean Hemispheric Surface Pressure (mb.) 72 Hours Before Onset of Mistral, Air Ministry Type A. (Brody, Reiter and Godfrey)

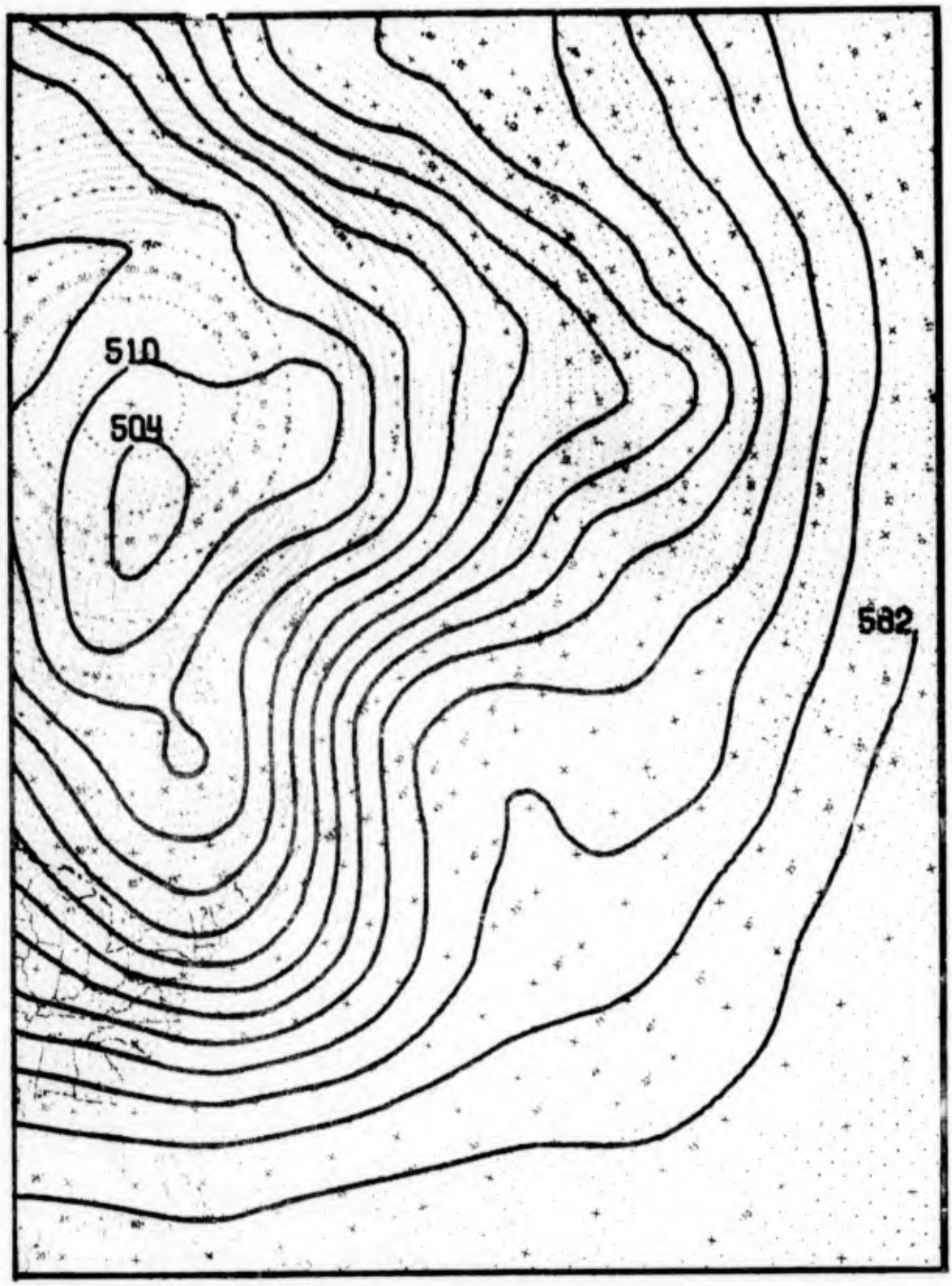

Figure B-26. Mean Hemispheric 500-Mb. Pattern (tens of geopotential meters) 72 Hours Before Onset of Mistral, Air Ministry Type A. (Brody, Reiter and Godfrey)

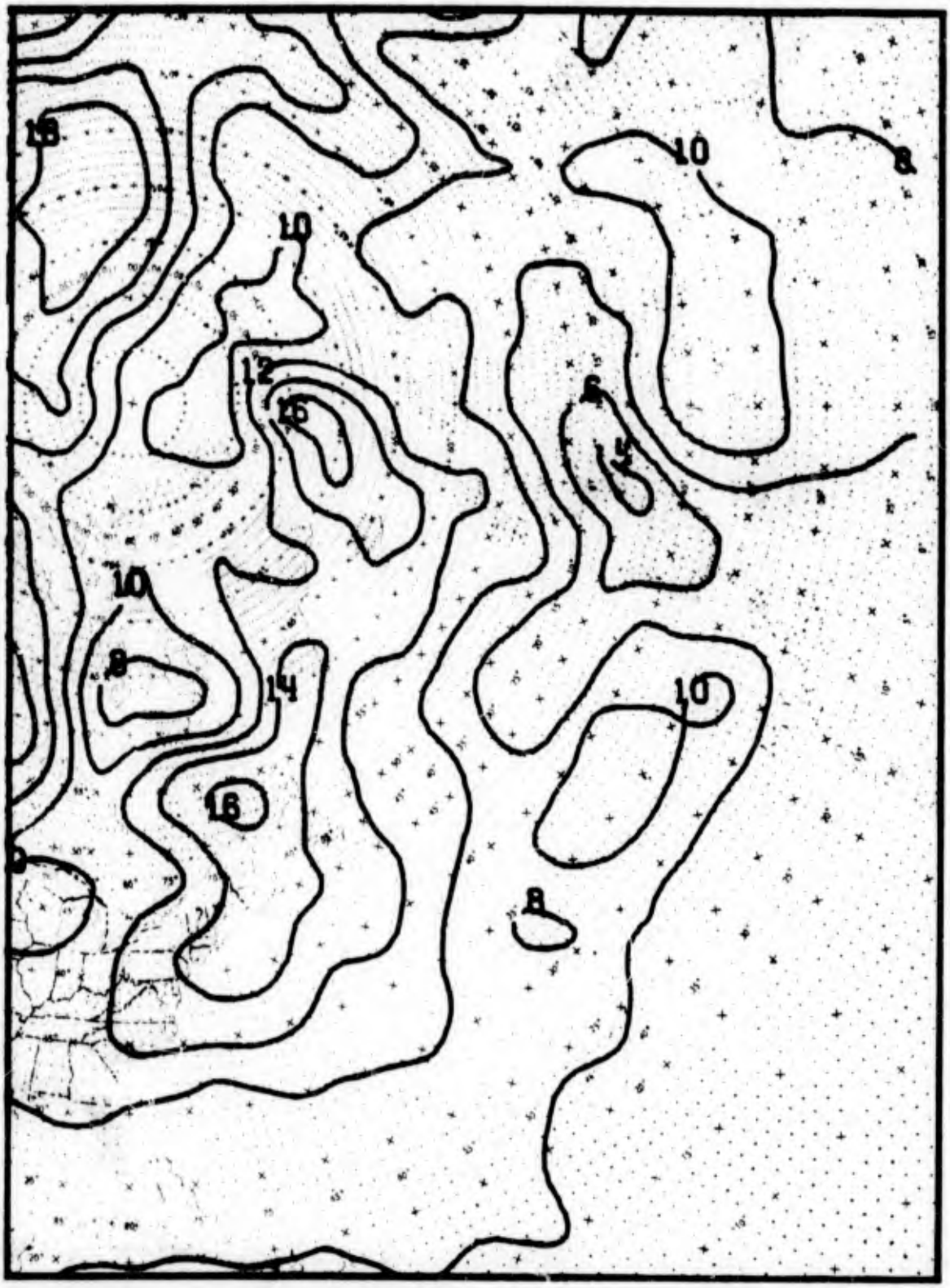

Figure B-27. Standard Deviations of Surface Pressure (mb.) 72 Hours Before Onset of Mistral, Air Ministry Type A. (Brody, Reiter and Godfrey)

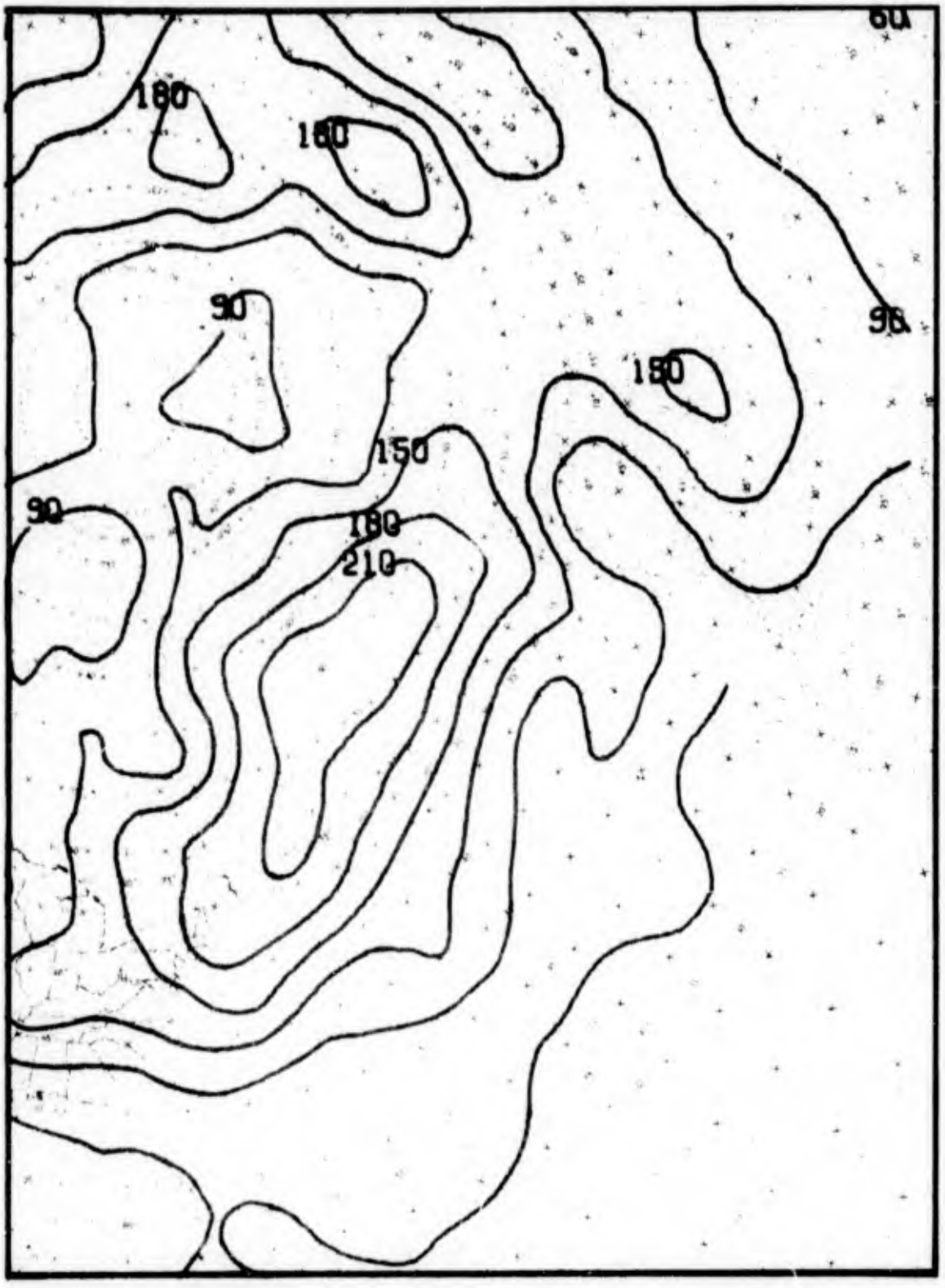

Figure B-28. Standard Deviations of 500-Mb. Heights (geopotential meters) 72 Hours Before Onset of Mistral, Air Ministry Type A. (Brody, Reiter and Godfrey)

APPENDIX C

STATISTICS OF THE ETESIAN.
FREQUENCY (%) AND STRENGTH (BEAUFORT) FOR THE THREE MOST FREQUENT WIND DIRECTIONS AT SELECTED ISLAND AND COASTAL STATIONS (AVERAGE OF OBSERVATIONS AT 0800, 1400 AND 2000 LT) (METAXAS).

Table C-1. Frequency (%) and Strength (Beaufort Scale) for Three Most Frequent Wind Directions (Average of Observations at 0800, 1400 and 2000 LT).

STATIONS	DIRECTION	MAY				JUNE				JULY				AUGUST				SEPTEMBER				OCTOBER			
		1,2,3	4,5	6	≥7	1,2,3	4,5	6	≥7	1,2,3	4,5	6	≥7	1,2,3	4,5	6	≥7	1,2,3	4,5	6	≥7	1,2,3	4,5	6	≥7
HELLENIKON	NW	6.7	2.3	0.1	0	8.2	1.8	0.2	0	7.4	1.5	0.1	0	7.1	1.4	0	0.1	5.0	0.8	0.1	0	3.8	1.1	0.1	0
716	N	7.7	2.3	0.4	0.2	9.2	4.9	0.2	0.1	12.3	9.5	1.2	0.4	14.3	9.8	1.3	0.1	19.1	7.4	0.6	0	17.3	6.6	0.2	0.3
1949-1968	NE	3.2	2.4	0.3	0.1	5.1	6.0	0.3	0.1	6.4	10.1	1.4	0.3	7.9	11.5	1.2	0.1	9.5	8.6	0.5	0	11.4	8.1	0.6	0
ALEXANDROUPOLIS	N	4.3	4.3	0.1	0	2.9	9.7	1.2	0	7.9	9.0	1.9	0	4.7	8.9	2.4	0.2	10.0	11.7	2.7	0.2	10.5	10.8	3.3	1.1
627	NE	12.9	3.7	0.1	0	12.6	4.9	0.4	0	11.9	12.2	1.8	0.1	10.6	13.2	1.4	0	11.9	13.5	0.8	0.2	13.4	12.9	1.2	0.2
1951-1960	E	4.5	2.2	0.1	0	4.2	1.3	0	0	4.1	2.2	0.1	0	4.4	2.6	0.1	0	4.3	2.7	0	0	4.4	1.2	0.1	0
LIMNOS	NW	8.4	4.8	0.4	0	12.5	8.5	0.7	0	11.4	9.4	1.0	0.2	12.6	6.9	0.4	0	5.8	4.5	0.8	0	2.5	2.1	0.1	0.1
651	N	2.6	0.8	0.2	0	3.5	2.6	0.6	0	3.8	6.3	1.2	0.7	4.9	4.7	0.7	0.2	4.7	4.4	0.9	0.3	2.0	1.9	0.2	0.2
1951-1960	NE	10.7	7.3	1.0	1.2	10.9	12.0	3.7	0.9	11.3	16.1	6.5	1.7	11.9	15.9	5.4	4.2	14.5	18.4	8.9	2.8	16.4	19.8	9.7	5.1
SKOPELOS	NW	3.7	2.9	0.2	0	6.3	4.0	0.4	0.3	3.5	6.3	0.9	0.5	3.5	4.2	1.2	0.7	2.1	3.2	1.3	0.2	1.6	1.4	0.5	0.2
662	N	17.1	4.3	0.4	0.1	17.3	4.1	1.2	0.4	18.8	5.1	0.4	0.1	12.8	4.9	0.7	0.5	11.3	3.7	0.9	0.3	7.8	7.3	3.4	0.2
1956-1968	NE	13.3	2.3	0	0	13.8	2.8	0.3	0.1	15.8	5.5	0.5	0	14.4	9.1	0.8	0.1	12.7	11.6	2.2	1.5	9.9	12.3	3.5	0.8
KIMI	NW	8.8	0.9	0	0	8.7	1.5	0.2	0	7.5	0.4	0.2	0	6.5	1.4	0.1	0	9.3	0.4	0	0	12.7	0.5	0.1	0
683	N	12.7	15.2	0.3	0.3	13.9	6.7	1.4	0.2	11.0	9.0	1.2	0.5	12.0	8.7	2.5	0.2	11.7	4.9	1.0	0.5	12.7	2.3	0.8	0
1955-1968	NE	17.1	7.6	1.7	0	19.2	10.5	2.5	0.6	21.2	17.8	2.4	0.4	25.4	14.0	2.6	0.3	27.7	14.8	3.3	0.2	28.9	13.4	3.0	0.4
SKYROS	NW	10.4	10.8	1.4	0	14.7	17.3	1.5	0.3	16.1	21.5	3.0	0.1	16.0	19.6	2.7	0.4	12.7	11.0	0.9	0.2	7.0	4.0	0.4	0.1
684	N	10.4	5.4	0.5	0.3	10.1	9.4	1.6	0.4	9.5	13.8	2.0	0.9	10.9	13.3	4.4	1.0	9.8	13.9	4.4	2.2	6.9	9.9	5.2	1.5
1951-1968	NE	5.7	2.6	0.2	0.2	6.1	2.9	0.4	0.5	4.9	3.4	1.1	0.5	5.2	3.4	0.9	0.4	5.7	6.5	3.1	2.7	7.3	7.9	5.4	6.0
ANDROS	NW	6.5	3.7	0.8	0.5	13.6	3.7	1.0	0.6	9.5	11.1	2.7	1.7	6.6	9.8	7.9	2.1	8.2	7.7	2.9	0.9	10.3	1.0	0.3	0
719	N	12.7	1.6	1.1	0.8	6.9	6.3	1.7	1.3	9.9	17.0	3.8	3.1	9.8	11.0	2.9	1.9	15.5	9.8	4.4	6.9	22.9	10.6	3.0	0.3
1932-1940	NE	17.1	2.5	0.3	0.1	20.3	7.5	1.4	0.5	15.8	6.8	1.7	0.9	18.0	8.0	2.6	0.9	14.7	2.3	2.2	1.4	6.5	2.5	0.6	0
SYROS	NW	4.0	0.7	0	0	12.3	1.3	0	0	14.4	3.5	0	0	8.7	1.1	0	0	4.4	0.6	0	0	4.3	1.3	0	0
730	N	13.5	19.3	0.1	0.1	16.1	14.8	3.7	0	16.2	35.4	3.8	0.6	18.6	35.7	3.3	0.7	17.7	32.5	5.1	0.1	16.5	24.7	2.6	0.7
1951-1959	NE	10.3	0.7	0	0	9.0	0.4	0.4	0	5.9	1.6	0.6	0	8.2	2.0	0.8	0	8.2	3.2	0	0	6.8	1.8	0	0
MILOS	NW	17.5	0.5	0.1	0	25.6	0.2	0	0	16.4	0.1	0	0	17.4	0	0	0	15.2	0	0	0	10.6	0.2	0	0.2
738	N	15.8	4.3	0.1	0	21.6	9.7	1.2	0	28.9	16.7	4.7	0.7	24.7	16.8	3.9	0.3	20.1	16.0	4.0	1.0	11.8	12.4	3.9	0.9
1951-1960	NE	3.7	3.7	0.1	0	4.5	4.9	0.4	0	3.4	8.4	2.2	0.4	6.4	10.2	2.5	0.2	5.1	11.6	2.6	0.2	6.2	8.7	2.5	0.3
NAXOS	NW	3.6	0.9	0.2	0.2	2.0	2.2	1.4	1.8	1.9	2.0	1.2	1.9	1.3	0.8	0.4	1.3	1.7	1.4	1.6	2.8	2.0	0.9	0.4	0.8
732	N	17.4	11.5	4.3	4.3	21.7	17.7	6.2	4.8	20.5	23.2	8.9	7.6	15.6	22.9	9.4	10.8	10.5	19.0	10.7	14.6	9.2	10.6	10.0	10.0
1956-1964	NE	7.0	5.2	2.8	1.6	9.6	6.7	1.6	0.4	9.9	9.1	2.7	1.2	8.5	10.9	3.8	2.7	5.8	6.6	2.3	2.5	4.4	4.7	3.3	3.9
THYRA	NW	8.3	5.4	1.1	0	12.3	9.0	1.1	0.1	9.4	10.9	1.0	0	8.2	11.0	1.0	0.4	7.5	7.5	1.1	0.1	6.4	4.7	0.8	0.1
744	N	5.2	6.7	2.2	0.1	3.6	8.2	1.5	0.1	4.6	22.0	9.4	0.6	3.0	22.4	10.2	0.2	4.1	23.8	8.5	0.4	6.3	11.7	1.6	0
1932-1940	NE	6.8	8.5	1.6	0	8.0	8.1	2.2	0.1	6.0	8.9	1.6	0.4	5.7	8.4	1.6	0.1	6.9	10.3	2.0	0.4	11.0	10.2	1.6	0.2
CHANIA	W	7.9	4.3	0.2	0	8.6	4.6	0.5	0.1	7.7	3.9	0.7	0	6.6	2.6	0.3	0	5.0	1.8	0.1	0.1	3.9	1.1	0	0
747	NW	13.5	1.9	0	0	17.6	2.1	0.1	0	18.0	4.6	0.2	0	14.4	2.0	0	0	10.5	1.8	0	0	7.0	0.8	0.1	0
1951-1968	N	14.3	1.3	0	0	17.2	2.3	0.1	0	19.1	4.0	0	0	18.6	4.1	0.1	0	18.1	6.1	0.1	0	12.8	5.4	0.4	0
HERAKLION	NW	18.5	18.3	0.5	0	21.7	22.8	1.1	0	25.4	34.4	1.5	0	22.6	29.4	1.1	0.2	19.2	18.1	0.7	0	13.4	8.8	0.2	0.1
754	N	15.7	12.8	0	0	14.2	4.6	0.3	0	11.8	5.9	0.1	0	13.6	6.9	0.3	0.1	15.4	10.8	0.2	0.1	16.3	4.9	0.4	0.1
1951-1960	NE	7.2	0.2	0	0	5.7	0	0	0	3.2	0.1	0	0	2.9	0	0	0	3.6	0.2	0	0	5.7	0.4	0.2	0
SITIA	NW	31.2	19.8	0.4	0.1	37.4	20.1	1.2	0	42.2	29.4	2.3	0.2	43.8	27.9	2.8	0.4	44.9	22.2	0.9	0.2	36.2	9.5	0.1	0
757	N	11.9	0.5	0.2	0	8.6	0.8	0	0	6.9	2.6	0.1	0	5.4	1.7	0.1	0	4.8	2.7	0	0	7.6	1.1	0	0
1953-1967	NE	5.1	0.1	0	0	4.1	0.2	0	0	1.2	0.7	0.1	0	0.8	0.3	0	0	1.7	0.2	0	0	2.8	0.3	0	0
MYTILINI	NW	9.0	4.7	0.1	0	14.5	7.0	0.4	0	16.8	9.8	0.6	0	15.9	8.8	0.4	0.1	14.1	7.3	1.5	0	10.1	0.8	0.1	0
667	N	18.5	5.8	0.3	0	25.8	8.0	0.1	0	31.2	12.3	1.4	0.6	28.5	12.0	1.9	0.7	20.6	12.7	3.6	0.3	14.8	7.3	2.0	1.2
1951-1960	NE	7.2	0.3	0	0	6.1	1.8	0.1	0	3.4	1.3	0.1	0	2.6	2.2	0	0	3.2	4.6	1.6	0	5.0	3.2	2.2	0.2
CHIOS	NW	1.9	0.2	0	0	2.3	0.3	0	0	1.8	0.4	0	0	1.2	0.8	0	0	3.2	0.6	0.1	0	4.8	0	0	0
704	N	15.8	6.7	0.2	0	19.0	7.3	0.3	0	24.5	19.8	0.7	0	19.4	18.4	0.7	0	15.9	11.5	1.8	0.4	16.8	9.4	1.6	0
1953-1967	NE	12.8	6.4	0.8	0.4	16.0	16.7	2.4	0	12.7	17.7	2.2	1.1	11.7	19.9	4.3	0.9	13.9	20.5	3.3	1.0	9.9	12.3	1.9	0.3
SAMOS	W	4.6	2.4	0.4	0	3.8	2.6	0.6	0.3	2.8	3.0	1.1	0.3	3.5	3.6	1.5	0.1	4.5	3.0	0.7	0.3	4.7	3.0	0.8	0.1
721	NW	27.8	11.5	1.0	0	45.1	13.7	2.9	0.7	42.9	27.1	2.7	0.5	39.8	24.6	3.3	0.2	33.5	16.9	2.4	0.9	21.6	8.6	0.6	0.2
1951-1960	N	8.9	1.5	0	0	7.8	2.9	0	0	7.1	2.7	0.3	0	9.1	2.1	0.1	0	9.3	3.5	0.7	0.2	10.2	2.8	0.1	0
KARPATHOS	W	29.8	8.1	0.6	0	41.6	20.7	1.4	0.2	37.4	30.0	3.5	0.5	44.4	25.6	2.6	0.1	46.3	21.2	1.2	0	40.5	8.8	0.2	0
748	NW	7.2	4.8	0.2	0.2	5.1	5.2	0.6	0.1	5.1	3.5	1.3	0.5	4.8	4.5	0.2	0	4.2	4.2	0.3	0.1	6.3	2.6	0.9	0
1951-1960	N	7.4	2.6	0.5	0.2	4.6	3.7	1.0	0	4.8	3.1	1.2	0.5	5.4	2.7	0	0	3.6	3.6	0.3	0	3.6	2.1	0.7	0

Table C-1. (Continued) Frequency (%) and Strength (Beaufort Scale) for Three Most Frequent Wind Directions (Average of Observations at 0800, 1400 and 2000 LT).

STATIONS	DIRECTION	MAY				JUNE				JULY				AUGUST				SEPTEMBER				OCTOBER			
		1,2,3	4,5	6	≥7	1,2,3	4,5	6	≥7	1,2,3	4,5	6	≥7	1,2,3	4,5	6	≥7	1,2,3	4,5	6	≥7	1,2,3	4,5	6	≥7
KOS	W	12.2	26.7	0	0	7.3	23.9	0.3	0	3.5	7.2	0	0	2.7	12.1	0.4	0	5.5	18.1	0.5	0	16.3	16.4	0.1	0
740	NW	5.7	32.2	0	0.1	10.6	43.9	1.3	0	15.2	66.5	4.2	0	16.3	61.6	1.6	0	13.7	44.1	3.1	0	7.9	23.3	1.3	0
1955-1964	N	0.2	1.8	1.7	0	1.4	3.5	1.2	0	0.1	0.8	0.2	0	0	1.6	1.3	0	0.2	5.1	2.2	0	0.1	2.1	0.7	0
RHODES	SW	4.1	0.7	0.1	0	3.1	9.8	0.2	0	3.6	3.2	0.5	0	3.6	3.4	0.4	0	5.8	3.1	0	0	6.0	0.5	0	0
749	W	38.1	18.2	1.1	0.2	33.7	44.8	3.1	0.2	30.8	45.4	5.3	0.1	36.1	40.8	3.2	0	33.1	29.2	1.7	0.2	24.1	10.9	0	0
1954-1963	NW	4.5	4.6	0.6	0	3.7	3.4	0.3	0	2.8	4.2	0.3	0	2.7	3.7	0.4	0	6.0	4.7	0.1	0	5.9	2.5	0	0.1
KERKYRA	W	11.1	0.9	0	0	13.0	1.1	0	0	13.7	1.2	0	0	11.1	0.8	0	0	7.1	0.5	0	0	4.9	0.2	0	0
641	NW	5.1	0.9	0	0	9.5	1.4	0.2	0	11.5	3.2	0	0	11.0	2.8	0	0	3.6	1.1	0	0	3.4	0.4	0	0
1951-1960	N	2.3	0.1	0	0	2.1	0	0	0	3.8	0.1	0	0	1.9	0.1	0	0	2.7	0.2	0	0	2.4	0	0	0
LEFKAS	W	7.3	3.1	0.4	0.1	8.8	5.2	0.8	0.8	7.4	4.4	1.0	0.2	9.4	3.2	0.8	0.5	7.4	1.3	0.3	0.4	3.4	1.3	0	0.2
669	NW	36.2	6.0	0.5	0	45.6	6.4	0.7	0.1	48.4	8.0	0.3	0	42.9	8.1	0.5	0.2	34.3	5.1	0.1	0.1	14.1	1.4	0.1	0.4
1951-1960	N	0.3	0	0	0	0.9	0.1	0	0	0.9	0	0	0	0.5	0	0	0	0.3	0.1	0	0	1.8	0.1	0	0
ARGOSTOLION	W	2.1	0.3	0	0	0.8	0.2	0	0	0.3	0.1	0	0	0	0	0	0	0.5	0	0	0	1.1	0.1	0	0
685	NW	35.1	3.9	0	0	40.0	9.2	1.0	0	48.5	10.0	0.7	0	45.0	8.3	0	0	29.5	2.9	0	0	21.4	0.8	0	0
1951-1960	N	5.0	0.5	0	0	6.7	0.4	0	0	6.8	0.8	0	0	7.2	0.3	0	0	8.9	0.7	0	0	3.3	0.9	0	0
ZAKYNTHOS	W	6.6	6.0	0	0.1	6.6	7.5	0.3	0.2	5.8	9.4	0.6	0	5.1	7.4	0.5	0	7.2	3.2	0.1	0.1	6.6	1.7	0	0
705	NW	9.9	8.5	0.4	0	10.3	10.9	0.1	0.1	12.7	18.6	0.8	0	12.7	14.6	0.8	0	12.6	11.4	1.0	0.2	9.6	4.9	0.1	0.1
1957-1968	NE	13.4	5.8	0.1	0	15.5	11.3	0.3	0	16.9	12.9	0.2	0	16.6	10.5	0.1	0.1	9.4	9.0	1.6	0.5	8.7	10.1	2.4	0.6
METHONI	W	18.5	23.9	1.8	0.2	19.0	25.5	2.6	0.3	21.0	22.5	1.5	0	17.2	22.8	1.7	0.2	10.2	17.2	0.6	0.1	6.1	9.0	0.8	0.1
734	NW	9.6	14.6	1.0	0.3	9.4	18.3	2.7	0.7	12.3	21.9	3.0	0.3	13.4	21.7	3.5	0.5	14.3	11.6	2.8	0.1	11.5	3.3	2.0	0
1951-1960	N	1.8	0	0	0	0.8	0	0	0	0.7	0.6	0	0	1.8	0.3	0	0	8.8	1.3	0	0	16.1	0.1	0	0
KITHIRA	NW	11.1	4.3	0.7	0	11.8	4.4	1.0	0.1	8.0	6.4	0.5	0.2	7.3	4.0	0.5	0.2	7.7	2.8	0.6	0	7.8	1.0	0	0
743	N	3.7	1.3	0.3	0	4.1	1.0	0.1	0.1	3.3	0.9	0.2	0.2	5.7	1.8	0	0.2	7.9	0.8	0.2	0	6.1	0.9	0.3	0.2
1951-1960	NE	11.7	4.6	1.4	1.6	12.4	8.0	0.6	0.4	17.7	9.9	3.0	1.6	14.3	13.4	3.1	1.7	15.9	15.2	4.4	4.7	8.9	19.3	4.0	8.8
ASTIPALEA	W	7.8	4.0	0.5	0.1	5.1	2.4	0.1	0	1.8	0.5	0	0.1	2.0	1.0	0.1	0	4.2	1.4	0.1	0	5.7	1.7	0.3	0.1
739	NW	5.6	3.5	0.6	0	8.1	11.8	4.4	0.4	6.0	16.8	8.8	2.6	7.2	18.3	8.4	2.8	5.0	8.7	3.5	0.8	2.7	3.4	0.6	0.1
1951-1968	N	22.1	16.6	2.2	0.8	21.1	21.0	5.6	0.8	16.3	26.9	7.6	1.7	15.7	25.3	4.6	1.8	23.0	25.6	6.1	3.2	21.5	20.0	4.2	1.7
PATPAI	SW	20.2	3.3	0.3	0	18.0	2.8	0.4	0	18.2	2.2	0.[illegible]	0	16.8	1.6	0.1	0	13.3	1.5	0.1	0	11.6	1.8	0.1	0.1
689	W	13.0	1.2	0	0.1	14.3	1.2	0	0.1	14.1	1.4	0	0	12.7	1.1	0.1	0	9.9	0.7	0.1	0	7.[illegible]	0.5	0	0.1
1951-1967	NW	9.2	0.5	0	0	9.8	0.4	0	0	6.9	0.7	0	0	6.7	0.5	0.1	0	5.5	0.4	0	0	6.8	0.5	0	0
PIREYS	NW	9.8	3.5	0.7	0.2	9.8	4.8	0.3	0.1	11.3	4.7	0	0.1	10.4	4.4	0.6	0	8.3	3.6	0.4	0	5.5	3.5	0	0
717	W	5.7	0.7	0	0	9.5	2.4	0	0	16.5	4.0	0.2	0	16.9	4.4	0	0	16.1	3.2	0.1	0	13.3	3.5	0.2	0.1
1955-1968	NE	8.0	1.9	0.1	0	9.1	2.1	0.2	0	12.2	4.0	0.3	0	14.8	4.1	0.3	0	21.2	3.8	0.5	0.2	26.5	3.4	0.5	0.3
CHALKIS	NW	8.3	0.3	0	0	6.5	4.4	0	0	6.8	7.7	0	0	6.7	6.8	0	0	7.5	6.0	0	0	6.8	4.3	0	0
697	N	11.6	5.9	0	0	14.2	12.0	0	0	16.0	15.7	0	0	15.5	19.4	0	0	14.1	15.3	0	0	13.2	13.6	0.1	0
1951-1960	NE	14.4	3.0	0.1	0	17.7	6.7	0	0	12.4	11.9	0	0	12.8	11.9	0	0	11.9	14.6	0	0	11.6	11.1	0.1	0
NAT.OBSERVATORY	NW	4.5	0.2	0	0	5.4	0.5	0	0	6.4	1.2	0.1	0	5.6	0.6	0.1	0	6.1	0.7	0	0	4.6	0.6	0	0
(ATHENS) 714	N	7.0	2.2	0.2	0.1	9.9	3.9	0.3	0	14.7	8.2	0.8	0.3	13.8	6.9	1.3	0.1	16.2	5.7	0.8	0.1	14.5	5.5	0.6	0.2
1949-1968	NE	5.7	2.3	0.2	0.2	9.0	4.3	0.5	0.1	11.5	8.1	0.9	0.1	13.7	9.1	1.3	0.2	12.3	6.4	1.1	0.1	12.5	7.5	0.7	0.2
NEA FILADELFIA	NW	3.0	0.7	0	0	3.8	1.0	0	0	2.6	0.4	0.1	0	2.7	0.6	0.1	0	2.0	0.7	0	0	1.3	0.1	0	0
701	N	2.0	0.9	0	0	2.3	1.2	0.1	0	4.0	3.3	0.4	0	3.8	2.0	0.1	0	3.2	1.3	0.1	0	2.0	0.8	0.3	0
1949-1968	NE	10.1	6.2	0.3	0.1	18.3	8.3	0.3	0	23.2	16.0	0.7	0.1	24.7	16.5	0.6	0.2	25.5	11.9	0.1	0.1	24.0	14.0	0.4	0.1
ELEFSIS	W	6.0	1.5	0.4	0.3	6.6	1.6	0.6	0.1	3.8	1.2	0	0	1.5	1.3	0.1	0	2.8	0.3	0.1	0	3.7	0.5	0.2	0
718	NW	5.4	1.2	0.2	0	4.0	0.6	0.2	0	7.6	2.6	0.2	0.2	6.2	1.7	0.2	0	5.5	1.8	0.2	0	5.8	1.6	0.2	0
1951-1960	N	14.7	3.9	0	0	19.9	6.8	0.8	0.6	23.7	13.6	1.7	0.7	26.2	12.0	2.4	0.6	27.3	10.4	1.1	0.2	26.7	9.2	1.2	0.5
MEGARA	W	4.2	3.2	0.4	0	6.0	2.6	0.4	0.1	6.4	3.5	0.4	0.1	7.5	4.8	0.3	0.1	5.4	2.0	0.1	0	6.0	1.7	0.1	0
708	NW	25.5	9.0	0.9	0.1	23.0	11.6	1.6	0.1	25.4	13.3	0.8	0.1	21.7	10.7	0.5	0	32.3	8.4	0.5	0	30.8	7.0	0.3	0
1950-1967	N	2.8	1.1	0.2	0	4.5	1.6	0.1	0.1	5.3	2.4	0.4	0.1	6.9	2.1	0.1	0	7.9	1.2	0.1	0	7.9	1.2	0.1	0
KARYSTOS	NW	4.0	0.5	0	0	3.2	3.5	0	0	1.3	1.1	0.1	0	0.8	0.2	0	0	1.[illegible]	0.7	0	0	2.4	0.3	0	0
703	N	12.9	10.9	0.9	0.4	14.2	21.9	2.0	0	19.0	35.7	7.6	0.6	17.2	35.3	8.0	0.7	17.7	33.3	2.6	0.1	11.5	25.3	4.5	0.1
1949-1968	NE	4.7	1.9	0.1	0	3.0	1.5	0.1	0	1.7	1.6	0	0	2.7	1.3	0	0	2.8	1.9	0	0	5.2	4.1	0.3	0.2
KAVALA	E	1.0	0.6	0	0	1.7	0.1	0	0	1.1	0.4	0	0	0.7	0.3	0	0	1.4	0.2	0.2	0	2.2	0.4	0.3	0
625	SE	17.3	15.0	0.2	0.3	20.3	13.0	0	0	16.0	9.8	0.2	0	15.1	9.8	0.1	0	20.8	10.9	0.2	0	15.5	4.4	0.3	0
1951-1960	S	10.0	4.8	0	0	8.9	5.6	0	0	9.3	8.3	0	0	15.7	7.1	0	0	5.5	2.3	0	0	10.6	2.7	0.1	0
VOLOS	W	3.4	0.3	0	0	4.1	0.5	0.3	0.1	2.7	0.3	0	0	2.2	0.3	0	0	3.9	0.3	0	0	5.7	0.3	0	0
661	NW	2.8	0.4	0	0	3.4	0.4	0	0	0.9	0.3	0	0	1.5	0.1	0	0	2.3	0.2	0	0	2.3	0.4	0	0.1
1956-1968	N	12.9	1.1	0.2	0.1	11.9	1.1	0.3	0.1	14.6	2.2	0.7	0.2	12.4	1.7	0	0	18.9	1.6	0.2	0	28.2	3.2	0.3	0.1